Anal. Methods Environ. Chem. J. 6 (3) (2023) 5-18

AMECJ

Research Article, Issue 3
Analytical Methods in Environmental Chemistry Journal
Journal home page: www.amecj.com/ir

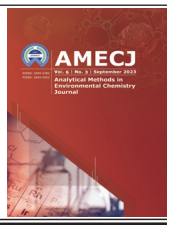

Adsorption of methylene blue dye onto bentonite clay: Characterization, adsorption isotherms, and thermodynamics study by using UV-Vis technique

Ahmed Jaber Ibrahim[a,*], Haneen Abdul Wahid Dwesh[a,b], and Ahmed R.Y. Al-Sawad [c]

[a] *Scientific Research Center, Al-Ayen University, ThiQar 64011, Iraq*
[b] *Ministry of Education, Directorate of Education Thi-Qar, Iraq*
[c] *College of Science, University of Sumer, Iraq*

ARTICLE INFO:

Received 3 June 2023
Revised form 9 Aug 2023
Accepted 28 Aug 2023
Available online 29 Sep 2023

Keywords:
Adsorption,
Methylene Blue,
Bentonite,
Thermodynamics,
Isotherms,
UV-Vis

ABSTRACT

This study uses the UV-Vis technique to describe the elimination of methylene blue dye from an aqueous solution by adsorption on an Iraqi bentonite clay surface. The batch approach was used to conduct adsorption studies carried out to evaluate the influence of factors of experimental like contact time (0–90 min), clay dose (0.1–0.35 g), and initial dye concentration (10–125 mg L^{-1}) at the range of temperatures (25-40°C). The Langmuir and the Freundlich isotherms were used to analyze the data; the Langmuir isotherm (R2 = 0.998) proved more appropriate for the equilibrium data. The thermodynamic properties of the adsorption process, including Gibbs free energy (ΔG^O), entropy(ΔS^O), and enthalpy (ΔH^O), were also studied. Since the (ΔG^O) and (ΔH^O) values were negative, it was clear that the adsorption process constituted an exothermic, spontaneous reaction. This investigation revealed that Iraqi bentonite clay effectively removed the dye methylene blue because of its high surface area. Methylene blue may be removed with an adsorption efficiency of up to 99.39 % at 25°C. By employing bentonite clay as an adsorbent surface, this research offers practical adsorption technology that is affordable and effective for treating wastewater.

1. Introduction

The production of textiles, leather tanning, cosmetics, paper, food processing, and pharmaceuticals are just a few industries whose effluents frequently contain dyes [1]. They have long been a source of ecological worry because of their toxic effects, carcinogenicity, mutagenicity, and teratogenicity [2]. Many physicochemical techniques, including adsorption, coagulation, chemical oxidation, advanced oxidation, and flocculation, are presently available to treat wastewater containing dyes [3-5]. Due to its incredible effectiveness, cheap operating cost, and straightforward operation technique, adsorption has drawn particular attention from researchers across the globe [6]. The main challenge in adsorption has continuously been developing new adsorbent materials to increase removal effectiveness. The greatest significant commercial adsorbents are alumina, activated carbon, polymers, clays, and silica [7,8]. Particularly, inexpensive natural clay is regarded as a suitable adsorbent since it is readily available, eco-friendly, non-toxic, has a high surface area, and has a variety of active sites on its surface [9,10]. This abundant clay may be used in many water purification processes [11]. Several researchers have documented using natural clays like halloysite,

*Corresponding Author: Ahmed Jaber Ibrahim
Email: ahmed.jibrahim@alayen.edu.iq
https://doi.org/10.24200/amecj.v6.i03.243

bentonite, montmorillonite, kaolinite, sepiolite, and smectite to purify several organic contaminants [12-17]. Also, modern and more advanced techniques have been used in the adsorption of organic pollutants from aqueous solutions in the recent period. These studies showed the possibility of using the adsorption process as a significant process for purifying wastewater and the possibility of using it in water purification systems [18,19].

The uses of Methylene Blue in the other domains must be carefully considered and supported by early safety research. This necessitates developing and optimizing a straightforward approach for detecting Methylene Blue in chemical samples. Numerous analytical techniques can be used to determine the amount of Methylene Blue because of its physicochemical characteristics. Several techniques can be listed, including capillary electrophoresis (CE), liquid chromatography (LC) combined with mass spectrometry (MS), diode array detection (DAD), and ultraviolet-visible spectroscopy (UV-VIS) [16]. This research studies the Methylene Blue adsorption as a sample of organic dye on natural Iraqi clay without treated (Bentonite) at several temperatures. Key operational parameters such as contact time, clay dose, and initial dye concentration have been considered for their effects. The adsorption process was computed using the isotherm models: Langmuir and Freundlich's models were used to assess the connection between experimental data, investigate the adsorbent's ability to maximize adsorption efficiency and compute thermodynamics parameters for the adsorption process.

2. Materials and methods

2.1. Instruments

Water Bath Oscillator (WB-80 - Bioevopeak Co., China), UV-Vis spectrophotometer (Edinburgh Instruments Ltd., UK), The amount of discrete wavelengths of UV or visible light that are absorbed by or transmitted through a sample in comparison with a reference or blank sample is measured by the analytical technique known as UV-Vis spectroscopy. Digital ultrasonic cleaner (VEVOR- USA), hotplate magnetic stirrer (Bioevopeak Co., Ltd., China), electronic balance (PR2202/E- Thermo Fisher Scientific Inc., USA), mesh sieves (20 µm-Retsch GmbH, Germany), and digital drying oven (Alterlab Co., Indonesia) were used.

2.2. Chemicals

All the chemical substances utilized in this investigation were sourced from reliable sources and were of the highest purity, including Methylene blue ($C_{16}H_{18}ClN_3S$, CAS number: 61-73-4) from Sigma-Aldrich. Iraqi Bentonite clay (Fig.1) was obtained from the western desert of Al-Anbar Governorate in Iraq. It is a fine particle of yellow colour and can absorb water. Table 1 shows the chemical components of Bentonite clay.

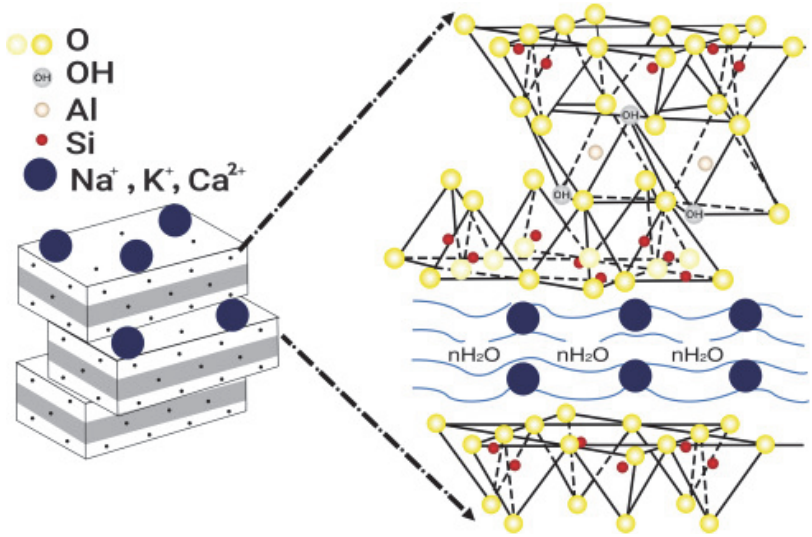

Fig. 1. Structural geometry of Bentonite [20]

Table 1. Chemical components of Bentonite [21]

Name	Formula	Percentage
Silica	SiO_2	% 65 – 50
Alumina	Al_2O_3	% 25 – 15
Ferric Oxide	Fe_3O_3	% 4 – 2
Magnesium Oxide	MgO	% 6 - 3
Calcium Oxide	CaO	% 2 – 0.5
Sodium Oxide	Na2O	% 5 – 0.5
Potassium Oxide	K_2O	% 1 – 0.2
Titanium Oxide	TiO_2	% 0.5 – 0.2

2.3. Preparation of clay powder

The Iraqi clay (Bentonite) used in this study was washed with Deionized water many times to eliminate contaminants and remove water-soluble substances such as salts and others. These clays were dried for five hours in an oven whose temperature was (200°C). The clays were ground in the physical chemistry laboratory at Alayen University, and the ground clay powders were subjected to a size sorting process using sieves designated for this purpose. The sorted particles used in this study were 20 µm (Particle size). After completing the sieving process, the clays were dried and kept in containers with tight lids (Fig.1).

2.4. Preparation of standard solution

To prepare different concentrations of Methylene blue (MB) dye, a standard concentration of dye (1000 mg L^{-1}) was diluted in double-distilled water (DDW). The stock solution was diluted appropriately to provide solutions for adsorption experiments. Using a UV-Vis spectrophotometer with a range of 200 - 800 nm, the maximum wavelength (λmax) of 664 nm was determined, corresponding to the highest absorption of the dye solution, as shown in Figure 2. Six concentrations were used to create the calibration curve, illustrating the relationship between absorbance and concentration: 5, 10, 15, 20, 40 and 50 mg L^{-1}. The standard curve between absorbance and concentration was created in Figure 3 after measuring the absorbance of these concentrations at the dye's λmax.

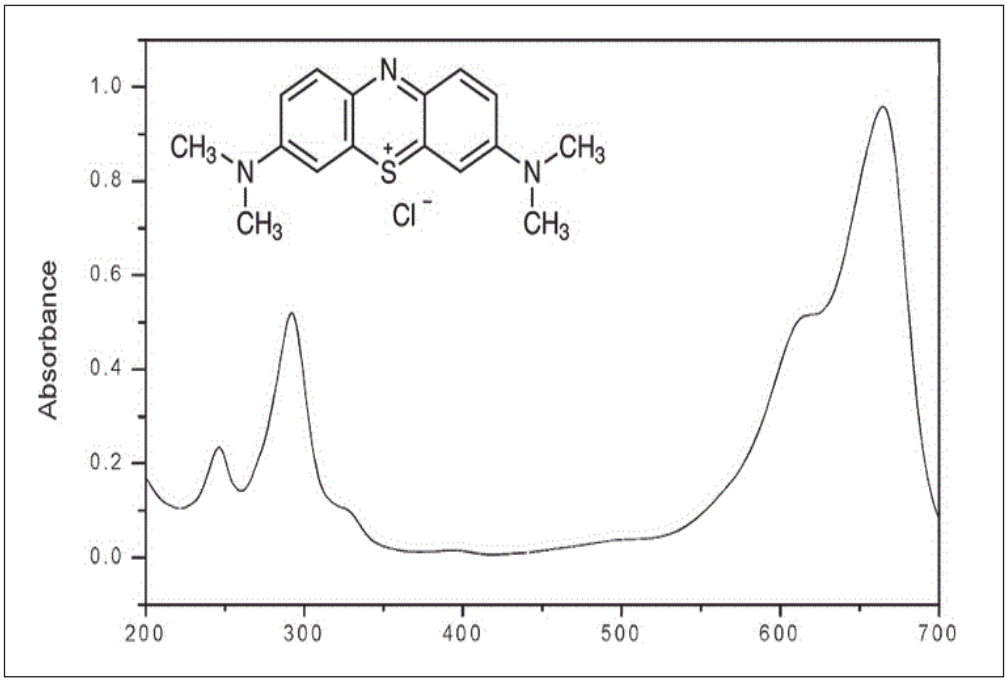

Fig. 2. UV-Vis spectrum of Methylene blue dye.

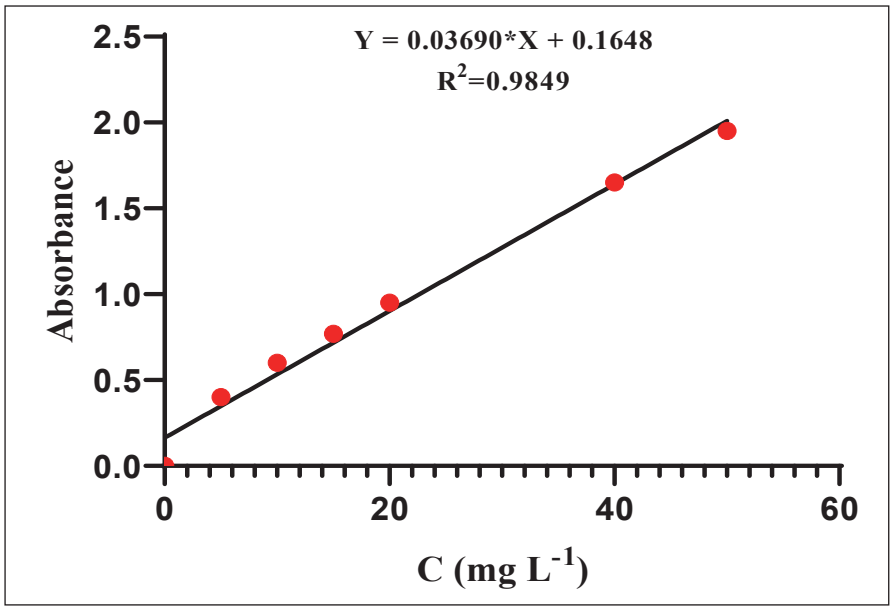

Fig. 3. Calibration curve of Methylene blue dye.

2.5. Adsorption process

The batch approach was used to conduct studies on MB adsorption onto Bentonite clay since it is straightforward and dependable at several temperatures. A set quantity of adsorbent was combined with 40 mL of an aqueous MB solution to conduct all batch adsorption studies in 100 ml Erlenmeyer flasks. Filtration was used to remove the adsorbent from the dye solution after a predetermined time. At the maximum adsorption wavelength of MB, λmax =664nm, the UV-Vis spectrophotometer was used to measure the dye concentration in the filtrate. The variation between the initial and final concentrations of the MB solution acquired before and after a connection between the adsorbent and the cationic MB solution was used to compute the concentration of dye absorbed by the adsorbent. Equations (1) are used to calculate the amount of MB dye adsorbed per unit mass of the adsorbent (mg g^{-1}) at time (t) [22].

$$Qe = V_{AS}(Co–Ce)/m \qquad \text{(Eq.1)}$$

V_{As}: Total volume of the adsorbent solution (*L*).
Co: Initial concentration of the dye (mg L^{-1}).
Ce: Concentration of the adsorbent solution at equilibrium (mg L^{-1}).
m: weight of the adsorbent (*g*).
Qe: amount of adsorbent at equilibrium (mg g^{-1}).

3. Results and Discussion

3.1. Determination of equilibrium time for adsorption system

The equilibrium time between the adsorbed clay surface and the adsorbed amount of dye must be evaluated. So, a concentration of 50 mg L^{-1} of MB dye solution was chosen and made in contact with (0.2 g) of bentonite clay powder at a temperature of (25°C). Then, the samples were taken from the solution at successive times and analyzed to find out the change in concentration with time. Determine the equilibrium time for the concentration of the dye adsorbed on the surface was equal to 45 minutes, as shown in Figure 4.

3.2. Determination of the clay dose

The influence of the adsorbent surface dose on the adsorption process of bentonite clay was investigated using a constant concentration of a solution of methylene blue dye (50 mg L^{-1}) and by taking different doses of bentonite clay at a temperature of (25°C) and 45 min of contact time. From the observation of Figure 5, we find that the shape of the curve begins to rise with the increase in the adsorbent surface dose. This height value indicates that the amount of adsorbent surface has reached saturation, which depends on the bentonite clay's physical properties [23]. The

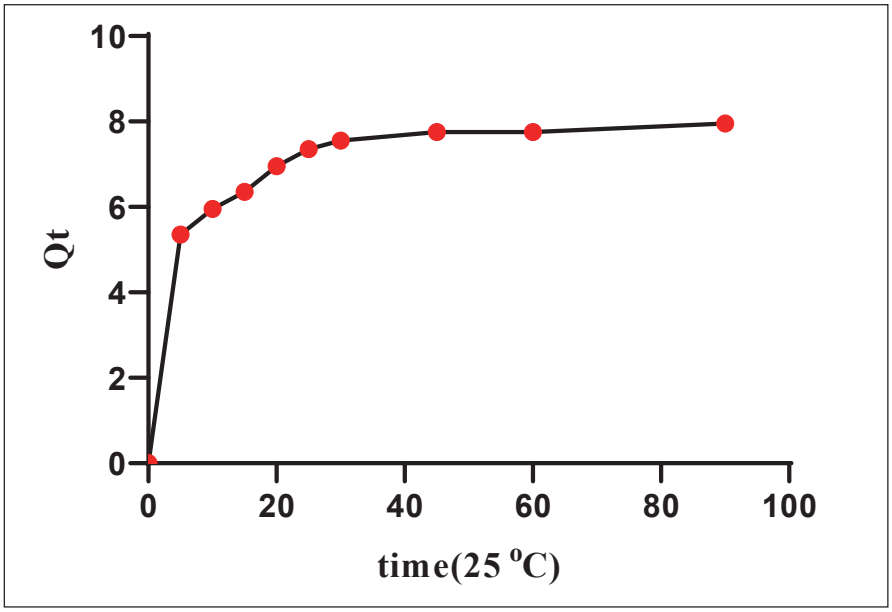

Fig. 4. Determination of the equilibration time for the dye solution adsorbed on the surface of bentonite clay

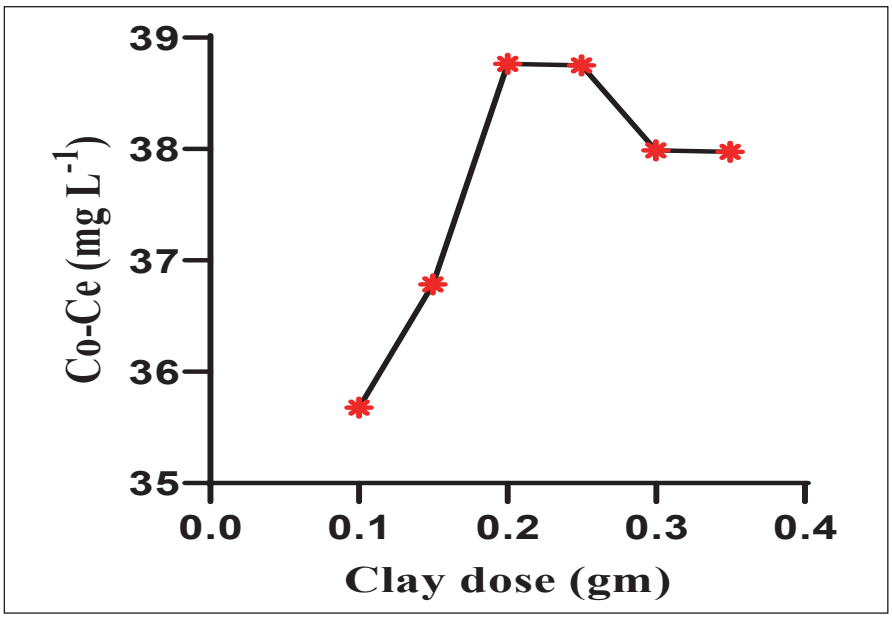

Fig. 5. Plot of *Co-Ce* vis different clay doses for adsorption of MB on the Bentonite clay.

results show that the best dose of bentonite clay for adsorption of the methylene blue dye solution is 0.2 gm.

3.3. Adsorption percentage

The adsorption percentage was calculated by Equation 2 [24].

$$percentage\ of\ dye\ adsorption = \frac{(Co - Ce)}{Co} * 100 \quad \text{(Eq.2)}$$

Since *Co* and *Ce* are the initial concentration (mgL^{-1}) of the dye solution and the concentration of dye (mgL^{-1}) adsorbed at equilibrium time, respectively. Table 2 shows the adsorption capacity percentage of MB dye on the surface of bentonite clay at the equilibrium time for studied temperatures.

Table 2. Adsorption percentage of dye on bentonite at studied temperatures.

Temperature (^{o}C)	adsorption capacity Percentage (%)
25	99.39
30	99.25
35	99.00
40	98.75

3.4. Adsorption isotherms

The adsorption study of MB dye from aqueous solutions on the surface of bentonite clay was conducted at different temperatures (25, 30, 35, and 40^{o}C) at initial concentrations of 10, 20, 30, 40, 50, 75,100, and 125 (mg L^{-1}) at a stirring speed of 150 rpm and at an equilibrium time of 45 min. The amount of adsorbent (*Qe*) corresponding to each value of the equilibrium concentrations (*Ce*) shown in Table 3 was calculated using Equation 1. The amount of adsorbent (*Qe*) was plotted against the equilibrium concentration (*Ce*) to give the general shape of the adsorption isotherms, as shown in Figure 6; it was possible to conclude that the adsorption follows the Langmuir equation (L_2-Type according to Giles classification).

The major shape of the adsorption isotherms of methylene blue dye on the surface of bentonite is identical to the type (L_2-Type according to Giles classification), which is characterized by a decrease in slope when increasing the concentration as the active sites decrease gradually until reaching the full coverage of the surface [25]. This behavior is attributed to the high affinity for the surface of the adsorbent at low concentrations of the adsorbent, which decreases with increasing concentrations, and this was consistent with previous studies [26,27]. Here, there is a need to give a clear idea of the nature and behavior of the clay inside the

Table 3. Adsorption values of MB dye on the bentonite surface clay at studied temperatures.

C_o (mg L^{-1})	298*K*		303*K*		308*K*		313*K*	
	Ce (mg L^{-1})	*Qe* (mg L^{-1})	*Ce* (mg L^{-1})	*Qe* (mg L^{-1})	*Ce* (mg L^{-1})	*Qe* (mg L^{-1})	*Ce* (mg L^{-1})	*Qe* (mg L^{-1})
10	0.014	1.997	0.021	1.995	0.037	1.992	0.062	1.987
20	0.034	3.993	0.049	3.990	0.081	3.983	0.132	3.973
30	0.069	5.986	0.096	5.980	0.145	5.970	0.223	5.955
40	0.141	7.971	0.185	7.963	0.256	7.948	0.366	7.926
50	0.303	9.939	0.3745	9.9251	0.473	9.905	0.625	9.875
75	1.135	14.772	1.273	14.745	1.437	14.712	1.680	14.664
100	5.033	18.993	6.699	18.660	6.816	18.636	7.190	18.562
125	17.171	21.565	18.923	21.215	20.77	20.846	23.85	20.23

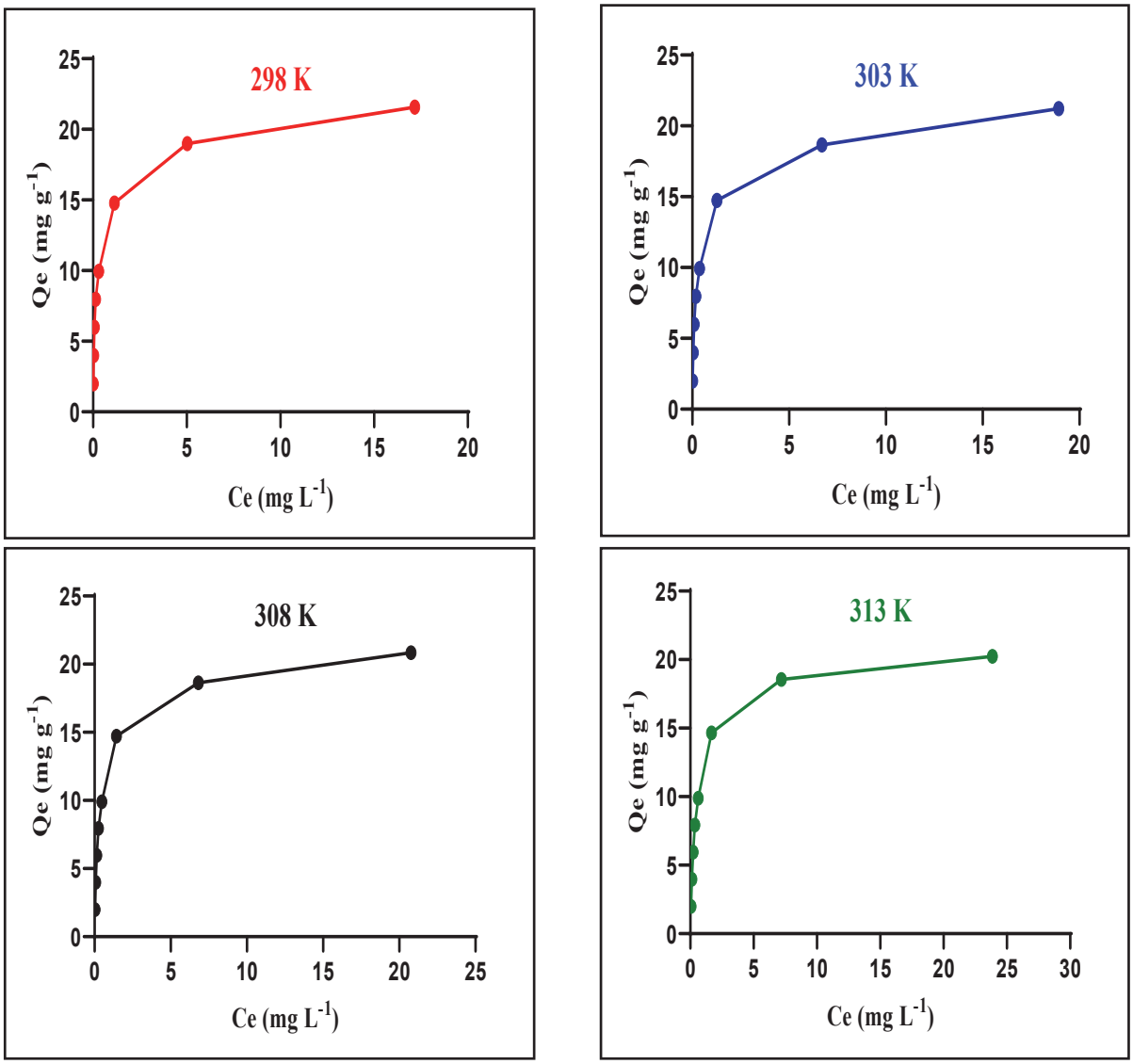

Fig. 6. Plot of Ce vis Qe for adsorption of MB dye on the Bentonite clay.

solution, as the surface of the clay material contains an abundance of active centers for adsorption due to the possession of wet clay particles by an Electrostatic double-layer [26]. We note from the adsorption isotherms on the surfaces of bentonite clay that the quantity of adsorption rises with rising concentration. This increase stops at a certain concentration, and after this concentration, the value of adsorption capacity stabilizes and remains constant no matter how the concentration of the dye in the solution increases, i.e. it reaches the state of saturation of the surface (Plateau Shape). That is, the adsorption is with a monomolecular layer, and the surface coverage of the material is homogeneous [28]. It can be explained that the rise in the amount of adsorption of methylene blue dye on the surface of bentonite may be because this clay surface contains effective sites that differ in physical and chemical properties, as well as the steric form [29], in addition to having the property of ion exchange (Ion - exchange) with other ionic species [30], as bentonite is one of the highly colloidal clays, in addition to its ability to retain the solution inside the layer due to the high plasticity and colloidal property that gives the characteristic of spreading the materials on the surface of the bentonite [31].

3.5. Langmuir isotherm model

The adsorption data of methylene blue dye on the surface of bentonite clay were processed in the same studied range of temperatures according to Langmuir in Equation 3 [32].

$$C_e/Q_e = \frac{1}{Q_{max} \cdot k_l} + \frac{C_e}{Q_{max}} \qquad \text{(Eq.3)}$$

Qe is the amount of dye adsorbed at equilibrium, and *Ce* is the concentration of the dye absorbed at equilibrium (mg L^{-1}). Both Qu max and kl are Langmuir experimental constants. From drawing the values of (*Ce/Qe*) vs. the concentration at equilibrium (*Ce*), a linear relationship was obtained (Fig.7). From it, we find the values of the Langmuir constants shown in Table 4 as the slope is equal to (*1/Qe*). The intersection is equal to ($1/Qe_{max}$ kl).

In general, it is noted from Table 4 that there is a gradual decrease in the value of kl and the maximum quantity of adsorption (Qe_{max}) with rising temperature and for all studied temperatures. This behavior indicates a decrease in dye adsorption with increasing temperature on the adsorbent surface. On the other hand, when taking the numerical average of the values of the correlation coefficient (R^2) for all the studied temperatures, it is noticed that its compatibility is on the surface of bentonite clay, where the numerical average of the values of the correlation coefficient (R^2) reached (0.998), and this means that the adsorption of methylene blue dye on the surface of bentonite made the Langmuir model more compatible.

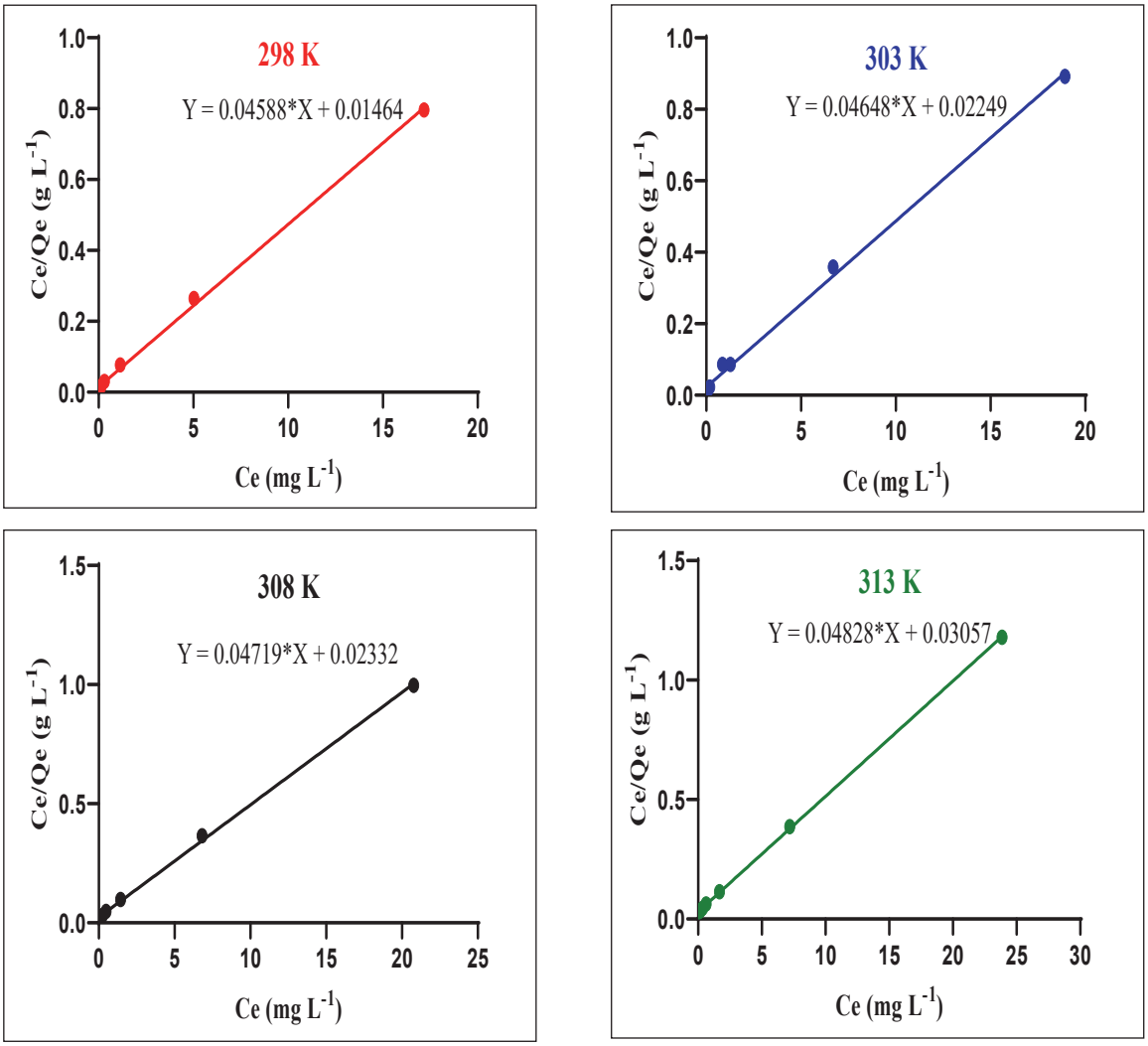

Fig. 7. Plot of *Ce* vis *Ce/Qe* for adsorption of MB dye on the Bentonite clay.

Table 4. Experimental Langmuir constants for adsorption of MB dye on the Bentonite clay

Temperature (K)	Qe max (mg L^{-1})	K_l (Lmg^{-1})	R^2
298	21.79599	3.13388	0.9987
303	21.51463	2.066696	0.9972
308	21.19093	2.023585	0.9992
313	20.71251	1.579326	0.9999

3.6. Frendlish isotherm model

The adsorption data were treated according to the linear of the Frendlish Equation 4 [33].

$$Ln\ Qe = ln\ kf + 1/n\ ln\ Ce \qquad (Eq.4)$$

Since: *Qe*: the quantity of dye adsorbed at equilibrium (mg g^{-1}). *Ce*: concentration of dye adsorbed at equilibrium (mg g^{-1}). Both (n) and (K_f) are experimental Frendlish constants. From drawing lnQe against lnCe, the values of the constant K_f were obtained from the straight-line segment, which expresses the surface adsorption capacity, while the values of the constant n were obtained from the slope of the straight line, which tells the intensity of adsorption. Table 5 shows the values of the Frendlish model's experimental constants and the correlation coefficient (R^2) values for the adsorption of methylene blue dye on the surface of bentonite clay. Figure 8 also shows the Frendlish isotherms for dye adsorption on the clay surface at the same

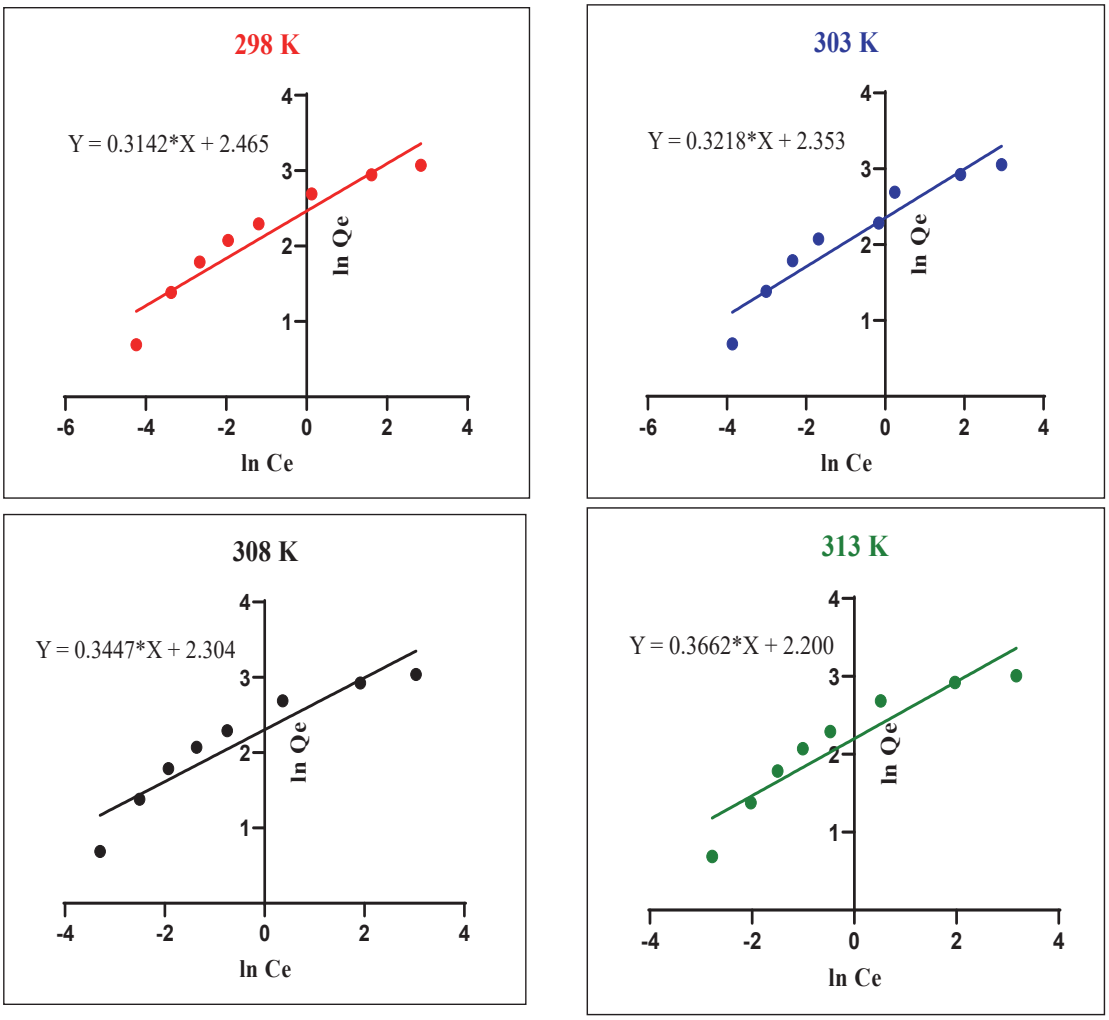

Fig. 8. Plot of ln *Ce* vis ln *Qe* for adsorption of MB dye on the Bentonite clay.

Table 5. Experimental Frendlish constants for adsorption of MB dye on the Bentonite clay

Temperature (K)	k_f (mg L^{-1})	N	R^2
298	11.763	3.182	0.9063
303	10.517	3.107	0.9102
308	10.014	2.901	0.8816
313	9.025	2.730	0.8649

studied temperature range.

It is noted from Table 5 that the values of the K_f constant generally decrease with rising temperature for the adsorption of methylene blue dye on the surface of bentonite clay, and this means that the adsorption process decreases with increasing temperature in general. As for the constant n, a relative decrease in its value is observed with an increase in temperature, and this means that an increase in temperature leads to a reduction in the affinity of the dye to stay in the solvent on the one hand and an increase in the adsorption of the MB on the surface of the bentonite on the other hand [34]. In comparison, the value of the numerical average of the correlation coefficient (R^2) for the bentonite surface according to the Frendlish model was (0.890). As opposed to that, when comparing the values numerical average of the correlation coefficient (R^2) of the Langmuir equation (0.998) and the Frendlish equation, we find that it is more applicable to the Langmuir equation. Thus, this equation is more suitable for describing the adsorption isotherm.

3.7. Adsorption Thermodynamics

The thermodynamics of the adsorption of MB dye on the surface of bentonite clay were calculated. Table 6 shows the computed values for those functions. The adsorption enthalpy (ΔH^O) value was determined from the slope of the linear Vant Hoff (Equation 5) from the Ln k plot against the reciprocal of temperature 1/T [35]. The plot of 1/T vis ln Qe for the adsorption of MB dye on the bentonite clay is shown in Figure 9.

$$ln\ K = -\Delta H^O / RT + Constant \qquad \text{(Eq. 5)}$$

Since: k: thermodynamic equilibrium constant, ΔH°: adsorption enthalpy, : the general gas constant (8.314 J mol^{-1} K^{-1}), *T*: absolute temperature (*k*), constant: Vant Hoff constant.

While the Gibbs free energy (ΔG^o) has been calculated from Equation 6 [36], the value of the change in entropy (ΔS°) was also found through the Gibbs formula for equilibrium as Equation 7 [37].

$$\Delta G^o = -RT\,LnK \qquad \text{(Eq. 6)}$$

$$\Delta G° = \Delta H° - T\Delta S \qquad \text{(Eq. 7)}$$

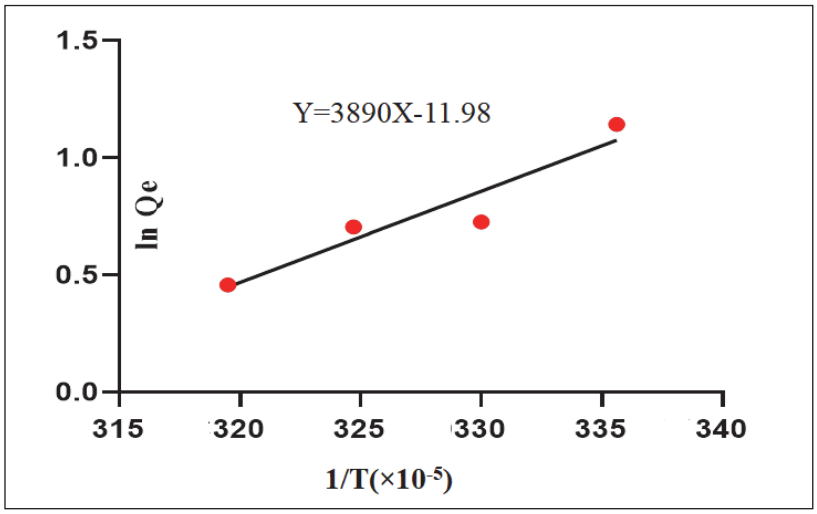

Fig. 9. Plot of 1/T vis ln Qe for adsorption of MB dye on the Bentonite clay.

Table 6. Thermodynamic parameters for the adsorption process

Temperature (k)	ΔH°	ΔG°	ΔS°
298	-32341.5	-2830.06	-99.0315
303	----------	-1828.77	-100.702
308	----------	-1804.97	-99.1444
313	----------	-1189.24	-99.5279

The results in Table 6 show that the values (ΔH°) for the adsorption of methylene blue dye on the surface of bentonite are negative, which means that the adsorption process is an exothermic reaction. The number of adsorbent particles decreases with the increase in temperature because the thickness of the adsorption layer will decrease with the increase in the temperature of the solution; this is because the rise in the temperature of the solution leads to the increase in the kinetic energy for the dye molecules adsorbed on the adsorbent surface, which leads to their separation from the adsorbent surface and their return to the solution [37]. This was confirmed by the kinetic study, where the adsorption capacity decreases with increasing temperature and for all studied concentrations. The experimental outcomes of the negative values of ΔG° for dye adsorption on the bentonite surface and for all temperatures indicate that the adsorption reaction is spontaneous in all its steps. The calculated negative entropy values (ΔS°) also indicate that the dye molecules are more uniform on the surface than in the solution.

4. Conclusion

The findings of this study show how effective Iraqi bentonite clay is at removing Methylene blue (MB) dye from aqueous solutions when used as an adsorbent surface. The optimal conditions for removing MB were 298 K of temperature, 0.2 gm of clay dose, and 45 min of contact time. The Langmuir isotherm (R2 = 0.998), according to the experimental results of adsorption isotherms, was more suitable for the equilibrium data. By analyzing the thermodynamic characteristics, it is possible to determine that the MB adsorption on Iraqi bentonite clay is an exothermic and spontaneous reaction. Also, this investigation revealed that Iraqi bentonite clay was effective at removing the dye MB because of its high surface area. MB dye was removed with an adsorption efficiency of up to 99.39 % at 25°C. This research offers practical adsorption technology that is affordable and effective for treating wastewater using bentonite clay as an adsorbent surface.

5. Acknowledgements

The structural formula of the Physical Chemistry Lab., Scientific Research Center, Alayen University supports this study.

6. References

[1] A.J. Ibrahim, ZnO nanostructure synthesis for the photocatalytic degradation of azo dye methyl orange from aqueous solutions utilizing activated carbon, Anal. Meth. Environ. Chem. J., 5 (2022) 5-19. https://doi.org/10.24200/amecj.v5.i04.200.

[2] A. Debroy, M. Yadav, R. Dhawan, S. Dey, N. George, DNA dyes: toxicity, remediation strategies and alternatives, Folia Microbiol., 67 (2022) 555-571. https://doi.org/10.1007/s12223-022-00963-8.

[3] F. Kooli, S. Rakass, Y. Liu, M. Abboudi, H.O. Hassani, S.M. Ibrahim, F. Wadaani, R. Al-Faze, Eosin removal by Cetyl trimethylammonium-Cloisites: influence of the surfactant solution type and regeneration properties, Mol., 24 (2019) 3015. https://doi.org/10.3390/molecules24163015.

[4] G. A. Ismail, H. Sakai, Review on effect of different type of dyes on advanced

oxidation processes (AOPs) for textile color removal, Chem., 291 (2022) 132906. https://doi.org/10.1016/j.chemosphere.2021.132906.

[5] A. J. Ibrahim, Adsorption behavior of Crystal Violet dye in aqueous solution using Co^{+2} hectorite composite as adsorbent surface, Anal. Meth. Environ. Chem. J., 6 (2023) 5-16. https://doi.org/10.24200/amecj.v6.i01.219.

[6] A.B. Fradj, A. Boubakri, A. Hafiane, S.B. Hamouda, Removal of azoic dyes from aqueous solutions by chitosan enhanced ultrafiltration, Res. Chem., 2 (2020) 100017. https://doi.org/10.1016/j.rechem.2019.100017.

[7] M. E. Ali, M. E. Hoque, S. K. Safdar Hossain, M. C. Biswas, Nanoadsorbents for wastewater treatment: next generation biotechnological solution, Int. J. Environ. Sci. Technol., 17 (2020) 4095-4132. https://doi.org/10.1007/s13762-020-02755-4.

[8] B. Bishayee, R. P. Chatterjee, B. Ruj, S. Chakrabortty, J. Nayak, Strategic management of nitrate pollution from contaminated water using viable adsorbents: An economic assessment-based review with possible policy suggestions, J. Environ. Manag., 303 (2022) 114081. https://doi.org/10.1016/j.jenvman.2021.114081.

[9] E. A. Ashour, M. A. Tony, Eco-friendly removal of hexavalent chromium from aqueous solution using natural clay mineral: activation and modification effects, N. Appl. Sci., 2 (2020) 1-13. https://doi.org/10.1007/s42452-020-03873-x.

[10] D. Dodoo, G. Appiah, G. Acquaah, T. D. Junior, Fixed-bed column study for the remediation of bauxite-liquid residue using acid-activated clays and natural clays, Heliyon, 9 (2023) e14310. https://www.cell.com/heliyon/pdf/S2405-8440(23)01517-7.pdf.

[11] A. Awasthi, P. Jadhao, K. Kumari, Clay nano-adsorbent: structures, applications and mechanism for water treatment, SN. Appl. Sci. 1 (2019) 1076. https://doi.org/10.1007/s42452-019-0858-9.

[12] W. Li, X. M. Liu, Experimental investigation of lithium isotope fractionation during kaolinite adsorption: Implications for chemical weathering, Geochim. Cosmochim. Acta, 284 (2020) 156-172. https://doi.org/10.1016/j.gca.2020.06.025.

[13] I. M. Minisy, N. A. Salahuddin, M. M. Ayad, Adsorption of methylene blue onto chitosan–montmorillonite/polyaniline nanocomposite, App. Clay Sci., 203 (2021) 105993. https://doi.org/10.1016/j.clay.2021.105993.

[14] Y.M. Vargas-Rodríguez, A. Obaya, J.E. García-Petronilo, G.I. Vargas-Rodríguez, A. Gómez-Cortés, G. Tavizón, J.A. Chávez-Carvayar, Adsorption studies of aqueous solutions of methyl green for halloysite nanotubes: Kinetics, isotherms, and thermodynamic parameters, Amer. J. Nanom., 9 (2021) 1-11. http://pubs.sciepub.com/ajn/9/1/1.

[15] J. Matusik, A. Koteja-Kunecka, P. Maziarz, A. Kunecka, Styrene removal by surfactant-modified smectite group minerals: Efficiency and factors affecting adsorption/desorption, Chem. Eng. J., 428 (2022) 130848. https//:doi.org/10.1016/j.cej2021.130848..

[16] U. Ortiz-Ramos, R. Leyva-Ramos, E. Mendoza-Mendoza, A. Aragón-Piña, Removal of tetracycline from aqueous solutions by adsorption on raw Ca-bentonite. Effect of operating conditions and adsorption mechanism, Chem. Eng. J., 432 (2022) 134428. https://doi.org/10.1016/j.cej.2021.134428.

[17] S. Gao, D. Wang, Z. Huang, C. Su, M. Chen, X. Lin, Recyclable NiO/sepiolite as adsorbent to remove organic dye and its regeneration, Sci. Rep., 12 (2022) 2895. https://doi.org/10.1038/s41598-022-06849-6.

[18] A.J. Ibrahim, Ultraviolet-activated sodium

perborate process (UV/SPB) for removing humic acid from water, Anal. Meth. Environ. Chem. J., 5 (2022) 5-18. https://doi.org/10.24200/amecj.v5.i03.191.

[19] J.A. Naser, T.A. Himdan, A.J. Ibraheim, Adsorption kinetic of malachite green dye from aqueous solutions by electrospun nanofiber Mat, Orient. J. Chem., 33 (2017) 3121-3129. http://dx.doi.org/10.13005/ojc/330654.

[20] P. Pourhakkak, M. Taghizadeh, A. Taghizadeh, M. Ghaedi, Adsorbent, Inter. Sci. Tech., 33 (2021) 71-210. https://doi.org/10.1016/B978-0-12-818805-7.00009-6.

[21] M. A. Rehman, T. Jafri, Stabilization of low plastic and high plastic clay using guar gum biopolymer, Int. J. Appl. Ind. Eng., 7 (2020) 329-343. http://dx.doi.org/10.22105/jarie.2020.247859.1195.

[22] I. Chaari, E. Fakhfakh, M. Medhioub, F. Jamoussi, Comparative study on adsorption of cationic and anionic dyes by smectite rich natural clays, J. Mol. Stru., 1179 (2019) 672-677. https://doi.org/10.1016/j.molstruc.2018.11.039.

[23] A. K. Dhar, H. A. Himu, M. Bhattacharjee, M. G. Mostufa, F. Parvin, Insights on applications of bentonite clays for the removal of dyes and heavy metals from wastewater: a review, Environ. Sci. Pollut. Res., 30 (2023) 5440-5474. https://doi.org/10.1007/s11356-022-24277-x

[24] A.N.M.A. Haque, R. Remadevi, O.J. Rojas, X. Wang, M. Naebe, Kinetics and equilibrium adsorption of methylene blue onto cotton gin trash bioadsorbents, Cellulose, 27 (2020) 6485-6504. https://doi.org/10.1007/s10570-020-03238-y.

[25] Y. Zhu, Y. Cui, Y. Peng, R. Dai, H. Chen, Y. Wang, Preparation of CTAB intercalated bentonite for ultrafast adsorption of anionic dyes and mechanism study, Colloids Surf. A., 658(2023) 130705. https://doi.org/10.1016/j.colsurfa.2022.130705.

[26] H. Çiftçi, Removal of methylene blue from water by ultrasound-assisted adsorption using low-cost bentonites, Chem. Phys. Lett., 802 (2022) 139758. https://doi.org/10.1016/j.cplett.2022.139758.

[27] A. Boukhemkhem, A. H. Pizarro, C. B. Molina, Enhancement of the adsorption properties of two natural bentonites by ion exchange: equilibrium, kinetics and thermodynamic study, Clay Mine., 55 (2020) 132-141. https://doi.org/10.1180/clm.2020.19.

[28] J. Serafin, B. Dziejarski, Application of isotherms models and error functions in activated carbon CO2 sorption processes, Micro. Meso. Mat., 354 (2023) 112513. https://doi.org/10.1016/j.micromeso.2023.112513.

[29] P. S. Kumar, G. J. Joshiba, C. C. Femina, P. Varshini, S. Priyadharshini, M. A. Karthick, R. Jothirani, A critical review on recent developments in the low-cost adsorption of dyes from wastewater, Desalin. Water Treat., 172 (2019) 395-416. https://doi.org/10.5004/dwt.2019.24613.

[30] S. B. Denison, P. D. Da Silva, C. P. Koester, P. J. Alvarez, K. Zygourakis, Clays play a catalytic role in pyrolytic treatment of crude-oil contaminated soils that is enhanced by ion-exchanged transition metals, J. Hazard. Mater., 437 (2022) 129295. https://doi.org/10.1016/j.jhazmat.2022.129295.

[31] Z. Tahr, A. Mohammed, J. A. Ali, Surrogate models to predict initial shear stress of clay bentonite drilling fluids incorporated with polymer under various temperature conditions, Arab J. Geosci., 15 (2022) 1449. https://doi.org/10.1007/s12517-022-10720-3.

[32] X. Guo, J. Wang, Comparison of linearization methods for modeling the Langmuir adsorption isotherm, J. Mol. Liq., 296 (2019) 111850. https://doi.org/10.1016/j.molliq.2019.111850.

[33] E. R. Orhue, A. Emomu, Freundlich, Langmuir and Temkin isotherm studies of silicon sorption on soils derived from

three parent materials in Edo State, Agro-Sci., 21 (2022) 1-12. https://doi.org/10.4314/as.v21i3.1.

[34] E. Y. Soh, S. S. Lim, K. W. Chew, X. W. Phuang, V. M. Ho, K. Y. Chu, R. R. Wong, L. Y. Lee, T. J. Tiong, Valorization of spent brewery yeast biosorbent with sonication-assisted adsorption for dye removal in wastewater treatment, Environ. Res., 204 (2022) 112385. https://doi.org/10.1016/j.envres.2021.112385.

[35] E. C. Lima, A. A. Gomes, H. N. Tran, Comparison of the nonlinear and linear forms of the van't Hoff equation for calculation of adsorption thermodynamic parameters (Δ S° and Δ H°), J. Mol. Liq., 311 (2020) 113315. https://doi.org/10.1016/j.molliq.2020.113315.

[36] L. Q. Chen, Chemical potential and Gibbs free energy, MRS. Bulletin., 44 (2019) 520-523. https://doi.org/10.1557/mrs.2019.162.

[37] I. Tahira, Z. Aslam, A. Abbas, M. Monim-ul-Mehboob, S. Ali, A. Asghar, Adsorptive removal of acidic dye onto grafted chitosan: a plausible grafting and adsorption mechanism, Int. J. Biol. Macromol., 136 (2019) 1209-1218. https://doi.org/10.1016/j.ijbiomac.2019.06.173.

Anal. Methods Environ. Chem. J. 6 (3) (2023) 19-35

AMECJ

Research Article, Issue 3
Analytical Methods in Environmental Chemistry Journal
Journal home page: www.amecj.com/ir

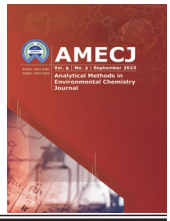

Determination of 2,4-dinitrophenylhydrazine using carbon paste modified with nanoparticles by cyclic voltammetry, high-performance liquid chromatography and spectrophotometry methods

Khalil Ibrahim Alabid [a,*] **and Hajar Naser Nasser** [a]

[a]*Analytical Chemistry - Department of Chemistry - Faculty of Science - Tishreen University – Syria*

ARTICLE INFO:

Received 12 May 2023
Revised form 25 Jul 2023
Accepted 17 Aug 2023
Available online 28 Sep 2023

Keywords:
2,4-Dinitrophenylhydrazine,
Graphene-carbon nitride nanoparticles,
Nitrogen carbon quantum dots,
Electrochemical,
High-performance liquid chromatography

ABSTRACT

The research deals with the manufacture of an electrode using modified carbon paste to determine 2,4-dinitrophenylhydrazine (2,4-DNPHZ), The modified carbon paste electrode (NiO-NCQD/g-C_3N_4/MCPE). The results show the presence of oxidation and reduction peaks, and it is subject to a quasi-reversible system; the best value of pH is (1) using sulfuric acid with a concentration of (0.1M), and scan rate is 100 mv sec^{-1}, it was linearity range of (1-1000) µM for oxidation, and (100-1000) µM for reduction, with correlation coefficient (R^2=*0.9717*) and (R^2=*0.9914*) for each of them, respectively. The proposed electrochemical method was compared with two methods they are spectrophotometry at a wavelength 360 (nm) and high-performance liquid chromatography (HPLC) at wavelengths (340 and 250) nm. It turned out that the electrochemical method (NiO-NCQD/g-C_3N_4/MCPE) was superior to the spectrophotometry method in terms of the detection limit. It turns out that there is no significant difference between (HPLC) and (NiO-NCQD/g-C_3N_4/MCPE) in terms of accuracy. The proposed electrochemical method is a new analytical method characterized by accuracy, repeatability, and reliability.

1. Introduction

The material of 2,4-Dinitrophenylhydrazine (2,4-DNPHZ) is a water pollutaFnt compound active in explosives. It belongs to the nitro-aromatic (NAC) and is a hydrazine derivative [1-3]. 2,4-Dinitrophenylhydrazine has weak decomposition in water [4] but is soluble in organic solvents such as (Methanol, Acetonitrile, Tetrahydrofuran THF… etc.) [4]. It forms a yellow color solution, and long-term exposure to 2,4-DNPHZ has many adverse health effects as a highly toxic compound [5]. It is used in industry as a detection reaction of ketones and aldehydes. It seeps through wastewater from industrial effluents and causes water pollution. Due to Figure 1, 2,4-Dinitrophenyl hydrazine is oxidized to 2,4-Dinitrophenyldizine material.

It is used in many applications, such as Alzheimer's detection [6]. It is also used as a surface enhancer for an adsorbent material such as magnetite or aluminum oxide to remove many heavy metal ions that are harmful to the environment, including Arsenic (As) and vanadium (V) [7-10]. It is used to determine the protein carbonyl [11] and in synthesizing Thiazolidin-4 as one of the biologically active drugs in treating malaria [12].

*Corresponding Author: Khalil Ibrahim Alabid
Email: khalilibrahimalabid@gmail.com
https://doi.org/10.24200/amecj.v6.i03.245

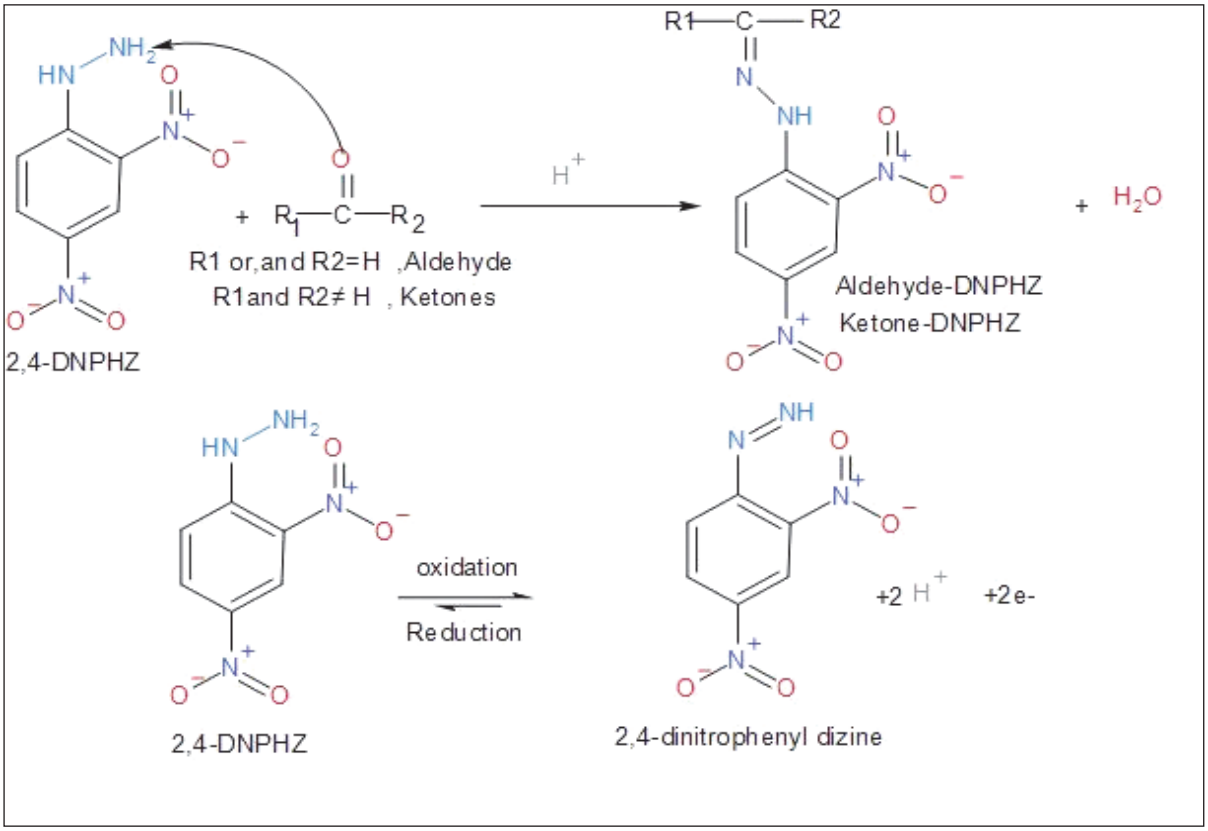

Fig. 1. Chemical equation for the reaction of 2,4-DNPHZ with aldehydes and ketones, and oxidation 2,4-Dinitrophenyl hydrazine to 2,4-Dinitrophenyldizine.

Through the reference study, it was found that there is a scarcity of direct methods for analyzing 2,4-dinitrophenylhydrazine; most of the reference studies used this compound as a reagent, where it was used as a selective reagent or as a derivatization reagent for the determination of aldehydes and ketones in spectroscopic, chromatographic, and electrochemical analytical methods. In high-performance liquid chromatography, it is also used in the measurement of free and bound malondialdehyde in plasma [13], determination of linear aliphatic aldehydes in heavy metal-containing waters [14], determination of malondialdehyde in normal human urine [15]. It is also used in analyzing carbonyl (aldehyde and ketones) in food, drug, and blood serum as a reagent of pre-column derivative in the HPLC technique [16]. It is used in the analysis of amino acids [17], aldehydes in air [18], total carbonyl in meat [19], and aldehydes in food samples [20]. In spectrophotometry, it is also used as a reagent in the analysis of many drugs using spectrophotometry [21-24], such as tetracycline hydrochloride [25], catechol, resorcinol [26], and nateglinide as a drug for the treatment of diabetes [27]. Interaction of haloperidol and 2,4-Dinitrophenylhydrazine used for the quantification in drug formulations [28], spectroscopic, cytotoxicity and molecular docking studies on the interaction between 2,4-dinitrophenylhydrazine derived Schiff bases with bovine serum albumin [29] at a wavelength near 360 nm [30]. In the electrochemical method, 2,4-dinitrophenylhydrazine was used in electrochemical methods such as Indirect determination of dopamine and paracetamol [31]. 2,4-dinitrophenylhydrazine and its derivatives can be removed from aqueous media using multi-walled carbon nanotubes (MWCNTs) [32]. Carbon nitride graphene (G-C_3N_4) is used in many applications, including removing and dissolving many organic pollutants [33-36]. Carbon paste electrodes (CPE) are important for chemically inert electrode

surface renewability, low ohmic resistance, easy fabricating, environmentally friendly, and low cost. However, its stability, kinetics, and selectivity are weak. To solve this problem, surface modification (MCPE) is resorted to by modifiers [37]. Cyclic voltammetry analysis is one of the important analytical methods through which the quantitative and qualitative analysis of the studied material can be done. In addition to the possibility of studying the behavior of the studied material, such as diffusion coefficient (*D*), charge transfer coefficient (α.nα), the mass transport (m_{trans}), constant (K^0), Gibbs free energy (*ΔG*), also, the highest occupied molecular orbital (*HOMO*), lowest unoccupied molecular orbital (*LUMO*), and others were used [37-38]. In previous studies, 2,4-Dinitrophenylhydrazine was used as a reagent in spectroscopic methods and as a derivation material for aldehydes and ketones in chromatographic analysis; this compound is one of the organic compounds harmful to the environment and has toxicity to many organisms. So, this research is also one of the important electrochemical analytical methods. It is an easy and simple method that can be applied in environmental monitoring and fields concerned with this compound. This research is one of the rare studies concerned with determining a 2,4-dinitrophenylhydrazine pollutant by an electrochemical method.

2. Experimental

2.1. Instrument and Reagents

SHIMADZU SPP-M20A high-performance liquid chromatography HPLC device connected to a Diode Array Detector, Chromatographic column C18, with dimensions of of 25cm×0.46cm×5µm, pH metric device, a device voltammetry by Metrohm made in Switzerland, model 797VA. The materials used are characterized by high purity, namely 2,4-Dinitrophenylhydrazine ($(O_2N)2C_6H_3NHNH_2$; CAS N.: 119-26-6) produced by Sigma, Germany. The monosodium phosphate (α-Naphthyl Acid Phosphate, Monosodium Salt; CAS N.: 81012-89-7), methanol (99.8%; CAS N.: Number: 67-56-1), concentrated sulfuric acid (95.0-98.0%; CAS N.: 7664-93-9; E.C. N.: 231-639-5), boric acid (CAS Number: 10043-35-3), phosphorous acid (CAS N.: 13598-36-2; M.W.: 82.00), sodium hydroxide (CAS N.: 1310-73-2; M.W.: 40.00), glassware of various sizes, boiled and cooled double distilled water (DW, Sigma, Germany) were used..

2.2. Preparation of Reagents and solutions

The 2,4-Dinitrophenylhydrazine standard solution was prepared. A group of solutions was prepared for the analytical methods.

2.2.1. Standard solution for Cyclic voltammetry (CV):

0.0792g of 2,4-DNPHZ powder is taken and transferred to a volumetric flask of 100 mL capacity to which is added an to get a water: ethanol solution 25:75 V/V solution of concentration 4mM.

2.2.2. Standard solution for the spectrophotometry method:

0.0396 g of 2,4DNPHZ powder is taken and transferred to a 100 mL of volumetric flask containing 24.823 mL double-distilled water, then 0.277 mL concentrated sulfuric acid and 75 mL ethanol are added, so its concentration is 396.0 mg L^{-1}, then the standard series (5,10,15, 20) mg L^{-1} is prepared from it which is stretching the chain with 0.1M sulfur acid.

2.2.3.Standard solution for HPLC:

0.0301g of 2,4DNPHZ powder is taken and transferred to a 100 mL volumetric flask and dissolved using a solution of 20% sulfuric acid; its concentration is 301 mg L^{-1}. The solution is left to cool down, and then the standard series (0.5-0.1; 1-5) mg L^{-1} is prepared in 20% sulfuric acid, filtered by a micro-membrane filter (0.45 µm) and then measured using high-performance liquid chromatography (HPLC). A temperature of 30°C with a flow rate of 1.0 mL per 1 min was used.

2.3. Procedure and preparation of NiO-NCQD/g-C_3N_4 adsorbent

An electrode was made (in the laboratory) from a glass tube open at both ends, then connected

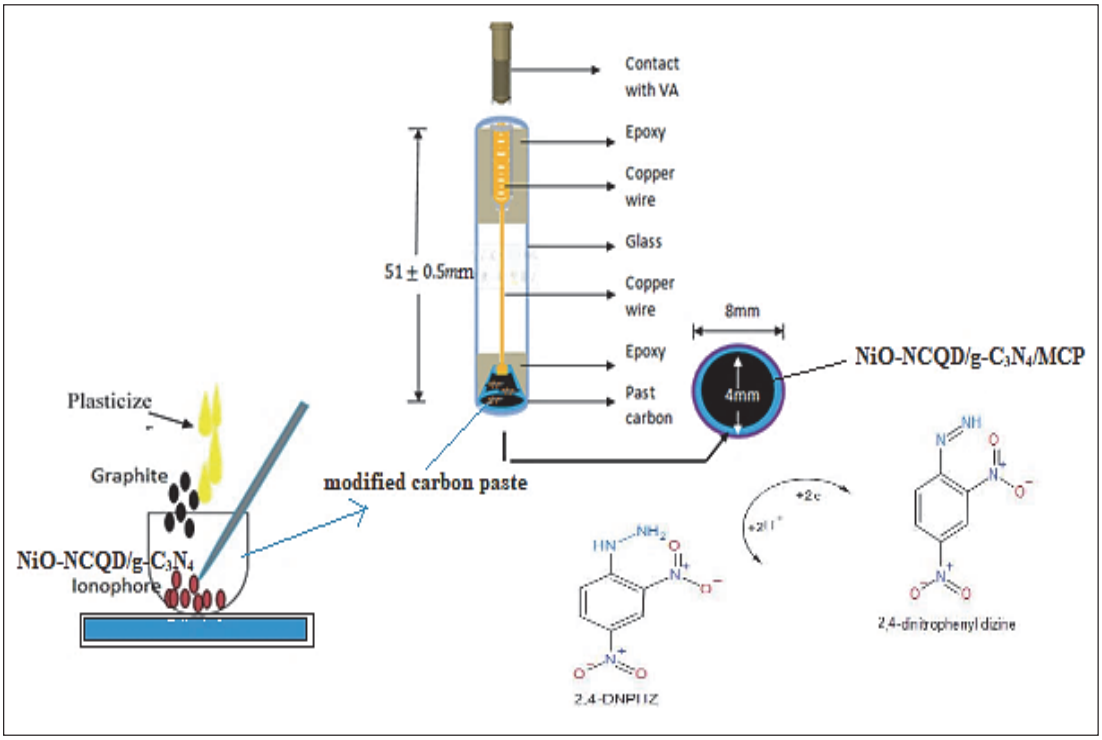

Fig. 2. Procedure based on components of the fabrication of a NiO-NCQD/g-C3N4/MCPE

by a copper wire and a support material. Then, a modified carbon paste was prepared and placed at the lower end of the electrode. Modified carbon paste using NiO-NCQD nano-composite (mix of NiO Nanoparticles (20nm) are added nitrogen quantum carbon dot as nanoadsorbent to get NiO-NCQD nanocomposite), graphene–nitride carbon g-C_3N_4, graphite and paraffin oil, for a total weight from modified carbon paste 0.5g, Symbolizes the factory electrode (NiO-NCQD/g-C_3N_4/MCPE), as in Figure 2. Nickel oxide nanoparticles studded with nitrogen quantum carbon dots were synthesized and characterized in previous work .[39] The 2,4-dinitrophenylhydrazine was determined using NiO-NCQD/g-C_3N_4/MCPE by cyclic voltammetry. Also, after sample preparation, 2,4-dinitrophenylhydrazine was measured by high performance liquid chromatography and spectrophotometry methods.

2.4. Preparation of acid and buffer solutions

2.4.1. Preparation of sulfuric acid solution:

The sulfuric acid solution is prepared at a concentration of 0.1M to get pH 1.

2.4.2.Preparation of monosodium phosphate buffer with H_2SO_4 solution:

A phosphate buffer was prepared from NaH_2PO_4 at a concentration of 0.1M, modified by a solution of H_2SO_4 (0.2 M) to get pH 1.

2.4.3.Preparation Britton–Robinson Buffer solution with H_2SO_4 solution:

Britton–Robinson Buffer solution (BRB) containing H_3PO_4 with a concentration of 0.04M, acetic acid CH_3COOH at a concentration of 0.04M and boron acid H_3BO_3 with a concentration of 0.04 M then modified with a solution H_2SO_4 with a concentration of 0.1M to get pH (1).

2.4.4.Preparation of monosodium phosphate buffer with H_3PO_4 solution:

A phosphate buffer was prepared from NaH_2PO_4 at a concentration of 0.1M and modified by a solution of H_3PO_4 (0.48M) to get pH 1.

2.4.5. Preparation of phosphorous acid solution:

Phosphorous acid solution is prepared at a concentration of 0.48M to get pH 1.

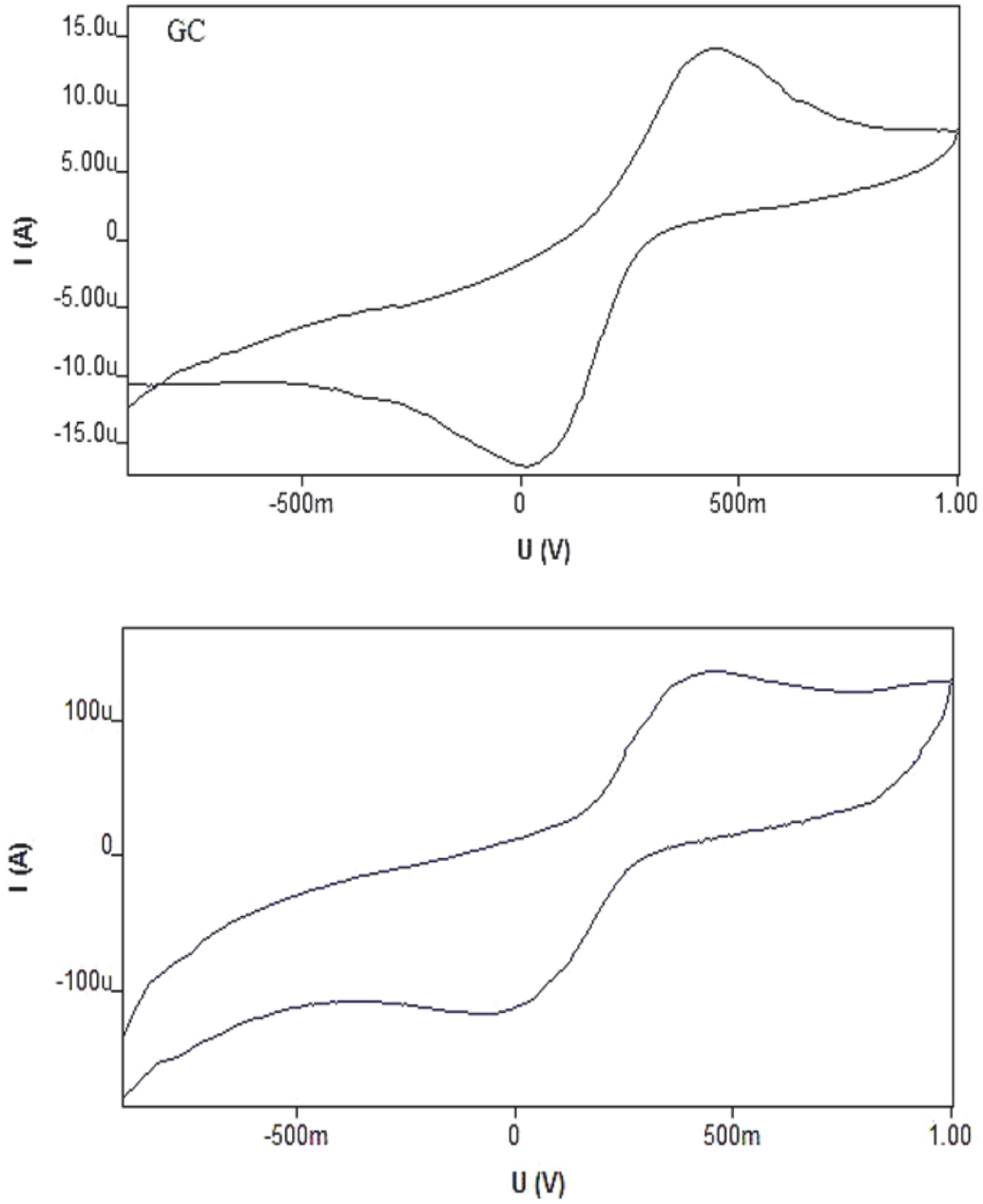

Fig. 3. Oxidation and reduction of ferrous ions using a 5mM electrode test solution of K4 [Fe (CN)$_6$].3H$_2$O in the presence of a 0.1M KCl on GC and (NiO-NCQD/g-C$_3$N$_4$/MCPE)

3. Results and Discussion

3.1. Ensure electrode manufacturing

The ferrous ions were oxidized using the prepared electrode (MCPE) and the glassy carbon electrode (GC), as shown in Figure 3. This electrode can be used in oxidation and reduction by comparing the curves. Also, electrochemistry based on carbon glassy electrodes was used for studying hydrazine and aldehydes [40].

3.2. Effect of the electrochemical percentage of the active material

The effect of the percentage of the active material on the peak current was studied in determining 2,4-DNPHZ, as in Figure 4. It was found that the best of them is 12% nickel oxide doped with quantum dots (NiO-NCQD) with 12% of carbon nitride sheets (C$_3$N$_4$), 38% of graphite powder (GP), and 38% of paraffin oil, as in Figure 4.

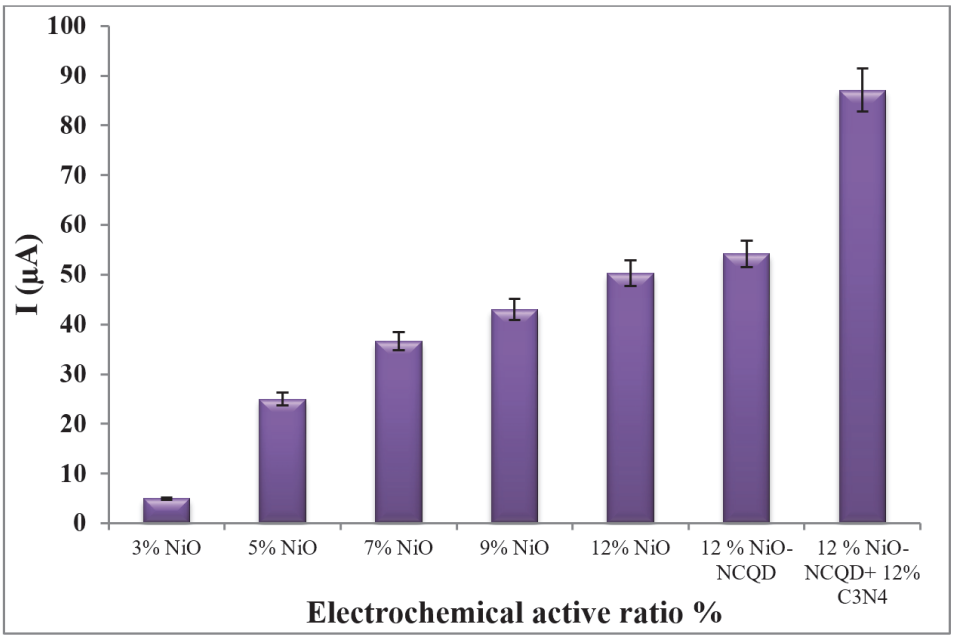

Fig. 4. Effect of the percentage of electrochemical active on the peak current for 2,4-DNPHZ

3.3. The Effect of pH

The Effect of pH was studied from pH 1 to 8 on peak current for 2,4-DNPHZ, shown in Figures 5a and 5b. Due to the Figure, the best recovery was obtained at pH 1.0 (Because of the appearance of an oxidation peak next to OX≈0.5V and the appearance of a return peak next to R≈-0.48V). The peak is clearer at pH =1, as for the rest of the pH (8-2), the height of the peak is not clear despite the increase in $I_{(P)}$ (µA) of the current. It was also observed in the range pH (8-2), where there is only an oxidation peak (ox), but there is no reduction peak (Red). Notice the appearance of an oxidation peak next to Eox≈0.5V and a reduction peak next to Ered≈-0.48V. The oxidation and reduction system is quasi-reversible because ΔE=0.98V is greater than 0.059.2, and $I_{ox}/I_{red} < 1$. Moreover, it is also noticed that the oxidation and reduction peak potential increases with decreasing the pH value, as in Figures 5a and 5b.

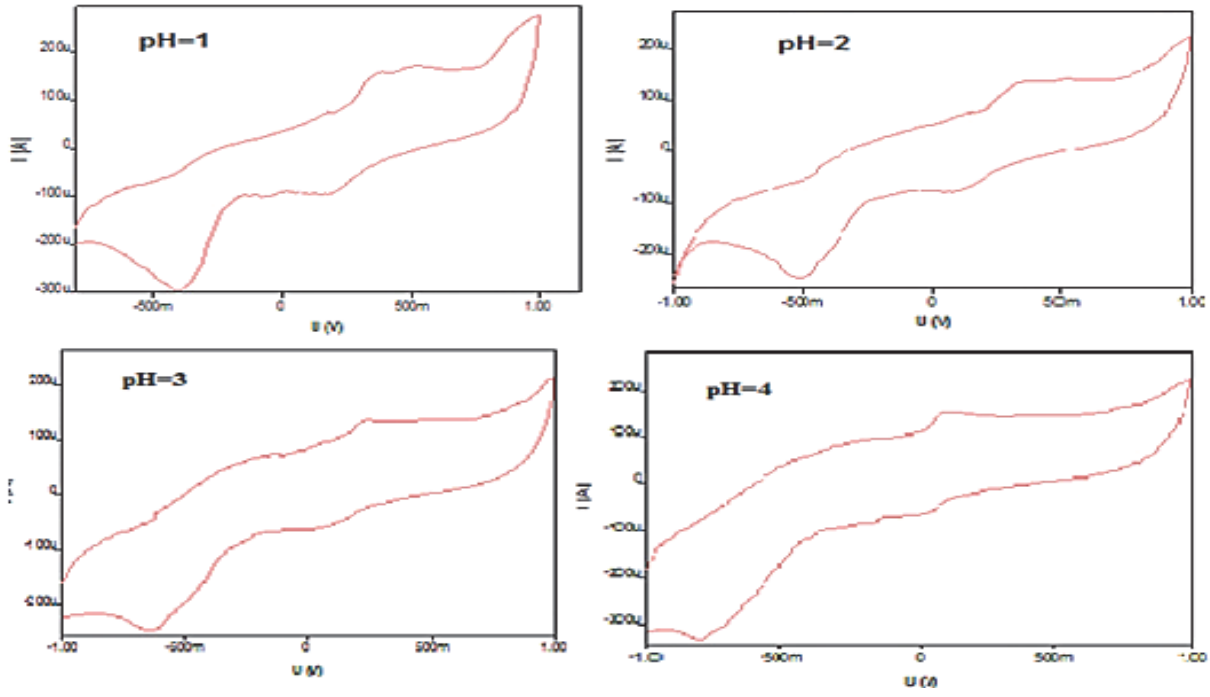

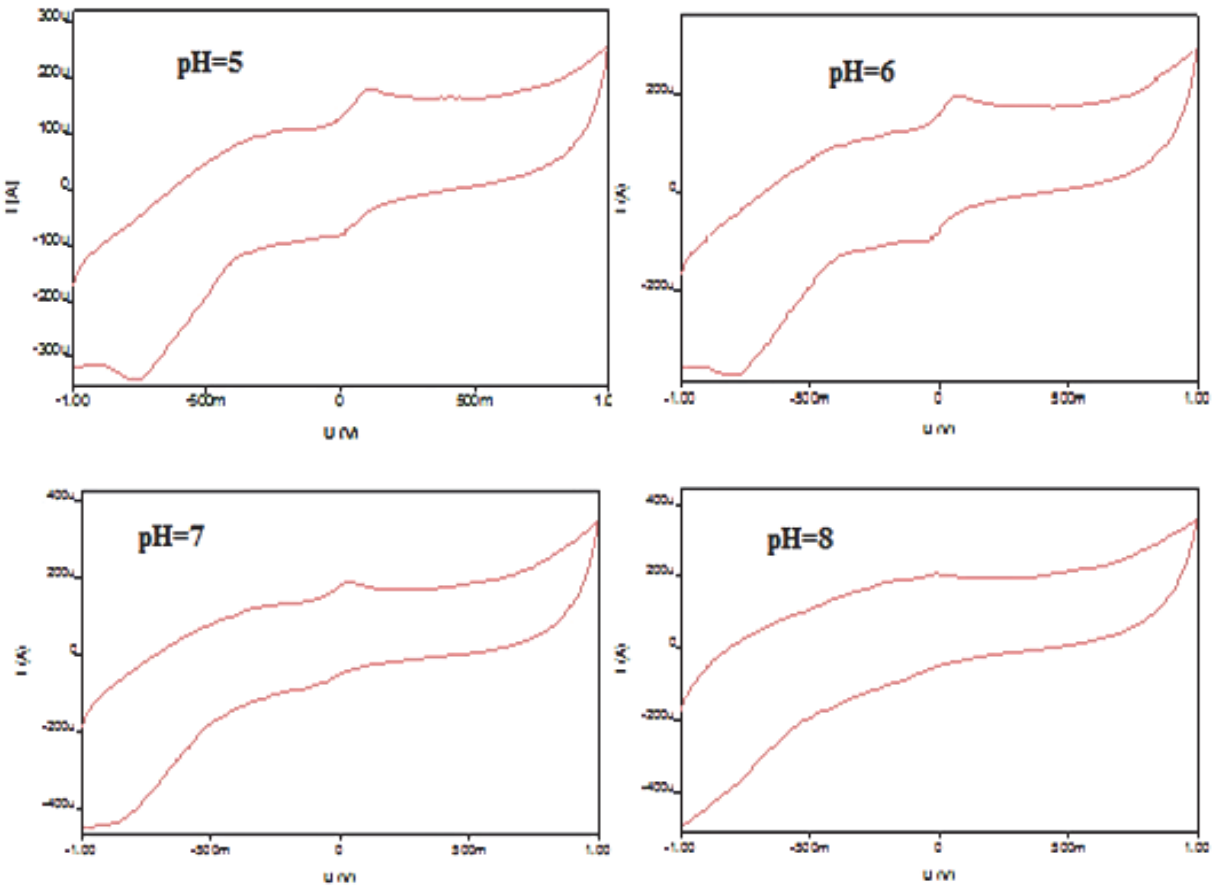

Fig. 5a. Effect of the pH from (1-8) on the peak of oxidation and reduction by (NiO-NCQD/g-C_3N_4/MCPE) for 2,4-DNPHZ

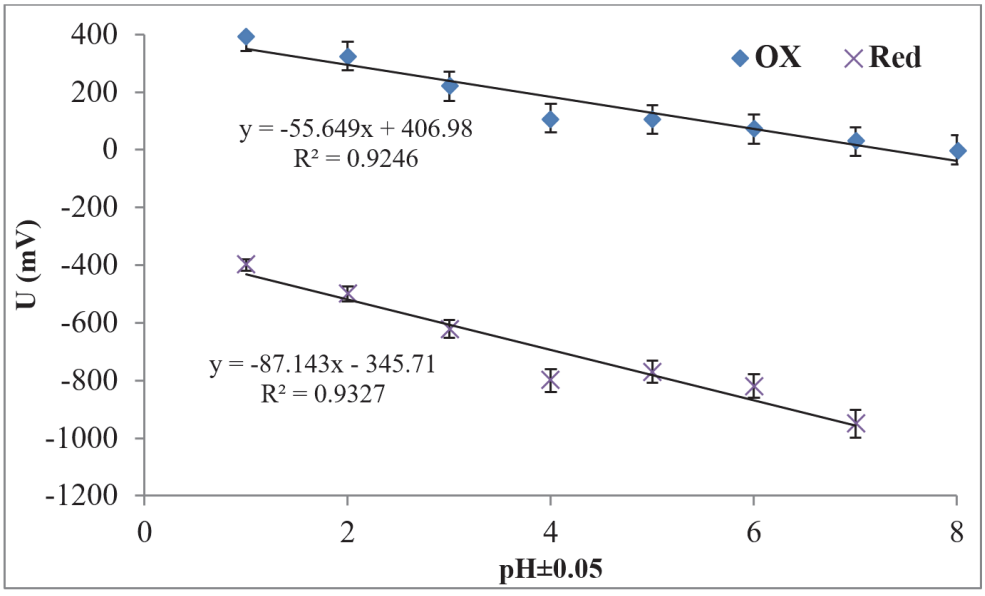

Fig. 5b. Effect of the pH from (1-8) on the peak of oxidation and reduction and effect of pH value on the peak potential U (mV) by (NiO-NCQD/g-C_3N_4/MCPE) for 2,4-DNPHZ

3.4. Effect of the type of acid

Several buffer and acid solutions were prepared at pH 1: sulfuric acid solution, monosodium phosphate with sulfuric acid, Britton–Robinson Buffer with sulfuric acid, monosodium phosphate with phosphorous acid, and phosphorous acid solution as in Figure 6. Due to Figure 6, sulfuric acid with a concentration of 0.1M was the best acid for determining 2,4-dinitrophenylhydrazine (2,4-DNPHZ) by (NiO-NCQD/g-C_3N_4/MCPE) at pH=1.

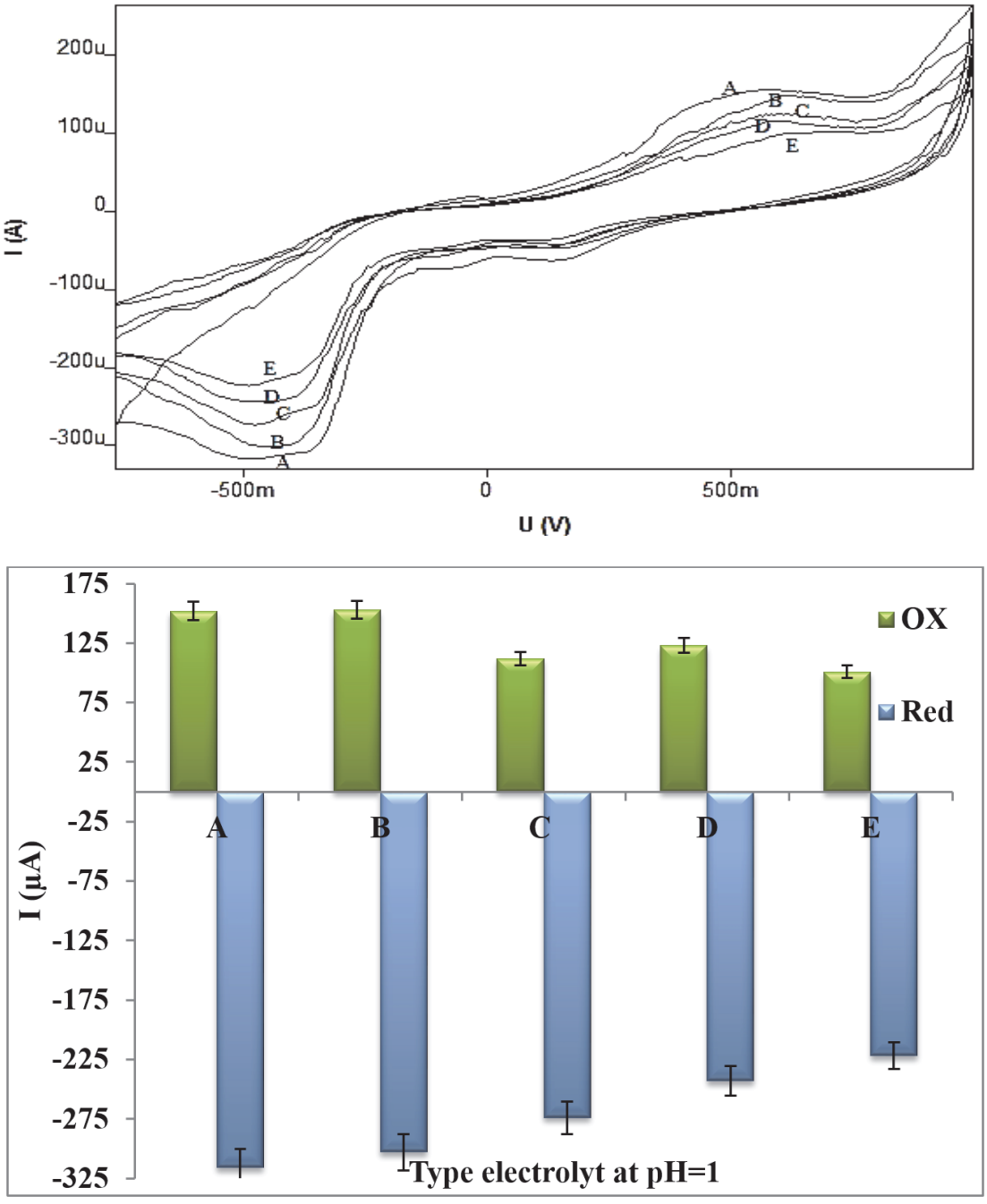

Fig. 6. Effect of the type of acid Effect on the I (µA) and Potential U(V) for both oxidation and redaction of 2,4DNPHZ effect of the kind of acid effect of on the I (µA) for both oxidation and redaction of 2,4DNPHZ A) H_2SO_4 (0.1M) pH=1 B) NaH_2PO_4 (0.1M) modified by H_2SO_4 (0.1M) until pH=1 C) BRB (0.04M for each) modified by H_2SO_4 (0.1M) until pH=1 D) NaH_2PO_4 (0.1M) modified by H_3PO_4 (0.48M) to get pH=1 E) H_3PO_4 (0.48M) pH=1

3.5. The effect of scan rate

The scan rate was studied within the range (10, 30, 50, 70, 100) mv sec $^{-1}$ on the peak current $I_{(P)}$ shown in Figure 7A. It also studied the relationship of the scan rate multiplied by the peak potential in terms of the peak current, as in Figures 7B and 7C. Due to the results, the best scan rate is 100 mv.sec^{-1}. It was found that the relationship is linear between each of the oxidation and reduction peaks with the peak current $I_{(P)}$.

3.6. Analytical Detection Limit

A standard series of 2.4-DNPHZ was prepared within the range (1, 25, 50, 75, 100, 250, 500, 750, 1000) µM as in Figures 7D-7F; the previous curves were drawn in terms of the concentration of 2,4-DNPHZ and the peak current strength for both oxidation and reduction as in Figure 7.

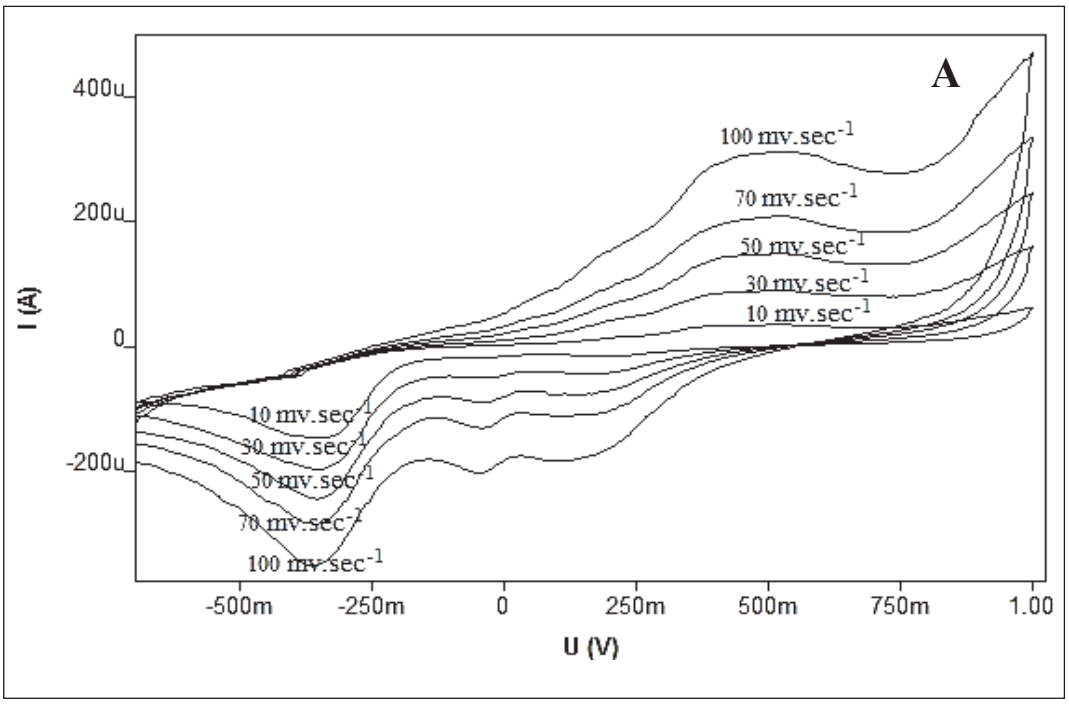

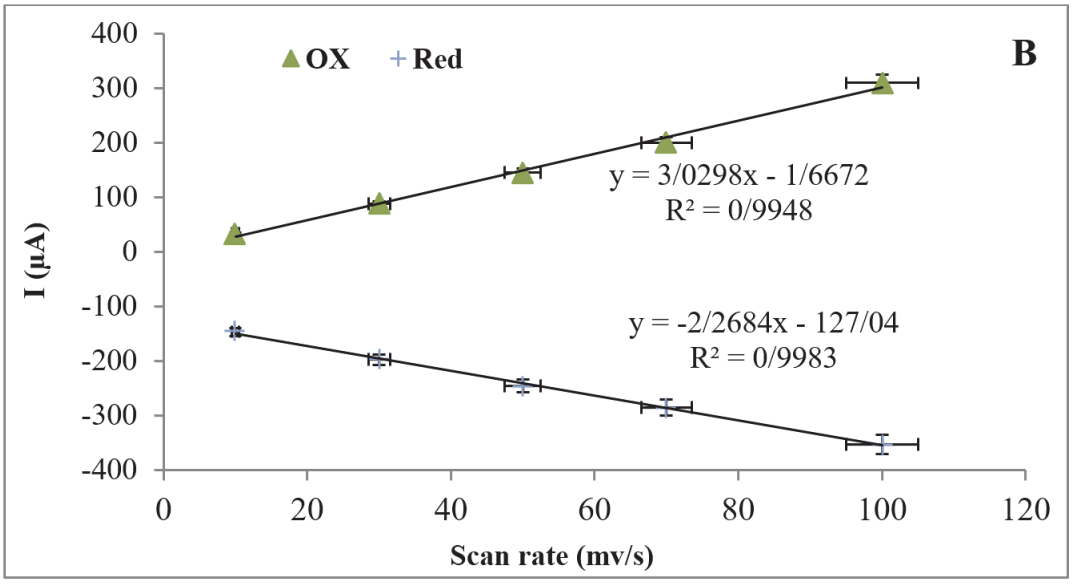

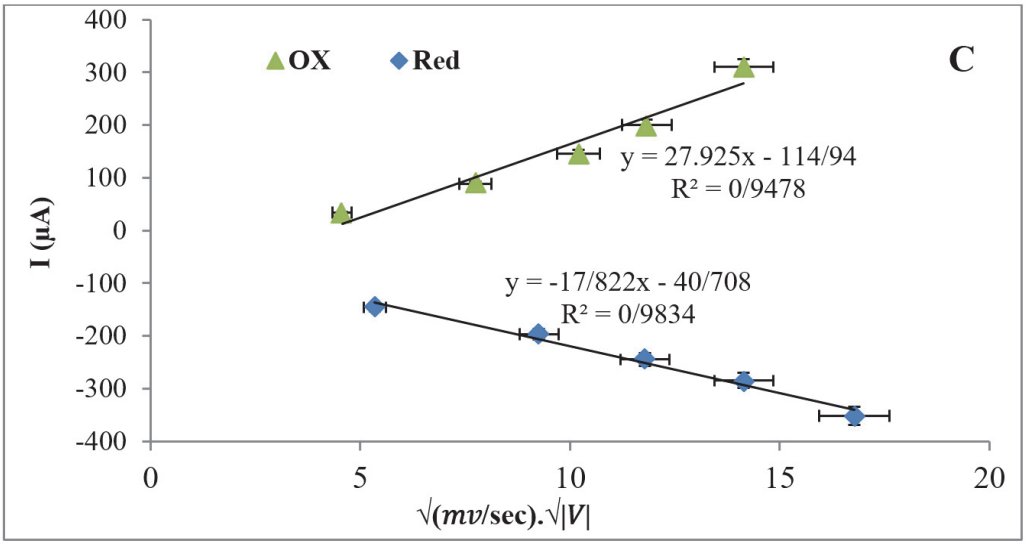
C
OX
Red
y = 27.925x - 114/94
R² = 0/9478
y = -17/822x - 40/708
R² = 0/9834
I (µA)
√(mv/sec).√|V|
400
300
200
100
0
-100
-200
-300
-400
0
5
10
15
20

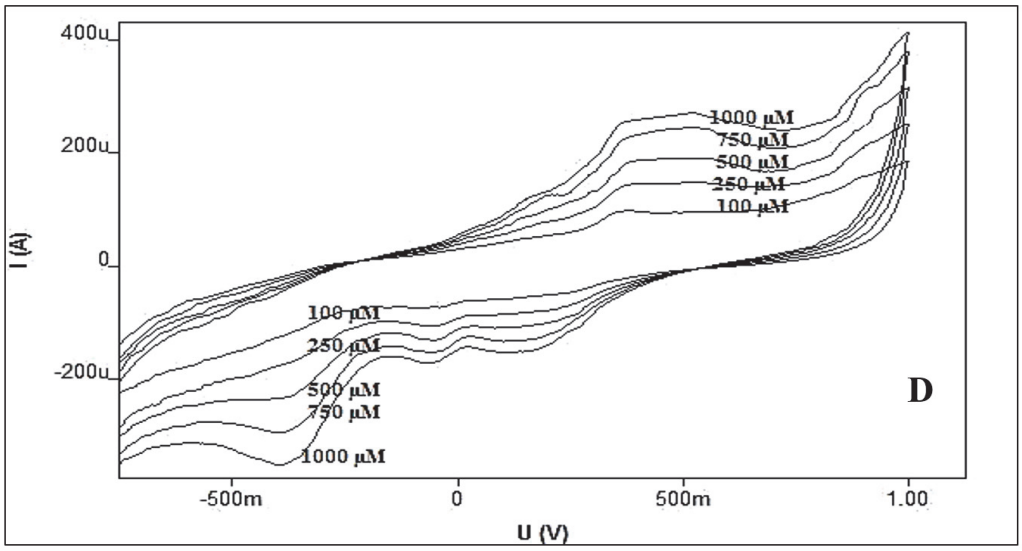
D
1000 µM
750 µM
500 µM
250 µM
100 µM
100 µM
250 µM
500 µM
750 µM
1000 µM
I (A)
U (V)
400u
200u
0
-200u
-500m
0
500m
1.00

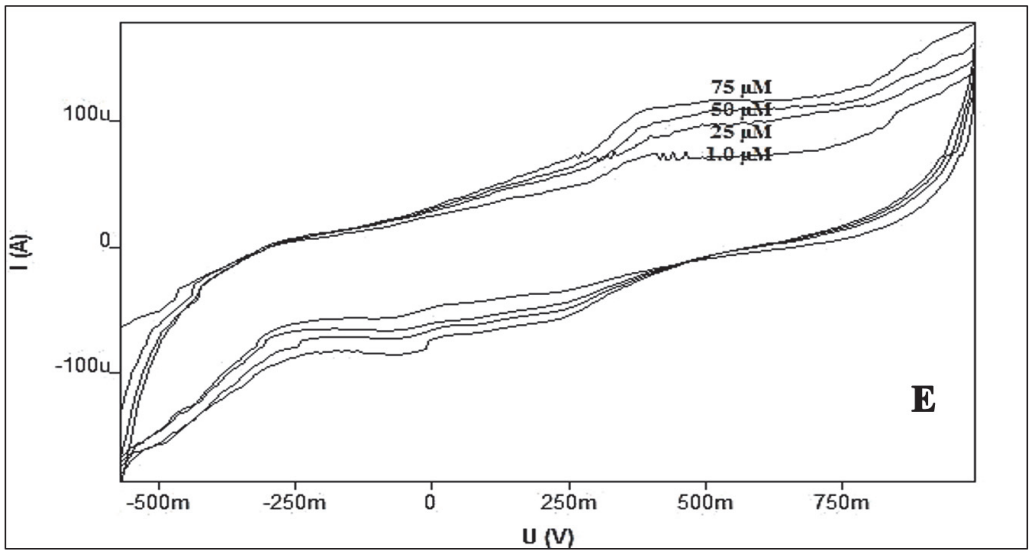
E
75 µM
50 µM
25 µM
1.0 µM
I (A)
U (V)
100u
0
-100u
-500m
-250m
0
250m
500m
750m

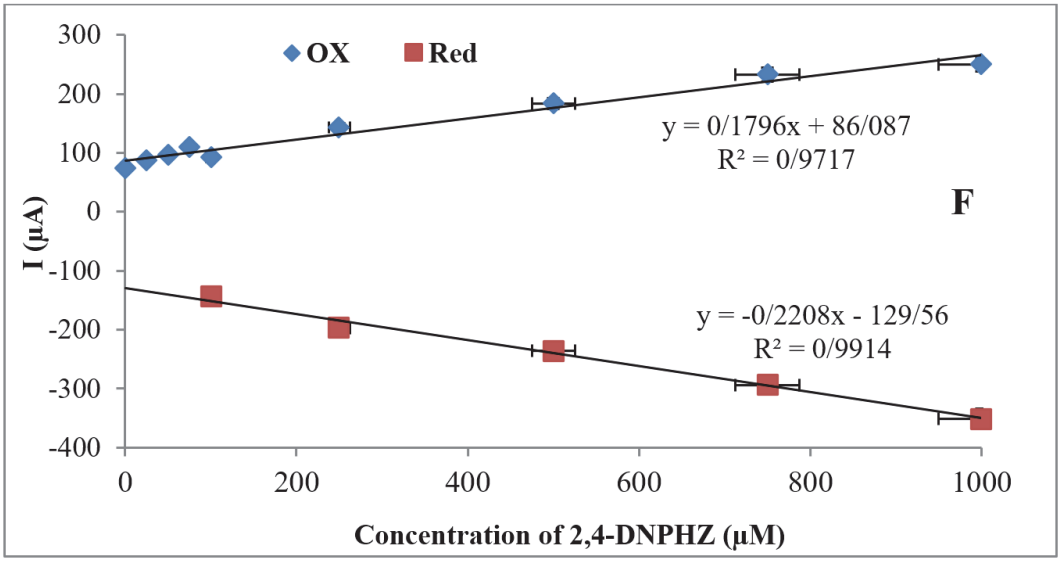

Fig. 7. Curve the oxidation-reduction peak of 2,4-DNPHZ

A) Effect of Scan rate on the peak current
B) Scan rate (mv/s) vs I(µA)
C) root effect of vs I(µA)
D) effect of concentration on peak current (100 -250 - 500 –750- 1000)µM
E) effect of concentration on peak current (1-25-50-75) µM
F) Curve concentration vs I (µA)

It was shown from the previous Figures that the field of linearity upon 2.4-DNPHZ lies within the range of (1-1000) µM for oxidation and (100-1000) µM for reduction with an equation of I_{OX}=0.1796$C_{2,4\text{-}DNPHZ}$ + 86.087 for oxidation and I_{Red}=-0.2208$C_{2,4\text{-}DNPHZ}$ - 129.56 for Redaction, with correlation coefficient R^2=0.9717 and R^2=0.9914 for each of them, respectively. Statistical treatments were calculated as Tabe 1. Concentrations are calculated from a mathematical relationship (Randles-Sevcik) of Equation 1.

3.7. Determine for 2,4-DNPHZ using spectrophotometry and HPLC

The 2,4-DNPHZ is analyzed based on spectrophotometry in Figures 8A and 8B. It was shown by spectral scanning that λmax= 360nm, a standard series of 2,4-DNPHZ was prepared. The absorbance was studied by concentration dependency, as in Figures (8A and 8B), that its equation is C_{ppm}=26.1491*A+0.2686, the minimum concentration that can be analyzed by UV-Vis spectrometry is 5 mg L^{-1}, so it was examined by chromatographic (HPLC) methods as well, in proportion to the detection limit of the proposed method. When determining this compound using high-performance liquid chromatography (HPLC), it was found that the retention time Rt≈1.9 min. Through the largest possible area in terms of wavelength, it was found that the best two wavelengths are 340nm and 250nm as in Figure 8C-8E. A standard series of 2,4DNDH is analyzed by HPLC within the range (5, 1, 0.5, 0.1) mg L^{-1}, as shown in Figure 8F. Statistical treatments were calculated for HPLC, where the number of measurements is three (n=3), the average taken Concentration $\bar{x}$ = 1.262626 µM (0.25g L^{-1}). The electrochemical method (NiO-NCQD/g-C3N4/

$$i_p = \mp 0.436 n F A_{real} C \left(\frac{nFvD}{RT}\right)^{\frac{1}{2}} \ldots\ldots\ldots\ldots\ldots\ldots quasi - reversible \qquad (Eq.1)$$

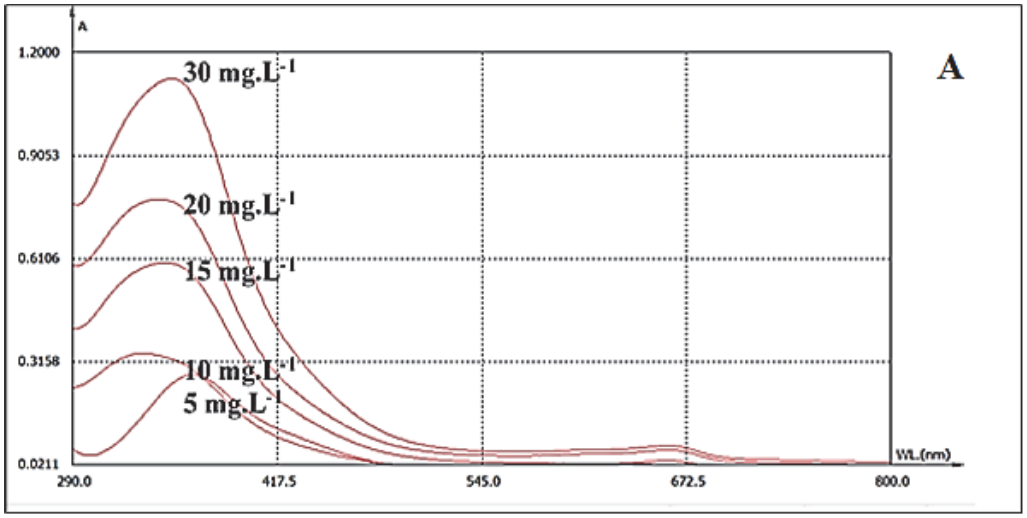
A
1.2000
0.9053
0.6106
0.3158
0.0211
30 mg.L-1
20 mg.L-1
15 mg.L-1
10 mg.L-1
5 mg.L-1
WL.(nm)
290.0
417.5
545.0
672.5
800.0
A

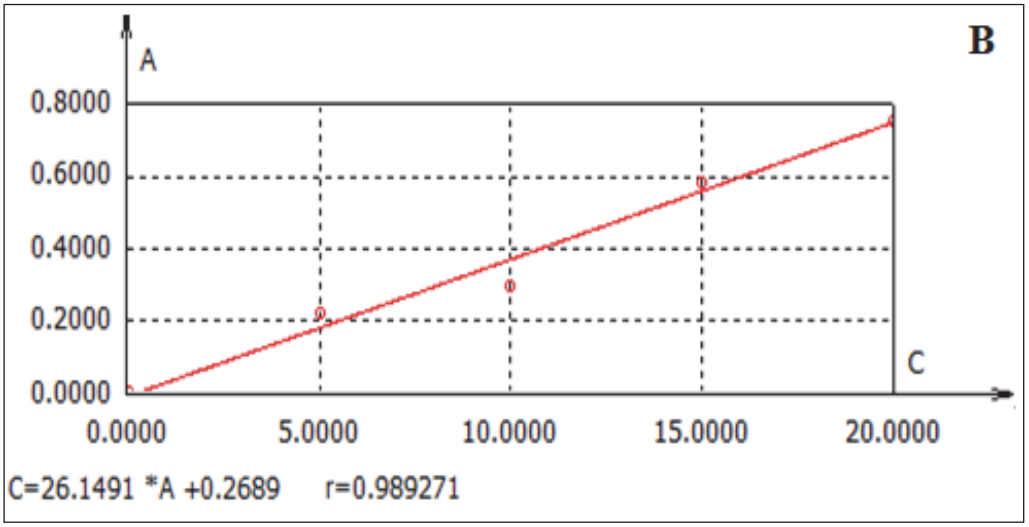
A
B
0.8000
0.6000
0.4000
0.2000
0.0000
C
0.0000
5.0000
10.0000
15.0000
20.0000
C=26.1491 *A +0.2689 r=0.989271

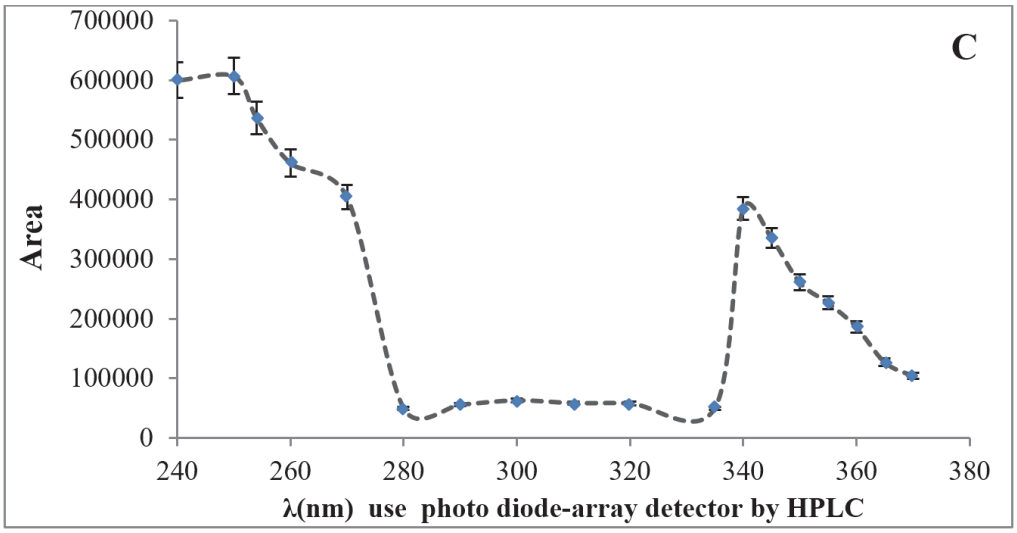
C
700000
600000
500000
400000
300000
200000
100000
0
Area
240
260
280
300
320
340
360
380
λ(nm) use photo diode-array detector by HPLC

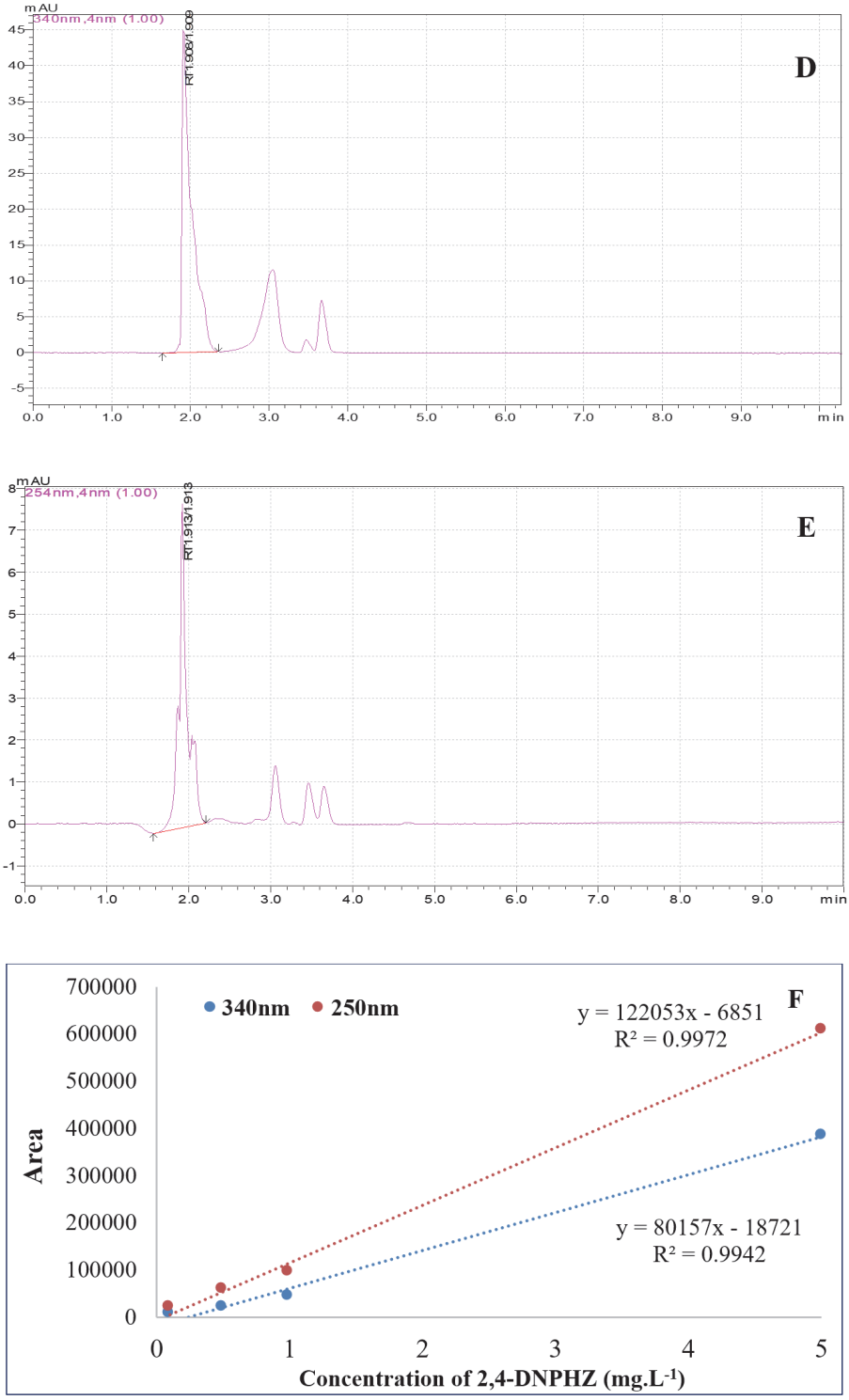

Fig. 8. Curve for 2,4-DNPHZ by High-performance liquid chromatography

A) absorbance vs wavelength,

B) absorbance vs concentration (5, 10, 15, 20) mg L^{-1}

C) wavelength (nm) vs. area by HPLC using a photodiode-array detector.

D) Using a photodiode-array detector, a chromatogram at a concentration of 5 mg L^{-1} at 340 nm.

E) chromatogram at a concentration of 5 mg L^{-1} at 254 nm

F) A standard series within the range (5-1-0.5-0.1) mg L^{-1} vs area.

MCPE) by (CV) of determining this pollutant is the best of the Spectrophotometry method. So, the electrochemical and chromatographic method is compared in Table 1.

The method proposed in this research (NiO-NCQD/g-C_3N_4/MCPE) is characterized by accuracy, reliability and good repeatability in Table 1. The results showed that the technique has a deviation of (0.02624747 µM), a relative standard deviation of a percent (2.08278875%), a quantitative detection limit (0.564097738 µM) and a detection limit (0.43843 µM). The value of the t-student was calculated (0.67361). So, the proposed method is characterized by reliability.

It turned out that the analysis using (HPLC) for analyzing the pollutant (2,4-DNDH) is characterized by analytical accuracy and validity. The results of the HPLC method were compared with (NiO-NCQD/g-C_3N_4/ MCPE) for the organic pollutant (2,4-DNDH). The value F-Test (3.819345) compared with the reference value F-Tab (19.000) at a confidence level of 95%. Comparing proposed methods based on the NiO-NCQD/g-C3N4/ MCPE with HPLC technique showed no significant difference between the two methods for determining (2,4-DNDH) in terms of accuracy.

4. Conclusions

In this study, the manufacture of an electrode using modified carbon paste (NiO-NCQD/g-C_3N_4/MCPE) was used to determine 2,4-dinitrophenylhydrazine (2,4-DNPHZ) by the cyclic voltammetry (CV). The modified carbon paste method was compared with high-performance liquid spectrophotometry (HPLC) and chromatography (UV-Vis). It turned out that the electrochemical method (NiO-NCQD/g-C_3N_4/MCPE) is superior to the spectrophotometry method in terms of detection limit (LOD). Also, there is no significant difference in accuracy between the HPLC method and NiO-NCQD/g-C3N4/MCPE method. The electrochemical method is a new analytical method characterized by accuracy, repeatability, and reliability with low cost.

5. References

[1] W. A. Adeosun, A. M. Asiri, H. M. Marwani, Real time detection and monitoring of 2, 4-dinitrophenylhydrazine in industrial effluents and water bodies by electrochemical approach based on novel conductive polymeric composite, Ecotoxicol. Environ. Safe., 206 (2020) 111171. https://doi.org/10.1016/j.ecoenv.2020.111171

[2] E. Zhang, P.Ju, Z. Zhang, H. Yang, L.Tang, X.Hou, J. J. Wang, A novel multi-purpose Zn-MOF fluorescent sensor for 2, 4-dinitrophenylhydrazine, picric acid, La^{3+} and Ca^{2+}: Synthesis, structure, selectivity, sensitivity and recyclability, Spectrochim. Acta Part A: Mol. Biomol. Spect., 222 (2019) 117207. https://doi.org/10.1016/j.saa.2019.117207

[3] K. Ahmad, A. Mohammad, P. Mathur, S. M. Mobin, Preparation of SrTiO3 perovskite decorated rGO and electrochemical detection of nitroaromatics, Electrochim. Acta, 215 (2016) 435-446. https://doi.org/10.1016/j.electacta.2016.08.123

[4] G. Zgherea, C. Stoian, S. Peretz, synthesis and physico-chemical characterization of 2.4-dinitrophenyl hidrazones derived from carbonyl compounds with some importance

Table 1. Analytical, statistical processors for Determination of (2,4-DNPHZ) by two methods (NiO-NCQD/g-C_3N_4/ MCPE) and (HPLC)

Method	concentration µ. mol L^{-1}	(n=3)	R (%)	SD (µ. mol.L^{-1})	RSD (%)
Adsorbent	1.25000	1.2602079	100.8166295	0.02624747	2.08278875
HPLC	1.262626	1.209843	95.81958	0.010157	4.239873

Adsorbent: NiO-NCQD/g-C_3N_4/ MCPE

in the study of food quality, Annals of the University Dunarea de Jos of Galati Fascicle VI-Food Technol., 33 (2009) 83-89. https://ores.su/en/journals/annals-of-the-university-dunarea-de-jos-of-galati-fascicle-vi-food-technology

[5] Y. Q. Lu, J. K. Jiang, W. D. Huang, Clinical features and treatment in patients with acute 2, 4-dinitrophenol poisoning, J. Zhejiang Uni. Sci. B, 12 (2011) 189-192. https://doi.org/10.1631/jzus.B1000265

[6] M. A. Smith, L. M.Sayre, V. E. Anderson, P. L. Harris, M. F. Beal, N. Kowall, G. Perry, Cytochemical demonstration of oxidative damage in Alzheimer disease by immunochemical enhancement of the carbonyl reaction with 2, 4-dinitrophenylhydrazine, J. Histochem. Cytochem., 46 (1998) 731-735. http://www.jhc.org

[7] F. Talebzadeh, S. Sobhanardakani, R. Zandipak, Effective adsorption of As (V) and V (V) ions from water samples using 2, 4-dinitrophenylhydrazine functionalized sodium dodecyl sulfate-coated magnetite nanoparticles, Sep. Sci. Technol., 52 (2017) 622-633. https://doi.org/10.1080/01496395.2016.1262873

[8] S. Sobhanardakani, M. Ahmadi, R. Zandipak, Efficient removal of Cu(II) and Pb(II) heavy metal ions from water samples using 2,4-dinitrophenylhydrazine loaded sodium dodecyl sulfate-coated magnetite nanoparticles, J. Water Sup. Res. Technol. AQUA, 65 (2016) 361-372. https://doi.org/10.2166/aqua.2016.100

[9] A. Afkhami, M. Saber-Tehrani, H. Bagheri, Simultaneous removal of heavy-metal ions in wastewater samples using nano-alumina modified with 2, 4-dinitrophenylhydrazine, J. Hazard. Mater., 181 (2010) 836-844. https://doi.org/10.1016/j.jhazmat.2010.05.089

[10] S. Sobhanardakani, R. Zandipak, 2, 4-Dinitrophenylhydrazine functionalized sodium dodecyl sulfate-coated magnetite nanoparticles for effective removal of Cd(II) and Ni(II) ions from water samples, Environ. Monit. Assess., 187 (2015) 1-14. https://doi.org/10.1007/s10661-015-4635-y

[11] I.Dalle-Donne,M.Carini,M.Orioli,,G.Vistoli, L. Regazzoni, G. Colombo, G. Aldini, Protein carbonylation: 2, 4-dinitrophenylhydrazine reacts with both aldehydes/ketones and sulfenic acids, Free Radical Biol. Med., 46 (2009) 1411-1419. https://doi.org/10.1016/j.freeradbiomed.2009.02.024

[12] P.D.Neuenfeldt,B.B.Drawanz,G.M.Siqueira, C. R.Gomes, S. M. Wardell, A. F. Flores, W. Cunico, Efficient solvent-free synthesis of thiazolidin-4-ones from phenylhydrazine and 2, 4-dinitrophenylhydrazine, Tetrahedron Lett., 51 (2010) 3106-3108. https://doi.org/10.1016/j.tetlet.2010.04.026

[13] J. Pilz, I. Meineke, C.H. Gleiter, Measurement of free and bound malondialdehyde in plasma by high-performance liquid chromatography as the 2, 4-dinitrophenylhydrazine derivative, J. Chromatogr. B Biomed. Sci. Appl., 742 (2000) 315-325. https://doi.org/10.1016/S0378-4347(00)00174-2 .

[14] Y.L. Lin, P.Y. Wang, L.L. Hsieh, K.H. Ku, Y.T. Yeh, C.H. Wu, Determination of linear aliphatic aldehydes in heavy metal containing waters by high-performance liquid chromatography using 2, 4-dinitrophenylhydrazine derivatization, J. Chromatogr. A, 1216 (2009) 6377-6381. https://doi.org/10.1016/j.chroma.2009.07.018.

[15] O. Korchazhkina, C. Exley, S.A. Spencer, Measurement by reversed-phase high-performance liquid chromatography of malondialdehyde in normal human urine following derivatisation with 2, 4-dinitrophenylhydrazine, J. Chromatogr. B, 794 (2003) 353-362. https://doi.org/10.1016/S1570-0232(03)00495-1.

[16] S. Uchiyama, Y. Inaba, N. Kunugita, Derivatization of carbonyl compounds with 2, 4-dinitrophenylhydrazine and their subsequent determination by high-performance liquid chromatography, J. Chromatogr. B, 879 (2011) 1282-1289. https://doi.org/10.1016/j.jchromb.2010.09.028

[17] R. Nawaz, T. Rasheed, T. Iqbal, M. Bilal, S. Majeed, Development of 2,4-dinitrophenylhydrazine-modified carbon paste electrode for highly sensitive electrochemical sensing of amino acids, Monatshefte für Chemie-Chemical Monthly, 151 (2020) 505-510. https://doi.org/10.1007/s00706-020-02580-y

[18] F. Lipari, S. J. Swarin, 2, 4-Dinitrophenylhydrazine-coated Florisil sampling cartridges for the determination of formaldehyde in air, Environ. Sci. Technol., 19 (1985) 70-74. https://doi.org/10.1021/es00131a007

[19] F. Soglia, M. Petracci, P. Ertbjerg, Novel DNPH-based method for determination of protein carbonylation in muscle and meat, Food Chem., 197 (2016) 670-675. https://doi.org/10.1016/j.foodchem.2015.11.038

[20] T.Wang,X.Gao,J.Tong,L.Chen,Determination of formaldehyde in beer based on cloud point extraction using 2, 4-dinitrophenylhydrazine as derivative reagent, Food Chem., 131 (2012), 1577-1582. https://doi.org/10.1016/j.foodchem.2011.10.021

[21] M. Al-Ani, L. U. Opara, D. Al-Bahri, N. Al-Rahbi, Spectrophotometric quantification of ascorbic acid contents of fruit and vegetables using the 2, 4-dinitrophenylhydrazine method, J. Food Agri. Environ., 5 (2007) 165. www.world-food.net

[22] P.S. Praveen, B. Anupama, V. Jagathi, G.D. Rao, Spectrophotometric determination of Tolperisone using 2,4-dinitrophenylhydrazine reagent, Int. J. Res. Pharm. Sci., 3 (2010) 317-320. www.ijrps.pharmascope.org

[23] P. Nagaraja, A. K. Shrestha, Spectrophotometric method for the determination of drugs containing phenol group by using 2, 4-dinitrophenylhydrazine, E-J. Chem., 7 (2010) 395-402. https://doi.org/10.1155/2010/328061

[24] H. Li, W. Goldberg, L. Verheyen, M. Foston, A method for the quantification of surface aldehyde content in cellulose nanocrystals using 2, 4-dinitrophenylhydrazine, SSRN J., (2022) 1-15. https://papers.ssrn.com/sol3/papers.cfm?abstract_id=4148789

[25] R. M. Khaleel, D. H. Mohammed, Spectrophotometric determination of tetracycline hydrochloride using 2, 4–dinitrophenyl hydrazine as coupling reagent, J. Phys. Conf. Ser., 1664 (2020) 012084. https://doi.org/10.1088/1742-6596/1664/1/012084.

[26] D. H. Mohammed, F. K. Omar, Spectrophotometric determination of catechol and resorcinol by oxidative coupling with 2, 4-dinitrophenyl hydrazine, Egypt. J. Chem., 64 (2021) 5061-5065. https://doi.org/10.21608/ejchem.2021.57506.3253

[27] M. Sireesha, R.S. Chandan, B.M. Gurupadayya,A.Shravya,Spectrophotometric determination of Nateglinide using 2, 4-dinitrophenyl hydrazine and potassium ferricyanide in pharmaceutical dosage form, Der Pharma Chem., 3 (2011), 497-506. https://www.derpharmachemica.com

[28] N. Rahman, S. Sameen, M. Kashif, Spectroscopic study on the interaction of haloperidol and 2, 4-dinitrophenylhydrazine and its application for the quantification in drug formulations, Anal. Chem. Lett., 6 (2016) 874-885. https://doi.org/10.1080/22297928.2016.1265898.

[29] S. Behera, R. Behura, M. Mohanty, R. Dinda, P. Mohanty, A.K. Verma, B.R. Jali. Spectroscopic, cytotoxicity and molecular docking studies on the interaction between 2, 4-dinitrophenylhydrazine derived Schiff bases with bovine serum albumin, Sens. Int., 1 (2020) 100048. https://doi.org/10.1016/j.sintl.2020.100048

[30] M. Kiamehr, B. Alipour, M. Nasrollahzadeh, S. M. Sajadi, Catalytic reduction of 2, 4-dinitrophenylhydrazine by cuttlebone supported Pd NPs prepared using Conium maculatum leaf extract, IET Nanobiotechnol., 12 (2018) 217-222. https://doi.org/10.1049/iet-nbt.2017.0005

[31] W. Boumya, M. Achak, M. Bakasse, M. A. El Mhammedi, Indirect determination of dopamine and paracetamol by electrochemical impedance spectroscopy

using azo coupling reaction with oxidized 2, 4-dinitrophenylhydrazine (DNPH): Application in commercial tablets, J. Sci. Adv. Mater. Dev., 5 (2020) 218-223. https://doi.org/10.1016/j.jsamd.2020.04.003

[32] M. P. Georgopoulou, C. V. Chrysikopoulos, Evaluation of carbon nanotubes and quartz sand for the removal of formaldehyde–(2, 4-dinitrophenylhydrazine) from aqueous solutions, Ind. Eng. Chem. Res., 57 (2018) 17003-17012. https://doi.org/10.1021/acs.iecr.8b03996

[33] A. Mohammad, M. Ehtisham Khan, M. Hwan Cho, Sulfur-doped-graphitic-carbon nitride (S-*g*-C_3N_4) for low cost electrochemical sensing of hydrazine, J. Alloys Compd., 816 (2020) 152522. https://doi.org/10.1016/j.jallcom.2019.152522

[34] I. Kolesnyk, J. Kujawa, H. Bubela, V. Konovalova, A. Burban, A. Cyganiuk, W. Kujawski, Photocatalytic properties of PVDF membranes modified with g-C3N4 in the process of Rhodamines decomposition, Sep. Purif. Technol., 250 (2020) 117231. https://doi.org/10.1016/j.seppur.2020.117231

[35] H. Mirzaei, M. H. Ehsani, A. Shakeri, M. R.Ganjali, A. Badiei, Preparation and photocatalytic application of ternary Fe_3O_4/GQD/g-C_3N_4 heterostructure photocatalyst for RhB degradation, J. Pollut., 8 (2022) 779-791. https://doi.org/10.22059/POLL.2022.331685.1202

[36] G. K. Jayaprakash, B. K. Swamy, S. Rajendrachari,S.C.Sharma,R.Flores-Moreno, Dual descriptor analysis of cetylpyridinium modified carbon paste electrodes for ascorbic acid sensing applications, J. Mol. Liq., 334 (2021) 116348. https://doi.org/10.1016/j.molliq.2021.116348.

[37] K. I. Alabid, H. N. Nasser, Study of the behavior and determination of phenol based on modified carbon paste electrode with nickel oxide-nitrogen carbon quantum dots using cyclic voltammetry, Anal. Methods in Environ. Chem. J., 6 (2023) 58-68. https://doi.org/10.24200/amecj.v6.i01.227

[38] K. I. Alabid, H. N. Nasser, An analytical method based on a modified carbon paste electrode by nanoparticles in optimal conditions for determining phenol in the liquid solutions and comparing it to high-performance liquid Chromatography, Anal. Methods in Environ. Chem. J., 6 (2023) 55-70. https://doi.org/10.24200/amecj.v6.i02.240

[39] K. I. Alabid, H.N. Nasser, Synthesis and characterization of nickel oxide with nitrogen quantum carbon dots as nanoadsorbent (NiO-NCQD) nanocomposite. Int. J. Nano Dimens., 14 (2023) 227-237. https://doi.org/10.22034/IJND.2023.1984570.2217

[40] W. Boumya, H. Hammani, F. Laghrib, S. Lahrich, A. Farahi, M. Achak, M. E.Mhammedi, Electrochemical study of 2, 4-dinitrophenylhydrazine as derivatization reagent and aldehydes at carbon glassy electrode, Electroanal., 29 (2017) 1700-1711. https://doi.org/10.1002/elan.201700019

Anal. Methods Environ. Chem. J. 6 (3) (2023) 36-53

AMECJ

Research Article, Issue 3
Analytical Methods in Environmental Chemistry Journal
Journal home page: www.amecj.com/ir

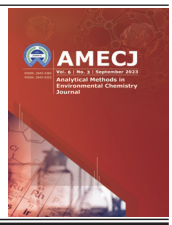

Virtual chemical analysis and machine learning-based prediction of polyethylene terephthalate nanoplastics toxicity on aquatic organisms as influenced by particle size and properties

Christian Ebere Enyoh[a,†], Chidi Edbert Duru[b], Qingyue Wang[a], and Senlin Lu[b]

[a]*Graduate School of Science and Engineering, Saitama University, 255 Shimo-Okubo, Sakura-ku, Saitama City, Saitama 8570-338, Japan.*

[b]*Department of Chemistry, Faculty of Physical Sciences, Imo State University, PMB2000 Owerri, Nigeria.*

[C] *School of environmental and chemical engineering, Shanghai University, Shanghai 200444, China.*

ARTICLE INFO:

Received 27 May 2023

Revised form 30 Jul 2023

Accepted 22 Aug 2023

Available online 28 Sep 2023

Keywords:
Analytical methods,
Artificial neural networks,
Fish,
Health risks,
Plastic pollution,
Simulation,
Toxicity

ABSTRACT

This study focuses on the chemical analysis and prediction of Polyethylene Terephthalate (PET) nanoplastics toxicity on aquatic organisms, considering the influence of particle size and properties. The effect PET NPs of different sizes (1, 4, 9, 16 and 25 nm coded NP1 to NP5) on aquatic organisms such as *Terpedo californica* (electric ray fish) and *Danio rerio* (zebrafish) as model species was evaluated by virtual chemical techniques and machine learning methodology based on Multilayer Perceptrons Artificial Neural Networks (MLP ANN) and Support Vector Machine. The PET NPs was built and characterized *in silico* and then docked on the acetylcholinesterase (TcAChE) and cytochrome P450 (Zf CYP450) of the organisms, respectively. The results showed that the binding affinities of the NPs increased steadily from – 7.1 kcal mol^{-1} to – 9.9 kcal mol^{-1} for NP1 to NP4 and experienced a drop at NP5 (– 8.9 kcal mol^{-1}) for TcAChE. The Zf CYP450 also had a similar pattern ranging from -5.2 kcal mol^{-1} to -8.1 kcal mol^{-1}. The MLP ANN showed an accuracy of 85.9 % and 77.3 %. In comparison, SVM showed a better PET NPs toxicity prediction with an accuracy of 99.5 % and 99.4% based on the inherent properties of TcAChE and Zf CYP450, respectively.

1. Introduction

Plastic manufacturing has continuously expanded from 1.5 million metric tonnes in 1950 to 368 million tonnes in 2019 [1], and it is omnipresent in our daily lives. Most plastic manufactured worldwide is used for single-use items [2]. As a result, plastic wastes, mostly made of single-use plastics, are now a growing global problem for environmental degradation. Due to a dramatic increase in the use of single-use plastics like gloves and N95 or surgical masks, the new coronavirus epidemic has exacerbated plastic pollution [3]. By 2050, landfills and aquatic bodies will contain nearly 12,000 million metric tonnes of plastic trash, endangering marine and terrestrial ecosystems [1] if current trends in plastic manufacture and waste management are allowed to continue. Natural weathering processes can cause discarded plastic to break down into microplastics (MPs; 100 nm—5 mm size) and/or nanoplastics (NPs < 100 nm) [4]. NPs could be consumed by biota because of their small size [4]. NPs are a fast-evolving topic important in various sectors, including human toxicity, food and environmental study [4].

*Corresponding Author: Christian Ebere Enyoh
Email: cenyoh@gmail.com
https://doi.org/10.24200/amecj.v6.i03.249

Ingestion of NPs can expose aquatic biota, which can then accumulate the particles and experience adverse effects [5]. The harmful effects of NP exposure in aquatic species include embryotoxicity, hepatotoxicity, growth inhibition of microalgae and fish larvae, reduced shrimp and plankton life spans upon long-term exposure, deterioration of intestinal tissues in sea bass, and changes in feeding behaviour, metabolism, and innate immunity in fish by Banerjee et al., 2021. Human exposure to NPs happens when they consume tainted food or drink or breathe in airborne plastic particles [1,6]. It has not been possible to analyze the consequences of NPs exposure in humans directly [7]; however, MP has been found in human feces [8], placenta, in both the maternal and fetal regions, and amniotic membranes [9]. Studies have often translated toxicity in some aquatic organisms to humans because of similar genetic traits [10]. The aquatic organism Zebrafish, which shares genetic traits with mammals, has been utilized extensively in MPs research for assessing environmental toxicity and studying genetic developments [10, 11]. Zebrafish and humans have a lot in common physiologically and genetically. Zebrafish and humans have around 70 % of the same genes, and 84 % of the genes associated with human illnesses are also present in zebrafish [12]. There are reports that due to their great sensitivity to toxic contaminants, embryos and juveniles of Zebrafish can be used effectively to examine the detrimental impacts of environmental pollutants on aquatic creatures and the poisonous process [13]. The toxicity of chemicals to zebrafish mainly involved the cytochrome P450 (CYP) enzymes [14]. The cytochrome P450 (CYP) enzymes catalyze oxidative transformation, which results in the activation or inactivation of a wide range of endogenous and foreign substances. This has implications for both healthy physiology and disease processes. The oxidative biotransformation of these xenobiotics may decide those chemicals' cellular and organ targets [15]. Many compounds that cause developmental abnormalities, such as cardiovascular, neurological, and connective tissue disorders, are substrates for CYPs. The CYP enzymes involved in xenobiotic metabolism may also play a role in producing morphogenic molecules or maintaining regions free of them, thereby defining the temporal and spatial domains in which morphogens act and facilitating the region-specific adjustments required for successful development [15]. On the other hand, an electric rays' fish (ERF) was also considered a model species for aquatic organisms in this study to evaluate the toxicity of NPs to benthic organisms as they often exist in the coral reefs, mud, or sandy bottoms [16]. ERFs are renowned for having the ability to generate an electric discharge that may range in voltage from 8 to 220 volts, depending on the species, and are used to defend themselves as well as to shock prey [17]. The species of the genus Torpedo may be the most well-known [16]. Its name appears on the underwater torpedo weapon. The word "torpere" means "to stiffen or paralyse" in Latin, referring to the impact the fish has on those who contact it [18]. The ERF is often found in shallow water up to 100 metres on coral reefs, mud, or sandy bottoms [19]. It mostly consumes invertebrates and tiny reef fish [16].

To evaluate the toxicity of pollutants to this organism, acetylcholinesterase (AChE) is the primary target. The AChE is a primary cholinesterase in organisms that catalyzes the breakdown of acetylcholine and some other choline esters that function as neurotransmitters. It is found mainly at neuromuscular junctions, where it terminates synaptic transmission. Drugs or toxins that inhibit AChE led to the persistence of high concentrations of acetylcholine within synapses, leading to increased cholinergic signalling within the central nervous system, autonomic ganglia and neuromuscular junctions.

Compounds that inhibit AChE irreversibly may lead to convulsions, bronchial constriction, muscular paralysis, and death by asphyxiation [20]. One important factor that can influence the toxicity of NPs to aquatic organisms is their size. Studies have shown that size affects the rate of ingestion of NPs to shrimp [21] and toxicity to human gastric cells [22]. In this study, the toxicity

of polyethylene terephthalate (PET) NPs of different sizes to aquatic organisms was studied using a molecular docking (MD) approach coupled with machine learning (ML) methodology, using the CYP450 in zebrafish and AChE in ERF as primary targets. By simulating the interaction between a small molecule and a protein at the atomic level, the MD method enables us to describe how tiny molecules behave at the target proteins' binding site and better understand fundamental biological processes [23]. The two primary steps in the docking procedure are predicting the ligand structure, positioning and orientation inside these sites and assessing the binding affinity, which is translated into toxicity. On the other hand, a group of algorithms called "machine learning (ML)" are used to analyze data and learn without being specifically trained to use it for forecasting. ML contains a variety of algorithms, including supervised, semi-supervised, unsupervised, and reinforced, depending on the application situation [24]. Using the supervised algorithm, which recognizes data patterns, gains knowledge from observations, and generates predictions, the dataset has labelled inputs and outputs [25]. These are employed in problems of classification, regression, and forecasting variety [24]. Machine learning (ML) has expanded to include research into the toxicity of microplastics, predicting effects on cell, immune, and reproductive systems, and identifying the accumulation of materials in organisms based on material properties [26,27]. As a result, ML is expected to emerge as a valuable tool for quickly assessing the potential biological impact of NPs. In this study, the properties data set collected from NPs structures designed and analyzed *in silico* were labelled using supervised ML and used to predict the toxicity of the PET NPs to the studied aquatic organisms.

2. Material and Methods

2.1. Preparation of PET Nanoplastics (NPs)

The PET NPs of different sizes were prepared *in silico* using the 3D atomistic in Biovia Material Studio 8. Firstly, a single 3D isotactic ethylene terephthalate homopolymer molecular model was sketched. Depending on the size of NPs, the number of chain lengths and repeat units were determined. Four PET NPs of different sizes were prepared and compared with a single monomer unit of PET MPs. The structure, chemical formula and molecular weight are presented in Table 1.

To increase the simulation's accuracy and efficiency, geometric optimization, namely energy reduction, is required for the developed PET NPs molecular models. The FORCITE module with COMPASS Forcefield was used to execute a geometry optimization work on the first formed molecular model with an unsatisfactory starting structure to reduce energy. The intelligent algorithm was optimized while the convergence tolerance energy and force were set to 0.001 kcal mol^{-1} and 0.5 kcal mol^{-1} A^{-1}, respectively, with 500 iterations. The optimized NPs structures were characterized to be sure they were in the nano-sized range. The results summary from the optimization and the characterization is presented in Table 3, which includes modifications to the total energy, surface area and occupied volume.

2.2. Effect of particle size on toxicity to aquatic organisms

2.2.1.Identification and preparation of enzyme targets

The 3D X-ray crystallographic structures of the acetylcholinesterase of *Terpedo californica* (electric ray fish) TcAChE with identity 1W76 and zebrafish cytochrome P450 (Zf CYP450) with identity 4R20 were retrieved from the protein data bank (PDB) which was shown in Figure1 [28]. The Chain A of the enzymes was used as a target to study the effect of chain length on nanoplastic toxicity. Their active sites were identified from the literature [14,29]. Removal of the interfering crystallographic water molecules and minimization of the protein was done using UCSF Chimera 1.14 [23,30,31].

Table 1. The PET NPs prepared in silico for the study

Samples	Chain length x repeat unit (nm)	Structure	Chemical formula	Molecular weight
PET 1	1 x 1 (1 nm)	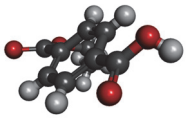	$C_{10}H_{10}O_4$	194.18
PET NPs 2	2 x 2 (4 nm)	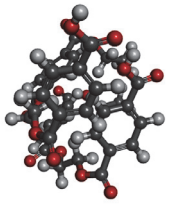	$C_{40}H_{36}O_{16}$	772.70
PET NPs 3	3 x 3 (9 nm)	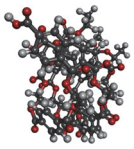	$C_{90}H_{78}O_{36}$	1747.66
PET NPs 4	4 x 4 (16 nm)	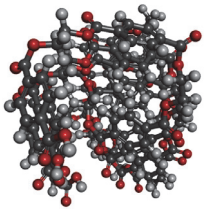	$C_{160}H_{136}O_{64}$	3082.85
PET NPs 5	5 x 5 (25 nm)	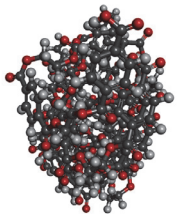	$C_{250}H_{210}O_{100}$	4814.28

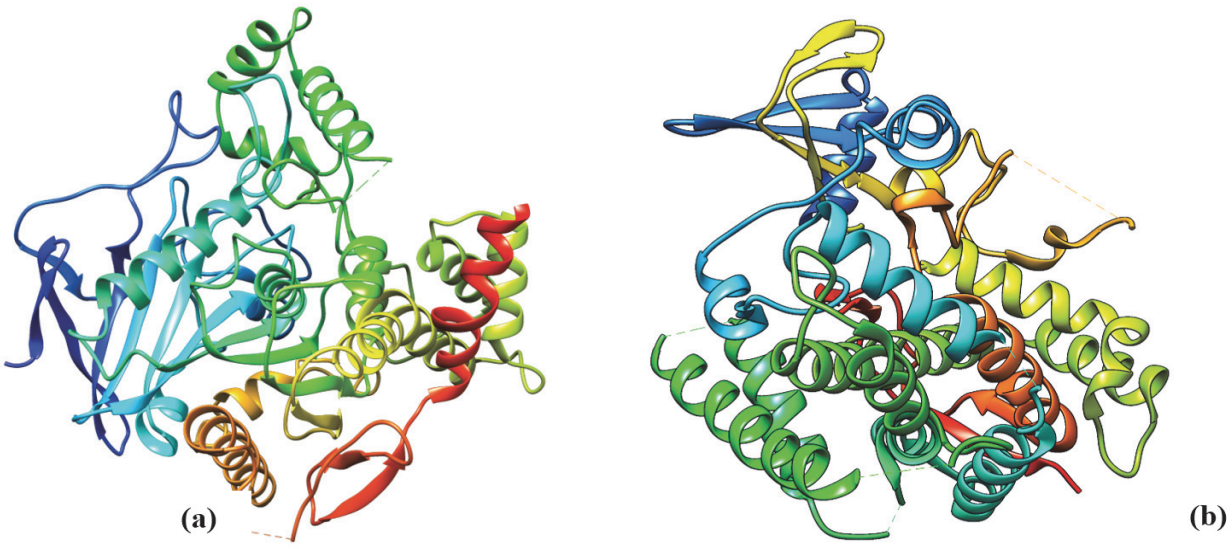

Fig. 1. Crystal structures of (a) TcAChE (b) Zf CYP450

2.2.2.Molecular docking studies

Site-directed docking of the nanoplastic compounds was performed on the active sites of the enzymes with Autodock Vina in PyRx software version 0.8 [32,33]. The amino acids at the active sites of the enzymes were identified in UCSF Chimera, and they were then selected and toggled on the enzyme surfaces in the Pyrx software. The specific sites on the receptors were set using the grid box with dimensions: center *x*: 88.622, center *y*: 55.838, center *z*: – 21.553, and size *x*: 30.496, size *y*: 27.705, size *z*: 18.659 for TcAChE, and center *x*: 3.640, center *y*: 5.221, center *z*: 50.783, and size *x*: 21.812, size *y*: 10.712, size *z*: 25.919 for Zf CYP450. At the end of the molecular docking, nine binding poses of the protein-ligand complex were generated, and their scoring results were also created. Hydrogen bonding and other hydrophobic interactions between the enzyme-ligand complex of the compounds were visualized using Biovia Discovery Studio 4.5 [34].

2.3. Machine Learning approach to model the toxicity of NPs to aquatic organisms

2.3.1.Artificial Neural Network (ANN)

This study uses Multilayer Perceptrons-based (MLP) Artificial Neural Networks (ANNs) as its machine learning strategy. ANNs are nonlinear models of interconnected "neurons," or units that can recognize patterns in various ways, including classification and prediction [25,26]. ANNs learn by seeing patterns in the data, and they store their newfound knowledge in weights, which are collections of connection strengths corresponding to regression coefficients. The MLP ANN employed in this work learns using backpropagation, where weights are adjusted following the processing of the whole data set or each datum. ANN weights evaluate the correlations between independent and dependent variables similarly to regression coefficients. However, ANN weights quantify local effects, whereas regression weights evaluate the global impacts of independent factors on dependent variables across all data [35].

An MLP comprises input, hidden, and output layers. Figure 2 presents an MLP ANN with four inputs (x1, x2, x3 and x4), one hidden-layer neuron and one output (f(x)). One can express the result of every hidden neuron (j) by utilizing the input values of Xi, weights, biases, and transfer function f(x) in the subsequent Equation 1.

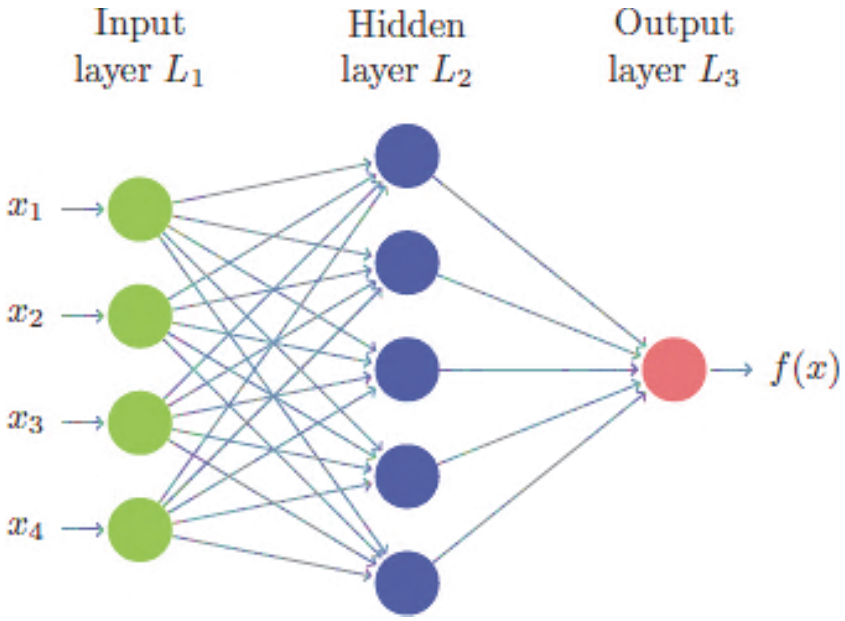

Fig. 2. An MLP ANN model with four input layers

Table 2. The range of data employed in ANN training

Parameter	Type	Minimum value	Maximum value
Binding affinity for AChE ($^{kcal\ mol-1}$)	Output	-7.1	-9.9
Binding affinity for CYP450 ($^{kcal\ mol-1}$)	Output	-5.2	-8.1
Molecular size (nm)	Input	1	25
Structure Energy ($^{kcal\ mol-1}$)	Input	13.51	200.16
Occupied volume ($Å^3$)	Input	168.32	3748.59
Surface area ($Å^2$)	Input	189.78	2148.33

$$H_j^o = f\left(\sum_{i=1}^{i} X_i \,.\, W_{ij} + b_j\right) \quad \text{(Eq. 1)}$$

The input and output variables used in this study for development are presented in Table 2. The input layer includes the independent variables, and the output layer contains the dependent variable. Equation 2 is used to express the final output (k) from the hidden layer result.

$$O_k^o = f\left(\sum_{i=1}^{i} H_j^o \,.\, W_{jk} + b_k\right) \quad \text{(Eq. 2)}$$

80 % of the data was used for training the ANN, while 20 % was used for testing. The batch training strategy, which produces the best results in data sets with minimal input variables, was used to train the network [36].

The MLP ANN makes an effort to calculate the weights connecting the input and output layers, representing the relative weights of the inputs into and outputs from the ANN "black box" or hidden layer [37]. In this study, the number of units in the hidden layer (excluding bias) varied for AChE and CYP450, respectively. At the same time, the activation function was based on hyperbolic tangent and linear. The arguments are transformed into values between -1 and +1 via the hyperbolic tangent, frequently employed in ANN modelling. This activation function is beneficial when the training data are normalized, as in the current research [35]. The hidden layer changes the input data into a collection of values and is then used by the output layer. The mathematical operations taking place in the hidden layer are what produce the ANN's nonlinear behaviour, making it a crucial part of the system [35,37]. In this study's case, the dependent variable, or binary classifications, is contained in the output layer. During training,, the ANN will examine the output layer's dependent variable and the input layer's independent variables to see how they specifically relate to one another. The hidden layer's nodes include mathematical functions that define the relationships. Once the connections (mathematical functions) have been established, the testing data will be used to validate them [38].

2.3.2.Support vector machine

SVM has several advantages compared to ANN, including its ability to avoid being trapped in local minima by mapping the nonlinear relationship between inputs and output(s), solving problems using only support vectors, and handling small data sets [37]. According to Yettou [39], the performance of an SVM model depends on the choice of kernel function and its parameters. The predicted output can be obtained using the SVM model as Equation 3.

$$y(x)_{pre} = \sum_{i=1}^{n} a_i \,.\, K\left(x_i, x_j\right) + b \quad \text{(Eq. 3)}$$

K(xi, xj) can be linear, polynomial, Gaussian or radial basis function kernel. αi and b denote the Lagrange multiplier and threshold parameter, respectively. In this study, the radial basis function kernel was used (Equation 4). The dataset used for the SVM is shown in Table 2. 20 support vectors were used in the model with a cost of 1 and gamma of 0.25. The gamma hyperparameter was selected before training the model and influenced the decision boundary's curvature.

$$f(x) = \sum_i^N a_i y_j \, exp\left(\frac{-||x-x_i||^2}{2\sigma^2}\right) + b \quad \text{(Eq. 4)}$$

2.3.3. Model evaluation metrics

Different statistical models, such as the average correlation factor (R^2), root mean square error (RMSE), and mean absolute error (MAE). The sum of square error (SSE) specified in Equations 5-8 was used to check and evaluate how well an ML model predicts the output (binding affinity, kcal mol^{-1}) [37].

$$R^2 = 1 - \frac{\sum(BA_{est} - BA_{exp})^2}{\sum(BA_{est} - \overline{BA}_{exp})^2} \quad \text{(Eq. 5)}$$

$$RMSE = \sqrt{\frac{1}{N}\sum(BA_{est} - BA_{exp})^2} \quad \text{(Eq. 6)}$$

$$MAE = \frac{1}{N}\sum(BA_{est} - BA_{exp}) \quad \text{(Eq. 7)}$$

$$SSE = \sum(BA_{est} - BA_{exp})^2 \quad \text{(Eq.8)}$$

Where:

- $(BA)_{est}$: is the estimated value of the binding affinity in kcal mol^{-1} by ANN model;
- $(BA)_{exp}$, is the experimental value of the binding affinity in kcal mol^{-1}; and
- : is the average value of binding affinity in kcal mol^{-1}

The goal should be to achieve the lowest error with (RMSE, MAE, and SSE) and the greatest with (R^2) correlations to obtain the optimal ANN model [37, 38].

3. Results and discussion

Although there is ample evidence that nanoplastics (NPs) are toxic to aquatic life, little is known about how these particles' sizes affect their toxicities. The binding affinity of NP2, NP3, and NP4 was higher than the control for TcAChE, indicating that they have a higher inhibitory potential at this site and, therefore, could impact more toxicity on the enzyme than the native inhibitor (-)-galanthamine. However, the abiraterone control for Zf CYP450 showed the highest toxicity with a binding affinity of -9.5 kcal mol^{-1} compared with the PET NPs. The validation of the model was tested by error analysis models, which confirmed that the SVM was at high accuracy. The study demonstrated that the size of PET NPs can influence their toxicity to aquatic organisms, and the surface area and reactivity (energy) of the NPs are important for their toxicity. Integrating chemistry analysis, machine learning, and environmental chemistry allows for accurately predicting Polyethylene Terephthalate (PET) nanoplastics toxicity on aquatic organisms, considering various particle sizes and properties.

3.1. Optimization and characterization of PET NPs

The prepared PET NPs were optimized and characterized. Geometry minimization is finding an arrangement in the space of a collection of atoms where the net inter-atomic force on each atom is acceptably close to zero and the position on the potential energy surface (PES) is a stationary point. Since this is the most stable configuration for the molecule and is most likely to occur in nature, geometry optimization aims to find the location where the energy is lowest [40]. The optimized energies, surface area and occupied volume were determined *in silico;* the results are presented in Table 3. After optimization, the PET NPs initial structure energy was reduced to 13.51, 91.78, 96.24, 200.16 and 176.47 kcal mol^{-1}, respectively, for 1 (1 nm) to 5 (25 nm). The most stable (geometry-optimized) forms of the NPs were used in the toxicity evaluation of aquatic organisms. The cornolly surface area of the nanoplastics is also presented in Figure 3. The surface area of the PET NPs ranged from 189.78 to 2148.33 $Å^2$, and the occupied volume of the PETs increased from

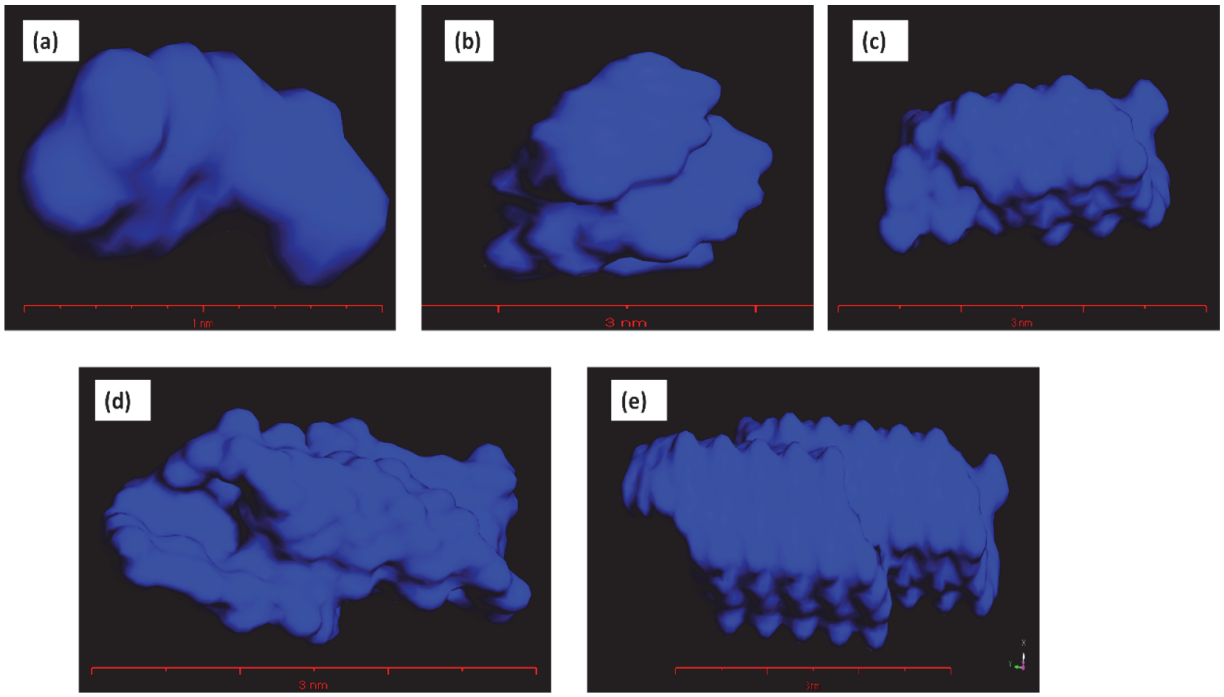

Fig. 3. Connolly surface plot of PET NPs for surface area and occupied volume determination. Figure (a) to (e) represents PET NPs 1 – 5.

Table 3. The PET NPs optimization and surface characterization results

Samples	Molecular Size (nm)	Energy (kcal mol-1) Initial	Final	Occupied volume (Å^3)	Surface area (Å^2)
PET NP 1	1	160.57	13.51	168.32	189.78
PET NPs 2	4	86874.58	91.78	734.18	651.47
PET NPs 3	9	137955.82	96.24	1441.39	1025.52
PET NPs 4	16	317658.71	200.16	2986.98	1783.66
PET NPs 5	25	8907.77	176.47	3748.59	2148.33

168.32 to 3748.59 Å^3 (Table 3). The surface area and occupied volume were determined based on the Connolly model [41R: SM]. Expectedly, the occupied volume and surface area increased with the PET NPs molecular sizes (Table 3). As the molecular sizes increase, the carbon to hydrogen increases as well, which has been shown to correlate to surface area [42R,43R; SM]. Enyoh [43] reported that the aging of PET microplastics increased the carbon-to-hydrogen ratio and, thus, the surface area of the material. Its surface area indicates how much overall space an object's surface takes up. Chemical reactions often proceed more quickly when a substance's surface area increases. However, the occupied volume measures the quantity of room inside an object. The surface area of the PET NPs confirmed that the PET NPs were nano-sized [44R; SM].

3.2. Effect of PET NPs size on toxicity to aquatic organisms through molecular docking

To evaluate the toxicity of NPs on aquatic organisms, the AChE of Electric ray fish (Terpedo californica) and CYP450 of Zebrafish (Danio rerio) were considered models. Acetylcholinesterase (AChE) is a primary cholinesterase in organisms that

catalyzes the breakdown of acetylcholine and some other choline esters that function as neurotransmitters. It is found mainly at neuromuscular junctions, where it terminates synaptic transmission. Drugs or toxins that inhibit AChE led to the persistence of high concentrations of acetylcholine within synapses, leading to increased cholinergic signalling within the central nervous system, autonomic ganglia and neuromuscular junctions. Compounds that inhibit AChE irreversibly may lead to convulsions, bronchial constriction, muscular paralysis, and death by asphyxiation [20]. However, CYP450 of zebrafish has increasingly been used in drug discovery and toxicology screening [30]. The CYP enzymes generally catalyze the oxidative transformation of many endogenous and exogenous chemicals, thereby functioning as a metabolizer of potentially toxic compounds in organisms. The CYP genes in zebra fish have been shown to have a high degree of sequence similarity with those of humans [15].

The binding affinities and the interactions of the enzyme-NP complex at the AChE active site are shown in Table 4. The decrease in binding affinity implies greater stability of the NP at the active site, which results in the inhibition of the enzyme activities. The binding affinities of the NPs increased steadily from – 7.1 kcal mol^{-1} to – 9.9 kcal mol^{-1} for NP1 to NP4 and experienced a drop at NP5 (– 8.9 kcal mol^{-1}). The binding affinity of NP2, NP3, and NP4 was higher than the control, indicating that they have a higher inhibitory potential at this site and, therefore, could impact more toxicity on the enzyme than the native inhibitor (-)-galanthamine. All the polymer chains from NP2 to NP4 fitted well into the binding pocket of AChE. Including an additional monomer unit in NP5 resulted in a constraint which manifested as a drop in the binding affinity of this polymer unit. A similar observation was reported in an experimental study by [22]. They evaluated polystyrene NPs of particle sizes (50, 100, 200, 500, 1000 or 5000 nm). They reported a toxicity trend in gastric cells in order of 50 > 5000 > 1000 > 500 > 200 > 100 nm. [21] reported an increase in mortality (toxicity to adult daggerblade grass shrimp *Palaemonetes pugio*) as MPs sizes increase. However, [45R; SM] found no effect of 200–600 µm PET MPs sizes on toxicity to *Scenedesmus* sp. The binding affinities of the different NPs and the control compound abiraterone at the Zf CYP450 active site are shown in Table 5. The control showed the highest toxicity with the binding affinity of -9.5 kcal mol^{-1} compared with the PET NPs, which ranged from -5.2 kcal mol^{-1} to -8.1 kcal mol^{-1}. The binding pocket of this protein could not accommodate two PET units from NP5, which manifested as a sharp drop in the binding affinity of the enzyme-NP5 complex. However, the toxicity pattern of the PET NPs on the Zf CYP450 active site is like AChE of Electric ray fish, indicating that increasing NP size will increase toxicity to a certain extent, followed by a reduction in toxicity due to inefficient enzyme-NP binding.

Table 4. The binding affinity of nanoplastic compounds on the TcAChE active site

PET NPs	NP-Protein complex	Binding affinity (kcal mol^{-1})	Protein-ligand interactions
Control	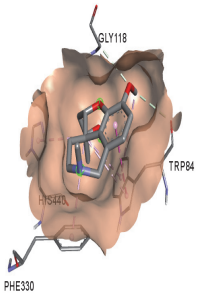	– 9.2	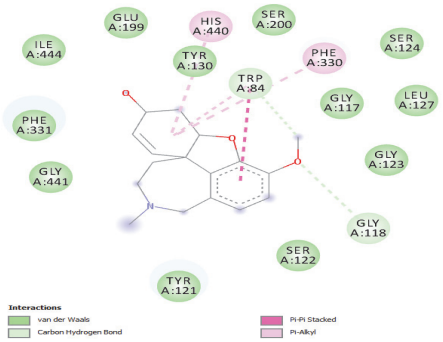

1	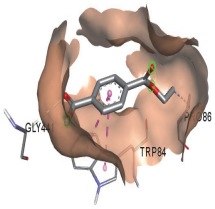	– 7.1	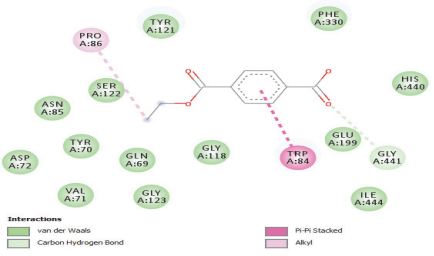
2	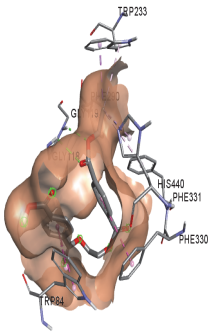	– 9.3	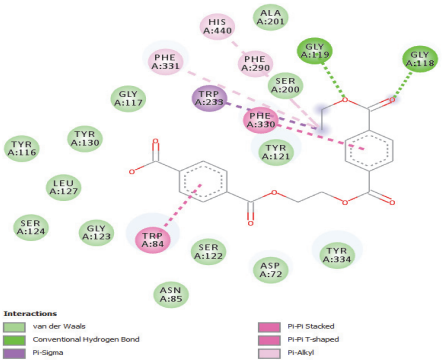
3	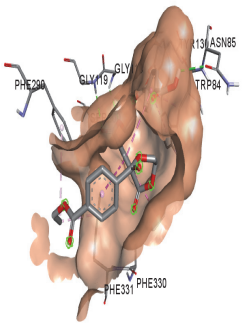	– 9.5	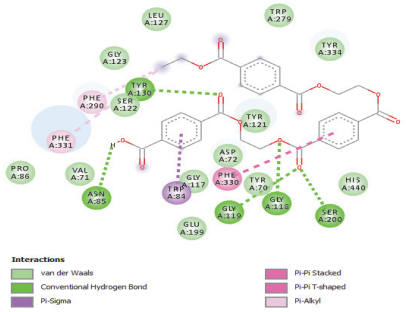
4	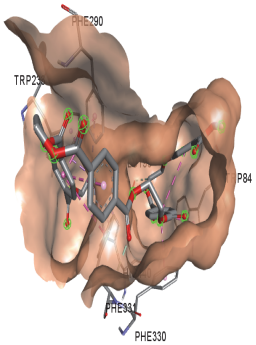	– 9.9	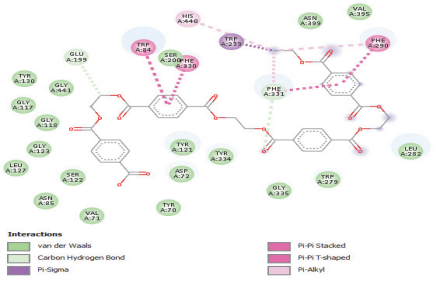
5	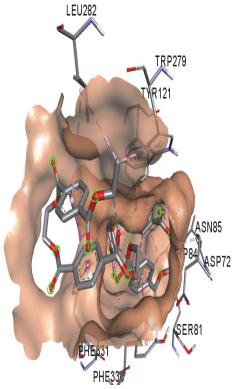	– 8.9	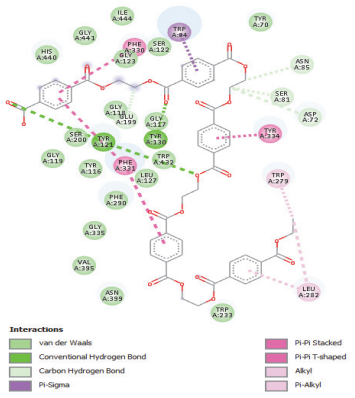

Table 5. The binding affinity of nanoplastics compounds on the Zf CYP450 active site

PET NPs	NP-Protein complex	Binding affinity (kcal mol^{-1})	Protein-ligand interactions
Control	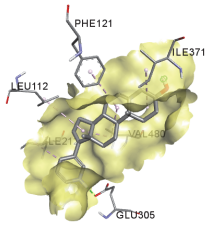	– 9.5	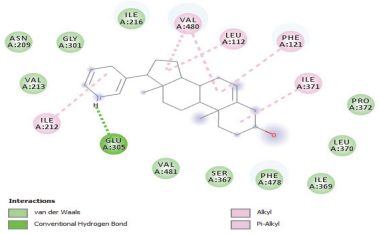
1	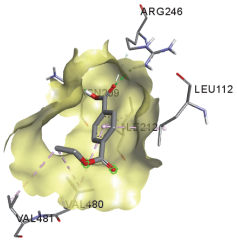	– 5.2	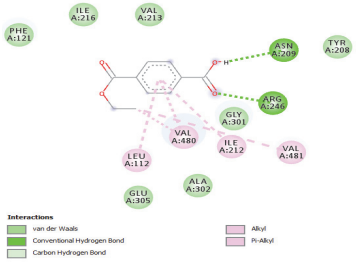
2	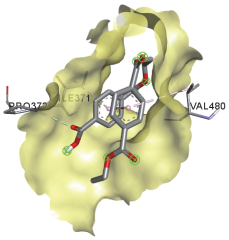	– 5.8	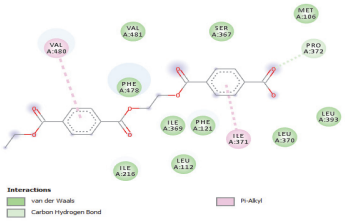
3	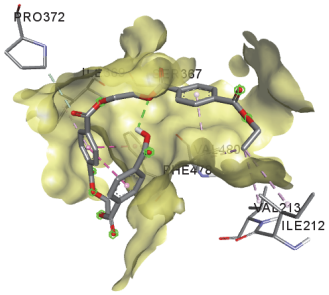	– 7.3	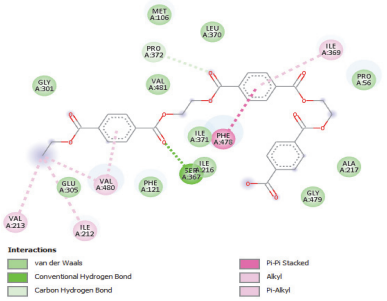
4	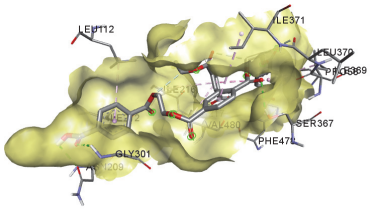	– 8.1	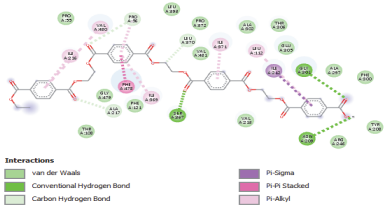
5	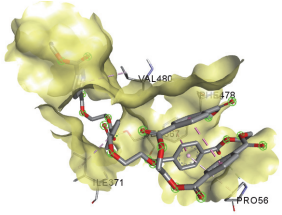	– 5.7	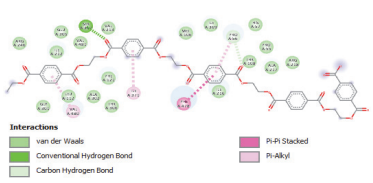

3.3. Toxicity evaluation via machine learning methodology

The toxicity of NPs is based on their structural characteristics, such as their molecular Size (MS), optimized energy, occupied volume (OC) and surface area (SA) at the active sites of TcAChE and Zf CYP450. The results showing the artificial neural networks, identification of the most important property and linear correlation of predicted binding affinity (toxicity) from machine learning and actual values from molecular docking are presented in Figures 4 to 5. The ANN for the two enzymes differed (Figure 4); AChE had 15 hidden layers (excluding bias), while CYP450 had just five each in the first and second hidden layers. Classification boundaries are simpler to define in the hidden layer than in the original space, which may be considered a mapping to a higher dimensional space. Out of the 20 SVM models tested model number 17 and 4 were best to predict the binding affinity to Tc AChE (Table S1, moved to supplementary material, SM) and Zf CYP450 (Table S2, moved to supplementary material, SM) based on the smallest root average squared error (RASE) values. These models had a cost of 2.49, and gamma and support vector (SV) of 0.499 and 4, respectively for Tc AChE, while for Zf CYP450, cost, gamma, and support vector (SV) were 3.71, 0.19 and 4, respectively.

The correlation of the predictive toxicity value from ANN and actual values obtained from the molecular docking were significant, with coefficients of 0.859 and 0.773 for Tc AChE and Zf CYP450, respectively (Figure 5a and 5b). However, the SVM algorithm showed a better correlation with the actual with coefficients of 0.995 and 0.994 for Tc AChE and Zf CYP450, respectively (Figure 5c and 5d). Correlation coefficient values > 0.9 are considered significant and acceptable [46R,47R,48R; SM]. Figures 5e and 5f compare the experimental values and those predicted by a Support Vector Machine (SVM) model. The results demonstrate that the points predicted by the SVM model align perfectly with the trend of the experimental points, indicating that the SVM model can accurately model the non-linear behavior of the reactivity descriptor of the PET NPs. In contrast, the performance of an Artificial Neural Network (ANN) model in this regard is not as good as that of the SVM model. The comparison between the experimental and predicted values is an essential step in evaluating the performance of machine learning models. The accuracy of the model's predictions is critical in determining its effectiveness in modelling the underlying system. In this case, the SVM model is shown to outperform the ANN model in modelling the complex and non-linear behavior of the reactivity descriptor of the PET NPs. This significant result highlights the importance of selecting the appropriate machine-learning model for a specific application.

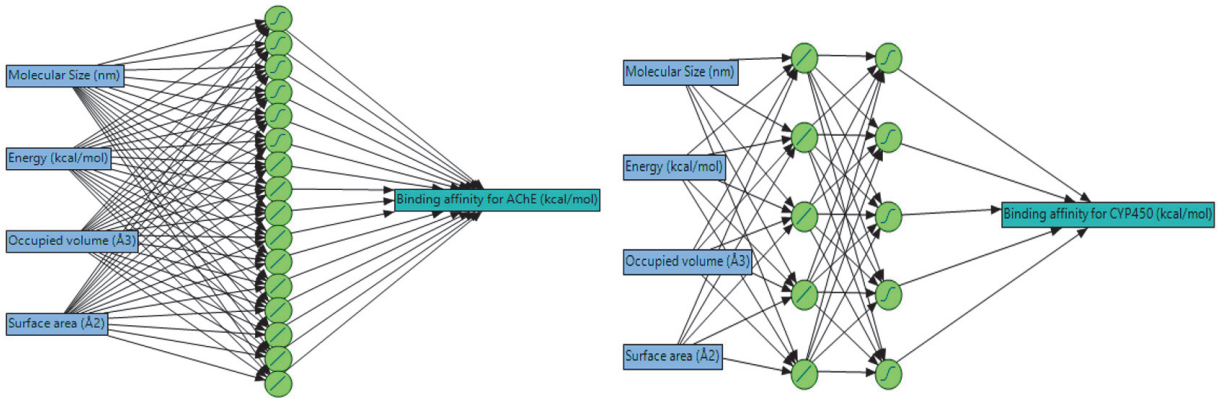

(a) **(b)**

Fig. 4. The artificial neural networks for predicting NPs toxicity based on their properties to (a) AChE and (b) CYP450.

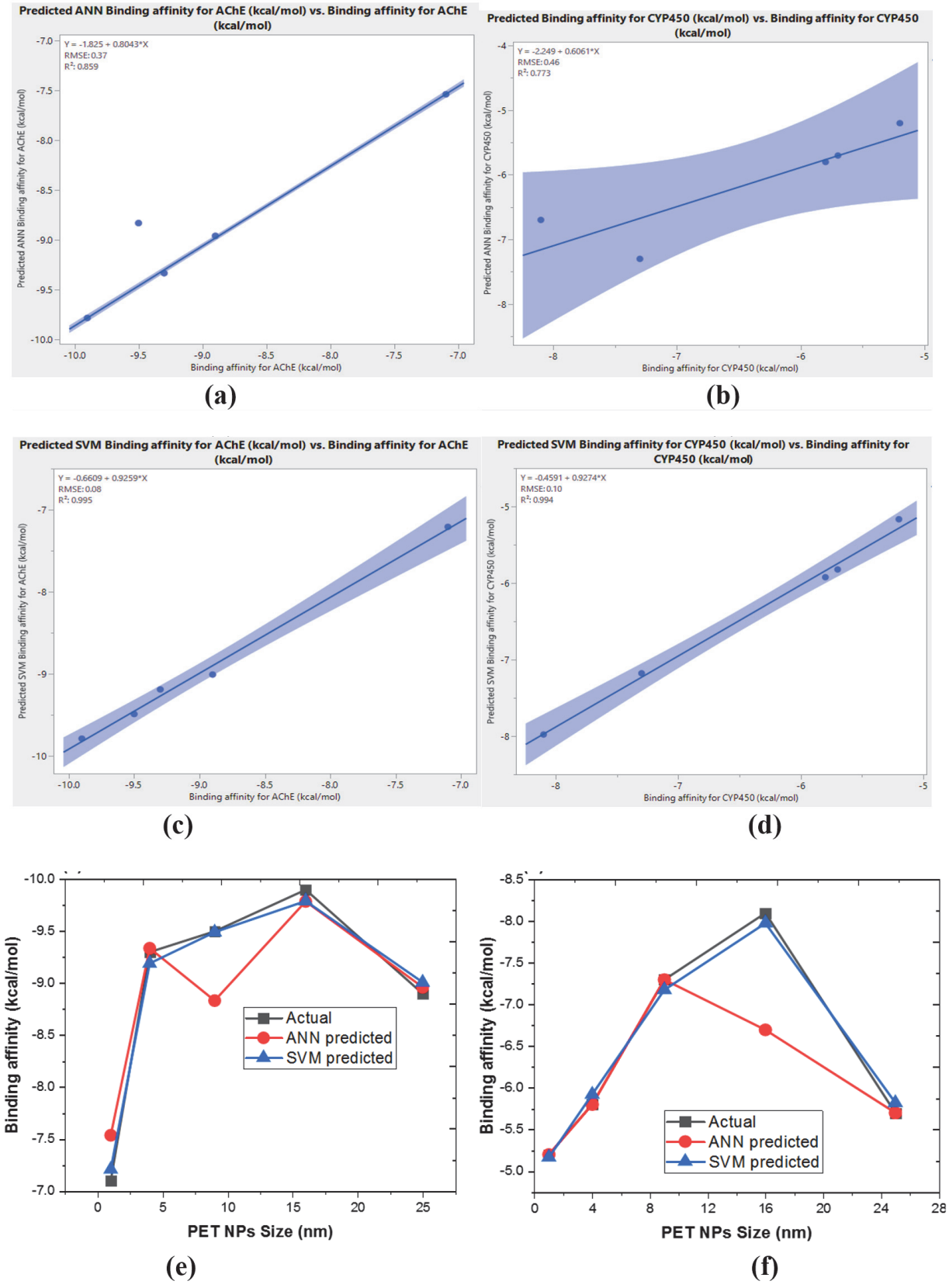

Fig. 5. The correlation of predicted binding affinity (toxicity) from ANN (a)-(b) and SVM (c)-(d) and actual values from molecular docking studies to AChE and CYP450. The comparative plot of the predicted binding affinity from ANN and SVM with actual values to (e) AChE and (f) CYP450

Furthermore, the SVM model's ability to accurately model the behavior of the reactivity descriptor of the PET NPs has significant implications for the field of nanotechnology. The reactivity descriptor is a critical property of the PET NPs that determines their reactivity and, therefore, their potential toxicity to aquatic organisms. Accurately modelling this property is essential for designing and optimizing these nanoparticles for various applications.

The most important NPs property for the toxicity varied with the proteins (Figures 6a and 6b). The NPs optimized energy and surface area were the main properties with normalized importance of 100 % that affect the toxicity of NPs at TcAChE and Zf CYP450 active sites, respectively. The NPs energy is indicative of their reactivity. Xie [49R; SM] recently found that nanoparticle chemical reactivity and surface area were important parameters influencing the toxicity of nanoparticles to algae. The results of a previous study using both in vivo and in vitro methodologies showed that the amount of surface area in contact with the mouse's biological system determines the response's amplitude, suggesting that surface chemistry phenomena are involved in biological reactivity [50R; SM]. Further, [51R; SM] reported that the surface area is the physiologically most efficient dosage meter for acute nanoparticle toxicity in the lung.

The efficacy of the constructed ANN and SVM model was additionally evaluated for reliability using error analysis models such as the root mean square error (RMSE), mean absolute error (MAE), and sum of square error (SSE). The error analysis results of the ANN and SVM are summarized in Table 6. The RMSE measures the difference between the toxicity values predicted by the model and the actual values [52R,53R; SM]. The values were 0.37 and 0.46 for AChE and CYP450, respectively, from the ANN, while 0.08 and 0.10 for SVM, indicating that the SVM is a better model. The MAE of each individual prediction error on all occurrences in the test set is the MAE of a model for the test set. The discrepancy between a forecast's expected value and its real value is known as a prediction error [54R; SM]. The ANN MAE for AChE and CYP450 were higher than those of SVM. Similar results were also obtained for the SSE. SSE is an accuracy metric that adds squared errors. When the data points are of equal magnitude, it is utilized to assess the forecasting model's accuracy [53R; SM]. The RMSE, MAE, and SSE values were lower for SVM, and the R^2 values were high for TcAChE and Zf CYP450, respectively, compared to ANN. These indicate that the system's prediction is more reliable for the SVM than the ANN model [55R; SM].

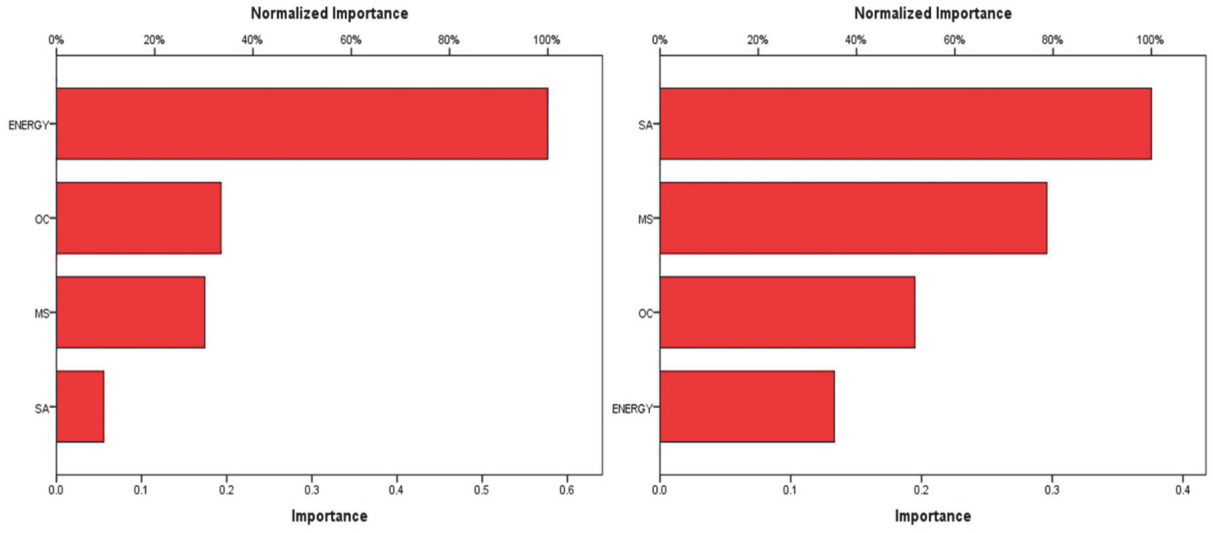

Fig. 6. The most important of NPs property from the ANN in predicting toxicity to (a) AChE (b) CYP450

Table 6. Error analysis results for the ANN

ML Algorithm	Model	AChE	CYP450
ANN	R^2	0.859	0.773
	RMSE	0.37	0.46
	MAE	0.55	0.65
	SSE	0.53	0.64
SVM	R^2	0.995	0.995
	RMSE	0.08	0.10
	MAE	0.06	0.07
	SSE	0.02	0.03

4. Conclusion

The present study examined the toxicity of Polyethylene Terephthalate Nanoplastics (PET NPs) to aquatic organisms through molecular docking and machine learning. The toxicity of the PET NPs increased with increasing size to a certain limit (16 nm), after which there was a drop in its toxicity due to inefficient enzyme-NP binding. Using the characteristics data from the PET NPs, the factors responsible for its toxicity were evaluated by the Machine Learning approach based on the Artificial Neural Network (ANN) and Support Vector Machine (SVM) model. The model was built for each component to predict the toxicity behavior of the PET NPs to zebrafish and electric ray fish, respectively. The predicted data obtained using SVM was at high accuracy for support vectors of 4, with $R^2 > 0.99$ and showed that surface area and reactivity (energy) were the most important properties for PET NPs toxicity. The study confirmed that the size of PET NPs can influence their toxicity to aquatic organisms, and the surface area and reactivity (energy) of the NPs are important for their toxicity.

5. Supplementary Materia l (SM)

Table S1 and S2 presented in SM. Also, more references from 41R- 55R moved to SM.

6. Conflicts of Interest

There are no conflicts of interest to declare.

7. Funding

This study was partially supported by the Special Funds for Basic Research (B) (No.22H03747, FY2022-FY2024) of Grant-in-Aid for Scientific Research of the Japanese Ministry of Education, Culture, Sports, Science and Technology (MEXT).

8. References

[1] A.W. Verla, C.E. Enyoh, E.N. Verla, K. Nwanorh. Microplastic–toxic chemical interaction: a review study on quantified levels, mechanism and implication, SN Appl. Sci. 1 (2019a) 1400. https://doi.org/10.1007/s42452-019-1352-0

[2] Y. Chen, A.K. Awasthi, F. Wei, Q. Tan, J. Li, Single-use plastics: Production, usage, disposal, and adverse impacts, Sci. Total Environ., 752 (2021) 141772. https://doi.org/10.1016/j.scitotenv.2020.141772

[3] S.A.L. Patrício, J.C. Prata, T.R. Walker, A.C. Duarte, W. Ouyang, D. Barcelò, Increased plastic pollution due to COVID-19 pandemic: Challenges and recommendations, Chem. Eng. J., 405 (2021) 126683. https://doi.org/10.1016/j.cej.2020.126683

[4] C.E. Enyoh, Q. Wang, T. Chowdhury, W. Wang, S. Lu, K. Xiao, M.A.H Chowdhury, New analytical approaches for effective quantification and identification of nanoplastics in environmental samples, Processes, 9 (2021) 2086. https://doi.org/10.3390/pr9112086

[5] C. E. Enyoh, L. Shafea, A. W. Verla, E. N. Verla, W. Qingyue, T. Chowdhury, M. Paredes, Microplastics exposure routes and toxicity studies to ecosystems: An overview,

Environ. Anal. Health Toxicol., 35(1) (2020) 1–10. https://doi.org/10.5620/eaht.e2020004.

[6] C.E. Enyoh, A.W. Verla, E.N. Verla, Airborne microplastics: a review study on method for analysis, occurrence, movement and risks, Environ. Monit. Assess., 191 (2019) 668. https://doi.org/10.1007/s10661-019-7842-0

[7] C.E. Enyoh, W. Qingyue, V.A. Wirnkor, T. Chowdhury, Index models for ecological and health risks assessment of environmental micro-and nano-sized plastics, AIMS Environ. Sci., 9 (2022) 51-65. https://doi.org/10.3934/environsci.2022004

[8] P. Schwabl, S. Köppel, P. Königshofer, T. Bucsics, M. Trauner, T. Reiberger, B. Liebmann, Detection of various microplastics in human stool: A prospective case series, Ann. Inter. Med., 171 (2019) 453–457. https://doi.org/10.7326/M19-0618

[9] A. Ragusa, A. Svelato, C. Santacroce, P. Catalano, V. Notarstefano, O. Carnevali, F. Papa, M. C. A. Rongioletti, F. Baiocco, S. Draghi, E. D'Amore, D. Rinaldo, M. Matta, E. Giorgini, Plasticenta: First evidence of microplastics in human placenta, Environ. Int., 146 (2021) 106274. https://doi.org/10.1016/j.envint.2020.106274

[10] A.P. Araújo, T. Marinho, T. Lopes, Toxicity evaluation of the combination of emerging pollutants with polyethylene microplastics in zebrafish: Perspective study of genotoxicity, mutagenicity, and redox unbalance, J. Hazard. Mater., (2022) 432. https://doi.org/10.1016/j.jhazmat.2022.128691

[11] J. Bhagat, L. Zang, N. Nishimura, Y. Shimada, Zebrafish: An emerging model to study microplastic and nanoplastic toxicity, The Sci. total environ., 728, (2020) 138707. https://doi.org/10.1016/j.scitotenv.2020.138707

[12] R.L. Bailone, H.C.S. Fukushima, V. Fernandes, Zebrafish as an alternative animal model in human and animal vaccination research, Lab. Anim. Res., 36 (2020) 13. https://doi.org/10.1186/s42826-020-00042-4

[13] M. Ignacio, K. Le Menach, M. Devier, M.P. Cajaraville, H. Budzinski, A. Orbea, Screening of the toxicity of polystyrene nano- and microplastics alone and in combination with benzo(a)pyrene in brine Shrimp Larvae and Zebrafish embryos, Nanomater., 12 (2022) 941. https://doi.org/10.3390/nano12060941

[14] P.S. Pallan, L.D. Nagy, L. Lei, E. Gonzalez, Structural and kinetic basis of steroid 17α,20-lyase activity in teleost fish cytochrome P450 17A1 and its absence in cytochrome P450 17A2, J. Biol. Chem., 290 (2015) 3248-268. https://doi.org/10.1074/jbc.M114.627265

[15] J.V. Goldstone, A.G. McArthur, A. Kubota, Identification and developmental expression of the full complement of Cytochrome P450 genes in Zebrafish, BMC Genom., 11 (2010) 643. https://doi.org/10.1186/1471-2164-11-643

[16] P.R. Last, W.T. White, M.R. de Carvalho, B. Séret, M.F.W. Stehmann, G.J.P. Naylor, Rays of the world. CSIRO Publishing, Comstock Publishing Associates, i-ix, pp. 1-790, 2016. https://www.cornellpress.cornell.edu/book/9781501705328/rays-of-the-world/#bookTabs=1

[17] S.W. Michael, Reef sharks and rays of the world. A guide to their identification, behavior, and ecology, Sea Challengers Monterey California publisher, 107 pages, 1993. https://doi.org/10.1017/S0025315400034998

[18] M. R. Aidan, ReefQuest Centre for Shark Research, Electric Rays publisher, 2008. http://www.elasmo-research.org/education/shark_profiles/torpediniformes.htm

[19] C. Sommer, W. Schneider, J.M. Poutiers, FAO species identification field guide for fishery purposes, the living marine resources of Somalia, FAO publisher, Rome, 376 pages, 1996. https://www.fao.org/3/y0770e/y0770e.pdf

[20] M.B. Colović, D.Z. Krstić, T.D. Lazarević-Pašti, A.M. Bondžić, V.M. Vasić, Acetylcholinesterase inhibitors: pharmacology and toxicology, Curr. Neuropharmacol., 11 (2013) 315-335. https://

doi.org/10.2174/1570159X11311030006

[21] A. D. Gray, J. E. Weinstein, Size- and shape-dependent effects of microplastic particles on adult daggerblade grass shrimp (*Palaemonetes pugio*), Environ. Toxicol. Chem., 36 (2017) 3074–3080. https://doi.org/10.1002/etc.3881

[22] A. Banerjee, L.O. Billey, W.L. Shelver, Uptake and toxicity of polystyrene micro/nanoplastics in gastric cells: Effects of particle size and surface functionalization, PLOS ONE, 16 (12) (2021) e0260803. https://doi.org/10.1371/journal.pone.0260803

[23] C.E. Duru, I.A. Duru, C.E. Enyoh, In silico binding affinity analysis of microplastic compounds on PET hydrolase enzyme target of Ideonella sakaiensis, Bull. Natl. Res. Cent., 45 (2021) 104. https://doi.org/10.1186/s42269-021-00563-5

[24] V. Zhou, Machine learning for beginners: An introduction to neural networks, Medium, 2019. https://towardsdatascience.com/machine-learning-for-beginners-an-introduction-to-neural-networks-d49f22d238f9

[25] C. Duru, C. Enyoh, I.A. Duru, M.C. Enedoh, Degradation of PET nanoplastic oligomers at the novel PHL7 target: Insights from molecular docking and machine learning, J. Niger. Soc. Phys. Sci., 5 (2023) 1154–1154. https://doi.org/10.46481/JNSPS.2023.1154

[26] F. Yu, X. Hu, Machine learning may accelerate the recognition and control of microplastic pollution: Future prospects, J. Hazard. Mater., 432 (2022) 128730. https://doi.org/10.1016/j.jhazmat.2022.128730

[27] X. Wu, Z. Qixing, M. Li, H. Xiangang, Machine learning in the identification, prediction and exploration of environmental toxicology: challenges and perspectives, J. Hazard. Mater., 438 (2022) 129487. https://doi.org/10.1016/j.jhazmat.2022.129487.

[28] C. E. Enyoh, Q. Wang, P. E. Ovuoraye, T. O. Maduka, Toxicity evaluation of microplastics to aquatic organisms through molecular simulations and fractional factorial designs, Chemosphere, 308(Pt 2) (2022) 136342. https://doi.org/10.1016/j.chemosphere.2022.136342

[29] H.M. Greenblatt, C. Guillou, D. Guénard, A. Argaman, S. Botti, B. Badet, The complex of a bivalent derivative of galanthamine with torpedo acetylcholinesterase displays drastic deformation of the active-site gorge: implications for structure-based drug design, J. Am. Chem. Soc., 126 (2004) 15405-15411. https://doi.org/10.1021/ja0466154

[30] R.T. Peterson, C.A. Macrae, Systematic approaches to toxicology in the zebrafish, Annu. Rev. Pharm. Toxicol., 52 (2012) 433-453. https://doi.org/10.1146/annurev-pharmtox-010611-134751

[31] C.E. Duru, Duru I.A., A. Bilar, Computational investigation of sugar fermentation inhibition by bergenin at the pyruvate decarboxylate isoenzyme 1 target of *Scharomyces cervisiae*, J. Med. Plants Stud., 8(6) (2020) 21-25. https://doi.org/10.22271/plants.2020.v8.i6a.1225

[32] C.E. Duru, Duru I.A., A.E. Adegboyega, In Silico identification of compounds from *Nigella sativa* seed oil as potential inhibitors of SARS-CoV-2 targets, Bull. Natl. Res. Cent., 45 (2021) 57. https://doi.org/10.1186/s42269-021-00517-x

[33] C.E. Enyoh, O.M. Tochukwu, C. E. Duru, S.C. Osigwe, C.B.C. Ikpa, Q. Wang, In silico binding affinity studies of microbial enzymatic degradation of plastics, J. Hazard. Mater. Adv., 6 (2022)100076. https://doi.org/10.1016/j.hazadv.2022.100076.

[34] BIOVIA, Dassault Systemes, San Diego, Discovery studio modeling environment, 2020. https://docslib.org/doc/9937570/biovia-discovery-studio%C2%AE-2020

[35] C.E. Enyoh, C.E. Duru, E. Prosper, Q. Wang, Evaluation of nanoplastics toxicity to the human placenta in systems, J. Hazard. Mater., 446 (2023) 130600. https://doi.org/10.1016/j.jhazmat.2022.130600

[36] H. Tang, K. C. Tan, Z. Yi, Neural networks: Computational models and applications. Heidelberg, Germany: Springer, 2007. https://link.springer.com/book/10.1007/978-3-540-69226-3

[37] C.E. Enyoh, Q. Wang, L. Senlin, Optimizing the efficient removal of ciprofloxacin from aqueous solutions by polyethylene terephthalate microplastics using multivariate statistical approach, Chem. Eng. Sci., 278 (2023) 118917. https://doi.org/10.1016/j.ces.2023.118917

[38] C.E. Enyoh, P. Ovuoraye, O. Isiuku, C. Igwegbe, Artificial neural network and response surface design for modeling the competitive biosorption of pentachlorophenol and 2,4,6-trichlorophenol to canna indica L. in Aquaponia, Anal. Methods in Environ. Chem. J., 6 (2023) 79-99. https://doi.org/10.24200/amecj.v6.i01.228

[39] A. Yettou, M. Laidi, A. El Bey, S. Hanini, M. Hentabli, O. Khaldi, and M. Abderrahim Ternary Multicomponent Adsorption Modelling Using ANN, LS-SVR, and SVR Approach – Case Study, Kem. Ind., 70 (2021) 509−518. https://doi.org/10.15255/KUI.2020.071 KUI-36/2021

[40] C.E. Enyoh, Q. Wang, W. Weiqian, C. Tanzin, H.R. Mominul, I. Md. Rezwanul, Sorption of per- and polyfluoroalkyl substances (PFAS) using Polyethylene (PE) microplastics as adsorbent: Grand canonical Monte Carlo and molecular dynamics (GCMC-MD) studies, Int. J. Environ. Anal. Chem., (2022) 1-19. https://doi.org/10.1080/03067319.2022.2070016

(References from 41R-55R showed in SM)

Anal. Methods Environ. Chem. J. 6 (3) (2023) 54-66

AMECJ

Research Article, Issue 3
Analytical Methods in Environmental Chemistry Journal
Journal home page: www.amecj.com/ir

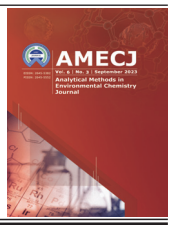

Starch nanocomposite containing hydroxyapatite and eggshell for absorbing methylene blue dye from aqueous solution

Negar Motakef Kazemi[a, *], and Nooshin Nassaj[b]

[a]*Department of Medical Nanotechnology, Faculty of Advanced Sciences and Technology, Tehran Medical Sciences(TMS), Islamic Azad University, Tehran, Iran*

[b]*Department of Nanobiomimetic, Faculty of Advanced Sciences and Technology, TMS, Islamic Azad University, Tehran, Iran*

ARTICLE INFO:

Received 29 Apr 2023
Revised form 15 Jul 2023
Accepted 14 Aug 2023
Available online 29 Sep 2023

Keywords:
Nanocomposite,
Starch,
Hydroxyapatite,
Eggshell,
Methylene blue,
UV-Vis spectrophotometer

ABSTRACT

Today, polymer nanocomposites (NCs) have become important as suitable candidates for nano absorbents due to their simplicity and cheapness. This research investigated a nano absorbent based on starch nanocomposite containing hydroxyapatite (HA) and eggshell inspired by nature to absorb methylene blue (MB) as a toxic cationic dye from aqueous solution. The effect of temperature, pH, and the ratio of hydroxyapatite and eggshell absorbent on the amount of absorption after immersion in an aqueous medium was measured. The samples were identified by the UV-Vis spectrophotometer, scanning electron microscope (SEM), X-ray energy dispersive spectrometry (EDS), Fourier transform infrared (FTIR), X-ray diffraction (XRD), and BET analysis. Based on the results, the biological nanocomposite of starch-containing 0.125 g hydroxyapatite and eggshell, inspired by nature, has the highest absorption (88%) of methylene blue dye from the aqueous solution quickly. Increasing temperature, increasing pH, and decreasing the amount of nano absorbent increased the absorption of methylene blue dye from the aqueous solution. The results show that starch nanocomposite containing hydroxyapatite and eggshell can absorb methylene blue dye and have good potential for various applications, especially in medical and industrial fields.

1. Introduction

Starch is widely used as a biodegradable, biocompatible, environmentally friendly and non-toxic material with renewable resources [1]. Regardless of its unique properties, starch has limitations such as poor processability, low mechanical properties, poor long-term stability, and high sensitivity to water, which are essential for developing starch nanocomposites. Starch nanocomposites comprise starch polymer as a base and nanometer-scale fillers as reinforcement [2]. Today, bio-based nanocomposites have expanded due to their distinct properties [3, 4]. The starch nanocomposite is a promising starting point for producing materials with environmentally friendly, biodegradable, low toxicity, low cost and biocompatibility properties. The development of new starch-based bio nanocomposites with improved properties has attracted specific applications, including food, agriculture, packaging, environmental remediation, textile, cosmetic, pharmaceutical, and biomedical fields [5, 6]. Hydroxyapatite with the general formula $Ca_{10}(PO_4)_6(OH)_2$ is used as a mineral, green and environmentally friendly adsorbent for wastewater treatment due to its extraordinary ability to absorb

*Corresponding Author: Negar Motakef Kazemi
Email: motakef@iaups.ac.ir
https://doi.org/10.24200/amecj.v6.i03.250

heavy metal ions, radionuclides, organic pollutants, and fluoride ions. The adsorption mechanisms of this compound include ion exchange reaction, surface complexation, and physical adsorption (such as electrostatic interaction and hydrogen bonding). Therefore, the use of hydroxyapatite nanocomposites has expanded today8 ,7]]. Eggshell has been used as recycled biological waste in the nanoscale to modify nanocomposites with an economical and simple method [9]. Nowadays, nanomaterials have attracted a lot of attention due to their small size and high surface area in various fields such as drug delivery [10], food packaging [11], energy [12], and absorption of dangerous substances [13]. Various physical, chemical, and biological methods have been developed to remove dyes from aqueous solutions (Table. 1). There are different physical methods, such as filtration processes (membrane, nanofiltration, ultra/microfiltration), reverse osmosis, ion exchange, irradiation, electrolysis, coagulation-flocculation, and adsorption to remove dye pollutants from wastewater [14, 15]. Currently, the use of adsorbents is of interest due to their high efficiency, economic feasibility, and simplicity of design for color removal [16]. Investigating the absorption rate of different pollutants is one of the critical applications of nanomaterials based on starch [17, 18], hydroxyapatite [7, 19] and eggshell [20-22]. Therefore, the absorption of starch nanocomposite containing hydroxyapatite and eggshell nanomaterials has been investigated in this research.

Water is one of the most important natural resources in the world for the survival of all living organisms and human growth. Wastewater has harmful effects on water and the environment. As one of the main effluents and pollutants, toxic dyes harm water, environment and living organisms [22]. Therefore, different physical, chemical, biological or combination methods are necessary for water purification [23]. Methylene blue is a heterocyclic molecule with the chemical formula $C_{16}H_{18}CIN_3S$, which is widely used in the pharmaceutical, textile, plastic, leather, cosmetics, and paper industries [24]. Methylene blue is a water-soluble, toxic, carcinogenic and non-biodegradable cationic dye [25]; hence, it can seriously threaten the ecosystem, and human health negatively affects the environment [26, 27]. Recently, methylene blue dye was absorbed by nanomaterials in aqueous solutions in an easy and efficient approach [28, 29]. Nano adsorbents based on starch [30, 31], hydroxyapatite and eggshell are important for methylene removal. Therefore, the importance and innovation of this research is the modification of starch nanocomposite with hydroxyapatite and eggshell to absorb methylene blue dye from aqueous solution as a biological nano absorbent inspired by nature.

2. Experimental

2.1. Reagents and Materials

Starch methylene blue was purchased from Merck (Germany). Hydroxyapatite was prepared from the Technical Research Campus of Yazd (Iran). The eggshell was procured in June 1400 from Sahar Brand Paya Bread Company (Iran). Normal soda solution (NaOH) and standard hydrochloric acid (HCl) were used by CAS numbers 1310-73-2 and 100317, respectively, from Merck Millipore.

Table 1. Comparison of MB removal methods [15].

Method	Techniques
Physical removal	Filtration processes (membrane, nanofiltration, ultra/microfiltration), Reverse osmosis, Ion exchange, Irradiation, Electrolysis, Coagulation-flocculation, Adsorption.
Chemical removal	Non-photochemical: Ozonation, Fenton system. Photochemical: UV light-assisted advanced oxidation process, catalyst-assisted advanced oxidation process, Electrochemical advanced oxidation processes.
Biological removal	Biodegradation of methylene blue dye, Biocatalytic degradation of methylene blue dye.

2.2. Methods

It Includes sample preparation (Eggshell nanoparticles, Starch-hydroxyapatite nanocomposite, Starch-eggshell nanocomposite, and Starch nanocomposite containing hydroxyapatite-eggshell) and general procedure.

2.2.1. Preparation of eggshell nanoparticles

First, the membrane attached to the eggshell was separated and cleaned several times with tap water. Place the washed eggshell in the oven at 105 ºC for two hours until it dries completely. Then, the dry eggshell was powdered and reached the nanometer scale using a ball mill.

2.2.2. Preparation of starch-hydroxyapatite nanocomposite

A 0.5% starch solution was prepared in distilled water. Then hydroxyapatite with ratios of 0.125, 0.25, 0.5 and 0.75% by weight was mixed in the starch solution. Finally, the final nanocomposite was isolated and dried.

2.2.3. Preparation of starch-eggshell nanocomposite

Nanoscale eggshell with ratios of 0.125, 0.25, 0.5 and 0.75% by weight was added to a 0.5% starch solution in distilled water and stirred. Finally, the final nanocomposite was isolated and dried. It should be noted that the nanocomposite with a ratio less than 0.125 was not investigated due to instability.

2.2.4. Preparation of starch nanocomposite containing hydroxyapatite-eggshell

Nanoscale hydroxyapatite and eggshell were added to 0.5% starch solution in distilled water and stirred. Finally, the final nanocomposite was isolated and dried.

2.2.5. Examination of methylene blue dye absorption

First, Landa Max of 3.0 mg L^{-1} (ppm) methylene blue solution was checked by spectrophotometer in the range of 250 to 700 nm, and the wavelength was determined at 664 nm. Then, the samples' absorption rate of methylene blue (3.0 mg L^{-1}) was checked at ambient temperature (25°C). Finally, the changes in temperature, pH of the solution, and the amount of nanosorbent were investigated for the optimal sample. 0.1 standard soda solution and 0.1 standard hydrochloric acid were used to adjust the pH. After shaking and centrifuging the sample (MB), the MB adsorbed on starch nanocomposite containing hydroxyapatite-eggshell at optimized pH and separated by centrifuge system before determination by the UV-Vis spectrometry (Fig. 1).

2.3. Characterization and Instrumental

The samples were investigated by methods of UV-Vis spectrophotometer to study methylene blue absorption, scanning electron microscope to evaluate shape and size, X-ray energy dispersive spectrometry for chemical analysis, Fourier

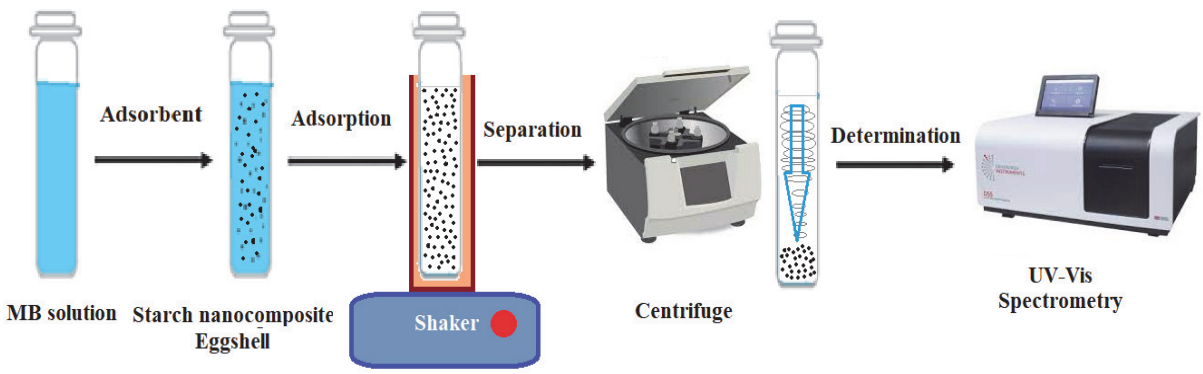

Fig. 1. A schematic diagram of methylene blue dye absorption

transform infrared to determine the functional groups, X-ray diffraction to check the crystal structure, and BET analysis to measure the surface area. In this research, ball mill machines made in Iran to prepare nanoscale eggshells, UV-Vis spectrophotometer PG Instrument model T80 made in Australia to study the amount of methylene blue absorption, scanning electron microscope TESCAN model MIRA lll made by the Czech Republic company with the copper coating to evaluate the shape and size. FTIR of Thermo device Avatar model made in USA by KBr tablets at room temperature to check the functional group. XRD device of Philips model PW1730 made in the Netherlands to determine the crystal structure. BET device of Bel model BELSORP MINI ll made in Japan to measure the surface area.

3. Results and discussions

3.1. Optimization parameters

The absorption percentage of methylene blue dye by 0.1 g of the samples was checked in 5 min (Table 2). Based on the results, eggshell nanoparticles have the highest absorption compared to hydroxyapatite. The nanocomposite has the highest absorption due to the synergistic effect of these compounds, but increasing the ratio of nanocomposite components has decreased the absorption percentage due to the accumulation and reduction of the contact surface. The nanocomposite sample of starch and 0.125 g of hydroxyapatite and eggshell had the highest absorption (88 %) and was chosen as the optimal sample.

Based on the temperature change results for the optimal sample, increasing the temperature up to 35 degrees has no apparent effect on absorption, but increasing the temperature up to 45 degrees has increased movement and absorption (Table 3). Based on the results of pH changes for the optimal sample, its increase caused an increase in absorption. The highest absorption was observed at pH 10, 94% (Table 4). Due to the results of changes in the amount of nano absorbent for the optimal sample, the increase in the amount of nano absorbent probably caused a decrease in absorption due to the increase in accumulation and the reduction in the available surface area (Table 5). Finally, the absorption of methylene blue by 0.0125 grams of starch nanocomposite sample and 0.125 grams of hydroxyapatite and eggshell was investigated as the optimal sample at a temperature of 45 degrees Celsius and a pH of 10, and 98% was calculated as the maximum absorption.

Table 2. Methylene blue absorption rate by the samples.

Sample	Absorption percentage(٪)
Eggshell	37
Starch	87
Hydroxyapatite	18
Nanocomposite with 0.125 g of eggshell	75
Nanocomposite with 0.25 g of eggshell	51
Nanocomposite with 0.5 g of eggshell	28
Nanocomposite with 0.75 g of eggshell	33
Nanocomposite with 0.125 g of hydroxyapatite	73
Nanocomposite with 0.25 g of hydroxyapatite	61.2
Nanocomposite with 0.5 g of hydroxyapatite	54
Nanocomposite with 0.75 g of hydroxyapatite	43
Nanocomposite (0.125g eggshell+0.125g Hydroxyapatite)	88
Nanocomposite (0.25 g eggshell+0.25 g Hydroxyapatite)	45
Nanocomposite (0.5 g eggshell+0.5 g Hydroxyapatite)	37
Nanocomposite (0.75 g eggshell+0.75 g Hydroxyapatite)	42

Table 3. Examination of temperature changes on the amount of methylene blue absorption by the optimal sample.

Temperature of solution (°C)	Absorption percentage (%)
25	88
35	83
45	92

Table 4. Examining pH changes on the amount of methylene blue absorption by the optimal sample.

pH	Absorption percentage(٪)
2	48
4	53
7	79
9	86
10	94

Table 5. Examining changes in the amount of nano absorbent on the absorption of methylene blue by the optimal sample.

The amount of Nano absorbent (g)	Absorption Percentage (%)
0.00625	97
0.01250	97
0.0250	95
0.0500	92
0.1000	88
0.2000	84
0.3000	72

3.2. Scanning Electron microscopy and EDS images

The shape and size of samples were checked by scanning electron microscope in Figure 2. It confirmed the results of spherical and uniform nanoparticles with an average nanometer size. Also, the absorption of methylene blue does not affect the shape and size of the nanocomposite.

The X-ray energy dispersive spectroscopy results are shown in Figure 3 and confirm the chemical composition. Based on these results, the elemental analysis of the samples was confirmed.

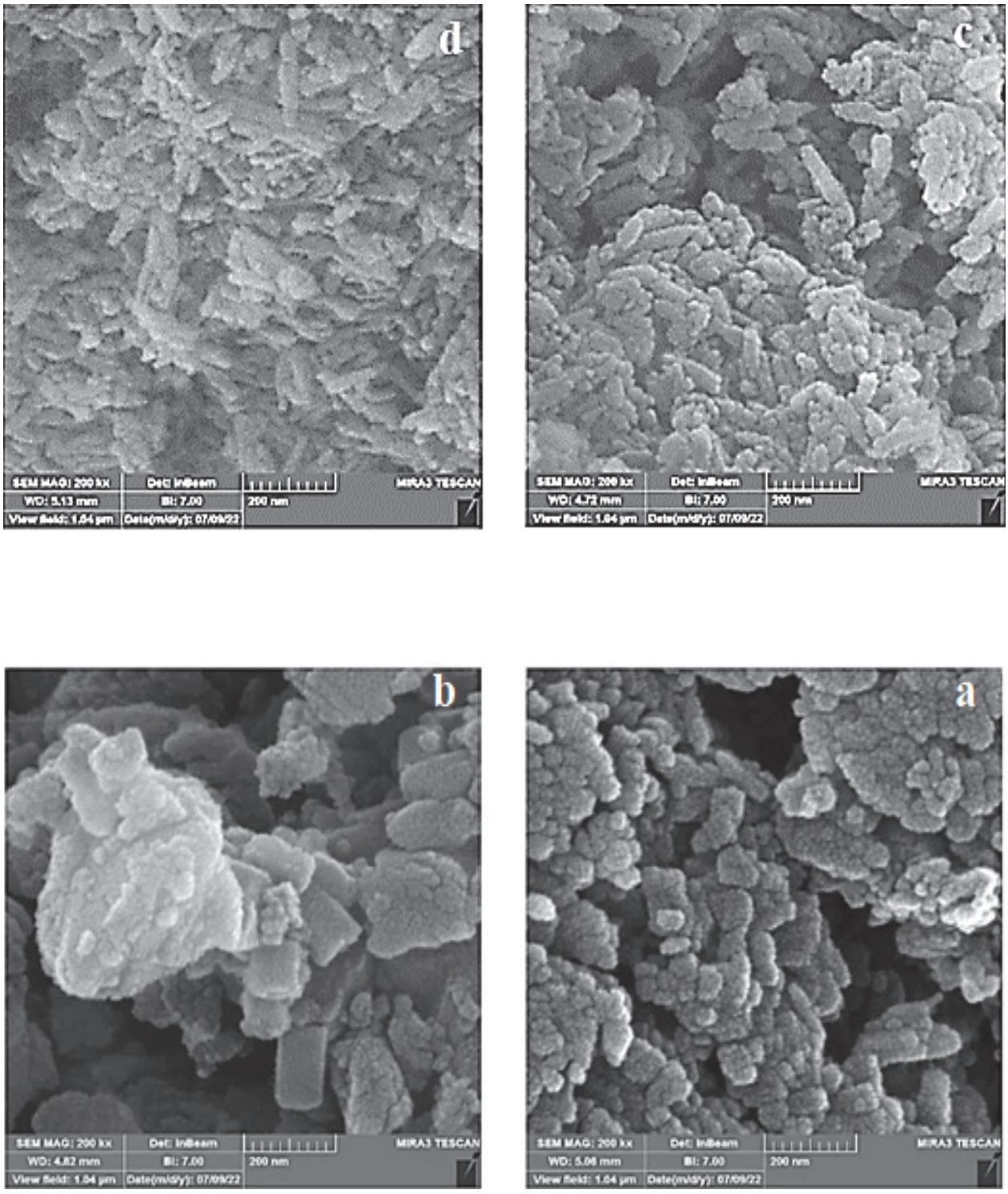

Fig. 2. SEM image of a) hydroxyapatite, b) eggshell, c) optimized nanocomposite before adsorption, and d) optimized nanocomposite after adsorption.

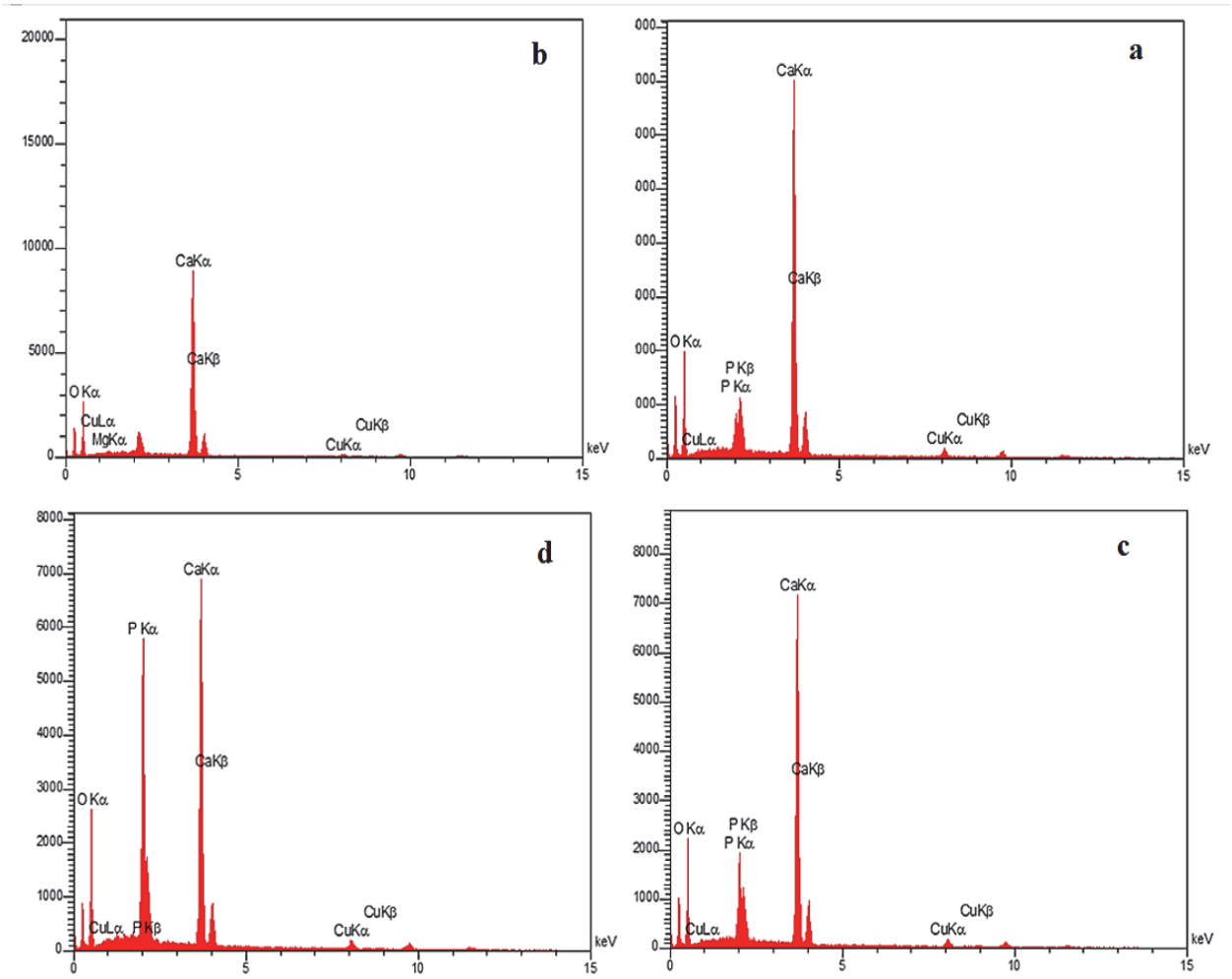

Figure 3. EDS image of a) hydroxyapatite, b) eggshell, c) optimized nanocomposite before adsorption, and d) optimized nanocomposite after adsorption

3.3. FTIR Spectra

The IR absorption spectra of the samples were recorded in the 400–4000 cm-1 range with KBr pellets. FTIR spectrum is shown in Figure 4 to identify functional groups. For starch, the 3000-3700 cm-1 peak indicates the O-H bond, which causes stretching vibrations of intermolecular and intramolecular hydroxyl groups. The peak in the range of 2600-2950 cm^{-1} indicates the C-H bond. The peak in the range of 1500-1800 cm^{-1} indicates the C=O double bond. As shown in the diagram, hydroxyapatite's peak in the wavelength range of 3700-3300 cm^{-1} is related to the O-H bond. The 1000 and 600 cm-1 peak indicates carbonate (CO_3^{-2}) and phosphate (PO_4^{3-}), respectively. For eggshells, the peak in the range of 3500 cm^{-1} indicates the O-H bond. The peak related to C=O and C=C bonds is observed in the 1600-1700 cm-1 range. Considering that a significant part of the eggshell is composed of calcium carbonate, the peaks below 1000 cm^{-1} correspond to CO_3^{-2} in calcium carbonate $CaCO_3$. The peak at 3434 cm-1 indicates O-H and N-H bonds for methylene blue. The CH=N bond is at 1599 $cm^{-1,}$ and the C=C bond is in the 1400-1500 cm-1 range. Peaks in the range of 1300-1400 cm^{-1} correspond to CH_2- and CH_3- and in the range of 1200 cm^{-1} correspond to C-N and N-N, 1176 cm^{-1} correspond to C-H and 1141 cm^{-1} correspond to C–N, and 1066 cm^{-1} corresponds to C–S–C. The FTIR results qualitatively confirm the nanocomposites' functional groups and aggregate peaks.

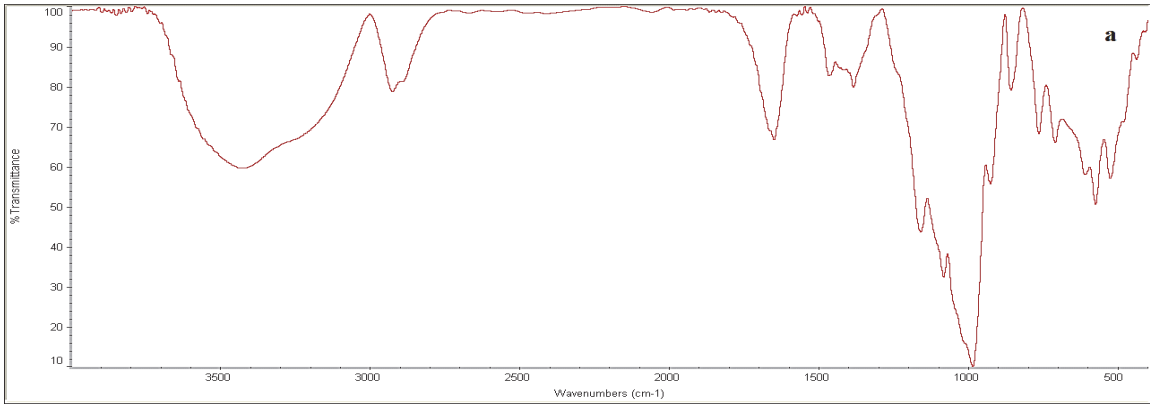
a
% Transmittance
Wavenumbers (cm-1)

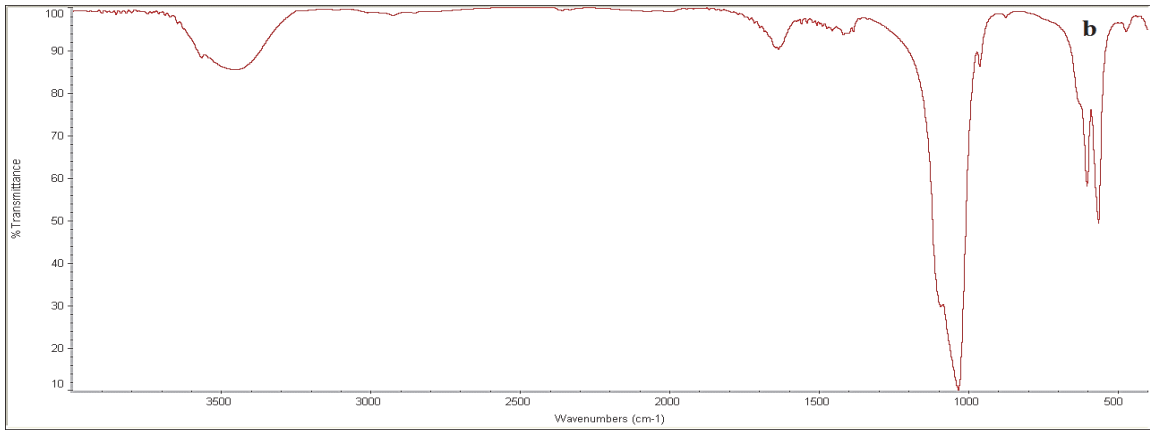
b
% Transmittance
Wavenumbers (cm-1)

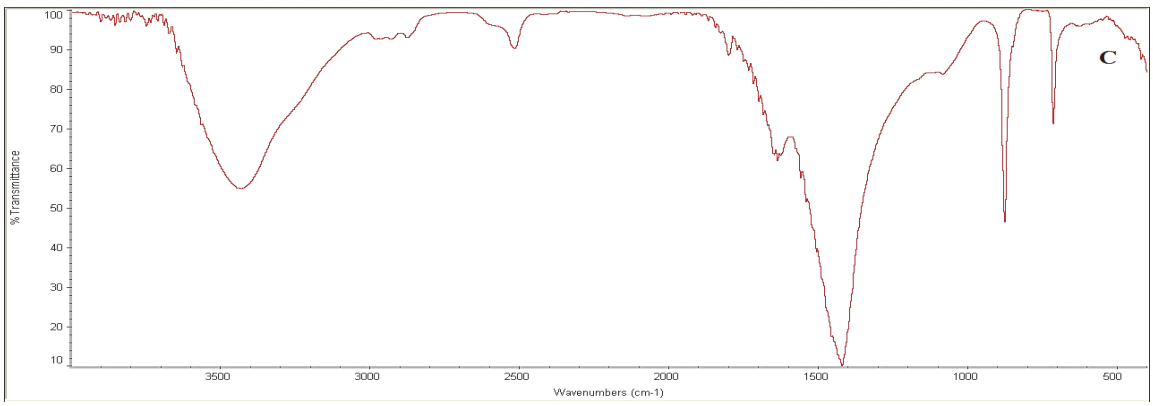
C
% Transmittance
Wavenumbers (cm-1)

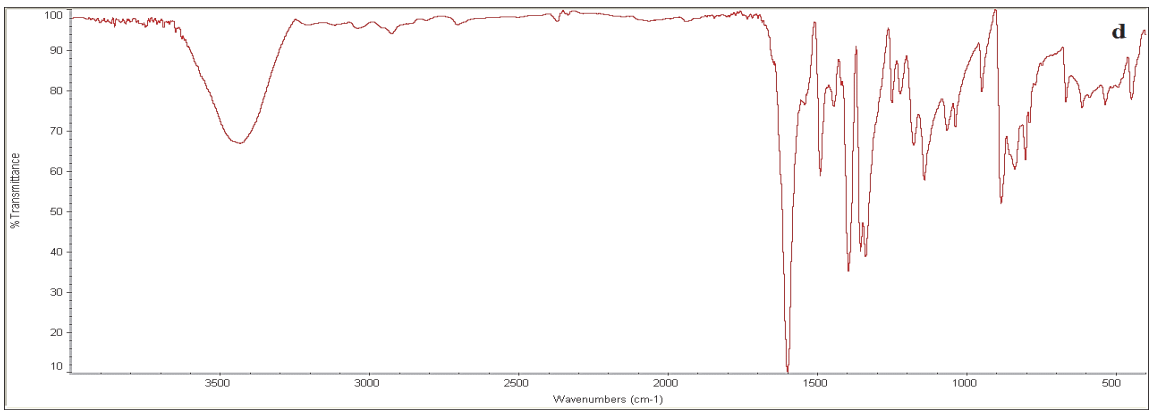
d
% Transmittance
Wavenumbers (cm-1)

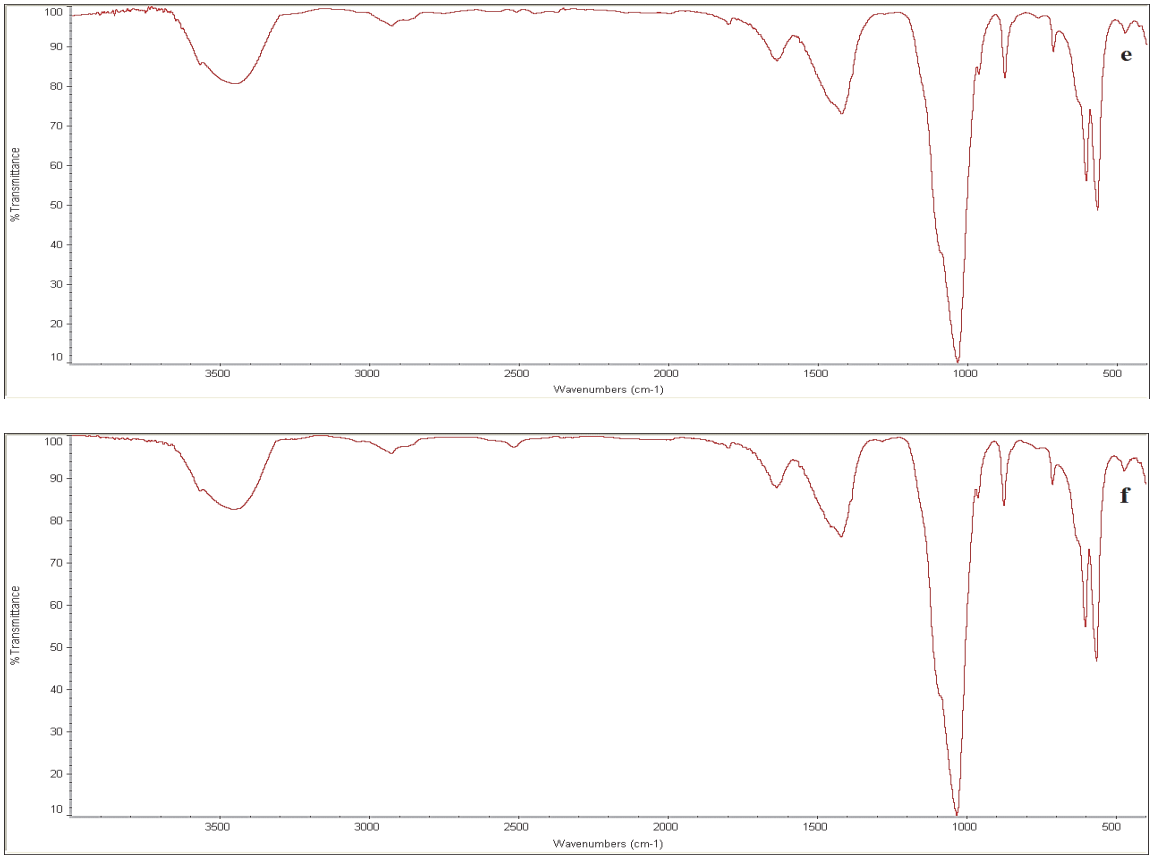

Fig. 4. FTIR spectra for a) starch, b) hydroxyapatite, c) eggshell, d) methylene blue, e) optimized nanocomposite before adsorption, and f) optimized nanocomposite after adsorption.

3.4. XRD pattern

The X-ray diffraction pattern was used to identify the crystal structure in 10° to 70° pairs (Figure 5), which proved the crystalline structure. Based on the results, characteristic peaks of eggshell and hydroxyapatite were observed in the final nanocomposite.

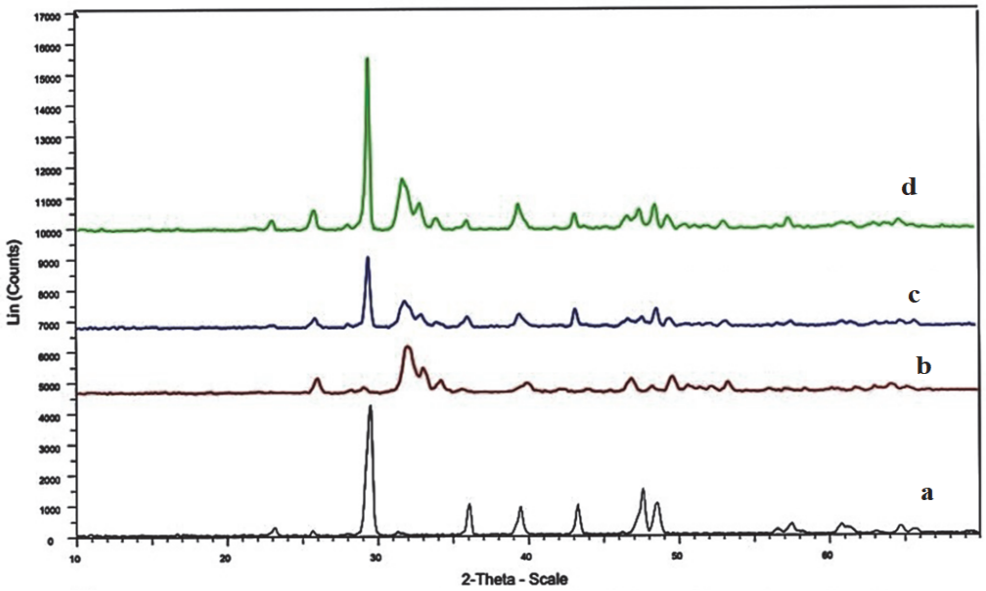

Fig. 5. XRD spectra for a) eggshell, b) hydroxyapatite, c) optimized nanocomposite before adsorption, and d) optimized nanocomposite after adsorption

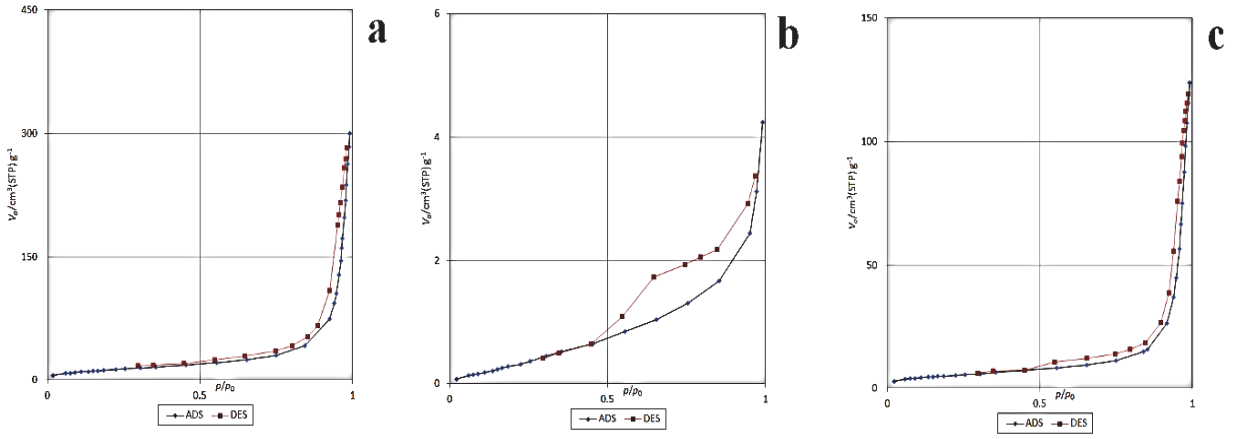

Fig. 6. BET analysis for a) hydroxyapatite, b) eggshell nanoparticles, and c) optimized nanocomposite.

3.5. BET Analysis

The results of adsorption and desorption isotherm to check the surface area are shown in Figure 6. Based on the surface area results for hydroxyapatite, eggshell, and nanocomposite, the optimal surface area is 47.08, 1.27, and 18.85 $m^2 g^{-1}$, respectively. In other words, hydroxyapatite has the largest surface area, which is confirmed by SEM results and the smaller size of nanoparticles.

3.6. Discussion

The spectrophotometer results showed that the nanocomposite of starch and 0.125 g of hydroxyapatite and eggshell have the highest absorption of methylene blue dye from the aqueous solution. In general, the increase in the percentage of nanocomposite components due to the decrease in the available surface has caused a reduction in the absorption percentage. Temperature changes have no noticeable effect on absorption. An increase in pH causes an increase in absorption due to more active sites, a decrease in the competition between positive charges and an increase in the adsorption of methylene blue through electrostatic attraction. These results confirm the previous report [32]. As a result, many OH- are available on the surface, and the adsorbent surface tends to be negatively charged. Hence, the affinity for exchanging OH^- ions with the cationic dye solution increases [33]. Based on the SEM results, hydroxyapatite was observed as spherical nanoparticles with an average size of 49 nm, eggshell spherical nanoparticles with an average size of 100 nm, and the presence of nanoparticles in the optimal nanocomposite before and after absorption was observed. Based on EDS results, oxygen (O), phosphorus (P) and calcium (Ca) elements were observed in hydroxyapatite [34] and oxygen, magnesium (Mg) and calcium in eggshells [35], according to other reports. FTIR results confirm the functional groups of starch [36], hydroxyapatite [37], eggshell [38], and methylene blue [39] based on previous reports. In the XRD pattern of hydroxyapatite, the peaks at 2θ are 26º, 32º, and 33º corresponding to the crystal plane (102), (211), and (300) according to the JCPDS standard card (896438) [40]. The high percentage of eggshell is composed of $CaCO_3$, and the 2θ peaks are equal to 29.1, 35.7º, 39.3º, 43.7º and 48.3º corresponding to the crystal plate (104), (110), (113), (202) and (116). The composition of $CaCO_3$ is according to the standard card 1934-002-99.

4. Conclusion

The optimal sample of starch nanocomposite and 0.125 g of hydroxyapatite-eggshell with 0.1 g and the pollutant concentration of 3 ppm showed absorption of 88% in 5 min. Based on the results, the optimal starch nanocomposite containing hydroxyapatite and eggshell nanostructures has the potential to absorb dye due to the small size of these compounds. Generally, increasing temperature, increasing pH and decreasing the amount of nano

absorbent has increased the absorption percentage of methylene blue dye from the aqueous solution. SEM confirmed the nanostructures for size and shape, EDS for elemental analysis, FTIR for functional groups, XRD for crystal structure, and BET for surface area. Therefore, the advantage of this bio-nano sorbent is a simple, fast and cheap preparation method with high dye absorption in a short time. Based on the results of this nanocomposite inspired by nature, it can show the future prospect of expanding research in various industries more than in the past.

5. References

[1] T. Jiang, Q. Duan, J. Zhu, H. Liu, L. Yu, Starch-based biodegradable materials: Challenges and opportunities, Adv. Ind. Eng. Polymer Res., 3 (2020) 8-18. https://doi.org/10.1016/j.aiepr.2019.11.003.

[2] NH. Zakaria, N. Muhammad, M.M.A.B. Abdullah, Potential of starch nanocomposites for biomedical applications, IOP Conf. Series: Mater. Sci. Eng., 209 (2017) 012087. https://doi.org/10.1088/1757-899X/209/1/012087.

[3] B. Sharma, P. Malik, P. Jain, Biopolymer reinforced nanocomposites: A comprehensive review, Mater. Today Commun., 16 (2018) 353-363. https://doi.org/10.1016/j.mtcomm.2018.07.004.

[4] R.H. Althomali, K.A. Alamry, M.A. Hussein, G.S. Tay, Versatile applications of biopolymer nanocomposites: A review, ChemistrySelect, 7 (2022) e202200843. https://doi.org/10.1002/slct.202200843.

[5] A. Gamage, P. Thiviya, S. Mani, P. Graceraj Ponnusamy, A. Manamperi, P. Evon, O. Merah, T. Madhujith, Environmental properties and applications of biodegradable starch-based nanocomposites, Polymers, 14 (2022) 4578. https://doi.org/10.3390/polym14214578.

[6] K.E. Rivadeneira-Velasco, C.A. Utreras-Silva, A. Díaz-Barrios, A.E. Sommer-Márquez, J.P. Tafur, R.M. Michell, Green nanocomposites based on starch: A Review, Polymers, 13 (2021) 3227. https://doi.org/10.3390/polym13193227.

[7] I. Lakmali Balasooriya, J. Chen, S. Menike Korale Gedara, Y. Han, M. Nirmali Wickramaratne, Applications of nano-hydroxyapatite as adsorbents: A review, Nanomater. (Basel), 12 (2022) 2324. https://doi.org/10.3390/nano12142324.

[8] N.A. Abdul Halim, M.Z. Hussein, M.K. Kandar, Nanomaterials-upconverted hydroxyapatite for bone tissue engineering and a platform for drug delivery, Int. J. Nanomed., 2021 (2021) 6477-6496. https://doi.org/ 10.2147/IJN.S298936.

[9] X. Huang, K. Dong, L. Liu, X. Luo, R. Yang, H. Song, S. Li, Q. Huang, Physicochemical and structural characteristics of nano eggshell calcium prepared by wet ball milling, LWT, 131 (2020) 109721. https://doi.org/10.1016/j.lwt.2020.109721.

[10] H. Jahangirian, E.G. Lemraski, T.J. Webster, R. Rafiee-Moghaddam, Y. Abdollahi, A review of drug delivery systems based on nanotechnology and green chemistry: green nanomedicine, Int. J. Nanomed., 2017 (2017) 2957-2978. https://doi.org/10.2147/IJN.S127683.

[11] C. Sharma, R. Dhiman, N. Rokana, H. Panwar, Nanotechnology: an untapped resource for food packaging, Front. Microbiol., 8 (2017) 1735. https://doi.org/10.3389/fmicb.2017.01735.

[12] E. Serrano, G. Rus, J. García-Martínez, Nanotechnology for sustainable energy, Renew. Sust. Energ. Rev., 13 (2009) 2373-2384. https://doi.org/10.1016/j.rser.2009.06.003.

[13] P. Kumari, M. Alam, W. Ahmed Siddiqi, Usage of nanoparticles as adsorbents for wastewater treatment: An emerging trend, Sustain. Mater. Technol., 22 (2019) e00128. https://doi.org/10.1016/j.susmat.2019.e00128.

[14] G.Crini,Non-conventionallow-costadsorbents for dye removal: A review, Bioresour. Technol., 97 (2006) 1061-1085. https://doi.org/10.1016/j.biortech.2005.05.001.

[15] P. Olusakin Oladoye, T. Oladiran Ajiboye,

E. Oyinkansola Omotola, O. Joel Oyewola, Methylene blue dye: Toxicity and potential elimination technology from wastewater, Results Eng., 16 (2022) 100678. https://doi.org/10.1016/j.rineng.2022.100678

[16] I. Anastopoulos, A. Hosseini-Bandegharaei, J. Fu, A.C. Mitropoulos, G.Z. Kyzas, Use of nanoparticles for dye adsorption: Review, J. Disper. Sci. Technol., 39 (2018) 836-847. https://doi.org/10.1080/01932691.2017.1398661.

[17] S. Ilahi Siddiqui, P. Narayan Singh, N. Tara, S. Pal, S. Ali Chaudhry, I. Sinha, Arsenic removal from water by starch functionalized maghemite nano-adsorbents: thermodynamics and kinetics investigations, Colloid Interface Sci. Commun., 36 (2020) 100263. https://doi.org/10.1016/j.colcom.2020.100263.

[18] P.N. Singh, D. Tiwary, I. Sinha, Improved removal of Cr(VI) by starch functionalized iron oxide nanoparticles, J. Environ. Chem. Eng., 2 (2014) 2252-2258. https://doi.org/10.1016/j.jece.2014.10.003.

[19] A. Nayak, B. Bhushan, Hydroxyapatite as an advanced adsorbent for removal of heavy metal ions from water: Focus on its applications and limitations, Mater. Today Proc., 46 (2021) 11029-11034. https://doi.org/10.1016/j.matpr.2021.02.149.

[20] O.G. Abatan, P.A. Alaba, B.A. Oni, K. Akpojevwe, V. Efeovbokhan, F. Abnisa, Performance of eggshells powder as an adsorbent for adsorption of hexavalent chromium and cadmium from wastewater, SN Appl. Sci., 2 (2020) 1-13. https://doi.org/10.1007/s42452-020-03866-w.

[21] T. Ravi, S. Sundararaman, Synthesis and characterization of chicken eggshell powder coated magnetic nano adsorbent by an ultrasonic bath assisted co-precipitation for Cr(VI) removal from its aqueous mixture, J. Environ. Chem. Eng., 8 (2020) 103877. https://doi.org/10.1016/j.jece.2020.103877.

[22] M.T. Yagub, T.K. Sen, S. Afroze, H.M. Ang, Dye and its removal from aqueous solution by adsorption: A review, Adv. Colloid Interface Sci. 209 (2014) 172-184. https://doi.org/10.1016/j.cis.2014.04.002.

[23] S. Dutta, B. Gupta, S.K. Srivastava, A.K. Gupta, Recent advances on the removal of dyes from wastewater using various adsorbents: A critical review, Mater. Adv., 2 (2021) 4497-4531. https://doi.org/10.1039/D1MA00354B.

[24] H.N. Hamad, S. Idrus, Recent developments in the application of bio-waste-derived adsorbents for the removal of methylene blue from wastewater: A review, Polymers, 14 (2022) 783. https://doi.org/10.3390/polym14040783.

[25] H. Hosseini, A. Zirakjou, D.J. McClements, V. Goodarzi, W.H. Chen, Removal of methylene blue from wastewater using ternary nanocomposite aerogel systems: Carboxymethyl cellulose grafted by polyacrylic acid and decorated with graphene oxide, J. Hazard. Mater., 421 (2022) 126752. https://doi.org/10.1016/j.jhazmat.2021.126752.

[26] I. Khan, K. Saeed, I. Zekker, B. Zhang, A.H. Hendi, A. Ahmad, S. Ahmad, N. Zada, H. Ahmad, L.A. Shah, T. Shah, Review on methylene blue: its properties, uses, toxicity and photodegradation, Water, 14 (2022) 242. https://doi.org/10.3390/w14020242.

[27] I. Mustafa, Methylene blue removal from water using H_2SO_4 crosslinked magnetic chitosan nanocomposite beads, Microchem. J., 144 (2019) 397-402. https://doi.org/10.1016/j.microc.2018.09.032.

[28] S. Abdul Mubarak, N. Bahrudin, N.N. Jawad, A.H. Hameed, B.H.S. Sabar, Microwave enhanced synthesis of sulfonated chitosan-montmorillonite for effective removal of methylene blue, J. Polym. Environ., 29 (2021) 4027–4039. https://doi.org/10.1007/s10924-021-02172-9.

[29] F. Marahel, B. Mombeni Goodajdar, L. Niknam, M. Faridnia, E. Pournamdari,

S.M. Doost, Ultrasonic assisted adsorption of methylene blue dye and neural network model for adsorption of methylene blue dye by synthesised Mn-doped PbS nanoparticles, Int. J. Environ. Anal. Chem. 103 (2023) 3059-3080. https://doi.org/10.1080/03067319.2021.1901895.

[30] T. Taweekarn, W. Wongniramaikul, C. Boonkanon, C. Phanrit, W. Sriprom, W. Limsakul, W. Towanlong, C. Phawachalotorn, A. Choodum, Starch biocryogel for removal of methylene blue by batch adsorption, Polymers, 14 (2022) 5543. https://doi.org/10.3390/polym14245543.

[31] Z. Mou, D. Liu, J. Lv, D. Chai, L. Bai, Z. Zhang, G. Dong, J. Li, W. Zhang, Insight into the highly efficient adsorption towards cationic methylene blue dye with a superabsorbent polymer modified by esterified starch, J. Environ. Chem. Eng., 10 (2022) 108425. https://doi.org/10.1016/j.jece.2022.108425.

[32] N. Motakef Kazemi, M. Odar, Adsorption and determination of Lead in water and human urine samples based on $Zn_2(BDC)_2(DABCO)$ MOF as polycaprolactone nanocomposite by suspension micro solid phase extraction coupled to UV–Vis spectroscopy, Anal. Methods Environ. Chem. J., 4 (3) (2021) 5-20. https://doi.org/10.24200/amecj.v4.i03.145.

[33] H. Faraji, A.A. Mohamadi, H.R. Soheil Arezoman, A.H. Mahvi, Kinetics and equilibrium studies of the removal of blue basic 41 and methylene blue from aqueous solution using rice stems, Iran. J. Chem. Chem. Eng., 34 (2015) 33-42. https://doi.org/10.30492/ijcce.2015.14750

[34] H.S. Ragab, F.A. Ibrahim, F. Abdallah, A.A. Al-Ghamdi, F. El-Tantawy, N. Radwan, F. Yakuphanoglu, Synthesis and *in vitro* antibacterial properties of hydroxyapatite nanoparticles, IOSR J. Pharm. Biol. Sci., 9 (2014) 77-85. https://doi.org/10.9790/3008-09167785.

[35] S.B. Hassan, V.S. Aigbodion, Effects of eggshell on the microstructures and properties of Al–Cu–Mg/eggshell particulate composites, J. King. Saud. Univ. Eng. Sci., 27 (2015) 49-56. https://doi.org/10.1016/j.jksues.2013.03.001.

[36] S.M. Ibrahim, Characterization, mechanical, and thermal properties of gamma irradiated starch films reinforced with mineral clay, J. Appl. Polym. Sci., 119 (2010) 685-692. https://doi.org/10.1002/app.32732.

[37] H. Gheisari, E. Karamian, M. Abdellahi, A novel hydroxyapatite–hardystonite nanocomposite ceramic, Ceram. Int., 41 (2015) 5967-5975. https://doi.org/10.1016/j.ceramint.2015.01.033.

[38] M.S. Tizo, L. Andre, V. Blanco, A. Cris, Q. Cagas, B. Rangel, B. Dela Cruz, J.C. Encoy, J.V. Gunting, R.O. Arazo, Efficiency of calcium carbonate from eggshells as an adsorbent for cadmium removal in aqueous solution, Sustain. Environ. Res., 28 (2018) 326-332. https://doi.org/10.1016/j.serj.2018.09.002.

[39] A.A. Alshehri, M. Ahmad Malik, Biogenic fabrication of ZnO nanoparticles using Trigonella foenum-graecum (Fenugreek) for proficient photocatalytic degradation of methylene blue under UV irradiation, J. Mater. Sci.: Mater. Electron., 30 (2019) 16156–16173. https://doi.org/10.1007/s10854-019-01985-8.

[40] A. Chandrasekar, S. Sagadevan, A. Dakshnamoorthy, Synthesis and characterization of nano-hydroxyapatite (n-HAP) using the wet chemical technique, Int. J. Phys. Sci., 8 (2013) 1639-1645. https://doi.org/10.5897/IJPS2013.3990.

Anal. Methods Environ. Chem. J. 6 (3) (2023) 67-88

AMECJ

Research Article, Issue 3
Analytical Methods in Environmental Chemistry Journal
Journal home page: www.amecj.com/ir

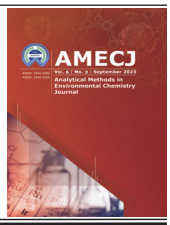

Analytical study on lead elimination by anionic clays: Characterization, adsorption kinetics, isotherm, thermodynamic, mechanism and adsorption

Salah Bahah[a,b,*]

[a] *Department of Environmental Engineering, Faculty of Science and Technology, University Bachir El Ibrahimi of Bordj Bou Arreridj, Algeria.*

[b] *Laboratory of Chemical Processes Engineering (LGPC), Department of Process Engineering, Faculty of Technology, University Ferhat Abbas Setif19000 ,1- Sétif, Algeria.*

ARTICLE INFO:

Received 20 May 2023
Revised form 30 Jul 2023
Accepted 19 Aug 2023
Available online 30 Sep 2023

Keywords:
Anionic clays,
Lead,
Adsorption,
Co-precipitation,
Functional groups

ABSTRACT

The co-precipitation method synthesized the synthetic anionicMg–Al and Ni-Al clays with three molar ratios (Mg/Al, Ni/Al). The samples were characterized by powder X-ray diffraction (XRD), Fourier transform infrared spectroscopy (FTIR), and scanning electron microscopy (SEM). No other crystalline phases were detected in the powder XRD patterns of the co-precipitated samples. The infrared spectra obtained all the functional groups that characterize these two types of anionic clays. SEM micrographs indicate the presence of particles and aggregates. The particles, or aggregates, are in the form of plates, supported by particles of acceptable sizes. The optimal pH for maximum lead adsorption is about 6.5 for both clays. The optimal adsorbent masses for the maximum percentages of lead removal are 0.2 g for Mg_3AlCO_3 and 0.25 g for Ni_3AlCO_3. The Mg_3AlCO_3 has a maximum adsorption capacity of lead, where q_m=73.42 mg g^{-1}. The adsorbed amount increases with increasing temperature for both types of clays studied. The equilibrium time of Pb^{2+} adsorption is reached after 5 min for both clays. The most appropriate models to describe the experimental data of adsorption kinetics and isotherms are pseudo-second-order and Langmuir. The detection limit (LOD) was 0.272 mg L^{-1}. The linearity range was 1 to 5 mg L^{-1}; the correlation coefficient in this range was 0.9997.

1. Introduction

Anionic clays, or Layered Double Hydroxides (LDHs), are mixed metal hydroxides that have a general formula expressed as$[(M^{II})_{1-x}(M^{III})_x(OH)_2]^{x+}(A^{m-}_{x/m})\cdot nH_2O]$. $M^{2+}$is a divalent cation (typically Mg, Zn, Ni, Co), $M^{3+}$is a trivalent metal cation (Al, Fe, Cr), A^{n-} is a charge anion, n/x is the molar ratio between di and trivalent cations, $M^{2+}/(M^{2+} + M^{3+})$, and m, the number of water molecules[1-3]. The structure of these clays consists of positively charged mixed metal hydroxide layers separated by charge-balancing anions and water molecules [4]. The cationic sheets containing $M(OH)_2$ in octahedral surroundings are linked by three edges, as in the brucite structure, between which compensating layers of anions are found [5]. These compounds have been the subject of much interest and research in recent years thanks to their interesting properties of anionic exchange [6,7], adsorption and porosity, which make it possible to envisage the intercalation of a large variety of anions (organic or inorganic)

*Corresponding Author: Salah Bahah
Email: basalah.univ@gmail.com
https://doi.org/10.24200/amecj.v6.i03.248

and the immobilization of various species, giving these hybrid materials a particular reactivity [6,7]. Therefore, LDH is considered a promising material [8]. Heavy metals are one of the main categories of water pollution; these releases pose a real danger to humans and their environment due to their stability and low biodegradability [9-11]. The use of the adsorption technique to remove heavy metals in aqueous solutions on different solid supports, especially on new materials such as anionic clays, has been the subject of much work [3, 5, 12]. Among the scientific results that use layered double hydroxides as adsorbents to remove lead are the studies of Yasin et al. (2014) [13]. The types of LDHs used to remove lead (Pb) from the aqueous solution are MgAl-NO_3 and Tartrate-MgAl. In this study, the maximum lead adsorption capacity calculated by the Langmuir model is 8.4 and 3.2 mg g^{-1} for Tartrate-MgAl and $MgAlNO_3$, respectively [13]. Yanming et al. (2017) [14] studied the removal of Pb^{2+} ions from an aqueous solution by glutamate intercalated in layered double hydroxide. The maximum retention capacity of Pb^{2+} is 68.49 mg g^{-1} [14]. The concentration of Pb and other metal ions can be determined by several techniques, which can be grouped under atomic spectrometry. Graphite furnace atomic absorption spectrophotometer (GF-AAS) is the best technique method. Several research studies use this technique to determine the lead concentration in the blood, like studies of Pacer et al. (2022) [15]. In addition, GF-AAS is an excellent method currently applied for trace lead concentration with high accuracy and precision [15, 16]. Like GF-AAS, inductively coupled plasma mass spectrometry and ICP-MS is other assay technique with precise and accurate results. However, it is a simple and rapid method compared to ICP-MS [17]. The comparative study carried out by Trzcinka-Ochocka et al. for the determination of lead and cadmium shows that validation parameters for ICP-MS and GF-AAS were similar. However, ICP-MS for Pb determinations is better than GF-AAS. Also, the detection limits (LOD) of ICP-MS are better than GF-AAS for lead analysis [18]. Inductively Coupled Plasma -Atomic Emission Spectroscopy (ICP-AES), sometimes named ICP-optical emission spectrometry (ICP-AES), is a device that results from the coupling between a high-frequency induced argon plasma and a spectrometer, which is used to calculate the concentration of metals in solid, liquid or gas samples. The LOD of the ICP-AES technique is lower than ICP-MS [19]. In addition, there are other lead dosage techniques without spectroscopic techniques, such as cyclic voltammetry (CV). Riyanto et al. showed that the electroanalysis method for lead determination in wastewater is accurate, precise, reproducible and inexpensive, with acceptable correlation [20]. Compared with spectroscopic techniques, the LOD of electroanalysis (0.929 mg L^{-1}) is higher than that of spectroscopic methods.

In this paper, lead removal from an aqueous solution was performed using two-layered double hydroxides, namely Mg_3AlCO_3 and Ni_3AlCO_3. The co-precipitation method prepared these two adsorbents with a molar ratio of (Mg/Al) equal to 3. Ni_3AlCO_3 can be considered among the LDHs not used to eliminate heavy metals from aqueous solution. The adsorption capacities of lead with two anionic clays at room temperature in optimized pH were compared and analyzed. We studied the effect of different parameters such as the Ni/Al ratio, pH, contact time, dose of adsorbent and temperature in the adsorption of Pb^{2+} ions from an aqueous solution. In addition, the mechanism and thermodynamic parameters were studied.

2. Experimental

2.1. Reagents and Materials

The products of magnesium nitrate hexahydrate ($Mg(NO_3)_2.6H_2O$; CAS 13446-18-9; Molecular Weight 256.41), Aluminum nitrate nonahydrate ($Al(NO_3)_3.9H_2O$; CAS Number: 7784-27-2; M. W.: 375.13) and Nickel nitrate hexahydrate ($Ni(NO_3)_2.6H_2O$; CAS 13478-00-7; Molecular Weight 290.79) used for the synthesis of $MgAlCO_3$ and $NiAlCO_3$ were purchased from Sigma, Germany. Sodium carbonates ($NaCO_3$), Sodium hydroxide (NaOH) and Lead nitrate $Pb(NO_3)_2$ were purchased from Merck.

2.2. Apparatus

The absorption measurements were made with AA-6200 Atomic Absorption Flame Emission Spectrophotometer SHIMADZU. Calibrating standard lead solutions were prepared by dilution from the stock solution (1000 mg L^{-1}). The linear working range was obtained between 1 to 5 mg L^{-1}. To estimate the sensitivity of the FAAS method, we calculated the limit of detection (LOD) and the limit of quantification (LOQ). The LOD and LOQ values were achieved at 0.272 mg L^{-1} and 0.825 mg L^{-1}, respectively.

2.3. Synthesis method

The LDHs studied are $NiAlCO_3$ (R=2, 3 et 4) and $MgAlCO_3$ (R=3). These clays were synthesized by the direct co-precipitation method, in which an aqueous solution containing appropriate amounts of nitrate elements (hydrated metal salts as sources) was added dropwise into an alkaline solution of Na_2C0_3 and NaOH at room temperature under vigorous stirring. During the synthesis, the pH was adjusted to pH 10. The resulting suspension was stirred for 18 hours at 65 °C. After cooling to room temperature, the precipitate was centrifuged and washed several times with bi-distilled water until there was no trace of nitrate ($AgNO_3$ test) and then dried overnight in an oven at 100 °C.

2.4. Adsorption method

The study of the adsorption of lead was performed by the batch method. The lead stock solution was prepared by dissolving Pb $(NO_3)_2$ in distilled water and diluting it to the desired concentration. Adsorption of Pb^{2+} on the selected clay was carried out in a 50 ml conical flask by taking 50 ml of a solution of the desired Pb^{2+} concentration to which 200 mg of the adsorbent was added. The adsorbate in the mixture was separated by centrifugation. An atomic absorption spectrophotometer determined the residual Pb2+ in the filtrate. All experiments except the pH variation study were performed at the stock solution pH. In the case of pH variation studies, a variable concentration of diluted NaOH and HCl solutions was used to adjust the pH. Figure 1 presents the adsorption method.

The adsorption of lead was calculated by Equation 1.

$$q_e = \frac{C_i - C_e}{m} * V \qquad \text{(Eq.1)}$$

Where q_e= lead adsorbed (mgg^{-1}); V = solution volume (L); C_i = initial concentration (mg $Pb^{2+}L^{-1}$); Ce (mgPb^{2+} L^{-1}) =equilibrium concentration and m adsorbent mass. % Removal of metal ions were calculated using Equation 2.

$$\text{Removal} = \frac{C_i - C_e}{C_i} * 100 \qquad \text{(Eq. 2)}$$

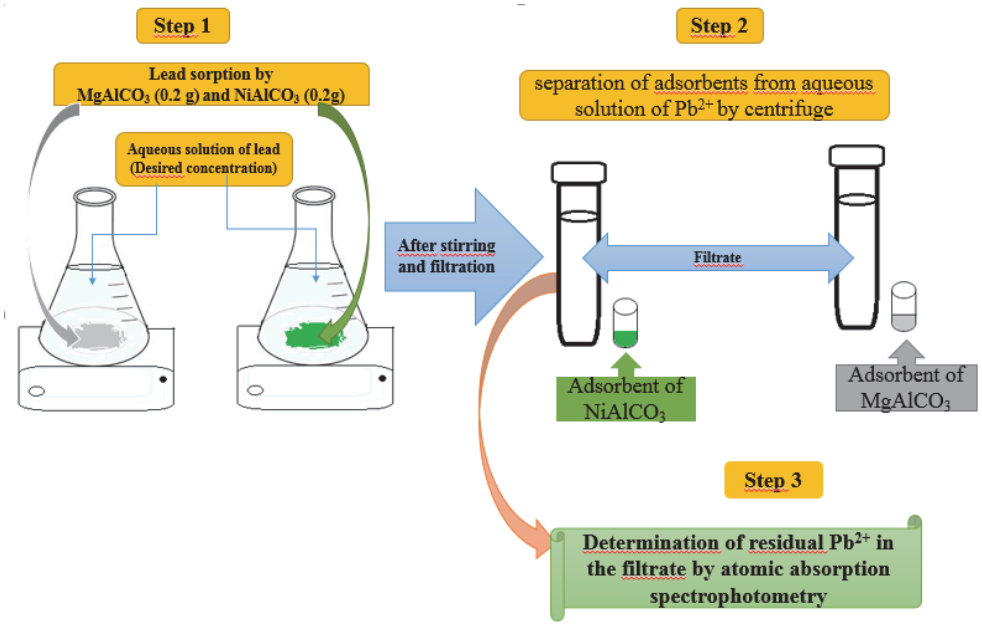

Fig. 1. Adsorption of lead by a batch method

3. Results and Discussion

3.1. Characterization

A Bruker D8 diffractometer with CuKα radiation (λ= 0.15406 nm) was used to study the structural properties of the clay. A scanning electronic microscopy instrument (S-4800), a Hitachi model (Japan), was utilized to study the surface properties. Fourier transform infrared spectroscopy (Perkin-Elmer model; USA) was applied to study the functional group of the adsorbent. Moreover, this last technique was used to examine the effect of the adsorption of Pb^{2+} on the different bands of the functional groups after adsorption. The infrared spectra were carried out between 4000 cm^{-1} and 400 cm^{-1}.

3.1.1.Characterization by XRD

The X-ray diffraction patterns of the prepared phases (Fig. 2a and 2b) are characteristic of layered double hydroxide materials (LDHs). Peaks 003 and 006 are sharp, narrow, and symmetric; the baseline is low and stable, which indicates a high degree of crystallinity and a typical structure of anionic clays. These reflections correspond to the layer order along the c-axis [21]. Inter-reticular distances are 7.70 °A and 7.75 °A for Ni/Al (R=3) and Mg/Al (R=3), respectively. These values are in order of those reported in similar studies by Kristina Klemkaite et al. [22]and Faour et al. [23]. The cell parameters of Ni_3AlCO_3 and $Mg_3AlCO_{3,}$ calculated as a = $2*d_{110}$ [24], are 3.04 and 3.06 °A, respectively. The constant c calculated using the equation $c=3*d_{003}$ [25] shows that the corresponding values for Ni_3AlCO_3 and Mg_3AlCO_3 are (23.10 °A) and (23.25 °A), respectively. These values always agree with those of Kristina Klemkaite et al. [22] and Faour et al. [23].

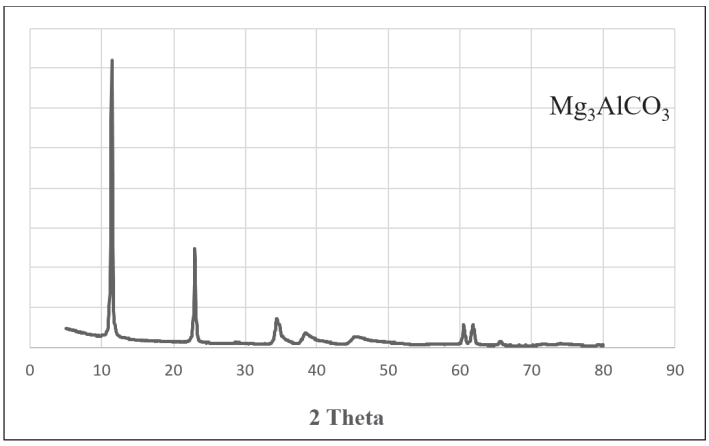

Fig. 2a. XRD patterns of Mg_3 Al–CO_3

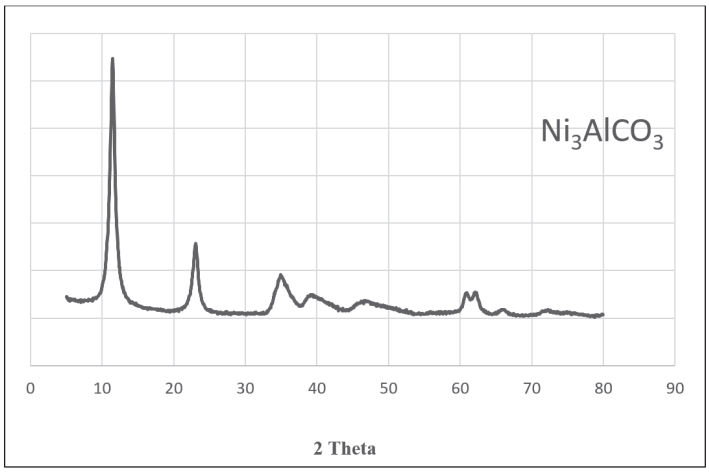

Fig. 2b. XRD patterns of Ni_3Al–CO_3.

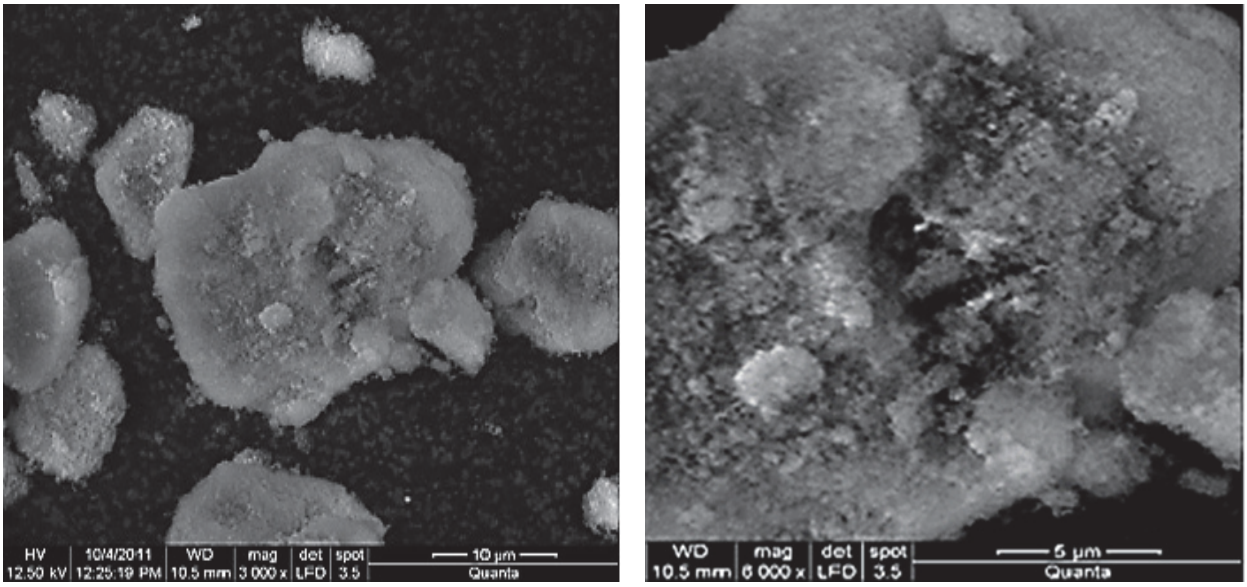

Fig. 3a. The SEM micrograph of (a) $Ni_3Al–CO_3$ (R=3)

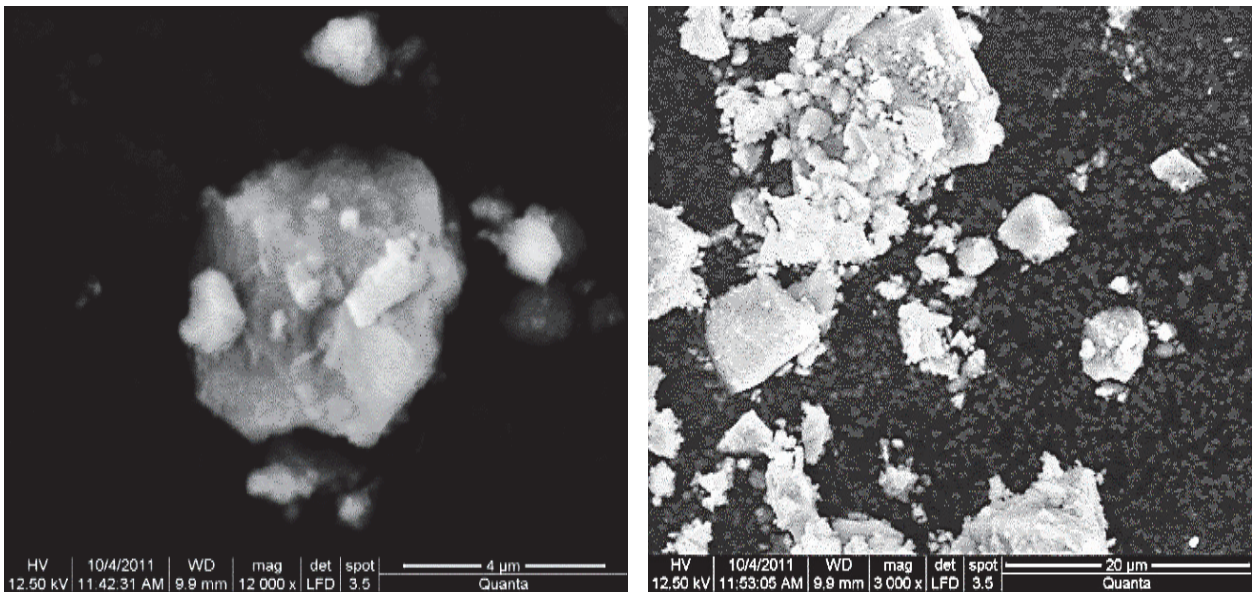

Fig. 3b. The SEM micrograph of $Mg_3Al–CO_3$(R=3).

3.1.2.Characterization by SEM

The images characterizing the surfaces of the different substrates are presented in Figure3a and 3b. The images at different magnifications show surfaces with large porosities and different types and sizes. The large inter-particle pores are occupied by particles of smaller sizes for both clays, which indicate the presence of inter-particle attraction forces that form large aggregates. The particles, or aggregates, are in the form of plates, supported by particles of acceptable sizes. Mg_3AlCO_3 particles are characterized by a rigid (compact) perimeter surrounding a highly porous surface.

3.2. Parameters of adsorption

In the following, we studied the effect of some parameters on lead adsorption, such as the solution's initial pH, the adsorbent's mass, contact time, molar ratio, and temperature. The concentration and volume of the aqueous lead solution were fixed at 50 mgL^{-1} and 50 mL, respectively, and the stirring speed was set at 400 rpm.

3.2.1.Effect of pH

To find the optimal pH corresponding to the maximum adsorption of lead in the aqueous solution, we studied the effect of this factor on the retention of Pb^{2+} at different pHs (from pH 3 to pH 9). The results obtained are shown in Figure 4. The amount retained as a function of the pH solution was determined from the concentration of Pb^{2+} remaining in the solution after equilibrium by the atomic absorption technique. According to Figure 4, the curves can be divided as a function of pH into two regions: the first one represents the domain of pH lower than 6.5 in which the percentage removal of Pb^{2+} retained on the selected anionic clays increases as the pH increases, reaching a maximum value at pH 6.5. At this optimum pH, the lead removal percentages are 95.4% and 81.34% for Mg_3AlCO_3 and Ni_3AlCO_3, respectively. The increase in Pb^{2+} adsorption on both types of LDHs with increasing pH can be explained by the decrease in H^+ ion concentration with increasing pH. Where the clay surface at low pH became positively charged due to the protonation reaction on the surfaces (formation of SOH^{2+}) [25], which leads to repulsive forces between Pb^{2+} ions and SOH^{2+}groups on the adsorbent surface [26]. According to Donglin Zhao, at pH values below 7, lead ions are present as Pb^{2+} in the solution. The adsorption reactions are surface complexation reactions, including two surface reactions. The chemical bonding reaction occurs between the metal ions and the surface functional groups, forming surface complexes of the inner sphere. In the second region, an electrostatic binding reaction occurs between metal ions and oppositely charged surface functional groups, forming surface complexes of the outer sphere at some distance from the surface. The complex adsorption of lead on LDH samples can be described as follows [25,26].

$$Sur\text{-}O^- + Pb^{2+} \rightarrow Sur\text{-}O^-\text{-}Pb^+ + H^+$$

Chemical binding adsorption

$$Sur\text{-}O^- + Pb^{2+} \rightarrow Sur\text{-}O^-\text{----}Pb^{2+}$$

Electrostatic binding adsorption

At pH greater than 6.5, for Mg_3AlCO_3, there is a slight decrease and then stability for lead removed until pH 9. These results almost agree with those found by Donglin Zhao et al., who used anionic clay based on Mg_2Al-LDH to remove lead [26]. For the anionic clay based on Ni_3AlCO_3, the characteristic curve shows a remarkable decrease in the amount of lead removed. At this pH range (pH > 6.5), according to ZHAO, Donglin et al. (2011) [26], lead in the aqueous solution takes the forms of Pb (OH) and Pb $(OH)_2$. Thus, the adsorption of Pb^{2+} on both LDHs occurred by precipitation reaction, as explained by several authors in this pH range (pH > 7) [26]. According to our results, it can be noted that the lead precipitation reaction is better catalyzed on the Mg_3AlCO_3 surface than that of Ni_3AlCO_3, where the amount adsorbed by Mg_3Al remains constant from pH 7.5 and higher compared to Ni_3Al-based clays, where the amounts of lead are decreased with the increase of pH (Figure 4).On the other hand, LIANG, Xuefeng et al. [25] conclude that the adsorption of Pb^{2+} on a clay-type Mg_2Al-Cl LDH results mainly from the precipitation induced by the surface. At optimum pH (pH = 6.5), the results show that the order of the quantity of lead retained for the clays used becomes Equation 3.

$$Q_{ads\ (MgAlCO3(R=3)} > Q_{ads\ (NiAlCO3(R=3)} \qquad \text{(Eq. 3)}$$

Whereas, at pH<5.5 (an acidic medium), the percentage of Pb^{2+} removal by Ni_3AlCO_3 HDL is higher than that of Mg_3AlCO_3 HDL, conversely for the pH > 5.5 range. This can be explained by the start of the lead precipitation reaction occurring in parallel with the complexation reaction from pH 5.5 to the optimum pH of 6.5.

3.2.2.Effect of adsorbent quantity

Different amounts of the adsorbent (0.05–0.3 g) were added to other conical flasks containing 50 mL of the aqueous solution of Pb^{2+} (pH 6.5). Figure 5 shows the variations of Pb^{2+} adsorbed amounts as a function of adsorbent mass for the two anionic clays studied with a contact time of 2 hours. The initial adsorbate concentration used is 50 mg L^{-1}. Lead removal percentages increase as the adsorbent

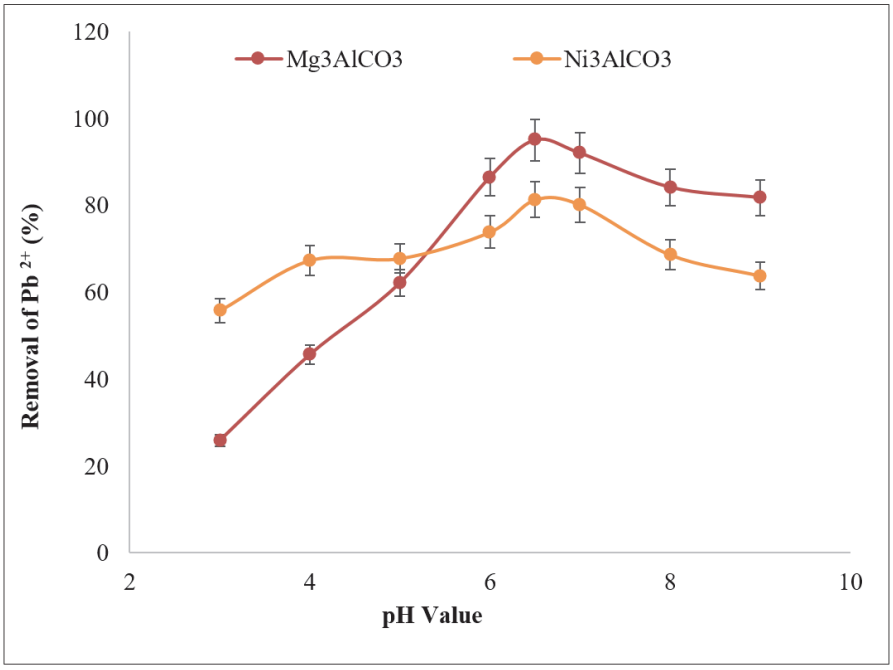

Fig. 4. Effect of initial pH on removal of Pb^{+2} ions onto $Mg3AlCO_3$ and $Ni3AlCO_3$.

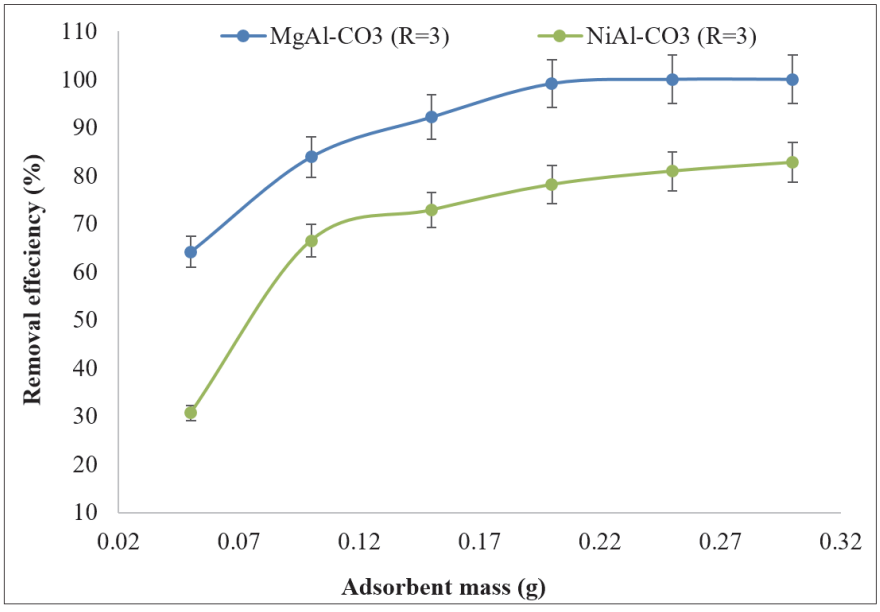

Fig. 5. Effect of mass on the adsorption of Pb^{2+} onto $Ni_3Al\text{-}CO_3$ and $Mg_3Al\text{-}CO_3$

mass increases from 0.05 g to 0.2 g. Above 0.2 g for Mg_3AlCO_3 and 0.25 g for Ni_3AlCO_3, the amount of Pb^{2+} retained remains almost constant regardless of the adsorbent mass. The maximum capacities corresponding to these masses are 95.25 % and 83.66 % for Mg_3AlCO_3 and Ni_3AlCO_3, respectively.

According to Figure 5, the amount of Pb^{2+} was adsorbed on the clays as Equation 4.

Qads (MgAlCO3(95.25%) > Qads (NiAlCO3(83.665) (Eq.4)

3.2.3.Effect of temperature

The effect of temperature on lead adsorption was studied at 20 °C, 30 °C, 40 °C, 50°C, and as well as pH of the solution. Figure 6 shows the percentage of lead removal as a function of temperature for Mg_3AlCO_3 and Ni_3AlCO_3. From the curves shown in Figure 6, the adsorbed amount increases with increasing temperature for both types of LDHs, where the lead removal percentages reach 94.16 % and 85.39 % for Mg_3AlCO_3 and Ni_3AlCO_3, respectively. The percentage of lead removal by Mg_3AlCO_3 is higher than that of Ni_3AlCO_3 for all temperatures. This may indicate that the adsorption of lead onto the active sites of LDHs studied is endothermic [27]. The increase in temperature can be enlarged and activate the adsorbent surface, which facilitates the mobility of lead ions from the bulk solution to the adsorbent surfaces and enhances the accessibility to the adsorbent active sites [27].

3.2.4.Effect of contact time and molar ratio

The study of the contact effect was carried out using four LDHs of the types Mg_3AlCO_3, Ni_2AlCO_3, Ni_3AlCO3, and Ni_4AlCO_3 (to see the molar ratio effect, (R=2, 3, and 4). The mass of the adsorbent used is 0.2 g, the concentration of Pb^{2+} in the solution is 50 mg $Pb^{2+}L^{-1}$, the stirring speed is 400 rpm, and the adsorption occurs at ambient temperature. The equilibration time is an important parameter that allows the determination of the rate of lead elimination, whether it is fast or slow, as well as the evaluation of the effectiveness of the absorbent. The shape of the curves shown in Figure 7 is typical of saturation curves with a slight quantitative difference. The Pb^{2+} retention kinetics consists of two distinct steps: an initial fast step with a contact time of up to 5 minutes for Mg_3AlCO_3 and Ni_3AlCO_3 and about 10 minutes for Ni_2AlCO_3 and Ni_4AlCO_3, respectively, and a slower second step in which retention reaches a plateau, indicating the achievement of balance. The equilibrium times for Ni_2AlCO_3 and Ni_4AlCO_3 represent the double time required for equilibrium compared to Mg_3AlCO_3 and Ni_3AlCO_3. This can be explained by the crystalline factor in Mg_3AlCO_3 and Ni_3AlCO_3, which is good compared to Ni_2AlCO_3 and Ni_4AlCO_3. The regular and repetitive distribution of atoms and functional groups bonded with these atoms, such as OH, facilitate the rapid attachment of Pb^{2+} ions to these surface functional groups. It is known that the elimination of Pb^{2+} for all adsorbents is done under the same conditions (temperature, stirring speed).

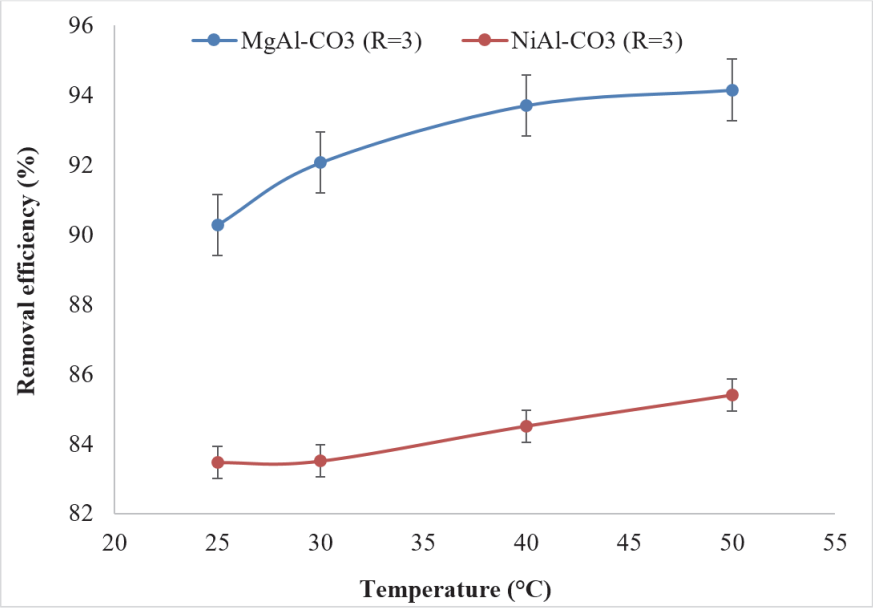

Fig. 6. Effect of temperature on Pb^{2+} adsorption on Mg_3AlCO_3 and Ni3$AlCO_3$

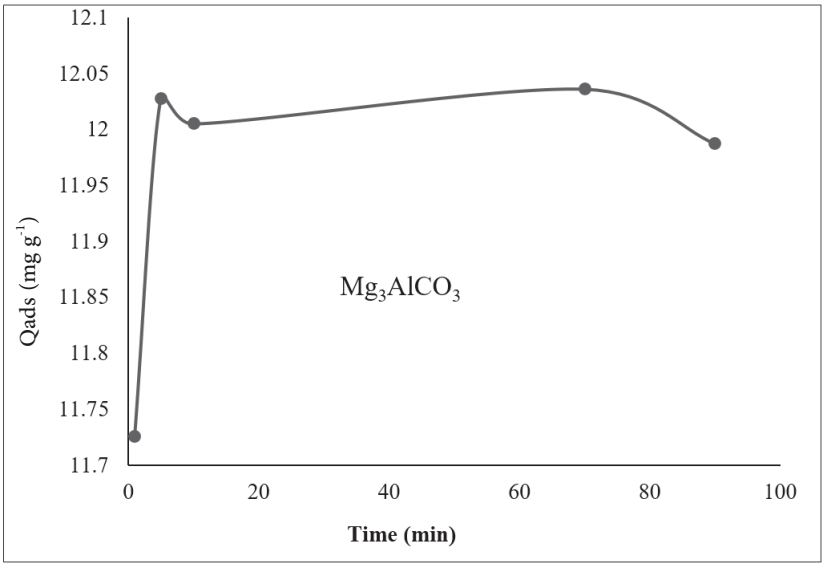
12.1
12.05
12
11.95
11.9
11.85
11.8
11.75
11.7
Qads (mg g-1)
Mg3AlCO3
0
20
40
60
80
100
Time (min)

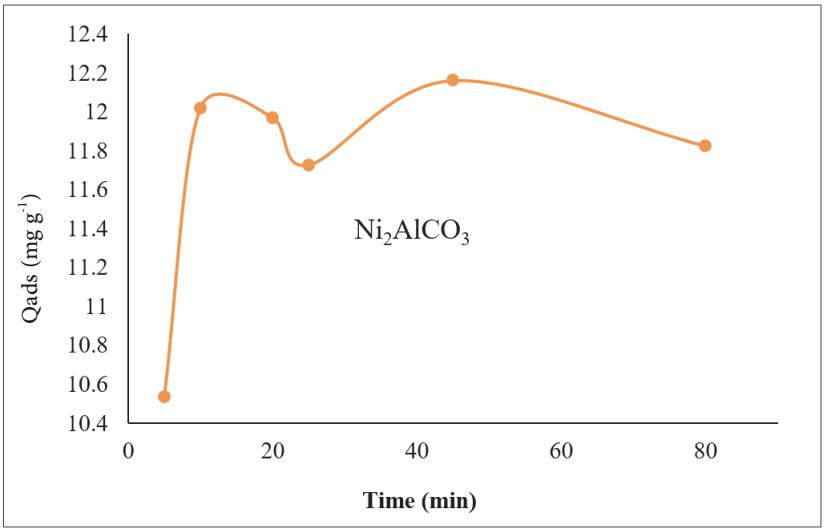
12.4
12.2
12
11.8
11.6
11.4
11.2
11
10.8
10.6
10.4
Qads (mg g-1)
Ni2AlCO3
0
20
40
60
80
Time (min)

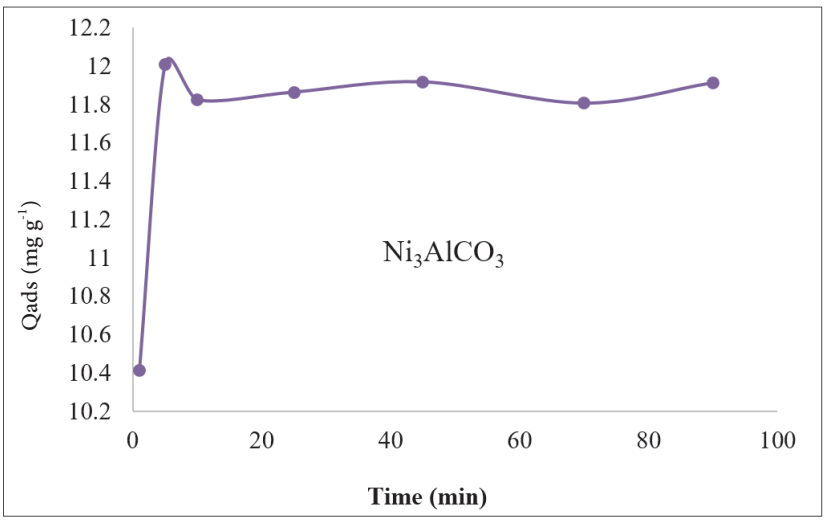
12.2
12
11.8
11.6
11.4
11.2
11
10.8
10.6
10.4
10.2
Qads (mg g-1)
Ni3AlCO3
0
20
40
60
80
100
Time (min)

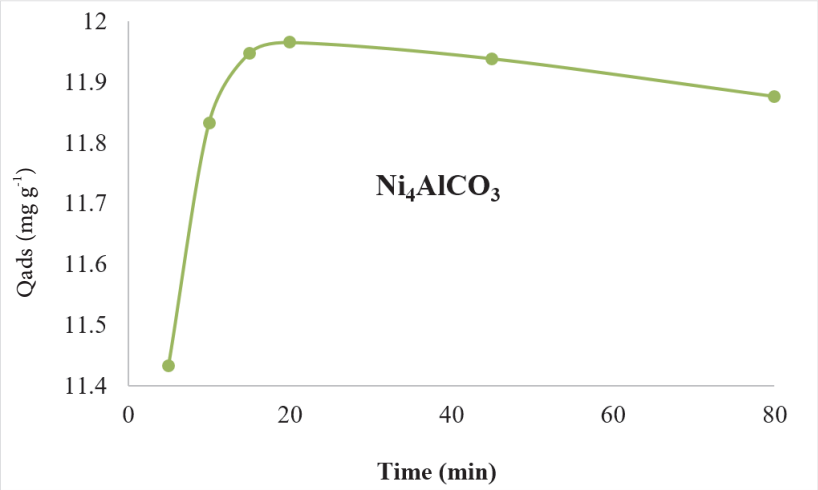

Fig. 7. Retention kinetics of Pb^{2+} on anionic clays studied

3.3. Kinetic models of adsorptions

To determine the most appropriate kinetic model, we have chosen three models, the most used for modelling adsorption kinetic data, which are: the pseudo-first-order (Equation 5), the second-order (Equation 6), and the intraparticle diffusion model (Equation 7). The corresponding equations in linear forms are presented as follows [28, 29].

$$\ln(q_e - q_t) = lnq_e - k_1.t \quad \text{(Eq.5)}$$

$$\frac{t}{q_t} = \frac{1}{k_2 q_e^2} + \frac{t}{q_e} \quad \text{(Eq.6)}$$

$$q_t = k_i t^{0.5} + C \quad \text{(Eq.7)}$$

Where q_e, q_t, t, k_1, k_2, k_i, and C are respectively the quantity of Pb^{2+} adsorbed at equilibrium (mg g^{-1}), the quantity of Pb^{2+} adsorbed at time t (mg g^{-1}), the time (min), the rate constant of the pseudo-first-order kinetic equation in g/mg min^{-1}, the rate constant of the pseudo-second-order kinetic equation in g/mg min^{-1}, the rate constant mg/g$min^{0.5}$, and the boundary layer thickness.

3.3.1.Pseudo first-order model.

The calculated results of the pseudo-first-order equation are presented in Table 1 and Figure 8. The values of the correlation coefficients are low, and the values of qe acquired by this method are contrasted with the experimental values. So, adsorption cannot be classified as pseudo-first order.

Table 1. Pseudo-first-order model parameters

Clay	Parameters
Mg_3AlCO_3	q_e (mg g^{-1}) exp = 12.00 q_e (mg g^{-1}) cal = 0.048 K_1 (mg $g^{-1}min^{-1}$) = 0.00057 R^2 = 0.00025
Ni_2AlCO_3	q_e (mg g^{-1}) exp = 11.96 q_e (mg g^{-1}) cal = 0.51 K_1 (mg $g^{-1}min^{-1}$) = 0.06 R^2 = 0.13
Ni_3AlCO_3	q_e (mg g^{-1}) exp =11.86 q_e (mg g^{-1}) cal =0.44 K_1 (mg $g^{-1}min^{-1}$) = 0.018 R^2 = 0.38
Ni_4AlCO_3	q_e (mg g^{-1}) exp =11.93 q_e (mg g^{-1}) cal = 0.11 K_1 (mg $g^{-1}min^{-1}$) = 0.025 R^2 = 0.072

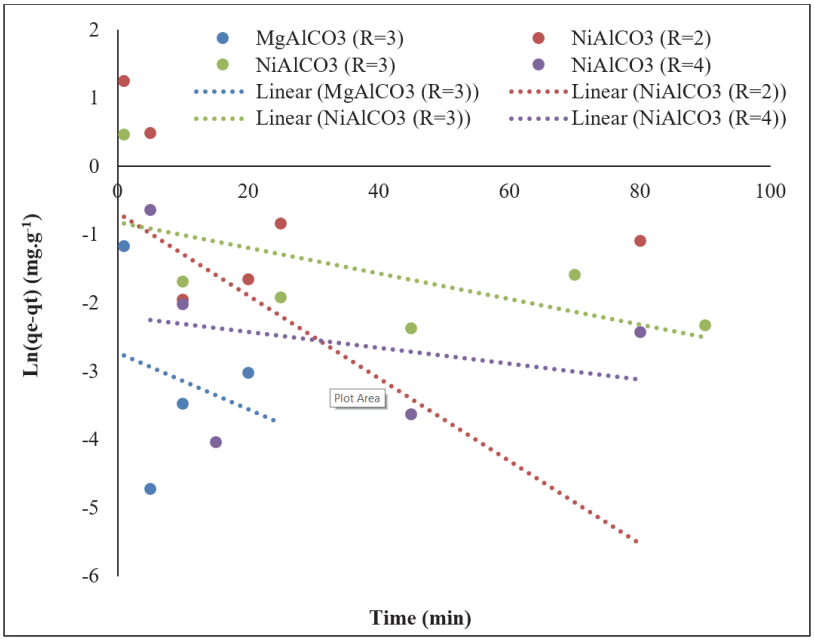

Fig. 8. Pseudo first-order model for anionic clays

3.3.2. Pseudo second-order model.

This model considers that the rate-limiting step in heavy metal adsorption is chemisorption and that chemisorptive bonds involving electron sharing or exchange between the absorbent and the adsorbent have been applied [5]. According to the high values of the regression constant R^2 = 0.99 for all the studied clays, the evolution of t/qt vs. t is presented by pseudo-second-order kinetics (Fig. 9). The parameters of the two kinetic models are shown in Table 2. From these results and in contrast to the first-order model, the amount of Pb^{2+} adsorbed at equilibrium determined experimentally is closer to that calculated using the second-order kinetic model (Table 2).

Table 2. Parameters of the pseudo-second-order model.

Clay	Parameters
Mg_3AlCO_3	q_e (mg g^{-1}) exp = 12.00 q_e (mg g^{-1}) cal =12.00 K_1 (mg $g^{-1}min^{-1}$) =-9.29 R^2 =1
Ni_2AlCO_3	q_e (mg g^{-1}) exp = 11.96 q_e (mg g^{-1}) cal = 11.93 K_2 (mg $g^{-1}min^{-1}$) = 0.487 R^2 = 0.99
Ni_3AlCO_3	q_e (mg g^{-1}) exp =11.86 q_e (mg g^{-1}) cal = 11.88 K_2 (mg $g^{-1}min^{-1}$) = 1.59 R^2= 0.99
Ni_4AlCO_3	q_e (mg g^{-1}) exp =11.93 q_e (mg g^{-1}) cal = 11.94 K_2 (mg $g^{-1}min^{-1}$) = 12.87 R^2 = 0.99

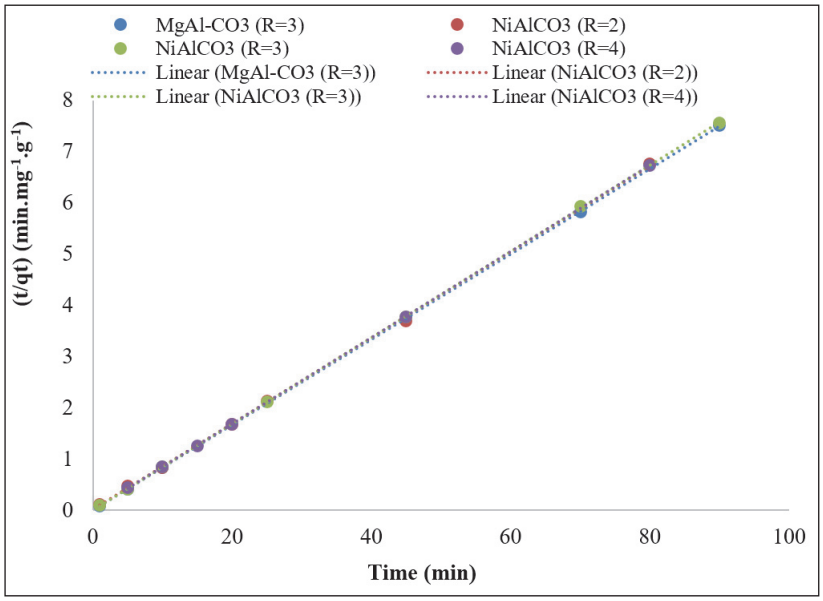

Fig. 9. Pseudo second-order model for anionic clays

3.3.3. Weber - Morris internal diffusion model

The Weber-Morris intra-particle diffusion model is the most used technique to identify the mechanism involved in the adsorption process. Intra-particle diffusion plots (q_t vs. $t^{0.5}$) (Fig. 10) were obtained from Equation 7. All the parameters of this model are presented in Table 3. Figure 10 indicates that straight lines do not pass through the point of origin before reaching the equilibrium state; therefore, the adsorption does not follow only the mechanism of intra-particle diffusion and that several processes affect the adsorption of Pb^{2+} and that intra-particle diffusion is not the limiting step for the whole reaction. The values of the constant C, which presents the thickness of the boundary layer, are in the order $C_{Mg3AlCO3} > C_{Ni2AlCO3} > C_{Ni3AlCO3} > C_{Ni4AlCO3}$. The values of C determine the boundary layer effect; higher values indicate a more significant impact [29].

Table 3. Parameters of the intra-particle diffusion model.

Clay	Parameters
Mg_3AlCO_3	$K_d = 0.135$ $C = 11.63$ $R^2 = 0.76$
Ni_2AlCO_3	$K_d = 1.54$ $C = 7.12$ $R^2 = 0.99$
Ni_3AlCO_3	$K_d = 0.68$ $C = 9.95$ $R^2 = 0.72$
Ni_4AlCO_3	$K_d = 0.32$ $C = 10.74$ $R^2 = 0.94$

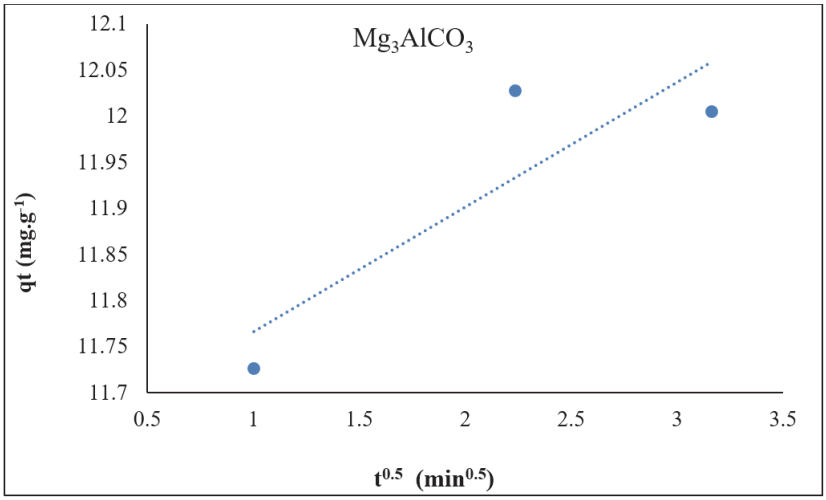
Mg3AlCO3
12.1
12.05
12
11.95
11.9
11.85
11.8
11.75
11.7
qt (mg.g-1)
0.5
1
1.5
2
2.5
3
3.5
t0.5 (min0.5)

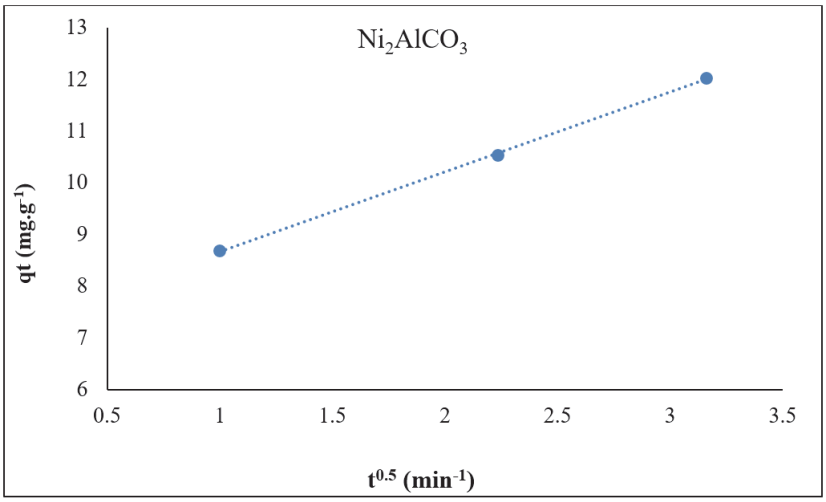
Ni2AlCO3
13
12
11
10
9
8
7
6
qt (mg.g-1)
0.5
1
1.5
2
2.5
3
3.5
t0.5 (min-1)

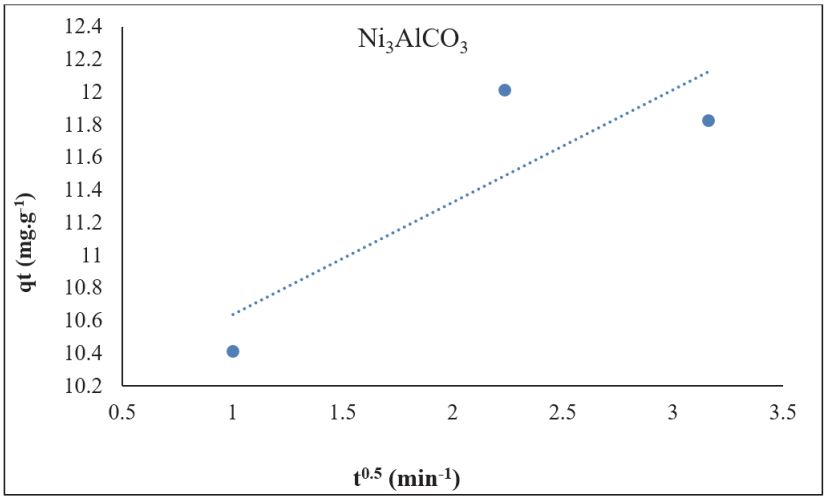
Ni3AlCO3
12.4
12.2
12
11.8
11.6
11.4
11.2
11
10.8
10.6
10.4
10.2
qt (mg.g-1)
0.5
1
1.5
2
2.5
3
3.5
t0.5 (min-1)

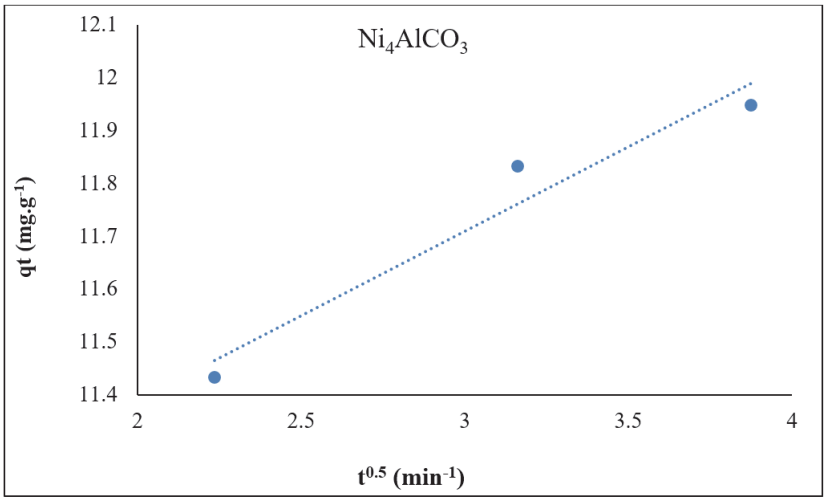

Fig. 10. Internal diffusion curves at a time less than 10 min

3.4. Lead retention equilibrium studies

To determine the adsorption characteristics of Mg_3AlCO_3 and $NiAlCO_3$ (R = 2, 3, and 4), a series of experiments are carried out in which solutions containing known concentrations of Pb^{2+} are in contact with the adsorbent. This study was carried out under the same conditions as the contact effect parameter, except for the concentrations of the Pb^{2+} solutions. After 24 hours, the solution concentration is measured when equilibrium has been established.

Figure 11 shows the curves of adsorbed amounts versus equilibrium concentrations for Pb^{2+} adsorption isotherms on Mg_3AlCO_3, Ni_2AlCO_3, Ni_3AlCO_3, and Ni_4AlCO_3 clays. The adsorption capacities of these clays are proportional to the metal concentrations. According to Giles et al., the allure of the isotherms is of type L [30]. Furthermore, the results showed that Mg_3AlCO_3 clay has a higher adsorption capacity than $NiAlCO_3$ (R = 2, 3, and 4).

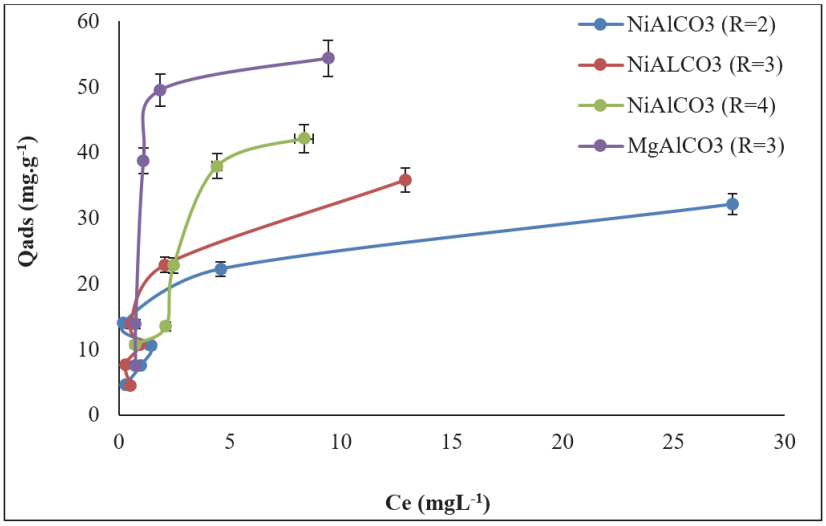

Fig. 11. Adsorption isotherms of Pb^{2+} on anionic clays studied.

3.4.1. Characterization of adsorbents before and after lead adsorption and mechanism

The infrared (IR) spectra of the raw Mg_3AlCO_3 and Ni_3AlCO_3 samples before and after the retention of lead at different concentrations are shown in Figure 12. The spectra are subdivided into three regions: between (1000 cm^{-1} and 400 cm^{-1}), (3000 cm^{-1} and 1000 cm^{-1}), and (4500 cm^{-1} and 3000 cm^{-1}). It can be noted that the IR spectra corresponding to the second region (1000 cm^{-1} to 3000 cm^{-1}) indicate two essential bands between (1650 cm^{-1} and 1660 cm^{-1}) and (1350 cm^{-1} and 1400 cm^{-1}) for both adsorbents before and after Pb^{2+} adsorption. These two bands are assigned to H2O and CO32-vibration modes, respectively. In the low-frequency region between 1000 cm^{-1} and 400 cm^{-1}, the infrared spectra after lead adsorption show intense vibration bands and are shifted compared to those of Mg_3AlCO_3 and Ni_3AlCO_3 before adsorption, as shown in Figure 12(a, b, c). For Mg_3AlCO_3, the vibration bands observed at 446.49 cm^{-1} and 554.49 cm^{-1} are attributed to the AlOH and MgOH bands, respectively [31]. After adsorption of the lead at different concentrations, the intensity of these bands increases and shifts slightly to high-frequency regions (447.49 cm^{-1} and 555.50 $cm^{-1,}$ respectively), which is explained by the fixation of Pb^{2+} ions on the lamellar layers to form bands of Pb-Al-OH and Pb-Mg-OH or M-O-Pb [32]. The band observed at 668.28 cm^{-1} for the Mg/Al-based clay before adsorption is assigned to the carbonate vibration mode [33]. After adsorption of Pb^{2+}, the spectrum does not show a remarkable shift of this band. The same remark was observed at the carbonate vibration band located at about 1357.79 cm^{-1} (Figure 12b) (second region). For the high-frequency region between (4500-3000 cm^{-1}), the vibration band of free hydroxyl groups located around 3446.55 cm^{-1} before adsorption is shifted to 3442 cm^{-1} for Mg_3AlCO_3 solids after lead adsorption for different concentrations. This shift, accompanied by the decrease of free OH band area after adsorption, is explained by the reduction of free OH in the hydroxyl layer, which reacts with Pb^{2+} ions according to Equation 8.

$$M\text{-}OH + Pb^{2+} \rightarrow M\text{-}O\text{- - -}Pb^{2+} + H^{+} \quad \text{(Eq. 8)}$$

As Equation 8, M is a divalent or trivalent cation (Mg or Al). For the adsorbent based on Ni_3AlCO_3, several bands were observed in the low-frequency region of the spectrum (<600 cm^{-1}) that characterize the lattice vibration modes [32]. The spectra indicate a slight shift with increasing peak intensity (sharp peak) at about 418.56 cm^{-1} for all Ni/Al-based HDLs after Pb^{2+} adsorption (Figure 12a). This band can be attributed to the formation of Al-O-Pb or Pb-Al-OH [32]. The infrared spectra also show the shift of the vibration band peaks from about 560.28 cm^{-1} and 594.99 cm^{-1} before adsorption to 562.25 cm^{-1} and 592.15 $cm^{-1,}$ respectively, for all Ni_3AlCO_3 clays after lead adsorption. The band's shift around 562 cm-1 has been assigned to hydroxyl groups associated with mainly Al [34], and bounds around 592 cm-1 have been given as hydroxyl groups associated with Al/Ni. The shift of these two bonds is assigned to the formation of M-O-Pb according to the reaction proposed above (case of Mg_3AlCO_3) (M = Ni^{2+} or Al^{3+}) [32]. Before the adsorption of Pb^{2+}, the strong and broad absorption band centred on 3483.20 cm^{-1} corresponds to the O–H stretching vibration of the layer surface and interlayer water molecules, and the band in 1652.88 cm^{-1} is due to the O–H bending vibration of water molecules. After adsorption of the lead, we notice the reduction and slight shift of the bands, which are centred towards a low frequency at 3482.53 cm^{-1}, indicating that the hydroxyl groups electrostatically attracted Pb^{2+} anions.

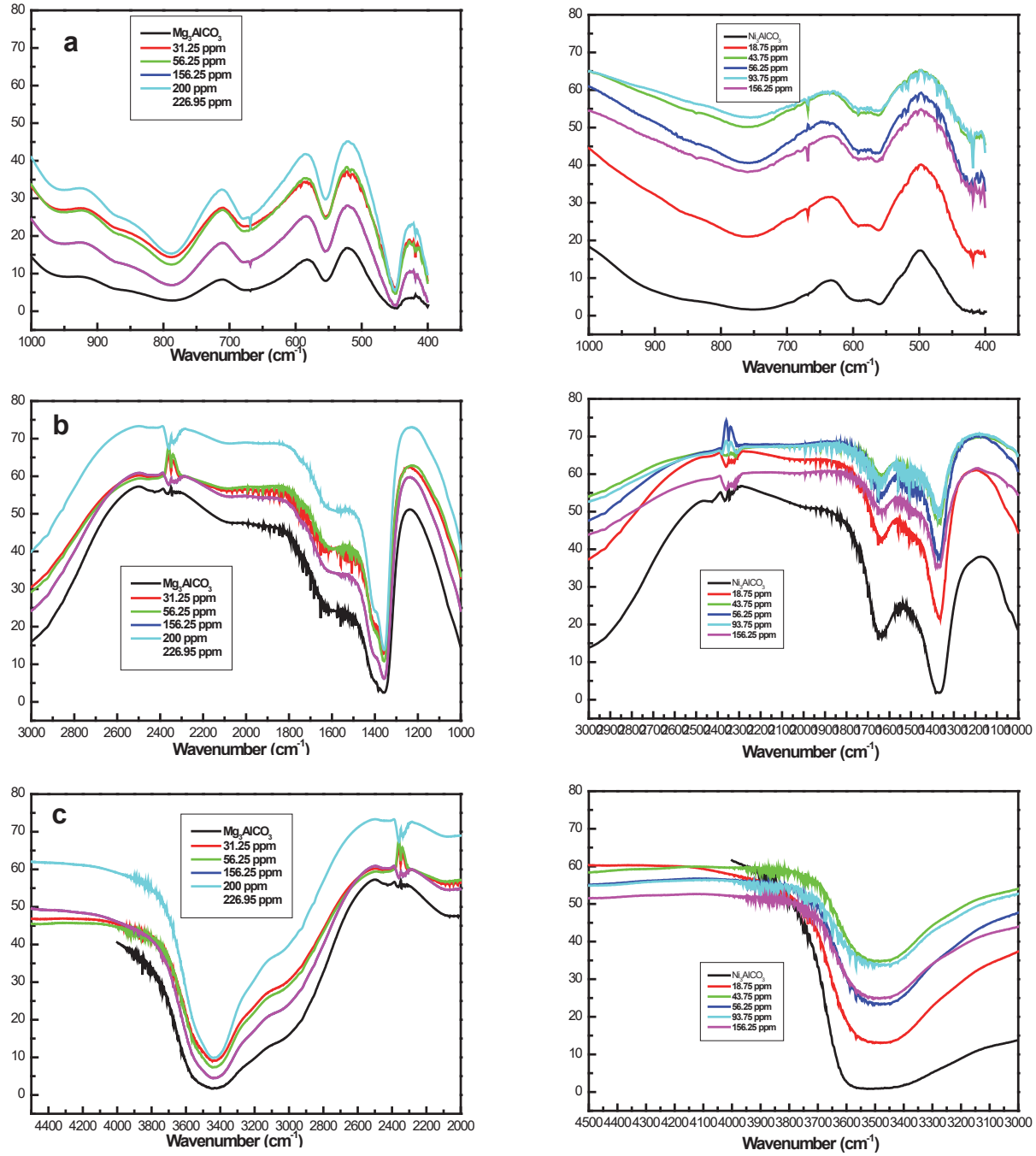

Fig. 12. FT-IR spectra of Mg_3AlCO3 and Ni_3AlCO_3 before and after uptake of lead at different concentrations. (a) region to 1000 cm^{-1} to 400 cm^{-1}, (b) region to 3000 cm^{-1} at 1000 cm^{-1}, and (c) region to 4500 cm^{-1} to 3000 cm^{-1}

3.4.2.Model of adsorption isotherms

Modelling adsorption isotherm data is essential for predicting and comparing adsorption performance. Lead (Pb) adsorption was modelled using Langmuir, Freundlich, and Temkin models. The linear equations that correspond to the three models are presented in Equations 9, 10, and 11 [28, 35].

$$\frac{C_e}{q_e} = \frac{1}{q_m K_L} + \frac{C_e}{q_m} \quad \text{(Eq. 9)}$$

$$\ln q_e = \frac{1}{n}\ln C_e + \ln(7) \quad \text{(Eq. 10)}$$

$$q_e = B.\ln A + B \quad \text{(Eq. 11)}$$

Where C_e, q_e, and q_m (mg g^{-1}) are the equilibrium concentration of lead (mg g^{-1}), the quantity of Pb^{2+} adsorbed at equilibrium (mg g^{-1}), and the maximum monolayer adsorption capacity of adsorbent (mg g^{-1}), respectively. n and K_F are the Freundlich adsorption constants. K_L is the Langmuir adsorption constant (Lmg^{-1}). This last parameter is used to calculate the dimensionless equilibrium parameter (R_L) that explains the favorability of the adsorption process; R_L is calculated from Equation 12 [35].

$$R_L = \frac{1}{1 + K_L C_0} \quad \text{(Eq. 12)}$$

B is a constant related to the heat of adsorption, which equals B = RT/b. R, T, and b are the gas constant (8.314 $J.mol^{-1} K^{-1}$), the absolute temperature (K), and the Temkin constant ($J\ mol^{-1}$). Typical adsorption isotherms for Pb^{2+} on all selected anionic clays are shown in Figures 13, 14 and 15, respectively, for the Langmuir, Freundlich, and Temkin models.

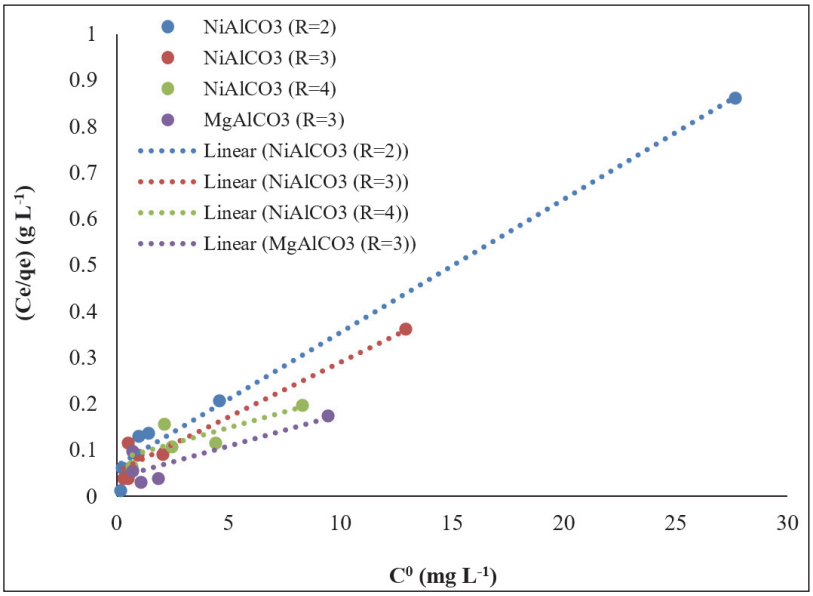

Fig. 13. Langmuir isotherm model of the studied anionic clays

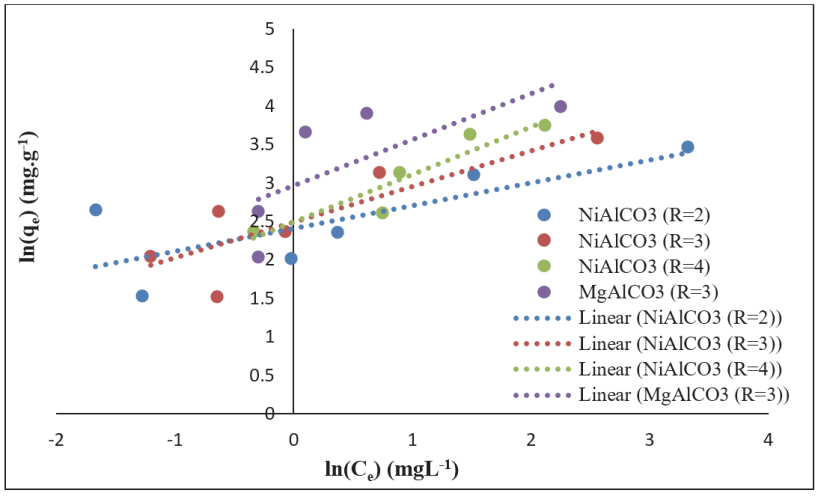

Fig. 14. Freundlich isotherm model of the studied anionic clays

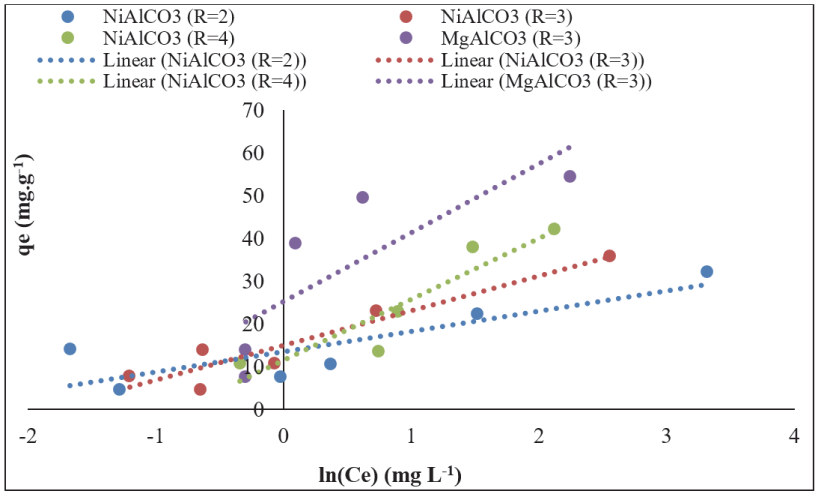

Fig. 15. Temkin isotherm model of the studied anionic clays

According to Figures (12 and 14) and the regression coefficients found and shown in Table 4, the Pb^{2+} adsorption data on all the anionic clays followed the Langmuir and Temkin models. The values of the equilibrium parameter without dimension R_L are between 0 and 1 for all the studied clays, showing that the adsorption of lead is favourable (Table 4).

The lead adsorption capacity values (Qm) found from the Langmuir model show that Mg_3AlCO_3 has a large adsorption capacity (73.42 mg g^{-1}). For Ni/Al-based clays, the Pb^{2+} ions adsorption capacity increases with the increase of the molar ratio, and Ni_4AlCO_3 has a Pb^{2+} adsorption capacity close to Mg_3AlCO_3.

Table 4. Parameters of Pb^{2+} adsorption isotherm models on selected anionic clays

Langmuir	**q_{max} (mg g^{-1})**	**b (L mg^{-1})**	**R_L**	**R^2**
Mg_3AlCO_3	73.42	0.33	0.04	0.73
Ni_2AlCO_3	35.71	0.44	0.05	0.98
Ni_3AlCO_3	43.47	0.44	0.05	0.95
Ni_4AlCO_3	72.51	0.17	0.07	0.66
Freundlich	**K_f**	**(n)**		**R^2**
Mg_3AlCO_3	19.29	1.67		0.52
Ni_2AlCO_3	11.14	3.37		0.60
Ni_3AlCO_3	12.05	2.15		0.72
Ni_4AlCO_3	12.08	1.62		0.95
Temkin	**K_t(L mg^{-1})**	**b**	**B_T (j mol^{-1})**	**R^2**
Mg_3AlCO_3	1.00	155.14	16.13	0.66
Ni_2AlCO_3	16.96	527.95	4.74	0.85
Ni_3AlCO_3	6.35	309.33	8.09	0.89
Ni_4AlCO_3	2.24	176.35	14.19	0.85

According to the correlation coefficients of the Freundlich model, the total experimental data on lead adsorption on anionic clays do not follow the Freundlich model (Table 4). The n value in the range of 1.62–3.37 indicates a favourable adsorption process. The correlation coefficients for the Temkin model of all the clays studied show that this last model adequately represents the experimental data on lead adsorption. The Temkin constant (BT) values presented in Table 4, related to the heat of sorption of Pb^{2+}, increase with the increase of the molar ratio of Ni/Al.

3.5. Thermodynamic parameters

To describe the thermodynamic behaviour of the absorption of Pb^{2+} ions in the aqueous solution, we use the following Equation13 and 14 [35, 36].

$$\ln K_D = \frac{-\Delta H}{RT} + \frac{\Delta S}{R} \quad \text{(Eq.13)}$$

$$\Delta G = -RT \ln K_D \quad \text{(Eq.14)}$$

where ΔH, ΔS, ΔG and T are the enthalpy, entropy, Gibbs free energy, and absolute temperature, respectively, and R is the gas constant (8.314 J k^{-1}. mol^{-1}), $K_D = (q_e/C_e)$, which depends on temperature. The thermodynamic parameters are determined starting from the lines of ln (k_D) vs. (1/T) in the linear domain of temperature, corresponding to the adsorption of lead, i.e., between 20°C and 50°C. The thermodynamic parameters are presented in Table 5. The positive values of enthalpy suggested the endothermic nature of the adsorption. They reflected the affinity of the adsorbent for Pb^{2+} ions [36]. The low H values for both adsorbents are 17.39 KJ mol^{-1} for Mg_3AlCO_3 and 4.97 for Ni_3AlCO_3, which are less than 40 KJ mol^{-1}. It shows a physical adsorption between Pb^{2+} ions and these clays [37]. Positive entropy values showed that the randomness at the solute-solution interface increases with the adsorption of Pb^{2+} in the adsorption process. Negative free energy values indicate a spontaneous process of the adsorption of Pb^{2+} by Mg_3AlCO_3 and Ni_3AlCO_3. These results obtained for Mg_3AlCO_3 agree with those found by Ayawei et al. [38].

4. Conclusion

As part of the study of layered double hydroxides and the possibility of using them as adsorbents to remove lead from water, we have synthesized in our laboratory two types of anionic clays by the direct co-precipitation method, namely Mg_3AlCO_3 and Ni_3AlCO_3. The analysis techniques used to characterize the LDHs show that the synthesized clays are materials from the family of layered double hydroxides. They have the same properties as the anionic clays of the Mg_3AlCO_3 and Ni_3AlCO_3 types. The pH, adsorbent mass, temperature, contact time, and molar ratio show that the adsorption capacity of Pb^{2+} by Mg_3AlCO_3 is higher than that of Ni_3AlCO_3. According to the Langmuir model,

Table 5. Thermodynamic parameters for the adsorption of Pb^{2+} by Mg_3AlCO_3 and Ni_3AlCO_3 at various temperatures

Adsorbent	ΔS (KJ.K^{-1}.mol^{-1})	ΔH (KJ.mol^{-1})	Temperature			
			298 K	303 K	313K	323 K
			K_d			
Mg_3AlCO_3	0.065	17.39	2.32	2.90	2.72	4.02
			ΔG (KJ.mol^{-1})			
			-2,08	-2.68	-3.42	-3.74
			K_d			
Ni_3AlCO_3	0.018	4.97	1.261	1.265	1.363	1.461
			ΔG (KJ.mol^{-1})			
			-0.576	-0.594	-0.80	- 0.102

Ni_4AlCO_3 and Mg_3AlCO_3 clays have a high lead adsorption capacity, and the maximum adsorption capacity values are 72.51mg g^{-1} and 73.42 mg g^{-1} for Ni_4AlCO_3 and Mg_3AlCO_3, respectively. At an optimal pH of 6.5, the removal percentages reach 95.4 % and 81.3 % for Mg_3AlCO_3 and Ni_3AlCO_3, respectively. The adsorbed amount increases with increasing temperature for both types of LDHs, where the lead removal percentages reach 94.16 % and 85.39 % for Mg_3AlCO_3 and Ni_3AlCO_3, respectively, and the adsorption capacities of Pb^{2+} were obtained ($Q_{Ni4AlCO3} > Q_{Ni3AlCO3} > Q_{Ni2AlCO3}$). The results showed that at pH below 6.5, the removal of Pb^{2+} may be achieved by complexation reactions, and the lead precipitated at higher pH. The experimental data on lead adsorption kinetics show that the pseudo-second-order model best describes the adsorption kinetics. The results of the applied Pb^{2+} adsorption isotherm models indicate that the Langmuir and Temkin models are the most adequate to represent the experimental data for both adsorbents. In addition, thermodynamic parameters show that the adsorption of lead by Mg_3AlCO_3 and Ni_3AlCO_3 is endothermic, spontaneous and random at the solute-solution interface.

5. Acknowledgements

The authors would like to thank the MESRS and DGRSDT (Ministère de l'Enseignement Supérieur et de la Recherche Scientifique et la Direction Générale de la Recherche Scientifique et du Développement Technologique- Algérie) for their Financial support.

6. Conflict of interest

We have no conflicts of interest to disclose.

7. References

[1] T.V. Toledo, C.R. Bellato, K.D. Pessoa, M.P. Fontes, Magnetic compounds based in hydrotalcites for removal of anionic contaminants in water, Quim. Nova., 36 (2013) 419–425. http://doi.org/10.1590/S0100-40422007000500005.

[2] M. Bouraada, F. Belhalfaoui, M.S. Ouali, Sorption study of an acid dye from an aqueous solution on modified Mg–Al layered double hydroxides, J. Hazard. Mater., 163 (2009) 463–467. http://doi.org/ 10.1016/j.jhazmat.2008.06.108

[3] L. D. Miranda, C. R., Bellato, M. P. Fontes, M. F. de Almeida, J. L. Milagres, L. A. Minim, Preparation and evaluation of hydrotalcite-iron oxide magnetic organocomposite intercalated with surfactants for cationic methylene blue dye removal, Chem. Eng. J., 254 (2014) 88-97. http://doi.org/10.1016/j.cej.2014.05.094

[4] R. Shi, P. Yangn, Y. Yin, X. Dong, J. Li. Fabrication of porous microspheres and network arrays of Zn–Al hydrotalcite-like compounds on Al substrate via facile hydrothermal method, Ceram. Int., 40 (2014) 6855–6863. http://doi.org/10.1016/j.ceramint.2013.12.005.

[5] E. Ramos-Ramírez, N. L. Gutiérrez Ortega, C. A. Contreras Soto, M. T. Olguín Gutiérrez, Adsorption isotherm studies of chromium (VI) from aqueous solutions using sol–gel hydrotalcite-like compounds, J. Hazard. Mater., 172 (2009) 1527–1531. http://doi.org/10.1016/j.jhazmat.2009.08.023

[6] S. V. Prasanna, P. V. Kamath, Anion-exchange reactions of layered double hydroxides: interplay between coulombic and H-bonding interactions, Ind. Eng. Chem. Res., 48 (2009) 6315-6320. http://doi.org/10.1021/ie9004332

[7] A. V. Radha, P. V. Kamath, C. Shivakumara, Mechanism of the anion exchange reactions of the layered double hydroxides (LDHs) of Ca and Mg with Al, Solid State Sci., 7 (2005) 1180-1187. http://doi.org/10.1016/j.solidstatesciences.2005.05.004

[8] M. Lakraimi, A. Legrouri, A. Barroug, A. DeRoy and J. P. Besse, Preparation of a new stable hybrid material by chloride–2,4-dichlorophenoxyacetate ion exchange into the zinc–aluminium–chloride layered double hydroxide, J. Mater. Chem., 10 (2000) 1007-1011. http://doi.org/10.1039/A909047I

[9] N. Drici. Hydroxydes doubles lamellaires, synthèse, caractérisation et propriétés.

Matériaux. Université Sorbonne Paris Cité, Français, NNT: 2015USPCD007, 2015. https://theses.hal.science/tel-01488539v1/file/edgalilee_th_2015_drici.pdf

[10] E. Géraud, V. Prévot, J. Ghanbaja, F. Leroux, Macroscopically ordered hydrotalcite-type materials using self-assembled colloidal crystal template, Chem. Mater., 18 (2006) 238–240. http://doi.org/10.1021/cm051770i

[11] K. Kadirvelu, M. Kavipriya, C. Karthika, M. Radhika, N. Vennilamani, S. Pattabhi, Utilization of various agricultural wastes for activated carbon preparation and application for the removal of dyes and metal ions from aqueous solutions, Bioresour. Technol., 87 (2003) 129-32. http://doi.org/10.1016/s0960-8524(02)00201-8.

[12] A. K. Jain, V. K. Gupta, A. Bhatnagar, Utilization of industrial waste products as adsorbents for the removal of dyes, J. Hazard. Mater., 101 (2003) 31-42. http://doi.org/10.1016/s0304-3894(03)00146-8.

[13] Y. Yasin, M. Mohamad, A. Saad, A. Sanusi, F. H. Ahmad, Removal of lead ions from aqueous solutions using intercalated tartrate-Mg–Al layered double hydroxides, Desalin. Water Treatment., 52 (2014) 4266-4272. http://doi.org/10.1080/19443994.2013.803935

[14] S. Yanming, L. Dongbin, L. Shifeng, F. Lihui, C. Shuai, M. A. Haque, Removal of lead from aqueous solution on glutamate intercalated layered double hydroxide, Arab. J. Chemy., 10 (2017) S2295-S2301. http://doi.org/10.1016/j.arabjc.2013.08.005.

[15] E. J. Pacer, C. D. Palmer, P. J. Parsons, Determination of lead in blood by graphite furnace atomic absorption spectrometry with Zeeman background correction: Improving a well-established method to support a lower blood lead reference value for children, Spectrochim. Acta Part B: Atom. Spect., 190 (2022) 106324. http://doi.org/10.1016/j.sab.2021.106324

[16] M. S. Tudosie, G. Caragea, D. M. Popescu, O. Avram, D. Serban, C. G. Smarandache, A. M. Dascalu, Optimization of a GF AAS method for lead testing in blood and urine: A useful tool in acute abdominal pain management in emergency, Exp. Ther. Med., 22 (2021) 1-8. http://doi.org/10.3892/etm.2021.10417.

[17] ZW. Zhang, S. Shimbo, N. Ochi, M. Eguchi, T. Watanabe, CS. Moon, M. Ikeda, Determination of lead and cadmium in food and blood by inductively coupled plasma mass spectrometry: a comparison with graphite furnace atomic absorption spectrometry, Sci. Total Environ., 205 (1997) 179-87. http://doi.org/10.1016/s0048-9697(97)00197-6.

[18] M. Trzcinka-Ochocka, R. Brodzka, B. Janasik, Useful and fast method for blood lead and cadmium determination using ICP-MS and GF-AAS; validation parameters, J. Clin. Lab. Anal., 30 (2016) 130-9. http://doi.org/10.1002/jcla.21826.

[19] D. Fuger, Mise en application de processus analytique complexe Analyse de métaux par ICP-AES. Robert Schuman–Département chimie, Université de Strasbourg, France, 2011. https://www.chemphys.fr/mpb/teach/ICP-AES/ICP-AES.pdf

[20] R. Riyanto, Determination of lead in waste water using cyclic voltammetry by platinum wire electrode, J. Sci. Data Anal., 14 (2014) 22-33. http://doi.org/10.20885/eksakta.vol14.iss2.art3.

[21] F. Delorme, A. Seron, M. Bizi, V. Jean-Prost, D. Martineau. Effect of time on the reconstruction of the $Mg_4Al_2(OH)1_2CO_3.3H_2O$ layered double hydroxide in a Na_2CO_3 solution, J. Mater. Sci., 41 (2006) 4876-4882. http://doi.org/10.1007/s10853-006-0304-4

[22] K. Klemkaite, I. Prosycevas, R. Taraskevicius, A. Khinsky, A. Kareiva, Synthesis and characterization of layered double hydroxides with different cations (Mg, Co, Ni, Al), decomposition and reformation of mixed metal oxides to layered structures, Open Chem., 9 (2011) 275-282. http://doi.org/10.2478/s11532-011-0007-9

[23] A. Faour, C. Mousty, V. Prevot, B. Devouard,

A. De Roy, P. Bordet, C. Taviot-Gueho, Correlation among structure, microstructure, and electrochemical properties of NiAl–CO_3 layered double hydroxide thin films, J. Phys. Chem. C, 116 (2012) 15646-15659. http://doi.org/10.1021/jp300780w

[24] F. Cavani, F. Trifiro, A Vaccari, Hydrotalcite-type anionic clays: Preparation, properties and applications, Catal. Today, 11 (1991) 173-301. http://doi.org/10.1016/0920-5861(91)80068-K

[25] L. Xuefeng, H. Wanguo, X. Yingming, Sorption of lead ion by layered double hydroxide intercalated with diethylenetriaminepentaacetic acid, Colloids Surf. A Physicochem. Eng. Asp., 366 (2010) 50-57. http://doi.org/10.1016/j.colsurfa.2010.05.012

[26] D. Zhao, G. Sheng, J. Hu, C. Chen, X. Wang, The adsorption of Pb (II) on Mg_2Al layered double hydroxide, Chem, Eng, J., 171 (2011) 167-174. http://doi.org/10.1016/j.cej.2011.03.082.

[27] M. Arshadi, M. J. Amiri, S. Mousavi, Kinetic, equilibrium and thermodynamic investigations of Ni (II), Cd (II), Cu (II) and Co (II) adsorption on barley straw ash, Water Resour. Ind., 6 (2014) 1-17. http://doi.org/10.1016/j.wri.2014.06.001

[28] J. B. Huo, G. Yu, Layered double hydroxides derived from MIL-88A (Fe) as an efficient adsorbent for enhanced removal of lead (II) from water, Int. J. Mol. Sci., 23 (2022) 14556. http://doi.org/10.3390/ijms232314556

[29] G. W. Kajjumba, S. Emik, A. Öngen, H. K. Özcan, S. Aydın, Modelling of adsorption kinetic processes—errors, theory and application, Advanced Sorption Process Applications, page 1-19, 2018. http://doi.org/10.5772/intechopen.80495

[30] C. H. Giles, T. H. MacEwan, S. N. Nakhwa, D. Smith, Studies in adsorption. Part XI. A system of classification of solution adsorption isotherms, and its use in diagnosis of adsorption mechanisms and in measurement of specific surface areas of solids, J. Chem. Soc. Resumed., 32 (1960) 3973–3993. https://doi.org/10.1039/JR9600003973

[31] V. Rives, Layered double hydroxides: present and future, Nova Science Publishers, Inc., New York, 2001, http://doi.org/10.1016/S0169-1317(02)00112-6

[32] R. Marangoni, M. Bouhent, , C. Taviot-Gueho, F. Wypych, F. Leroux. Zn2Al layered double hydroxides intercalated and adsorbed with anionic blue dyes: A physico-chemical characterization, J. Colloid Interface Sci., 333 (2009) 120-127. http://doi.org/10.1016/j.jcis.2009.02.001

[33] T.N. Moroz, Formation of spinel from hydrotalcite-like minerals and destruction of chromite implanted by inorganic salts, App. Clay Sci., 18 (2001) 29–36. http://doi.org/10.1016/S0169-1317(00)00027-2

[34] P. Benito, I. Guinea, F. M. Labajos, V. Rives, Microwave-assisted reconstruction of Ni, Al hydrotalcite-like compounds, J. Solid State Chem., 181 (2008) 987-996. http://doi.org/10.1016/j.jssc.2008.02.003

[35] A. A. Inyinbor, F. A. Adekola, G. A. Olatunji, Kinetics, isotherms and thermodynamic modeling of liquid phase adsorption of Rhodamine B dye onto Raphia hookerie fruit epicarp, Water Resour. Ind., 15 (2016) 14-27. http://doi.org/10.1016/j.wri.2016.06.001

[36] J. X. Lin, S. L. Zhan, M. H. Fang, X. Q. Qian, H. Yang, Adsorption of basic dye from aqueous solution onto fly ash, J. Environ. Manage., 87 (2008) 193-200. http://doi.org/10.1016/j.jenvman.2007.01.001

[37] B. Houari, S. Louhibi, K. Tizaoui, L. Bouklihacene, B. Benguella, T. Roisnel, V. Dorcet, New synthetic material removing heavy metals from aqueous solutions and wastewater, Arab. J. Chem., 12 (2019) 5040-5048. http://doi.org/10.1016/j.arabjc.2016.11.010

[38] N. Ayawei, C. Y. Abasi, D. Wankasi, E. D. Dikio, Layered double hydroxide adsorption of lead: equilibrium, thermodynamic and kinetic studies, Int. J. Adv. Res. Chem. Sci., 2 (2015) 22-32. https://www.arcjournals.org/pdfs/ijarcs/v2-i5/3.pdf

Anal. Methods Environ. Chem. J. 6 (3) (2023) 89 - 102

AMECJ

Research Article, Issue 3
Analytical Methods in Environmental Chemistry Journal
Journal home page: www.amecj.com/ir

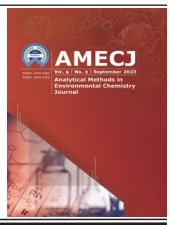

Chemical analysis of Eucalyptus and Rosemary essential oils using gas chromatography-mass spectrometry (GC-MS) and evaluation of their toxicity against the most common urban pest

Marzieh Asgari[a], Moloud Kazemi[b], Mohammad Mahmoudi Sourastani[c], and Mona Sharififar[d, *]

[a] *MSc student of Biology and Vector Control, School of Public Health, Jundishapur University of Medical Sciences, Ahvaz, Iran*

[b] *Department of Pharmaceutics, School of Pharmacy, Jundishapur University of Medical Sciences, Ahvaz, Iran.*

[c] *Department of Horticultural Sciences, Faculty of Agriculture, Shahid Chamran University of Ahvaz, Ahvaz, Iran.*

[d] *Department of Medical Entomology and Vector Control, School of Public Health, Jundishapur University of Medical Sciences, Ahvaz, Iran.*

ARTICLE INFO:

Received 23 May 2023

Revised form 28 Jul 2023

Accepted 13 Aug 2023

Available online 30 Sep 2023

Keywords:
Gas chromatography-mass spectrometry,
Eucalyptus,
Rosemary,
Essential oil,
Blatella germanica,
Toxicity,

ABSTRACT

Using plant essential oils (EOs) as a pesticide alternative has gained increasing interest as a promising strategy to reduce the harmful effects of chemical pesticides. This study aims to investigate the chemical composition of *Eucalyptus globulus* Labill and *Rosmarinus officinalis* L. essential oils and evaluate their impacts against *Blattella germanica* L. under laboratory conditions. The essential oils were prepared from dried leaves using hydro-distillation (HD) as a chemical extraction method. The gas chromatography-mass spectrometry (GC-MS) was employed to analyze and identify their chemical compounds. Bioassays were conducted using the standard contact method recommended by the World Health Organization, and the data were analyzed using the probit regression model. By GC-MS analysis, the major components included 1,8-cineole (50.67%), alpha-pinene (17.48%), limonene (4.26%) for eucalyptus and alpha-pinene (20.67%), camphor (10.69%), 1,8-cineole (9.38%), Borneol (9.02%), comphene (7.15%), and limonene (4.88%) for rosemary. The LD_{50} values were 9. 27, 10.54, and 3.23 %, and LD_{95} values increased to 27.2, 22.3 %, and 14.3% for rosemary, eucalyptus, and their mixture. The EOs mixture had a higher repellent effect with a repellency rate of 98.9% at a concentration of 3% compared to 93.3% and 90% at a concentration of 5% for rosemary and eucalyptus alone. The mixture of eucalyptus and rosemary EOs can be a promising alternative for controlling the German cockroach.

1. Introduction

Essential oils are a liquid that is chemically extracted from plants by different solvents. Essential oils are liquefied versions of plants such as *Eucalyptus globulus* Labill. and *Rosmarinus officinalis.* The extraction methods include steam distillation (SD), solvent extraction (SE), enfleurage, cold extraction (CE), and water distillation (WD). Also, pressure and temperatures affect the extraction procedure or sample preparation of essential oil.

*Corresponding Author: Mona Sharififard
Email: sharififard-m@ajums.ac.ir, sharififardm@yahoo.com
https://doi.org/10.24200/amecj.v6.i03.256

Steam distillation is a common method used for extracting essential oils from plants by chemistry methods b and analysis by UV-Vis, GC-FID, GC-MS, HPLC, LC-MS, solvent-microwave, and FTIR techniques. Solvent microwave extraction was also used to prepare essential oil [1,2]. The German cockroach (*Blattella germanica* L.) is one of the most important and common urban pests that can significantly threaten public health. This cockroach species exists in human environments, including restaurants, hotels, hospitals, and food storage areas. It can mechanically transmit disease-causing agents such as bacteria, viruses, fungi, protozoa, and parasite eggs to humans through their digestive system. Therefore, controlling this pest is of great importance. This cockroach species can also cause allergic reactions, including severe respiratory distress [3, 4]. The overuse of synthetic pesticides has led to the development of resistance in many populations of German cockroaches, highlighting the need for alternative pest control strategies [5]. On the other hand, insect resistance is one of the major consequences of pesticides in recent decades, resulting from excessive and indiscriminate chemical pesticides. Excessive use of pesticide compounds has led to resistance in various populations of health-importance pests and insect vectors. It has caused the emergence of insects resistant to various insecticides [6]. The high toxicity of chemical insecticides to humans and wildlife and environmental contamination has led to extensive research in recent years to introduce low-risk compounds for pest control [7-8]. Given the public concerns about chemical pesticides in residential areas, finding safe alternatives for urban pest control is a serious necessity [9]. GC–MS was used for essential oil analysis, and extracting, separating, and identifying essential oils (EOs) from a natural plant was studied. The chemical compounds in EOs were separated and analyzed by gas-chromatography-mass–spectrometry (GC–MS). The different chemical components are compared with two extraction methods [10]. An analytical chemistry method was used based on the identification and determination of linalool in essential oils. The internal standard method was used based on headspace solid phase microextraction (SPME) and gas chromatography–mass spectrometry (GC-MS). The experiments showed the effectiveness of the internal standard method based on the regression analysis of the calibration curve with perfect linearity ($R2 \geq 0.98$) [11]. Over 20 plant essential oils and their components have been listed as low-risk pesticides by environmental protection agencies. They are exempt from registration requirements [12]. Rosemary and eucalyptus are two plants that have been studied in recent years for their insect toxicity and repellent effects against pests. Rosemary (*Rosmarinus officinalis* L.) from Lamiaceae is a perennial herb that grows as small evergreen shrubs in countries around the western Mediterranean Sea. The yield of rosemary essential oil by steam distillation is high, and it has a wide range of applications in the pharmaceutical, cosmetic, and food industries [1]. *Eucalyptus* spp., a genus belonging to the Myrtaceae family, has more than 800 different species, and although it originates from the continent of Australia, it has been grown in many tropical and subtropical regions due to its high adaptability and rapid growth for obtaining wood, gum, cellulose, and essential oils. Essential oils and extracts isolated from the aerial parts of this plant have been used in traditional medicine [13]. The use of essential oils as plant-based pesticides has numerous advantages. Firstly, complex mixtures of active compounds present in essential oils can often exhibit synergistic effects that can slow down pesticide-resistant growth in pest populations. Additionally, mixtures of two or more essential oil components have been shown to exhibit synergistic, additive, or antagonistic effects on various insects, including spiders, nematodes, house flies, plant mites, and moths. Synergistic toxic interactions are relevant to pest management and the development of effective natural product formulations, and they enable us to achieve higher mortality rates with lower amounts of active ingredients [14-15]. There are many plants' essential oil components that have insecticidal effects. Some

essential oils contain compounds such as carvacrol, thymol, and eugenol, which have insecticidal properties. Other essential oils contain compounds like citronellal, geraniol, and limonene, known for their insect-repellent properties. In addition to these compounds, many essential oils contain other volatile organic compounds that can have insecticidal or insect-repellent properties. These include terpenes, aldehydes, ketones, and esters. The other components in the essential oils that contribute to their insecticidal properties depend on the specific plant from which the essential oil is extracted. Each plant has a unique combination of essential oil components contributing to its insecticidal properties. It's worth noting that the precise mechanisms by which these essential oil components exert their insecticidal effects are not always fully understood. Some compounds may interfere with the insect's nervous system, while others may disrupt its feeding or reproductive systems [16-19]. Although the insecticidal activity of plant extracts against numerous agricultural and storage pests and some medical pests has been demonstrated, few studies have been conducted on the German cockroach [1]. This study investigates the chemical composition of essential oils extracted from *R. officinalis* and *E. globulus* using gas chromatography-mass spectrometry (GC-MS). Furthermore, this study evaluates these essential oils' toxicity and repellent activity alone and in combination as an environmentally friendly method against the German cockroach (*B. germanica*). Essential oils as a pesticide alternative have become increasingly popular due to their environmentally friendly nature. By conducting this research, we aim to contribute to the development of safer and more efficient pest control methods using plant-based essential oils.

2. Materials and Methods

2.1. Instrument

A gas-chromatography-mass spectrometer (GC-MS) was used to analyze and identify rosemary and eucalyptus essential oil compounds (Hewlett-Packard 6890, Agilent Technology, Santa Clara, California, USA). The Clevenger-type apparatus was used for sample preparation of necessary oil extraction by two chemistry methods (Fig.1).

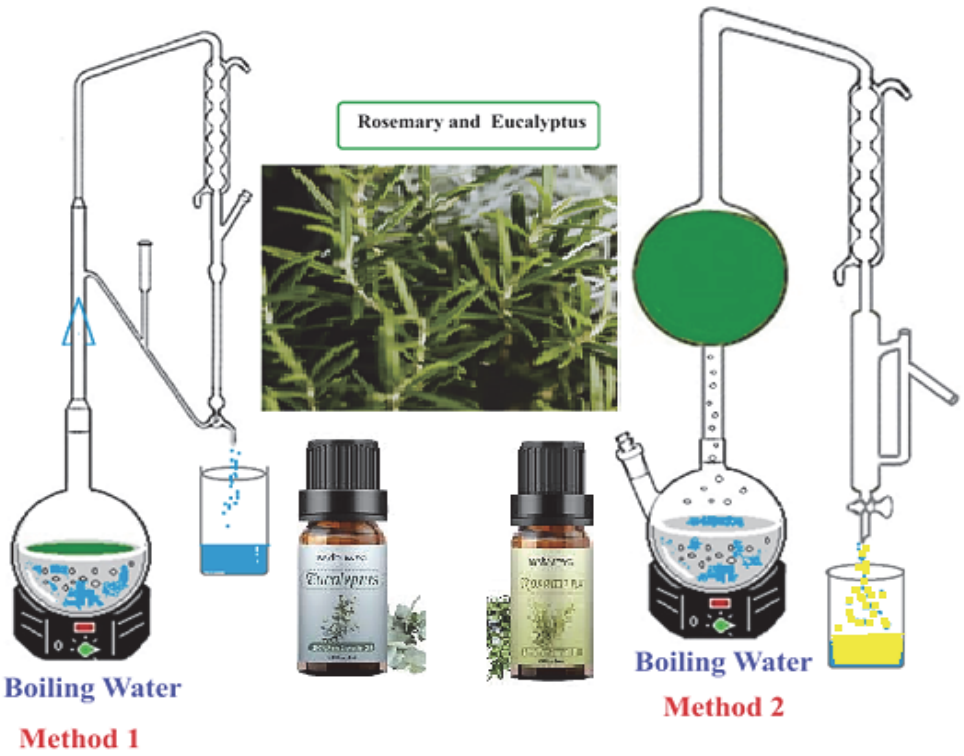

Fig.1. The Clevenger-type apparatus was used for sample preparation of essential oil by two extraction methods.

2.2. Plant collection

The fresh leaves of the *E. globulus* and *R. officinalis* plants were collected from the herbal garden of Chamran University in Ahvaz, Iran. Collected rosemary and eucalyptus specimens were identified by the Department of Horticultural Sciences at Chamran University in Ahvaz.

2.3. Extraction procedure of essential oil

Dry samples (100 g) of rosemary and eucalyptus were poured into a 1L flask. Then, 600 cc of deionized water was added to the flask and subjected to hydro-distillation in a Clevenger-type apparatus. In the Clevenger apparatus, rosemary and eucalyptus are mixed with water and boiled at 100^{0}C. After boiling, volatile components evaporated (in a position of steam distillation). In addition, the steam moved to a bed of rosemary and eucalyptus plants. In both methods, two layers of liquid and oil-rich phases were achieved. The oil phase was separated by separating funnels. Also, compounds in water are frequently distilled, water saturated with mixtures of rosemary and eucalyptus plants and their combinations are collected in the oil phase. The essential oil extraction process lasted approximately four h to 100 °C (Fig. 2). Then, the extracts were exsiccated by anhydrous sodium sulphate and stored in a dark glass vial at 4°C in a refrigerator for further experiment.

2.4. Rearing of the German cockroaches

The study was conducted on a susceptible strain of German cockroach kept in the Medical Entomology and Vector Control laboratory of Jundishapur University of Medical Sciences for one year. The cockroaches were reared in plastic containers with open mouths (Boucal) and fed on breadcrumbs, biscuits, and baguette crumbs. The containers were kept in a germinator at 27±3°C and 55±5% humidity under a 12:12 L: D.

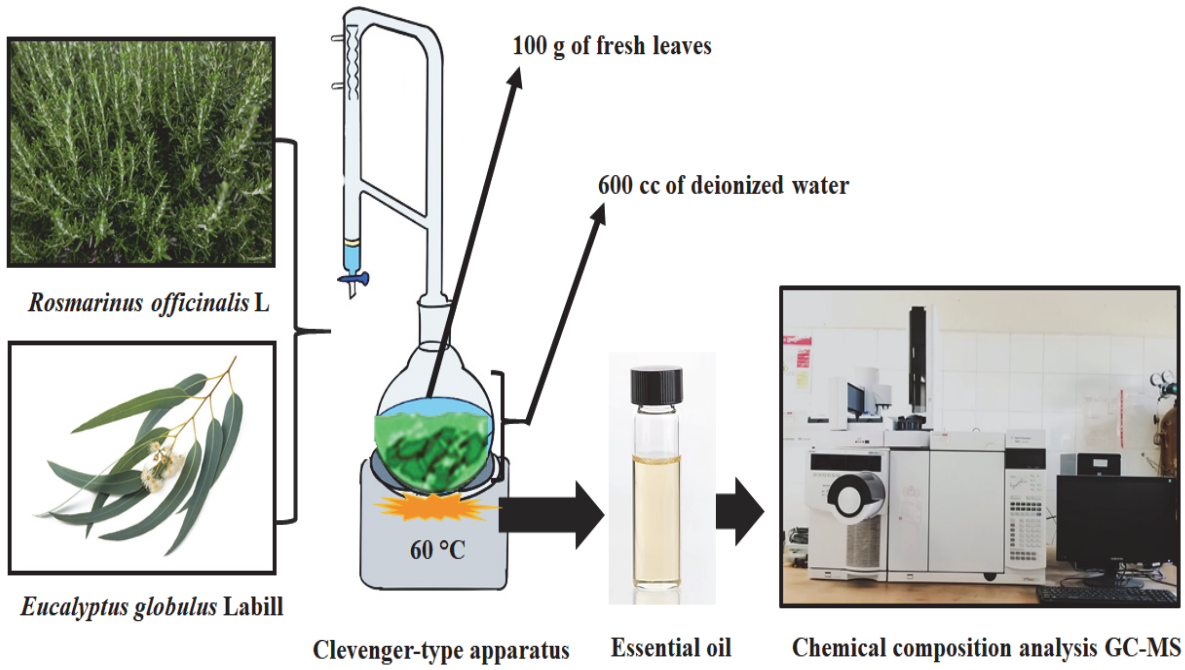

Fig. 2. The procedure of collecting plants, extracting, sample preparation, and GC-MS analysis of essential oils

2.5. Plant Analysis by Gas-chromatography-mass spectrometer (GC-MS)

GC-MS was used for EOs analysis (Fig. 2). It is equipped with HP–5MS column (30 m× 0.25 mm× 0.25 µm). The initial temperature used was 40 °C for 1 min and was later raised to 220 °C at a rate of 3 °C/min and finally raised to 270 °C for 5 min at a rate of 20 °C/min. Other parameters of the GC-MC machine included carrier gas Helium (99/999%), injector temperature (260 °C), detector temperature (FID, 270 °C), split-less mode, ionization potential of 70eV, scan rate of 1 scan/sec, the scan range of m/z 40–48 was used for all analysis. The essential oil constituents were identified by comparing their retention indices mass spectra fragmentation with those in a stored Wiley 7n.1 mass computer library and those of the National Institute of Standards and Technology (NIST).

2.6. Toxicity and Repellency assay

To assess the sensitivity of German cockroaches to the essential oils, the tarsal contact bioassay method recommended by the World Health Organization was used [20]. Different concentrations of eucalyptus and rosemary essential oils (5%, 7.7%, 10%, 14.1%, and 20%) were prepared using acetone as a solvent before analysis by GC-MS. Then, 2 mL of each concentration was applied to the inner surface of 500 mL glass jars. After the solvent evaporated, ten males or high-instar nymphs were released into each jar, and the jars were covered with mesh lids. The cockroaches were exposed to the treated surface for 30 minutes, transferred to clean jars, and kept at 27±2°C, 55±5% RH, and a 12:12 L: D. The control group was treated with acetone. The number of dead cockroaches was recorded after 24 hours. The bioassay was performed in four replicates. To evaluate the repellency of eucalyptus and rosemary essential oils against German cockroaches, plastic containers (17 × 10 × 5 cm) were used. The inner side of the container`s walls was lined with Vaseline to prevent the escape of cockroaches. The bottom of each container was covered with filter paper and divided into two equal parts by a line. Different concentrations (1%, 3%, 5%, and 7%) of each essential oil and their mixture in a 1:1 ratio was prepared with acetone [$(CH3)_2CO$] as solvent. One side of the filter papers was treated with 2 mL of each concentration. Ten adult cockroaches were released in the center of each container. They were kept under 27±2°C, 55±5% RH, and 12:12 L: D conditions. The containers were checked after 24 and 48 hours, and the number of dead and alive cockroaches in each half of the filter paper was recorded. The control group was treated with 2 mL of acetone. The test was performed in four replicates. The repellency percentage was calculated using Equation 1.

$$\text{Repellency}\,(\%) = 100 - (T \times 100)/N \qquad \text{(Eq.1)}$$

T: The number of cockroaches in the treated half of the filter paper.
N: The total number of released cockroaches.

2.7. Combined Insecticidal Effect

A proportion of eucalyptus (1:1) and rosemary essential oils was combined, and different concentrations (5%, 7.7%, 10%, 14.1%, and 20%) were prepared using acetone as a solvent. The contact bioassay method, as described above, was used, and the mortality of the cockroaches was recorded after 24 hours. The test was performed in four replicates.

2.8. Statistical GC-MS Analysis

Data were first corrected using the Abbott formula and mortality of the control group. Then, a probit regression analysis (dose-response analysis) was performed. Furthermore, the data were analyzed through ANOVA with mean comparisons and SPSS 24 software for statistical analysis.

3. Results and Discussion

3.1. GC-Mass Analysis

The GC-Mass analysis of eucalyptus and rosemary essential oils is represented in Table 1. The significant components of eucalyptus essential oil typically include 1,8-cineole (Eucalyptol, 1,3,3-Trimethyl-2-oxabicyclo[2.2.2]octane, 1,8-Cineole, 1,8-Epoxy-

p-menthane; 50.67%), α-pinene ((1S,5S)-2,6,6-Trimethylbicyclo[3.1.1]hept-2-ene(−)-α-Pinene); 17.48%), Aromadendrene (1,1,7-Trimethyl-4-methylenedecahydro-1H-cyclopropa[e] azulene; 4.27%) and limonene (1-Methyl-4-(prop-1-en-2-yl)cyclohex-1-ene; 4.26%), while the major components of rosemary essential oil typically include alpha-pinen ((1S,5S)-2,6,6-Trimethylbicyclo[3.1.1]hept-2-ene (−)-α-Pinene); 20.67%), verbenone (rel-(1R,5R)-Pin-2-en-4-one; 11.8%), camphor (1,7,7-Trimethylbicyclo[2.2.1] heptan-2-one; 10.69%), 1,8-cineole (9.38%), Borneol ((1R,2S,4R)-1,7,7-trimethylbicyclo[2.2.1] heptan-2-ol; 9.02%) and comphene (7.15%). Limonene in both essential oils has been almost the same (4.26 and 4.28%). In addition, chemical analysis of rosemary (*officinalis*) and eucalyptus (*globulus*) is shown in Figure 3.

3.2. Toxicity assay

The probit analysis also showed that the insecticidal effect or lethal doses of the mixture of rosemary and eucalyptus essential oils in the mean of LD_{50} and LD_{95} values decreased to nearly one-third compared to essential oils used separately. In other words, the results indicated the synergistic effect of combining these two essential oils (Table 2). The lethal dose values of 50% and 95% of rosemary and eucalyptus essential oils do not significantly differ due to the overlap of the confidence interval ranges. However, each has a significant difference with a mixture of EOs due to the lack of overlap in confidence intervals.

Table1. Constituents of *Rosmarinus officinalis* and *Eucalyptus globulus* essential oils by GC-MS analyses.

Rosmarinus officinalis (GC-MS)			Eucalyptus globulus (GC-MS)		
RT	***Major Constituents (%)***	***Components***	***RT***	***Major Constituents (%)***	***Components***
7.825	20.67	α-Pinene	7.819	17.48	α-Pinene
8.208	7.15	Camphene	9.015	0.79	β-Pinene
9.003	0.71	β-Pinene	9.461	1.05	β-Myrcene
9.318	2.39	3-Octanone	9.833	0.2	1-Phellandrene
9.456	2.45	β-Myrcene	10.565	4.26	Limonene
10.182	0.32	α-Terpinene	10.731	50.67	1,8-Cineole
10.423	1.82	p-Cymene	11.452	0.68	γ-Terpinene
10.554	4.88	Limonene	12.328	2.48	α-Terpinolene
10.634	9.35	1,8-Cineole	14.92	1.26	4-Terpineol
11.435	0.26	γ-Terpinene	15.309	1.99	α-Terpinolene
12.316	0.6	α-Terpinolene	20.31	0.17	δ-Cadinene
12.666	1.98	Linalool	21.265	1.29	α-Gurjunene
13.987	10.69	Camphor	21.838	0.2	Calarene
14.622	9.02	Borneol	22.015	4.27	Aromadendrene
14.834	0.93	Pinocamphone	23.394	1.47	Ledene
14.92	1.22	4-Terpineol	23.84	0.15	Naphthalene
15.326	2.13	β-Fenchyl	24.046	0.25	δ-Cadinene
15.893	11.8	Verbenone	25.122	0.39	Azulene
17.97	3	Bornyl acetate	26.387	0.61	γ-Gurjunene
19.44	0.23	3-Terpinolenone			
21.512	0.95	t-Caryophyllene			
22.364	0.18	α-Humulene			
25.483	0.29	Isocaryophillene			

RT: Retention time

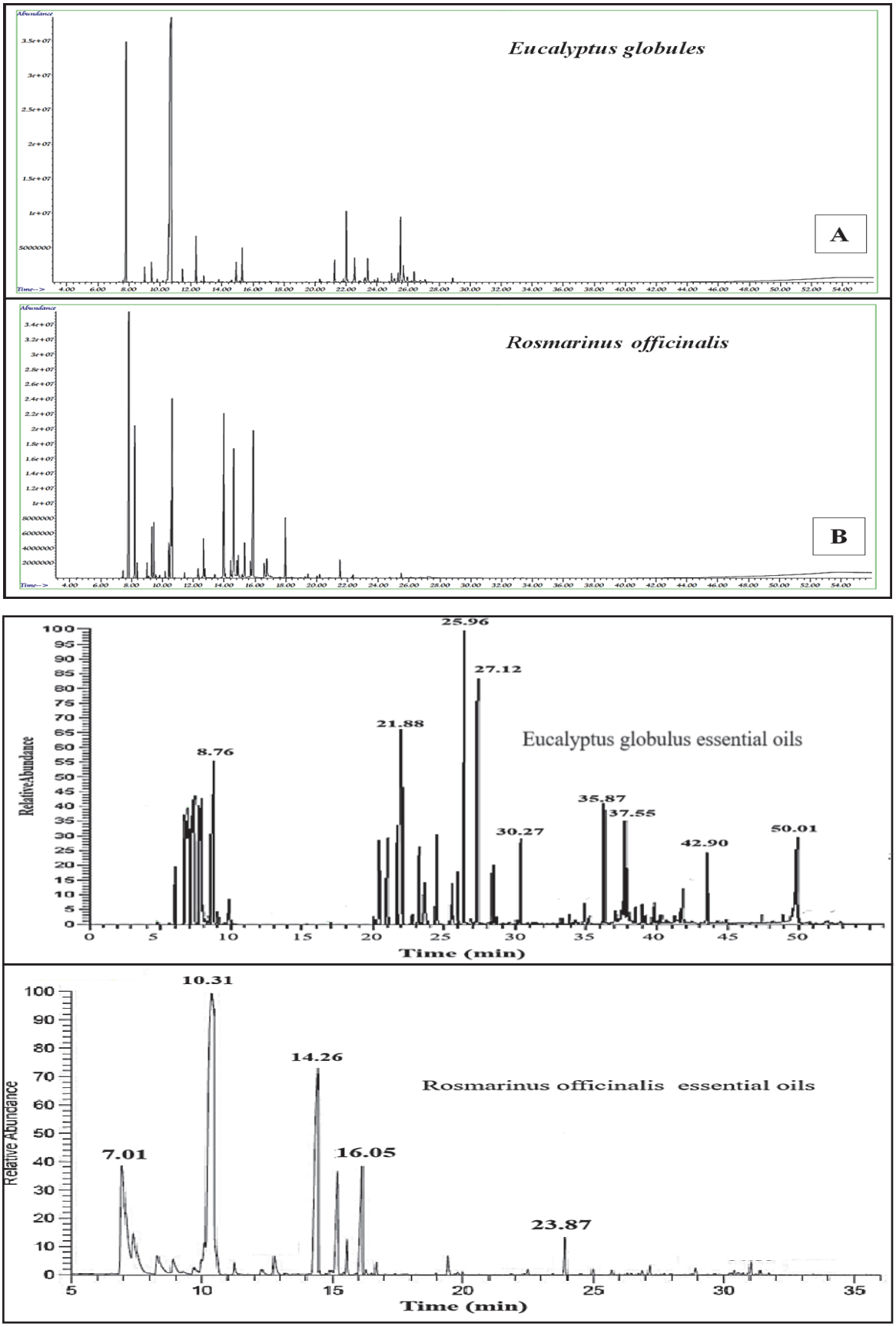

Fig. 3. GC-MS chromatogram based on chemical analysis for essential rosemary oil (Rosmarinus officinalis L.) and eucalyptus (Eucalyptus globulus Labill).

Table 2. Lethal doses of rosemary and eucalyptus essential oils and their mixture against *B. germanica* under laboratory conditions.

Essential oil	LD_{50} (Cl)	LD_{95} (Cl)	Slop (±SE)	N^2 (df)
Eucalyptus	10.54 (9.2 – 12.1)	27.2 (21 – 42.4)	3.9 ± 0.63	12.85 (13)
Rosemary	9.27 (8.11 - 10.51)	22.31 (17.9 – 32.2)	4.3 ± 0.63	6.41 (13)
Eucalyptus+ Rosemary	3.23 (0.83 – 4.85)	14.3 (10.3 – 31.14)	2.26 ± 0.67	8.73 (13)

The results of this insecticidal activity showed that the cockroach mortality rate ranged from 10% to 93% for rosemary and 8.6% to 90% for eucalyptus, depending on the concentration used in the study on susceptible German cockroach males by the contact surface method. The highest mortality effect for both essential oils was observed at a concentration of 20%. However, no significant difference in the percentage of cockroach mortality was observed between 14.1% and 20% concentrations of rosemary. Eucalyptus essential oil showed the highest effect at a concentration of 20%, with a mortality rate of 90%, while the lowest was at a concentration of 5%, with a mortality rate of 6.6%. The average mortality rate in the mixture of two essential oils ranged from 70% to 96.6%, indicating that the insecticidal effect of the mix of two essential oils at the same concentrations was much more significant than that of essential oils alone. The comparison of mortality means among different treatments revealed that significant differences were observed in the percentage of mortality means when using rosemary and eucalyptus essential oils individually. However, there was no significant difference in the mortality rate observed at different concentrations of the two essential oils when combined (Fig. 4).

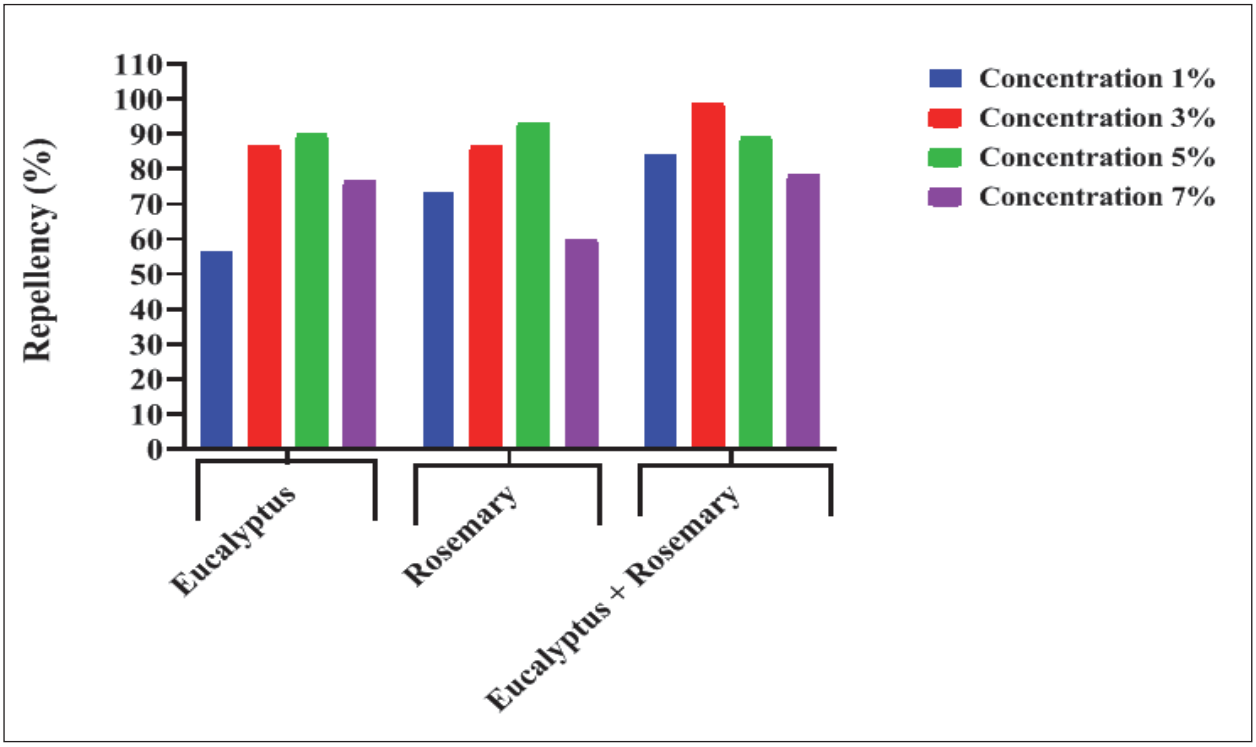

Fig. 4. Toxicity percentages of concentrations of eucalyptus, rosemary, and their mixture against B. germanica after GC MS analysis

As observed, there is a significant difference in the repellency percentages among eucalyptus, rosemary, and their mixture against *B. germanica* at concentrations of 1%, 3%, 5%, and 7% after 24 hours (P_{value}<0.0001). In the single essential oil treatments, the repellency rate increases from 1% to 5% concentration, with the highest repellency rate observed at 5% concentration (90 and 93.3% for eucalyptus and rosemary), followed by a decreasing trend at 7% concentration. However, in the mixed essential oil treatment, the repellency rate increases from 1% to 3% concentration. Then, it decreases to 7%, with the highest repellency rate at 3% concentration (98.9%). Therefore, it can be concluded that at equal concentrations of the three treatments, the mixed essential oils had a higher efficacy compared to the single essential oils. Additionally, the effective concentration for the mixed treatment was 3%. In contrast, the highest repellency rate for the single essential oil treatments was observed at a concentration of 5% (Fig. 5).

3.3. Discussion

Water distillation (WD) was used for extracting essential oils from plants as a chemistry procedure and analyzed by different methods such as UV-Vis, GC-FID, GC-MS, HPLC, LC-MS, and solvent-microwave. Solvent microwave extraction was also used to prepare essential oil [1,2]. Many extractions were obtained from different samples such as plants, human matrix, water samples by water distillation (WD), SPME, DSPME, LLE, DLLME. IL-SPE, and ultrasound assisted-dispersive ionic liquid-suspension SPE [21-27]. The German cockroach is a common household pest that can cause significant health problems for humans. Essential oils, as a natural alternative to synthetic insecticides, have gained popularity recently. In this study, we investigated the toxicity and repellency of eucalyptus and rosemary essential oils and their mixture against the German cockroach under laboratory conditions. The results showed that essential oils of rosemary and eucalyptus, grown in the climatic conditions of

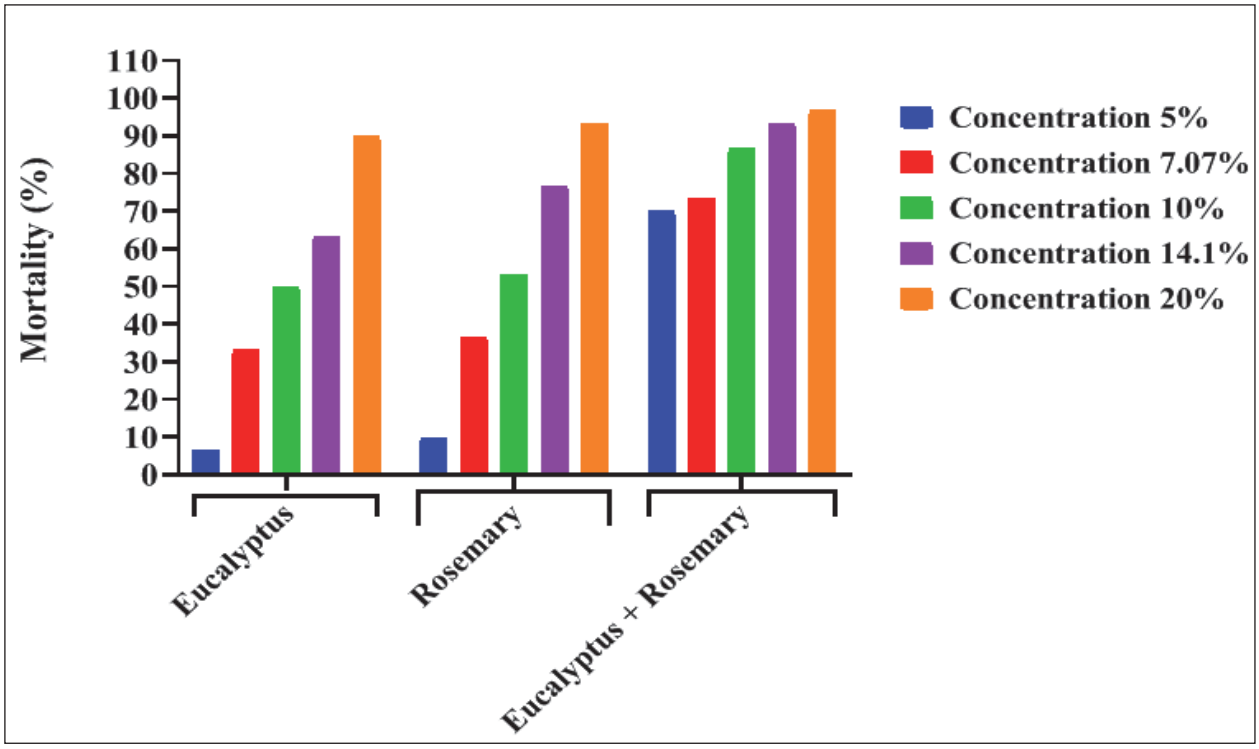

Fig 5. Repellency percentages of concentrations of eucalyptus, rosemary, and their mixture against B. germanica after GC MS analysis

Khuzestan province, have a suitable potential for controlling the German cockroach, especially when used in combination. The main components of eucalyptus essential oil detected by *GC-MS* were 1,8-cineole, α-pinene, and limonene. In contrast, the major components of rosemary essential oil include α -pinen, camphor, 1,8-cineole, borneol comphene and limonene. Limonene in both plant essential oils has been almost the same (4.26% and 4.28%). Gas chromatography-mass spectrometry (*GC-MS*) is a commonly used technique for analyzing plant essential oils. It can also detect the presence of adulterants or contaminants in essential oils, which can help ensure their purity and quality. 1,8-cineole, α-pinene, and limonene are three types of terpenes commonly found in various plants' essential oils. Each of these compounds has insecticidal or repellent properties to varying degrees1,8- .cineole, or eucalyptol, is a colourless terpene oxide commonly found in eucalyptus oil and other essential oils such as rosemary. It has been found to have insecticidal properties against various insects, including mosquitoes, flies, and cockroaches. Its mode of action is thought to be disrupting the insects' nervous system, leading to paralysis and death [12-20, 28]. α-pinene is a monoterpene that is commonly found in essential oils of pine trees, as well as in other plants such as rosemary and eucalyptus. It has been found to have repellent properties against several insect species, including mosquitoes and flies. Its mode of action is thought to be through blocking the olfactory receptors of the insects, making it difficult for them to locate their targets [29, 30]. Limonene is a monoterpene that is commonly found in essential oils of citrus fruits, as well as in other plants such as rosemary and peppermint. It has been found to have insecticidal properties against several insect species, including mosquitoes, fruit flies, and cockroaches. Its mode of action is thought to be disrupting the insects' cell membranes, leading to cell death [31]. Overall, these terpenes have shown promise as natural insecticides or repellents. However, their effectiveness may vary depending on the specific insect species and the concentration and formulation of the terpenes used. Further research is needed to understand their potential as alternatives to synthetic pesticides. Many studies have investigated the effectiveness of different essential oils against this cockroach species, all of which have indicated the high potential of these natural compounds for killing and repelling the German cockroach. The insecticidal and repellent properties of eucalyptus and rosemary essential oils against the American cockroach were also demonstrated, with a dose of 32.54 µg cm^{-2} and 35.97 µg cm^{-2} resulting in 50% mortality, which is comparable to the doses of chemical insecticides [1]. The repellent and insecticidal effects of eucalyptus and rosemary essential oils against the brown-banded cockroach, *Supella longipalpa,* were demonstrated, with rosemary essential oil causing 100% mortality and 94.5% repellency at concentrations of 2.5% to 30%. Eucalyptus essential oil causes 100% mortality with 27.7% to 51.7% repellency [9]. Clove oil, thyme oil, and peppermint oil had potent insecticidal activity against German cockroaches, with mortality rates ranging from 82% to 100% [32]. Another study found that essential oils from lavender, peppermint, and tea trees had insecticidal activity against German cockroaches, with mortality rates ranging from 70% to 100% [33]. In addition to their insecticidal properties, essential oils have also been found to have repellent effects against German cockroaches. Essential oils from catnip and Osage orange had strong repellent effects against German cockroaches, with repellency rates ranging from 82% to 100% [34]. Other essential oils that have insecticidal or repellent effects against German cockroaches include cinnamon, lemongrass, and eucalyptus [35, 36]. However, the effectiveness of these oils may vary depending on factors such as the concentration and formulation of the oil, as well as the specific strain of cockroaches being targeted. The combination of eucalyptus and rosemary essential oils had a synergistic effect on the German cockroach, with the LC_{50} and LC_{95} values decreasing significantly to one their compared to individual essential oils, with an LC50

value of 3.23% and 14.3%. Some essential oils have shown a synergistic effect when combined with other compounds, which can increase their insecticidal activity against German cockroaches. One study investigated the synergistic effect of thymol, a compound found in thyme essential oil, and piperonyl butoxide, a common insecticide synergist, against German cockroaches. The combination of thymol and piperonyl butoxide had a greater insecticidal effect than either compound alone, with mortality rates of up to 100% [37]. Another study investigated the synergistic effect of eucalyptus oil and limonene, a compound found in citrus fruits, against German cockroaches. The combination of eucalyptus oil and limonene had a synergistic effect on the fumigant toxicity of the oils against German cockroaches, increasing their mortality rates [38]. In addition, the synergistic effect of essential oils from five different plants, including peppermint, cinnamon, lemongrass, and piperonyl butoxide, against German cockroaches had a synergistic effect on the insecticidal activity against German cockroaches, with mortality rates ranging from 81% to 100% [39, 40]. The use of essential oils in combination with synergists has shown promise as an effective approach to control German cockroaches. However, further research is needed to fully understand the mechanism of action and optimize the formulation and application of these compounds [39, 40].

4. Conclusion

Overall, plant essential oils analyzed with GC-MS have shown promise as natural insecticides and repellents against German cockroaches. Our findings suggest that the combination of eucalyptus and rosemary essential oils has a potent insecticidal effect against the German cockroach and can be an effective natural alternative to synthetic insecticides. The synergistic effect of the two essential oils can be attributed to their different chemical compositions, determined by GC-MS after sample preparation method and act on various targets in the insect's body. Further studies are needed to evaluate the effectiveness of the essential oil combination against other insect pests and to investigate the safety and practicality of using essential oils as insecticides on the field scale.

5. Acknowledgements

This article is derived from the master's thesis of Ms. Marzieh Asgari and was supported financially by the Deputy of Research and Technology of Jundishapur University of Medical Sciences, Ahvaz, with the project code OG-0106 and ethics code IR.AJUMS.REC.1401.031.

6. Conflicts of Interest

The authors declare that there is no conflicts of interest.

7. References

[1] R. Ye, K. Tian, Extraction process optimization of essential oil from *Mellissa officinalis* L. using a new ultrasound-microwave hybrid-assisted Clevenger hydrodistillation, Ind. Crops Prod., 203 (2023) 117165. https://doi.org/10.1016/j.indcrop.2023.117165

[2] F. Chen, X. Du, A new approach for preparation of essential oil, followed by chlorogenic acid and hyperoside with microwave-assisted simultaneous distillation and dual extraction (MSDDE) from *Vaccinium uliginosum* leaves, Ind. Crops Prod., 77 (2015) 809-826. https://doi.org/10.1016/j.indcrop.2015.09.058

[3] M. M. Tavakoli, B. Davari, H. Nasirian, A. Salehzadeh, S. Moradkhani, A. H. Zahirnia, Investigation of insecticidal properties of *Rosmarinus officinalis* L. and *Lavandula angustifolia* Mill essential oils against German cockroach in laboratory conditions, Feyz Med. Sci. J., 25 (2021) 994-1002. https://feyz.kaums.ac.ir/article-1-4254-en.html

[4] A. Kakeh-Khani, M. Nazari, H. Nasirian, Insecticide resistance studies on German cockroach (*Blattella germanica*) strains to malathion, propoxur and lambdacyhalothrin, Chula Med. J., 64 (2020) 357-365. https://

doi.org/10.14456/clmj.2020.45

[5] C.A. Damalas, I.G. Eleftherohorinos, Pesticide exposure, safety issues, and risk assessment indicators, Int. J. Env. Res. pub. Health, 8 (2011) 1402-1419. https://doi.org/10.3390/ijerph8051402

[6] X.Y. Pan, F. Zhang, Advances in biological control of the German cockroach, Blattella germanica (L.), Biol. Control, 142 (2020) 104104. https://doi.org/10.1016/j.biocontrol.2019.104104

[7] Y.C. Yang, H.S. Lee, J.M. Clark, Y.J. Ahn, Insecticidal activity of plant essential oils against *Pediculus humanus capitis* (Anoplura: Pediculidae), J. Med. Entomol., 41 (2004) 699-704. https://doi.org/10.1603/0022-2585-41.4.699

[8] A. Bolandnazar, M. Ghadamyari, M. Memarzadeh, J. Jalali Sandi, Repellent and lethal effect of essential oils of rosemary, peppermint and eucalyptus and thyme extract, formulated as nano-and microemulsions, on *Bemisia tabaci* (Homoptera: Aleyrodidae) under greenhouse condition, J. Entomol. Soc. Iran., 38 (2018) 81-97. https://doi.org/10.22117/jesi.2018.116014.1152

[9] M. Sharififard, F. Safdari, A. Siahpoush, H. Kassiri, Insecticidal and repellency properties of *Eucalyptus* sp. essential oil against *Supella longipalpa* (Dictyoptera: Blatellidae), an important vector of tropical and infectious diseases, in hospitals and residential areas, Iran. J. Infect. Dis., 19 (2014) 67-71. http://www.iiccom.org/current_issue.asp

[10] C. D. Zhang, X. Y. Hu, H. S. Wang, GC–MS analysis of essential oil extracted from Acori tatarinowii Rhizoma: An experiment in natural product analysis, J. Chem. Educ., 98 (2021) 3004–3010. https://doi.org/10.1021/acs.jchemed.1c00451

[11] B. Obi Johnson, A. M. Golonka, Determination of Linalool in essential oils by SPME-GC-MS: Using the internal standard method, J. Chem. Educ., 99 (2022) 917–923. https://doi.org/10.1021/acs.jchemed.1c00212

[12] S. Gaire, M. E. Scharf, A. D. Gondhalekar, Synergistic toxicity interactions between plant essential oil components against the common bed bug (*Cimex lectularius* L.), Insects, 11 (2020) 133. https://doi.org/10.3390/insects11020133

[13] A. Ebadollahi, W.N. Setzer, Analysis of the essential oils of *Eucalyptus camaldulensis* Dehnh. and *E. viminalis* Labill. as a contribution to fortify their insecticidal application, Nat. Prod. Commun., 15 (2020) 1-10. https://doi.org/ 10.1177/1934578X20946248

[14] R. Pavela, G. Benelli, Essential oils as ecofriendly biopesticides? challenges and constraints, Trends plant Sci., 21 (2016) 1000–1007. https://doi.org/10.1016/j.tplants.2016.10.005

[15] L. Wuv, X. Huo, X. Zhou, D. Zhao, W. He, S. Liu, H. Liu, T. Feng, C. Wang, Acaricidal activity and synergistic effect of thyme oil constituents against carmine spider mite (*Tetranychus Cinnabarinus* (Boisduval), Molecules, 22 (2017) 1873. https://doi.org/10.3390/molecules22111873

[16] R. Pavela, Essential oils for the development of eco-friendly mosquito larvicides: a review, Ind. Crops Prod., 76 (2015) 174-187. https://doi.org/10.1016/j.indcrop.2015.06.050

[17] M. B. Isman, M. L. Grieneisen, Botanical insecticide research: many publications, limited useful data, Trends Plant Sci., 19 (2014) 140-145. https://doi.org/10.1016/j.tplants.2013.11.005

[18] S. Shi, X. Zhang, X. Liu, Z. Chen, H. Tang, D. Hu, H. Li, GC-MS analysis of the essential oil from *Seseli mairei* H. Wolff (Apiaceae) roots and their nematicidal activity, Molecules, 28 (2023) 2205. https://doi.org/10.3390/molecules28052205

[19] C. Regnault-Roger, C. Vincent, J.T. Arnason, Essential oils in insect control: low-risk products in a high-stakes world, Annu. Rev. Entomol., 57 (2012) 405-424. https://doi.org/10.1146/annurev-ento-120710-100554

[20] WHO, Instructions for determining the

susceptibility or resistance of adult mosquitos to organochlorine, organophosphate and carbamate insecticides: diagnostic test, WHO/VBC/81.806. Geneva: World Health Organization,1981. https://apps.who.int/iris/handle/10665/69615

[21] Z. Karamzadeh, J. Rakhtshah, N.M. Kazemi, A novel biostructure sorbent based on ysSB/MetSB@ MWCNTs for separation of nickel and cobalt in biological samples by ultrasound assisted-dispersive ionic liquid-suspension solid phase micro extraction, J. Pharm. Biomed. Anal., 172 (2019) 285-294. https://doi.org/10.1016/j.jpba.2019.05.003

[22] K. Merchant, M.D. Mobarake, Ultrasound-assisted solid-liquid trap phase extraction based on functionalized multi wall carbon nanotubes for preconcentration and separation of nickel in petrochemical wastewater, J. Anal. Chem., 74 (2019) 865-876. https://doi.org/10.1134/S1061934819090090

[23] N. Esmaeili, Ultrasound assisted-dispersive-modification solid-phase extraction using task-specific ionic liquid immobilized on multiwall carbon nanotubes for speciation and determination mercury in water samples, Microchem. J., 154 (2020) 104632. https://doi.org/10.1016/j.microc.2020.104632

[24] J. Rakhtshah, N. Esmaeili, A rapid extraction of toxic styrene from water and wastewater samples based on hydroxyethyl methylimidazolium tetrafluoroborate immobilized on MWCNTs by ultra-assisted dispersive cyclic conjugation-micro-solid phase extraction, Microchem. J., 170 (2021) 106759. https://doi.org/10.1016/j.microc.2021.106759

[25] M. Habibnia, A. Rashidi, Simultaneously speciation of mercury in water, human blood and food samples based on pyrrolic and pyridinic nitrogen doped porous graphene nanostructure, Food Chem., 403 (2023) 134394. https://doi.org/10.1016/j.foodchem.2022.134394

[26] N. Esmaeili, J. Rakhtshah, E. Kolvari, Rapid speciation of lead in human blood and urine samples based on mwcnts@ dmp by dispersive ionic liquid-suspension-micro-solid phase extraction, Biol. Trace Elem. Res., 199 (2021) 2496-2507. https://doi.org/10.1007/s12011-020-02382-7

[27] Sh. Teimoori, New extraction of toluene from water samples based on nano-carbon structure before determination by gas chromatography, Int. J. Environ. Sci. Technol., 20 (2023) 6589–6608. https://doi.org/10.1007/s13762-023-04906-9

[28] A. Tawatsin, S. D. Wratten, R. R. Scott, U. Thavara, Repellency of volatile oils from plants against three mosquito vectors, J. Vector Ecol, 26 (2001) 76-82. https://onlinelibrary.wiley.com/journal/19487134

[29] S. S. Cheng, H.T. Chang, S. T. Chang, K. H. Tsai, W. J. Chen, Bioactivity of selected plant essential oils against the yellow fever mosquito *Aedes aegypti* larvae, Bioresour. Technol., 89 (2003) 99-102. https://doi.org/10.1016/S0960-8524(03)00008-7

[30] V.A. Cruz, N.J. Ferreira, H.P. Cornelio-Santiago, Oil extraction from black soldier fly (Hermetia illucens L.) larvae meal by dynamic and intermittent processes of supercritical CO_2 – Global yield, oil characterization, and solvent consumption, J. Supercrit. Fluids, 195 (2023) 105861. https://doi.org/10.1016/j.supflu.2023.105861

[31] W.S. Choi, B.S. Park, S.K. Ku, S.E. Lee, Repellent activities of essential oils and monoterpenes against *Culex pipiens* pallens, J. Am. Mos. Control. Assoc., 18 (2002) 348-351. https://pubmed.ncbi.nlm.nih.gov/12542193/

[32] R. Pavela, Insecticidal properties of several essential oils on the house fly (*Musca domestica* L.), Pest. Manag. Sci., 22 (2007) 274-278. https://doi.org/10.1002/ptr.2300

[33] E. Enan, Insecticidal activity of essential oils: octopaminergic sites of action, Comp. Biochem. Physiol. Part C Toxicol.

Pharmacol., 130 (2001) 325-337. https://doi.org/10.1016/S1532-0456(01)00255-1

[34] K. Huang, D. Zhang, J. J. Ren, Screening of the repellent activity of 12 essential oils against adult German Cockroach (Dictyoptera: Blattellidae): preparation of a sustained release repellent agent of binary Oil-γ-CD and its repellency in a small container, J. Econ. Entomol., 113 (2020) 2171–2178., https://doi.org/10.1093/jee/toaa162

[35] C. J. Peterson, J. R. Coats**,** Catnip essential oil and its nepetalactone isomers as repellents for Mosquitoes, recent developments in invertebrate repellents, ACS publisher, Chapter 4, pp 59-65, 2011. https://doi.org/10.1021/bk-2011-1090.ch004

[36] O. Koul, S. Walia, G. S. Dhaliwal, Essential oils as green pesticides: potential and constraints, Biopestic. Int., 4 (2008) 63-84. https://www.koulresearch.org/journal.htm

[37] R. Jannatan, R. Rahayu, Fumigant toxicity and repellency of citronella grass essential oil (Cymbopogon nardus (L.) Rendle) to German cockroaches (Blattella germanica L.), Eur. J. Biol. Res., 11(2021) 267-273. http://dx.doi.org/10.5281/zenodo.4670508

[38] R. Nikzad, M.R. Youssefi, Comparison of lethal effect of carvacrol, thymol, permethrin and cypermethrin toxicants on German cockroaches (Blattella germanica), Vet. Res. Biol. Prod., 131 (2021) 61-67. https://doi.org/10.22092/VJ.2020.128751.1671

[39] A. K. Phillips, A.G. Appel, Fumigant toxicity of essential oils to the German cockroach (Dictyoptera: Blattellidae), J. Econ. Entomol., 103 (2010) 781-90. https://doi.org/ 10.1603/ec09358.

[40] I. Zibaee, P. Bahari Khorra, Synergistic effect of some essential oils on toxicity and knockdown effects, against mosquitos, cockroaches and housefly, Arthropods, 4 (2015) 107-123. http://www.iaees.org/publications/journals/arthropods/articles/2015-4(4)/2015-4(4).asp

Anal. Methods Environ. Chem. J. 6 (3) (2023) 103-120

AMECJ

Research Article, Issue 3
Analytical Methods in Environmental Chemistry Journal
Journal home page: www.amecj.com/ir

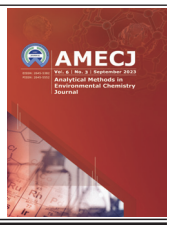

Comparative analysis of groundnut oil quality in the north-central zone of Nigeria: Determination and evaluation of heavy metals, fatty acids, phospholipids, and iodine values in groundnut oil

Ijah Silas Ioryue [a]*, and Terngu Timothy Uzah [b]
[a] *Department of Biochemistry, Federal University of Technology, Ikot Abasi, Nigeria,*
[b] *Department of Chemistry Federal University of Petroleum Resources, Efrum, Nigeria*

ARTICLE INFO:
Received 11 May 2023
Revised form 21 Jul 2023
Accepted 17 Aug 2023
Available online 29 Sep 2023

Keywords:
Analysis,
Groundnut oil,
Atomic absorption spectrometer,
Fatty acid,
Phospholipids,
Gas chromatography

ABSTRACT
The research presents a comparative analysis of the quality of locally produced groundnut oil (*Arachis hypogaea*) sold in the north-central zone of Nigeria markets (Benue, Nasarawa, Kogi, Kwara, Niger and Plateau States). The aim was to assess and compare the qualities of the oils and to know the safety of human consumption. The groundnut oil produced biodiesel, shampoo lubricants, and soap-making industries. The concentrations of the heavy metals were analyzed with atomic absorption spectrometry (AAS). It showed that the lead, zinc, and copper (Pb, Zn, Cu) were within the FAO/WHO recommended limit, while Cd (0.201-0.331 mg kg^{-1}) was above the limit (0.07 mg kg^{-1}). Also, the gas chromatography (GC-FID) results indicated that twelve fatty acids (linoleic > oleic > palmitic > stearic > lignoceric > arachidic acid > behenic > erucic > arachidonic > margaric > linolenic > palmitoleic) were obtained in the groundnut oils in all markets and fatty acids include caprylic acid, capric acid, lauric acid, and myristic acid were absent in oils. In addition, the magnitude of six phospholipids (phosphatidylcholine > phosphatidylethanolamine > phosphatidylinositol > phosphatidylserine > phosphatidic acid > lysophosphatidylcholine) were also achieved, respectively. The results showed that iodine, peroxide, saponification value and refractive index were below the FAO/WHO recommended level, and the acid value was higher than the normal range.

1. Introduction

Groundnut oil is a tasting oil derived from the groundnut plant (Arachishypogaea), a species in the legumes family (Fabaceae). Some common synonyms for groundnut are peanut, earthnut, goober, pinder, and ground pea. It is called "*abum*" by the Tiv people, "emansak" by the Ibibios, "epa" by the Yorubas, "Gyada" by the Hausas and Asiboko by the Ibos. In 1753, Linnaeus described the domesticated groundnut species as Arachis (derived from the Greek "arachis," meaning a weed), hypogaea (meaning an underground chamber) or a weed with fruit produced below the soil. Groundnut is eaten fresh or roasted and is used in cooking, confectionery and pressed for edible oil. Palm oil and groundnut oil are both vegetable oils. Vegetable oils are water-insoluble, edible liquids derived from plants, which consist predominantly of long-chain fatty acid esters derived from the

*Corresponding Author: Ijah Silas Ioryue
Email: silasoo4real@gmail.com
https://doi.org/10.24200/amecj.v6.i03.239

simple alcohol glycerol. Oil plays a crucial role in our everyday life. There are different types of oils, including edible, non-edible, essential oils [1], etc. Edible oils include palm oil, coconut oil, groundnut oil, etc. Rubber seed oil is an example of non-edible oil. Essential oils include Jasmine oil, sandalwood oils, etc. The quality of groundnut oil could be affected by improper post-harvest handling, processing and storage. Again, there is widespread speculation that groundnut oil is being adulterated for profit maximization. The adulteration ranges from using dyes, water and other illegal food additives, which could affect the quality of these oils regarding nutritional value, wholesomeness, utilization, safety and shelf-life. The percentage of free fatty acid, moisture and dirt content generally determines the quality of this oil. The produce is traditionally bought on a 5% free fatty acid basis with penalties for exceeding this figure [2]. Hence, there is a need to assess the quality of groundnut oils sold in major markets in the north-central zone of Nigeria. Heavy metals have relatively high densities of 4.0g cm^{-1} and above [3]. Heavy metals in trace amounts are of significant benefit to man. Inadequate trace elements in diet may constitute a health problem that may be devastating. In large doses, heavy metals are generally characterized as toxic or poisonous. Since trace elements provide nutritional value, they are sometimes called micronutrients [3]. Groundnut oils are essential daily condiments because of their various uses in our everyday lives. Unfortunately, it has been reported that some brands of groundnut and palm oils are adulterated with diesel automobile hydrocarbon oil, which is miscible with vegetable oils. This impurity is alleged to change the quality of vegetable oils and consequently negatively affect consumers [4]. Vegetable oils and fats contain trace levels of various metals depending on many factors such as species, soil used for cultivation, irrigational water, variety and stage of maturity, pollution, mode of processing, storage, and contaminations. These metals may enter the food material from the soil through mineral uptake by crops, food processing, and environmental contamination (as in fertilizer application). Metals play essential negative and positive roles in human life [5]. Hence, there is a need to determine the concentration of heavy metals, trace elements and some physicochemical parameters in these groundnut oils in the north-central zone so that consumers will know the qualities of these groundnut oils. Atomic absorption spectroscopy (AAS) is a widely used analytical technique for determining heavy metals concentration in water, fats and oils [6-8]. It is a sensitive and reliable method for measuring trace amounts of heavy metals in water and oil samples. AAS has been used in several studies to assess drinking water quality and food samples from various sources, including oils. Gas chromatography (GC) Flame ionization detector (FID) is a well-established technique which is used to identify and quantify the incorporation of fatty acids into lipid pools. Chromatographic separation of lipids is typically extracted from the sample using the solubility of lipids in solvent mixtures of chloroform and methanol. Sodium chloride is added to facilitate the separation of the mixture into aqueous and organic lipid-containing phases [9]. Complex lipid classes of interest can be separated from the total lipid extract by solid phase extraction (SPE).

The study aimed to assess the quality and Nutritional values of locally produced groundnut oil in the northern central zone of Nigeria (Benue, Nasarawa, Kogi, Kwara, Niger and Plateau states). Therefore, the AAS and GC-FID determined the physicochemical parameters, the concentration of heavy metals, and the concentration of fatty acids and phospholipids in groundnut oil.

2. Material and Methods

2.1. Reagents and Materials

The reagents used for the analysis were all analytical grades purchased from Emole Nigeria (NO: 33 Old Otukpo Road high level, Makurdi, Benue State, Nigeria). Cadmium, lead, zinc, and copper standard solutions (500 mL; 1000 mg L^{-1}) purchased from Merck, Germany. The reagents such as nitric acid (CAS number : 7697-37-2), sulfuric acid

(CAS number: 7664-93-9), hydrochloric acid (CAS number: 7647-01-0), hydrogen peroxide (CAS number: 7722-84-1), sodium hydroxide (CAS number: 1310-73-2), sodium thiosulphate (CAS number: 7772-98-7), glacial acetic acid (CAS number: 64-19-7), potassium hydroxide (CAS number: 1310-58-3), potassium iodide (CAS number: 7681-11-0), ethanol (CAS number: 64-17-5), tetrachloromethane (CAS number: 56-23-5), chloroform (CAS number: 67-66-3), Wiji's solution (CAS number: 7790-99-0), phloroglucinol (CAS number: 108-73-6), diethyl ether (CAS number: 60-29-7), methanol (CAS number: 67-56-1), boron trifluoride (CAS number: 7637-07-2), n-hexane (CAS number: 110-54-3) were purchased from Merck, Germany. Also, the phenolphthalein indicator (Sigma), starch indicator (Sigma), polyethylene bottles (plastic bottles), weighing balance, beakers, oven, filter paper, deionized water (DW), bottles, bath water and heating were used for analysis groundnut oil.

2.2. Instrumental

The measurements were made from Ahmadu Bello University Zaria Laboratory for the analysis of heavy metal samples using a Phoenix 986 atomic absorption spectrometer (Biotech Engineering Management Co. Ltd, UK) and Shimadzu GC-FID (model GC-2014; Sweden) for the analysis of Fatty acids and phospholipids in the groundnut oils. Cadmium, lead, zinc and copper hollow cathode lamps were operated according to the AAS manufacturer's instructions.

2.2.1. Atomic Absorption Spectrophotometer

A Phoenix 986 model (Biotech Engineering Management Co. Ltd, UK) atomic absorption spectrometer with four hollow cathode lamp positions was employed. The light sources of the different elements were hollow-cathode lamps from Cathoden, UK. The light beam through Air-Acetylene was controlled by an aperture for measuring absorbance in different slit widths depending on the calculated element. The oxidant rate was 4.5 L $min^{-1,}$ and the fuel rate (C_2H_2) was 1.5 L min^{-1}. The most sensitive Cd, Cu, Pb and Zn absorption lines were used [10]. Standard solutions were inspired into the flames after the burner had been allowed to operate for 5-10 min. This way, thermal equilibrium was attained before any final adjustment to the absorbance mode, measuring time, burner height, gas flows or amplifier gain. In this case, maximum sensitivity will be expected. All absorbance values are the average of ten readings recorded successively from the different absorbance modes. The background absorption is measured and subtracted from the total absorption to determine the actual atomic absorption signal. For this reason, a continuum source of deuterium arc lamp in ultraviolet has been used to measure only the background contribution to the absorption signal, which has essentially zero atomic absorption sensitivity at the regular resolution for atomic absorption instruments. In this case, the background correction is automatically carried out by a background correction system [11]. The limit of detection (LOD) and limit of quantification (LOQ) for heavy metal (Pb, Zn, Cu, Cd) determination was achieved by AAS and is shown in Table 1. The lowest qualitative and quantitative concentrations for the tested linearity range were calculated for each metal according to the guidelines of ICH,2000. LOD and LOQ were calculated using the expression m × S/c, where m = 3.3 for the LOD and 10 for the LOQ, S is the standard deviation of the intercept, and c is the slope of the calibration curve tested for linearity.

Table 1. The LOD and LOQ of AAS For heavy metal determination

Parameter	Pb	Zn	Cu	Cd	Average
LOD(mg L^{-1})	0.088	0.052	0.077	0.028	0.06125
LOQ (mg L^{-1})	0.433	0.208	0.231	0.112	0.2455

2.2.2. Gas chromatography analysis

Shimadzu GC-FID model GC-2014 Sweden was equipped with a flame ionization detector and capillary column (30 m, 0.53 mm) with a stationary phase fused silica. The chromatographic conditions were detector temperature 280°C, injector temperature 250°C, initial column temperature 120°C for 1 min, programmed to increase at a rate of 10°C per minute up to 200°C and then at four °C per minute up to the final temperature of 220°C. Nitrogen and hydrogen for chromatography R, as the carrier and auxiliary gas, respectively, have a 1.3 mL min^{-1} flow rate. As a determination, one µL of the derived sample was injected, alternatively with a sample volume/internal standard ratio of 80/20. Fatty acids and phospholipids were identified by comparing the standards' retention times and relative retention times with those of the samples. The quantification was by internal standardization using the methyl esters of lauric acid as the internal standard. The value of fatty acids and phospholipids were calculated according to AOCS methodology (mg per 100 g^{-1}) [12].

2.3. General Procedure

First, the *groundnut oil (Arachis hypogaea)* samples were prepared by digestion procedure, and then parameters such as iodine value, the concentration of free fatty acid, Acid value, color, odour, peroxide value, saponification value and refractive index were determined. Also, heavy metals (Cd, Pb Zn and Cu), Fatty acids and phospholipids in groundnut oil were determined.

2.3.1. Digestion of groundnut oil (Arachis hypogaea)

First, 2.0 g of each sample was weighed in a beaker. Concentrated nitric and sulphuric acids (5cm^3) were added, followed by hydrogen peroxide (2cm^3), then heated on a heating mantle until a clear solution was obtained. The content of the beaker was allowed to cool and then filtered. The resulting solutions were made up to 50cm^3 using de-ionized water and then transferred into a plastic bottle for metal analysis by the AAS method [13].

2.3.2. Procedure for determination of parameters in groundnut oil

Acid value was determined by the titrimetric method of Kupwade and Desai [14]. 5g of the oil sample was weighed, and 75 mL of hot, neutral alcohol was added with a few drops of phenolphthalein. The mixture was shaken vigorously and titrated with 0.1M NaOH solution with constant shaking until the pink coloration remained permanent. The acid value was calculated using Equation 1(V= titration endpoint value).

$$\text{Acid value}=(V\times 5.6) / (\text{Weight of sample}) \quad \text{(Eq.1)}$$

The iodine value was determined according to the titrimetric method of Pearson [15]. 2.0 g of oil sample was weighed into a dry glass stopper bottle of 250 mL Capacity, and 10 mL of carbon tetrachloride was added to the oil. About 20 mL of Wij's solutions were then added and allowed to stand in the dark for 30 min. 15 mL of (10%) potassium iodide and 100 mL of water were added and then titrated with 0.1M sodium thiosulphate solution using starch as indicator just before the endpoint. A blank was also prepared alongside the oil samples. The iodine value was calculated by Equation 2.

$$\text{Iodine value}= (V_2-V_1)\times 1.269 / \text{Weight (g)} \quad \text{(Eq.2)}$$

Where V_2= titre value for blank, V_1= titre value for sample(s)

The peroxide value was evaluated according to AOAC [16]. A 2.0 g oil sample was weighed into a tube, and 1g of powdered potassium iodide with 20 mL of solvent mixture (glacial acetic acid and Chloroform) was added. This was then placed in boiling water for 30s. The content was poured into a flask containing 20 mL of 5% iodide solution. The tube was washed with 25ml of distilled water and titrated with 0.002N sodium thiosulphate solution using

starch as an indicator. A blank was prepared alongside the oil samples. Peroxide was obtained by Equation 3.

$$\text{Peroxide Value} = \frac{2(V1 - V2)\ \text{mEq/kg}}{\text{Weight of sample (g)}} \quad \text{(Eq.3)}$$

Where V_2= titre value for blank, V_1= titre value for sample(s)

The Saponification value was determined according to the titrimetric method of Pearson [15].

2.0 g of oil sample was weighed into a conical flask, and 25 mL of alcoholic potassium hydroxide was added. The solution was heated in boiling water for one hour. 1 mL of 1% phenolphthalein was added and titrated with 0.5N HCl. A blank was prepared alongside the oil samples. The formula calculated the value by Equation 4.

$$\text{Saponification Value} = \frac{5.61N(A - B)}{W} \quad \text{(Eq.4)}$$

Where N= Concentration of HCl acid used,
A= Volume of H_2SO_4, for blank (mL),
B= Volume of H_2SO_4 (mL),
56.1= Equivalent weight of potassium hydroxide,
W= weight of oil

The colour of the oil samples was determined by visual comparison, while the odour of the oil samples were determined using a glass stoppered bottle rinsed with 4 M HCl internally and externally and rinsed with distilled water. The bottle was halfway filled with the oil sample and shaken vigorously for about 2 minutes. The stopper was then removed, and the odour was observed by putting nostrils near the mouth of the bottle. The rancidity of the oil samples was determined qualitatively using the Kries Test, as described by Pearson [15]. 5.0 cm^3 of the oil samples was placed in a 100 cm^3 test tube vigorously mixed with 5cm^3 of 0.1% phloroglucinol solution in diethyl ether and 5 cm^3 of concentrated HCI for about 20s. The presence of pink colour indicates incipient rancidity. The refractive index (RI) was determined using a mathematical expression [17] and shown in Equation 5.

$$RI = 1.45765 + 0.0001164/V \quad \text{(Eq.5)}$$

RI: the Refractive Index
V : Iodine Value

2.3.3. Procedure for analysis of fatty acid, phospholipid, and heavy metals

50 mg of the extracted fat content of the sample was saponified (esterified) for five) minutes at 95^{0}C with 3.4 mL of 0.5M KOH in dry methanol (CH_3OH). The mixture was neutralized by using 0.7M HCl. 3 mL of the 14% boron trifluoride in methanol was added. The mixture was heated for five minutes at the temperature of 900^{o}C to achieve a complete methylation process. The fatty acid methyl ester was thrice extracted from the mixture with redistilled n-hexane. The content was concentrated to 1.0 mL for Gas Chromatography analysis (GC-FID), and 1µm was injected into the injection pot of GC-FID. The modified method of Liu *et al.* [18] was employed to determine the extracted oil phospholipid content. 0.01g of the extracted fat was added to the test tubes to ensure complete dryness of the oil for phospholipid analysis. The solvent was completely removed by passing the stream of nitrogen gas on the oil. 0.4 mL of chloroform was added to the test tube's content, followed by the addition of 0.10 mL of the chromogenic solution. The range of the tube was heated at the temperature of 100^{0}C in a water bath for about 1min and 20s. The content was allowed to cool to the laboratory temperature, and 5 mL of the hexane was added, and the tube with its content shook gently several times. The solvent and the aqueous layer were allowed to be separated, and the hexane layer was recovered and allowed to be concentrated to 1.0 mL for gas chromatography analysis (GC) using a pulse flame photometric detector (FPD). Also, the heavy metals determined by F-AAS after sample preparation (Acid digestion; microwave) of groundnut oil (Fig.1)

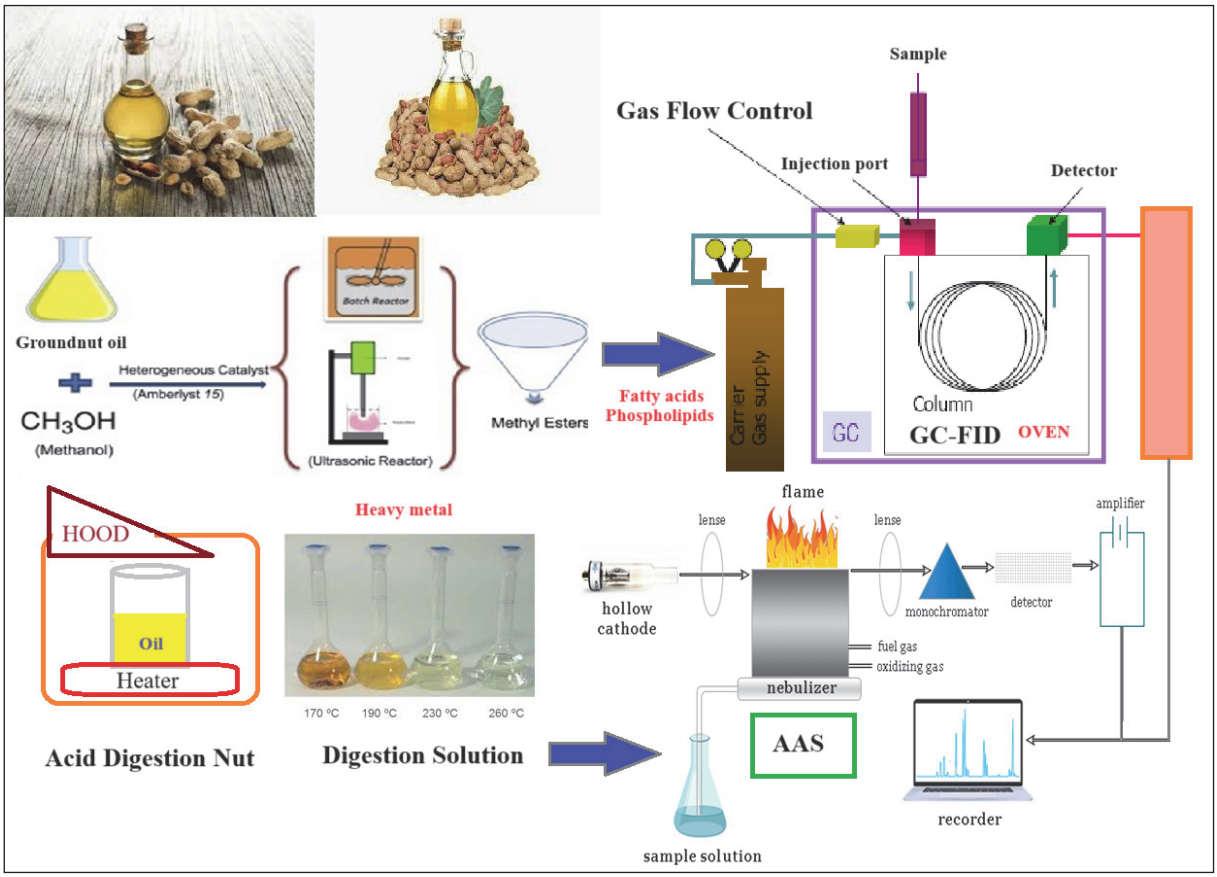

Fig.1. Procedure for sample extraction/separation of fatty acid, phospholipid and heavy metals from groundnut oil before determination by GC-FID and F-AAS

2.4. Scope of the study, collection of oil samples, and study area

The study was restricted to parameters such as iodine value, fatty acid/phospholipid concentration, acid value, colour, odour, peroxide value, saponification value, refractive index, heavy metals, Fatty acid and phospholipid in groundnut oil in North central Nigeria. The concentration of heavy metals (Cd, Pb Zn and Cu), fatty acid and phospholipid in groundnut oil were determined by F-AAS and GC -FID, respectively. The study covered an analysis of groundnut oil in 2022. Groundnut oil was bought from six states in north-central Nigeria markets for two months (September and October 2022). Three groundnut oil samples of 100 cm^3 each were collected from three sellers in each market, giving eighteen samples. The collected oil samples were packed in polyethylene bottles and stored below 20°C until analyses were used. The study was conducted in north-central Nigeria, one of Nigeria's geopolitical zones. It comprises six states, including the federal capital territory, Abuja. The states include Benue, Nasarawa, Plateau, Kogi, Niger and Kwara (Fig. 2).

3. Results and Discussion

The results obtained from the physical and chemical analysis of locally produced groundnut oil (Arachis hypogea oil) sold in six markets in North Central Nigeria are presented in Table 2, 3 and Figure 3. The physical parameters of the ground nut oil are shown in Table 2. Also, the oil's heavy metal contents, the percentage composition of fatty acids, saturated and unsaturated fatty acids, and phospholipids were presented in Tables 4, 5, 6 and 7 and Figures 3, 4, 5 and 6. Oil constitutes a significant composition of

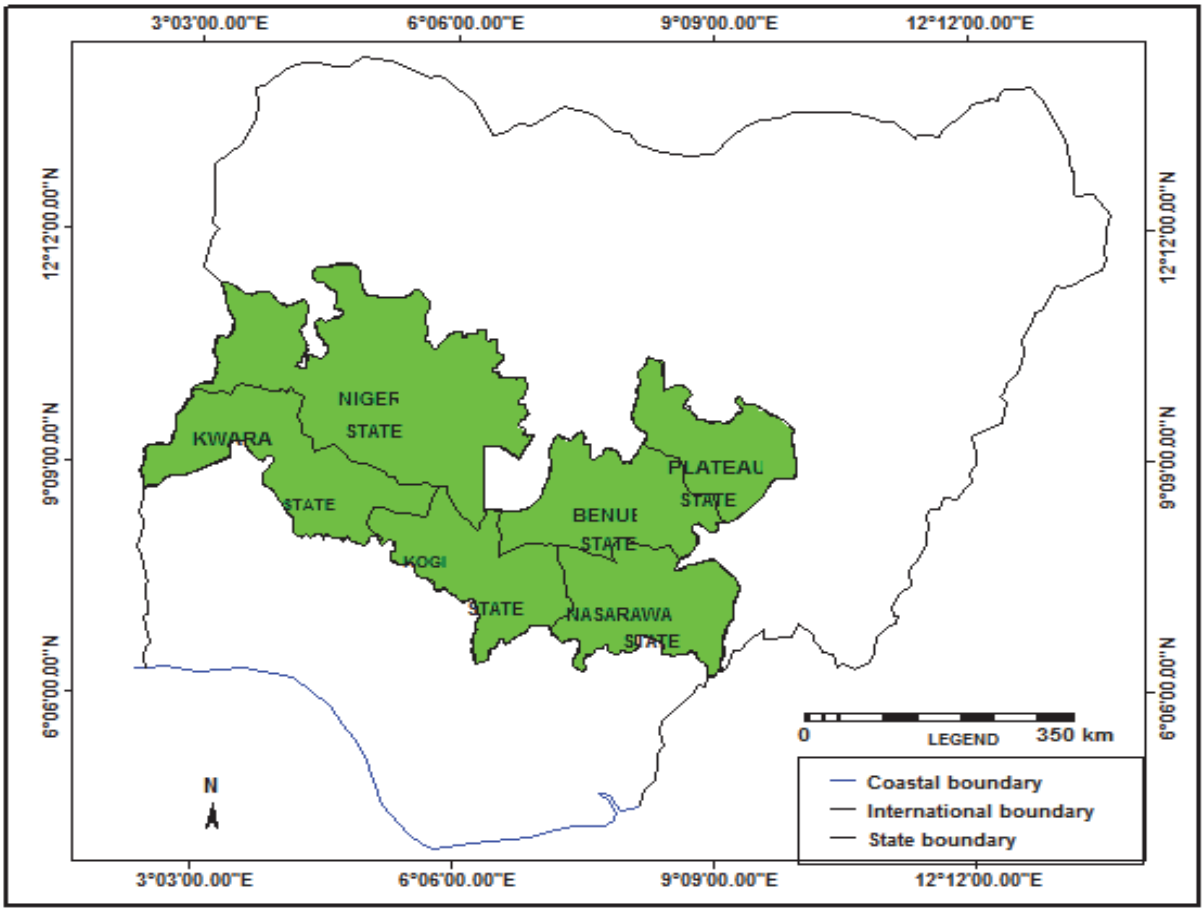

Fig. 2. Map of north central Nigeria showing the sampling states.

our daily diet consumption, and its market growth is now considered for its acceptability and economy, not minding the composition and nature.

3.1. Physical parameters

The sampled groundnut oil in Makurdi, Lafia and Lokoja was amber-yellow, while Jos, Minna and Ilorin were golden yellow. No abnormal odour of the sampled oil was noticed; hence, it was agreeable or acceptable. The state of all the oil was liquid (Table 2).

Table 2: The physical parameters of the groundnut oil purchased in the North Central Nigeria markets

Market	Colour	Odour	State (25°C)
Makurdi	Amber Yellow	Agreeable	Liquid
Lafia	Amber Yellow	Agreeable	Liquid
Jos	Golden Yellow	Agreeable	Liquid
Minna	Golden Yellow	Agreeable	Liquid
Lokoja	Amber Yellow	Agreeable	Liquid
Ilorin	Golden Yellow	Agreeable	Liquid

3.2. Chemical properties of the oil

The study indicated that oil in the Makurdi market was relatively high in fat content (135%), while the Lokoja market has the lowest value (70%), as shown in Table 3 and Figure 3. The order of fats content was Makurdi<Jos< Ilorin<Minna<Lafia<Lokoja. The iodine value is a measure of the total unsaturation of oils, as well as an indicator of their susceptibility to oxidation. The iodine values of all oil samples from the Northcentral markets were below the WHO specification (86-166 g I2/100g of oil) range. The higher the iodine number, the more C=C bonds in the fat [19]. This shows that the groundnut oil samples from the Lokoja market contain higher unsaturated fatty acids than any other market sampled. The chemical analysis of iodine value indicated that the Lokoja market has the highest value, followed by the Lafia market. The increasing order was Lokoja >Lafia> Minna >Makurdi> Jos >Ilorin. A high iodine value denotes a high degree of unsaturation caused by the extent of oxidation and degree of heat treatment during oil processing. The peroxide value is the weight of active oxygen contained in one gram of oil or fat [20]. Peroxide value measures peroxides and hydroperoxides formed in the initial phases of lipid oxidation. It, therefore, determines the degree of oil oxidation and indicates the level of deterioration of oils and fats. Freshly refined oil should have no peroxide value. In this study, it was observed that the groundnut oil from all the markets showed peroxide values (Table 3 and Figure 3) lower than the FAO/WHO (14) recommendation range(≤10 mili equivalent oxygen per kg), thus indicating less susceptibility to oxidation with Lokoja market having the highest (1.13 meq per kg) and Minna market having the lowest (0.42 meq per kg). According to Hassan [21], a low peroxide value indicates the oil's oxidative stability and a high peroxide value indicates poor oil resistance to peroxidation during storage [22]. Therefore, it is likely that storage for a long time may lead to rancidity of the oil. A rancid taste often becomes noticeable when the peroxidative value exceeds 20 meq per kg [23]. Peroxide value is critical for examining the quality and stability of fats and oils, stages of oxidation and spoilage extent [24]. Thus, the ground nut oil obtained from these locations will not harm human health due to its nonprone oxidation. The acid value is used to measure the quality of the oil since the acid value indicates the extent of hydrolysis and deterioration. The higher the fatty acid value, the higher the level of free fatty acids, which translates into decreased oil quality. The acid values from Lafia and Minna markets were approximately similar in value. In this study, the acid value in all the markets was higher compared to FAO/WHO [10] specification (≤ 0.6 mg KOH per gram of oil), and it followed Lokoja >Lafia >Minna>Jos> Ilorin >Makurdi order. The high acid values indicate free fatty acids present in the groundnut oil, which may be due to exposure to atmospheric oxygen or due to the method used for the extraction. According to Demian [25], acid values measure the extent to which glyceride in the oil has been decomposed by lipase and other actions such as light and heat. The determination is often used as a general indication of the condition and edibility of oil. According to Badmos *et al*. [26], a low acid value indicates the stability of oils over a long period and protection against rancidity and peroxidation. No rancidity was detected in any of the sampled groundnut oil in north-central Nigeria (Table 3 and Figure 3).

The saponification value measures the fatty acids' average molecular weight (or chain length). It is a measure of oxidation during storage and indicates the oil deterioration. An increase in saponification value in oil increases the volatility of the oils. It enhances the quality of the oil because it shows the presence of lower molecular weight components in 1.0 g of the oil, which will yield more energy on combustion [27]. The saponification values from the Northcentral markets were below the FAO/WHO [10] specification (187-196 mg KOH per gram of oil) range. This property makes it less useful in soap making. The lower saponification value observed in this study suggests that the mean molecular weight of fatty acids is high, as low saponification indicates the presence of long-chain

fatty acids, and higher saponification value indicates lower chain fatty acids since saponification value is inversely proportional to the average molecular or chain length of the fatty acid. The study shows that the Jos market has the highest saponification (142.25 mg KOH per gram) while the Minna market has the lowest value (37.23 mg KOH per gr). The increasing order of saponification was Minna >Lokoja>Ilorin>Lafia >Makurdi >Jos. All the groundnut oil sampled has the same refractive index (1.46) in North Central Nigeria.

Table 3. Chemical Analysis of the groundnut oil sold in north-central Nigeria

Market	Fat content (%)	Iodine Value (wij's)	Peroxide value (meq kg^{-1})	Acid Value (%)	Rancidity	Saponification value(mgKOH g^{-1})	Refractive Index
Makurdi	135	1.35	0.70	4.43	Nil	127.02	1.46
Lafia	78	1.73	0.60	2.12	Nil	113.10	1.46
Jos	128	0.67	0.80	2.52	Nil	142.25	1.46
Minna	89	1.67	0.42	2.22	Nil	37.23	1.46
Lokoja	70	2.62	1.13	1.62	Nil	46.44	1.46
Ilorin	97	0.12	0.84	3.01	Nil	52.46	1.46

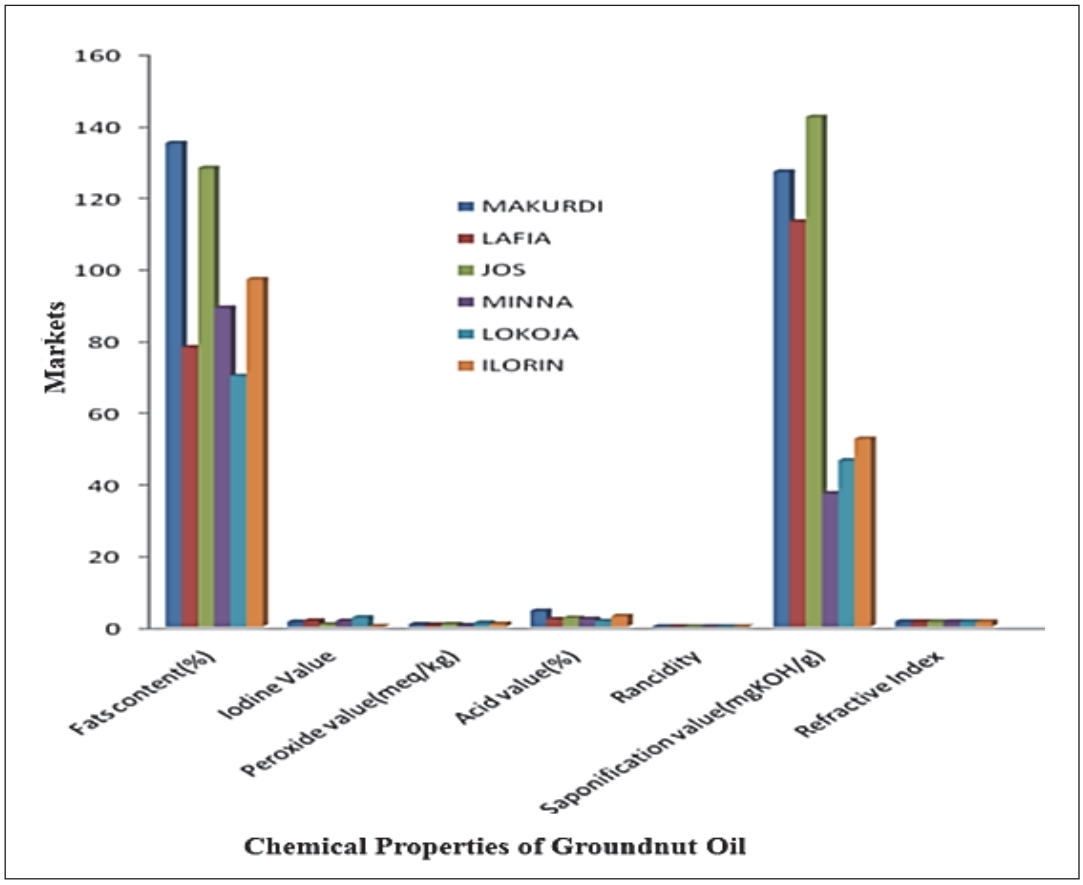

Fig.3.Chemical properties of the groundnut oil sold in north-central Nigeria

3.3. Heavy metals analysis

Lead serves no useful purpose in the human body, but its presence in the body can lead to toxic effects, regardless of the exposure pathway. In this study, the minimum (0.052 mg kg^{-1}) and maximum (0.114 mg kg^{-1}) levels of lead in the groundnut oil recorded were approximately equal to the threshold limit of lead established by WHO [28]. The highest and lowest values were noticed from Lafia and Ilorin markets, respectively. Lead in the oil may result from anthropogenic activities such as using leaded petrol during extraction. The order of lead in the oil was Ilorin>Makurdi>Jos>Lokoja>Minna>Lafia (Table 4 and Figure 4). *Cadmium* mean concentration (Saponification of groundnut oil) in the groundnut oil samples in North central Nigeria was above the recommended limit of daily tolerable intake level of 70 µg for Cd for the average 70kg man and 60 µg of Cd per day for average 60 kg woman [4]. The highest and lowest values were found in Lafia and Jos, respectively (Table 4 and Figure 4). The increased order of cadmium was Jos<Makurdi<Minna<Ilorin< Lokoja< Lafia. The element is toxic even at low levels, resulting in nausea, vomiting, abdominal cramps, headache, diarrhea, and shock. The increase in the mean levels of Cd observed in the groundnut oil was attributed to environmental pollution from emissions from municipal waste incinerates, industrial effluents, and plants' absorption. *Zinc* content of the samples ranged from 0.119 -0.061 mg kg^{-1}. However, the concentration of zinc in the oil samples from the four markets (Makurdi, Jos, Lokoja and Ilorin) analyzed were within the threshold limit (0.1mg kg^{-1}) specified by WHO [28], while Lafia and Minna market values were above the threshold limit established by the world health organization (WHO). Therefore, groundnut oils from these four markets were within the acceptable nutritional margins regarding zinc (Table 4 and Figure 4). *Copper* is essential for the human body, but high intake can cause adverse health problems like headaches, stomachaches, dizziness, vomiting and diarrhea [29]. In Figure 4, the copper content of samples of groundnut oil from all the markets was below the threshold limit; this may probably be a result of low industrial activity in the area, low contamination of the soil in which the groundnut seed used in the production of the oil were cultivated [30]. The highest and lowest values from the research were 0.110 and 0.011 mg kg^{-1}, respectively. The order was Jos>Makurdi>Minna>Ilorin>Lokoja>Lafia. The maximum level of Cu tolerable for a healthy man and woman is 0.9 mg kg^{-1} daily. The results obtained were within acceptable limits of Cu specified by the WHO. Also, heavy metal and VOCs can be extracted /separated from different matrix by nanotechnology before determination by F-AAS, ET-AAS and GC-FID [31-37].

Table 4. Mean Concentration of heavy metals (mg kg^{-1}) in groundnut oil Purchased in North Central Nigeria

Market	Pb	Cd	Zn	Cu
	Mean	Mean	Mean	Mean
Makurdi	0.061	0.202	0.061	0.105
Lafia	0.110	0.333	0.119	0.011
Jos	0.062	0.201	0.063	0.110
Minna	0.113	0.212	0.115	0.103
Lokoja	0.072	0.331	0.071	0.101
Ilorin	0.052	0.322	0.082	0.102
FAO/WHO,1999	0.114	0.07	0.1	0.9

S.D: Standard Deviation

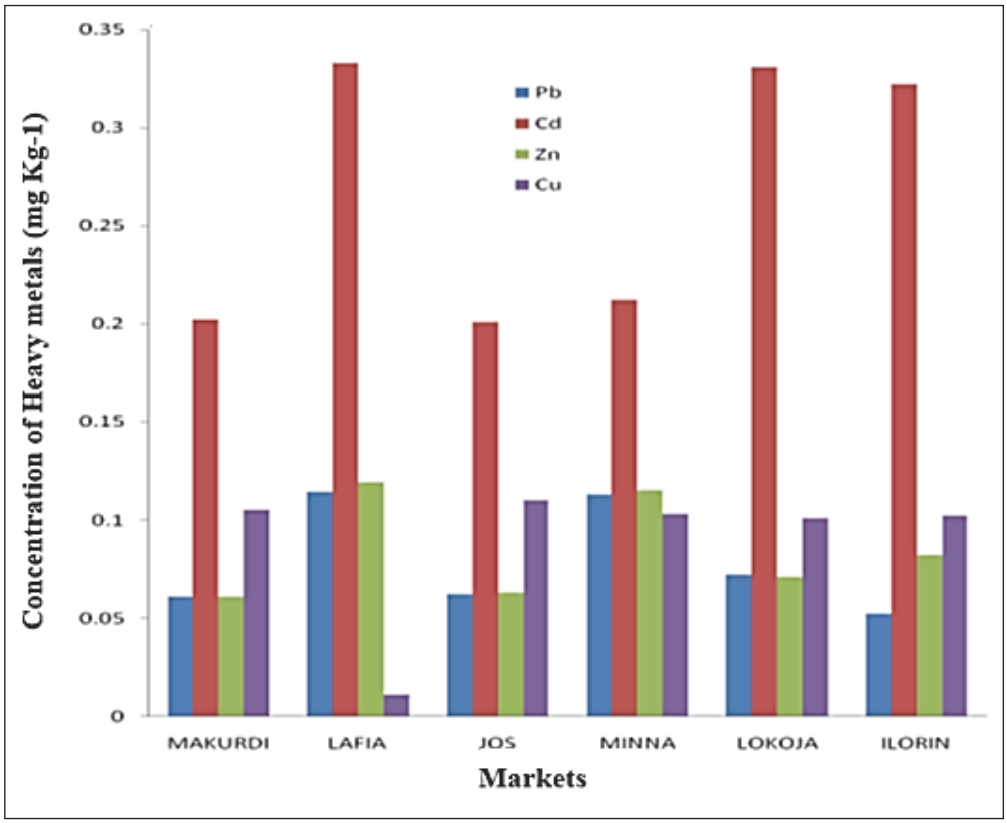

Fig. 4. Concentration of heavy metals (mg kg^{-1}) in groundnut oil

3.4. Analysis of fatty acids composition

Table 5 and Figure 5 show the percentage composition of fatty acids in locally produced groundnut oil in six markets in north-central Nigeria. The results indicated twelve fatty acids in the oils. Comparatively, fatty acid detected in both markets in North central Nigeria includes palmitic acid, palmitoleic acid, margaric acid, stearic acid, oleic acid, linoleic acid, linolenic acid, arachidic acid, arachidonic acid, behenic acid, erucic acid and lignoceric acid. Fatty acids absent in the oils include caprylic, capric, lauric, and myristic acid. The order of fatty acid composition in all the samples in all the markets is linoleic > oleic > palmitic > stearic > lignoceric > arachidic acid > behenic > erucic >arachidonic > margaric >linolenic>palmitoleic acids. Phospholipids results showed six phospholipids: phosphatidylcholine, phosphatidylethanolamine, phosphatidylinositol, phosphatidylserine, phosphatidic acid and Lysophosphatidylcholine. The order of magnitude was phosphatidylcholine > phosphatidylethanolamine > phosphatidylinositol > phosphatidylserine > phosphatidic acid > Lysophosphatidylcholine [23]. The study establishes that all the fatty acid types present were found in the sampled locally produced groundnut oil in all the markets in north-central Nigeria. This result obtained was like that of Kupwade and Desai [14], except that they detected caprylic acid, capric, lauric, and myristic acids and detected oleic acid to be the most predominant, with a percentage of 58.68%. Linoleic acid, the predominant acid in all the sampled markets, is an omega-six fatty acid and plays a vital role in pro-inflammatory reactions, blood clots, and allergic reactions.

Table 5. Percentage composition of fatty acid in locally produced groundnut oils

Fatty acid	Makurdi Market	Lafia Market	Jos Market	Minna Market	Lokoja Market	Ilorin Market
Caprylic acid (C8:0)	0.00	0.00	0.00	0.00	0.00	0.00
Capric acid (C10:0)	0.00	0.00	0.00	0.00	0.00	0.00
Lauric acid (C12:0)	0.00	0.00	0.00	0.00	0.00	0.00
Myristic acid (C14:0)	0.00	0.00	0.00	0.00	0.00	0.00
Palmitic acid (C16:0)	13.58	12.51	11.59	12.65	13.68	12.55
Palmitoleic acid (C16:1)	0.02	0.70	0.03	0.87	0.71	0.02
Margaric acid (C17:0)	0.08	0.05	0.06	0.09	0.09	0.06
Stearic acid (C18:0	4.27	4.59	4.37	4.69	5.00	4.91
Oleic acid (C18:2)	38.25	40.75	39.46	38.43	40.87	40.46
Linoleic acid (C18:2)	42.39	36.38	43.49	42.49	36.48	42.29
Linolenic acid (C18:3)	0.06	0.56	0.06	0.57	0.06	0.55
Arachidic acid (C20:0)	0.38	0.71	0.39	0.63	0.78	0.33
Arachidonic acid C20:4)	0.09	0.42	0.42	0.09	0.09	0.42
Behenic acid (C22:0)	0.16	2.89	2.99	0.17	0.16	2.87
Erucic acid (C22:1)	0.12	0.23	0.13	0.24	0.22	0.23
Lignoceric acid (C24:0)	0.39	0.22	0.83	0.22	0.37	0.21

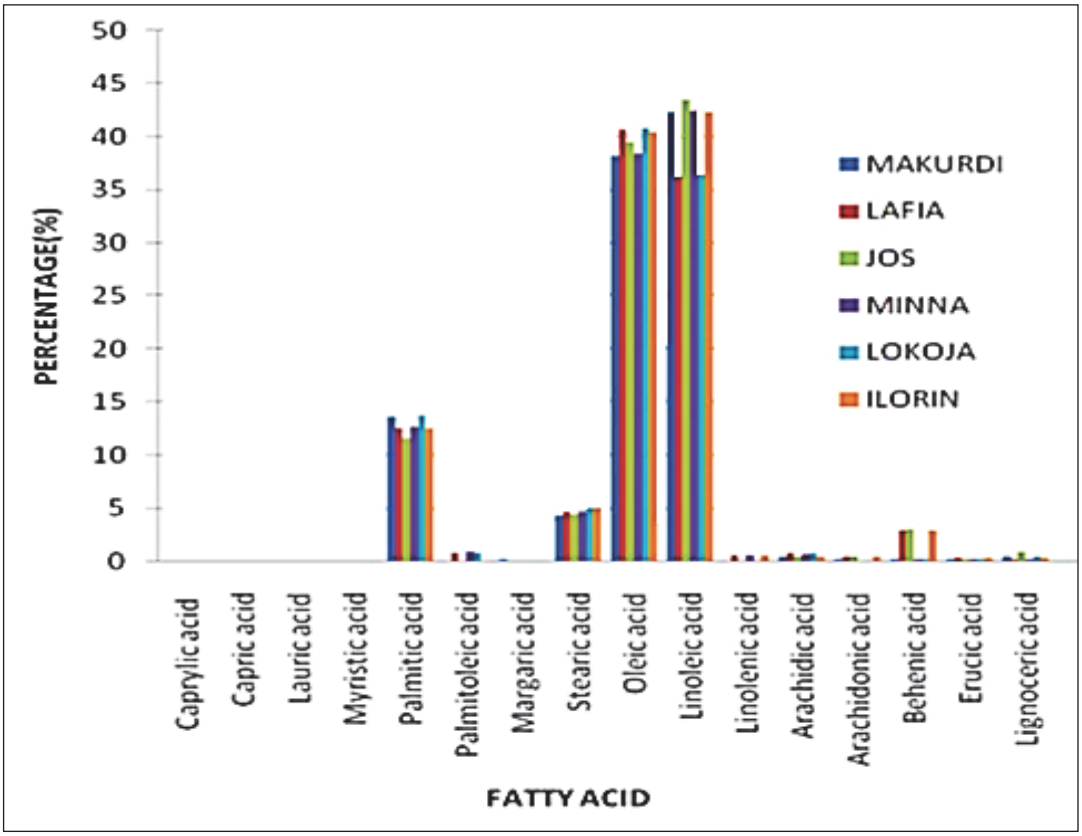

Fig. 5. Percentage of saturated and unsaturated fatty acids found in locally produced groundnut oil in north-central Nigeria

The result of the percentage composition of saturated, unsaturated, and monounsaturated fatty acids are presented in Table 6 and Figure 6, which showed that the percentage composition of total unsaturated fatty acid is more than saturated and monounsaturated fatty acid in all the locally produced groundnut oil marketed in North central Nigeria (Makurdi, Lafia, Jos, Lokoja, Minna and Ilorin) with Makurdi (81.85%) and Jos (78.03%) having the highest and lowest values respectively. The highest composition of TSFA, MUFA and PUFA was found in Lafia (20.97%), Ilorin (41.88%) and Jos (42.80%), while the lowest composition was found in Lokoja (18.85%), Makurdi (38.39%) and Minna (37.22%) respectively. The higher the composition of unsaturated fatty acid, the higher its potential as an industrial feedstock and vice versa. In the polymer industry, unsaturated fatty acids are converted to epoxides poly oils, precursors in making plastics. The order of fatty acids was TUFA>PUFA>MUFA>TSFA.

Table 6. Percentage of saturated, unsaturated, and monounsaturated fatty acids composition

Fatty acid	Makurdi market	Lafia market	Jos market	Minna market	Lokoja market	Ilorin market
TSFA%	18.86	20.97	18.96	20.79	18.85	20.79
TUFA%	81.85	79.03	78.03	81.49	79.21	81.83
MUFA%	38.39	41.68	38.39	41.77	38.48	41.88
PUFA%	42.56	37.35	42.80	37.22	42.11	37.76

* % = Percentage; * TSFA = Total saturated fatty acid
* TUFA = Total unsaturated fatty acid.
* MUFA = Monounsaturated fatty acid.
* PUFA = Polyunsaturated fatty acid.

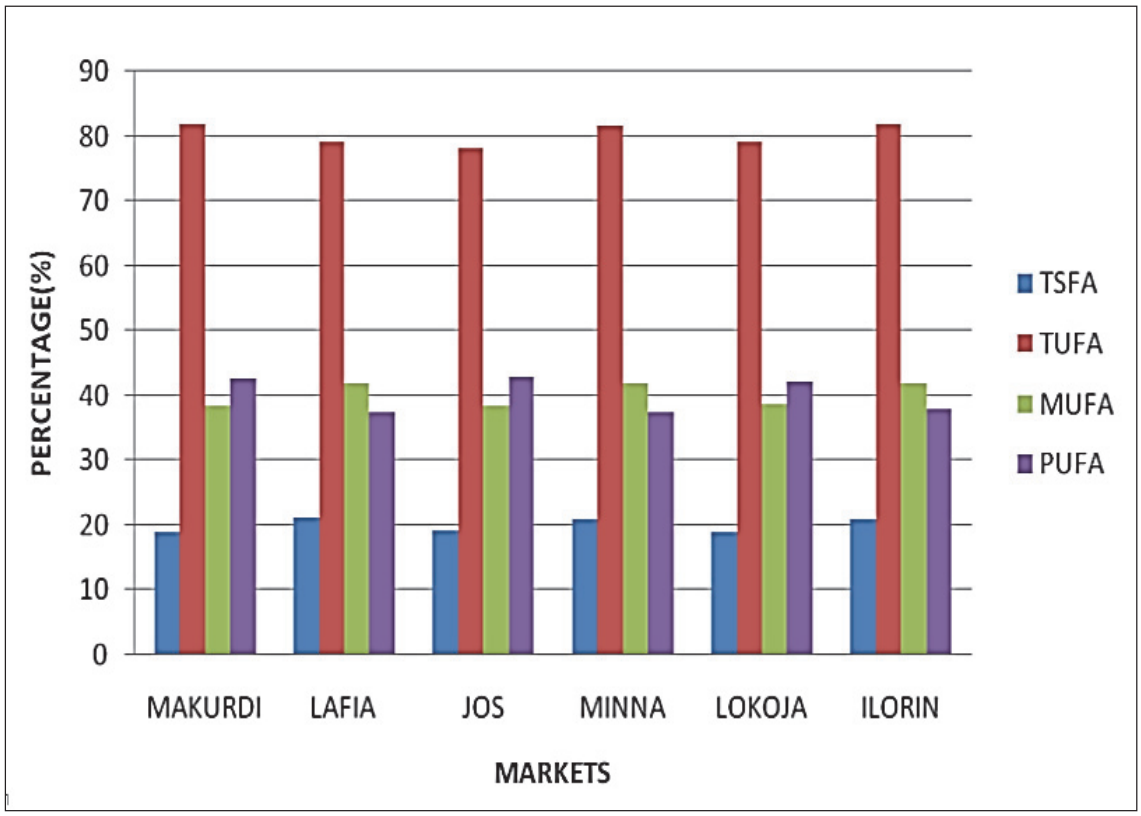

Fig. 6. Percentage of saturated, unsaturated, and monounsaturated fatty acids composition in north-central Nigeria

* TSFA = Total saturated fatty acid * TUFA = Total unsaturated fatty acid;
* MUFA = Monounsaturated fatty acid * PUFA = Polyunsaturated fatty acid;

3.5. Analysis of phospholipids composition

The phospholipids analyzed in locally produced groundnut oil sold in north central Nigeria are presented in Table 7 and Figure 7. Six phospholipids were identified, with phosphatidylcholine having the most significant percentage of phospholipid composition in all the markets and sampled groundnut oil. In contrast, lysophosphatidylcholine had the least in all the markets. The order of magnitude was phosphatidylcholine > phosphatidylethanolamine > phosphatidylinositol > phosphatidylserine > phosphatidicacid > lysophosphatidylcholine.

The highest concentration of phosphatidylcholine was found in Ilorin market (349.22) and the least in Makurdi market (259.86). This research analysis agrees with Adeyeye et al. [38] who reported phosphatidylcholine as the most abundant phospholipid in animals and plants as the main building blocks of membrane bilayers. Phosphatidylcholine, known to reduce body fat and required in the body for cell functioning Williams, Dowhan [39], was detected in large oil concentrations.

Table 7. Percentage composition of phospholipids found in locally produced Groundnut oil in north central Nigeria (mg per 100 gram)

Phospholipid	Makurdi Market	Lafia Market	Jos Market	Minna Market	Lokoja Market	Ilorin Market
Phosphatidylethanolamine	84.87	64.35	85.78	65.53	83.86	63.34
Phosphatidylcholine	259.86	347.04	295.86	346.11	260.84	349.22
Phosphatidylserine	3.39	9.93	3.45	9.68	3.29	9.90
Lysophosphatidylcholine	1.18	2.52	1.19	2.51	1.17	2.50
Phosphatidylinositol	79.53	67.89	78.60	68.98	79.43	69.89
Phosphatidic acid	2.93	10.81	2.99	10.76	2.79	10.18

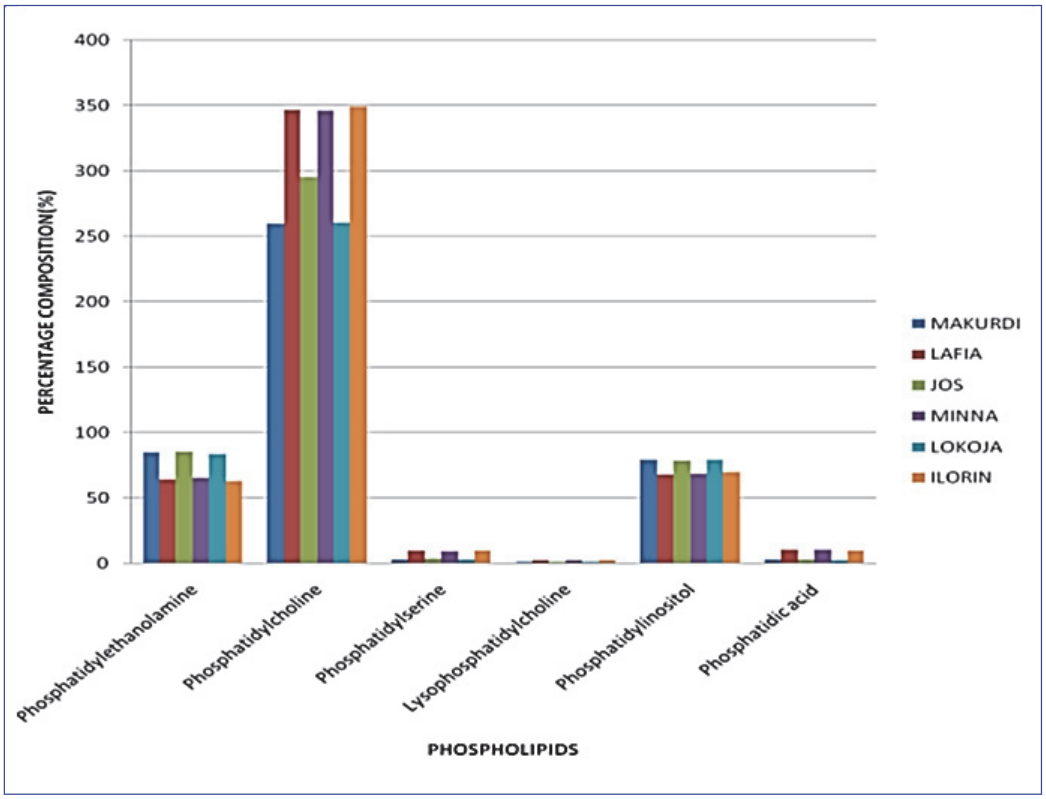

Fig. 7. Percentage composition of phospholipids found in groundnut oil in north-central Nigeria

4. Conclusion

The work compared locally produced groundnut oils produced and sold within and around north-central Nigeria markets. The assessment of the physicochemical parameters of the groundnut oil samples revealed that iodine, saponification, and peroxide values were lower than the threshold limit values (TLVs) except for acids greater than the reference value (FDA/WHO). Heavy metals (Zn, Pb, Cu, and Cd) contents of the groundnut oil from the six markets were detected by F-AAS and GC-FID. The results showed cadmium and zinc appeared to be the predominant metal contaminants and were the only elements that exceeded the recommended safe dietary exposure level. The oils had twelve fatty acids, which include palmitic acid (C16:0), palmitoleic acid (C16:1), margaric acid (C17:0), stearic acid (C18:0), oleic acid (C18:1), linoleic acid (C18:2), linolenic acid (C18:3), arachidic acid (C20:0), arachidonic acid (C20:4), behenic acid (C22:0), erucic acid(C22:1) and lignoceric acid (C24:0). It establishes that capric acid, caprylic acid, lauric acid and myristic acids are absent in the oil while linoleic acid was the highest in composition in all the sampled oil in all the markets in north central Nigeria followed by oleic acid which GC-FID analyzed. The oils show potential for industrial application as biodiesel, lubricants, plastics, and soap due to the presence of unsaturated and some saturated fatty acids. However, the oils will also help make shampoo. The assessment of phospholipid levels of the groundnut oils was also carried out with GC-FID, producing six phospholipids, namely phosphatidylcholine, phosphatidylethanolamine, phosphatidylinositol, phosphatidylserine, phosphatidic acid and Lys phosphatidylcholine. Phosphatidylcholine can help treat liver diseases and serves as a precursor of choline, a compound in the synthesis of acetylcholine, which can improve memory and muscle function.

5. Recommendation

It is recommended that further research into the use of these oils for some industrial processes be embarked upon, and medical value should be checked. Also, groundnut oil contains high levels of phosphatidylcholine, among other legumes. Hence, it is advised that people should consume locally produced groundnut oil more often than other vegetable oils.

6. Significance of the Study

Groundnut oil is the chief source of edible oil. For the production of soap, margarine, and cosmetics and with the growing awareness in environmental pollution, groundnut oil is to be analyzed to ascertain its pollution level and nutritional value. This study is significant for the following reasons;

(i) To provide a physicochemical database for groundnut oil that could be used as a basis for future studies.

(ii) To create awareness of its contamination/ pollution level.

7. Acknowledgement

The authors would like to express unique words of thanks and their acknowledgement to the Faculty of Sciences, Ahmadu Bello University Zaria, Nigeria, for their support and to the chief Technologist for his encouragement in carrying out this study.

8. References

[1] M. M. Azam, K. T. Ramya, R. Abdul Fiyaz, B. C. Ajay, A. Waris, Hidden treasures of edible oils and their health benefits, Popular Kheti, 7(3) (2019) 53-56. www.popularkheti.com

[2] C.W.S. Hartley, The oil palm, Longman Scientific & Technical ; Wiley, Harlow, Essex, England, New York, 3rd Edition, 958, 1988. https://www.worldcat.org/title/oil-palm-elaeis-guineensis-jacq/oclc/17505983

[3] W. Jadaa, H.K. Mohammed, Heavy Metals–Definition,NaturalandAnthropogenicSources of Releasing into Ecosystems, Toxicity, and Removal Methods – An Overview Study, J. Ecol. Eng., 24 (2023) 249-271. https://doi.org/10.12911/22998993/162955

[4] K.Asemave, S.T. Ubwa, B.A. Anhwange, A.G. Gbaamende, Comparative evaluation of some

metals in palm oil, groundnut oil and soybean oil from Nigeria, Int. J. Mod. Chem., 1 (2012) 28-35. https://modernscientificpress.com/journals/ijmchem.aspx

[5] P. Agbaire, Nutritional and antinutritional levels of some local vegetables from Delta State, African J. Food Sci., 6 (2012) 8-11. https://doi.org/10.5897/AJFS11.175

[6] M.G. Idris, D. Umaru, A.N. Aliyu, I.H. Musa, Atomic absorption spectroscopy analysis of heavy metals in water at Daura gypsum mining site, Yobe state, Nigeria, J. Founds. Appls. Phy., 8 (2021) 227–234. http://sciencefront.org/ojs/index.php/jfap/article/view/184

[7] P.A. Adeoye, Z. Saidu, I.A. Kuti, J. Ibrahim, B.A. Adabembe, Assessment of heavy metals uptake by vegetables cultivated on soil receiving industrial wastewater in Minna, Nigeria, Arid Zone J. Eng. Techn. Environ., 14 (2018)101-110. https://www.azojete.com.ng/index.php/azojete/article/view/128/90

[8] S. Umar, A. Muhammad S. Elijah, Assessment of heavy metal contamination in groundwater from motorized boreholes In Maitumbi, Tipa garage area, Minna, Niger state, Sci. World J., 18 (2023) 212-215. https://dx.doi.org/10.4314/swj.v18i2.7

[9] G.C. Burdge, P. Wright, E.A. Jones, S.A. Wootton, A method for separation of phosphatidylcholine, triacylglycerol, non-esterified fatty acids and cholesterol esters from plasma by solid-phase extraction, Br. J. Nutr., 84 (2000)781–787. https://doi.org/10.1017/S0007114500002154

[10] J.G. Puentes, A.J. Moya, M.D. La Rubia, Comparative study of the presence of heavy metals in edible vegetable oils, Appl. Sci., 13 (2023) 3020. https://doi.org/10.3390/app13053020

[11] A. A. Shaltout, M. A. Ibrahim, Detection limit enhancement of Cd, Ni, Pb and Zn determined by flame atomic absorption spectroscopy, Can. J. Anal. Sci. Spect., 52 (2007) 276-286 https://www.scribd.com/document/528781981/CJASS-2007

[12] AOCS, Official Method Ce1b-89, Fatty acid composition of marine oils by gas liquid chromatography (GLC), in Collison, M. W. (ed.) official methods and recommended practices of the American oil chemists' society. 7th ed. Champaign, Illinois, USA, American Oil Chemists' Society Press, 2017. https://myaccount.aocs.org/PersonifyEbusiness/Store/Product-Details/productId/111772

[13] S. Kheirati, M.F. Akrami, B.H. Moshtaghi, F. Pourramezani, S. Jambarsang, H. Kiani, S.E. Khalili, The chemical composition and heavy metal content of sesame oil produced by different methods: A risk assessment study, Food Sci. Nutr., 9 (2023) 2886-2893. https://doi.org/10.1002/fsn3.2245

[14] R.V. Kupwade, V.M. Desai, Estimation of acid value, % of FFA and cholesterol content in groundnut oil collected from local rural farmers in Sangli, Int. J. Res. Anal. Revs. (IJRAR), 6 (2019) 516 – 517. http://www.ijrar.org/IJRAR1AAP130.pdf

[15] D. Pearson, The chemical Analysis of food, 6th ed., Churchill Publisher, London, Pages 604, 1970. https://www.amazon.com/chemical-analysis-foods-David- Pearson/dp/0700014578

[16] F. J. Baur, L. G. Ensminge, The Association of Official Analytical Chemists (AOAC), J. Am. Oil Chem. Soc., 54 (1977) 171–172. https://doi.org/10.1007/BF02670789

[17] D. R. Erickson, Practical Handbook of Soybean Processing and Utilization, Elsevier, 1st Edition, pages 130, 2015. https://doi.org/10.1016/C2015-0-04084-9

[18] Y. Liu, L. Li, Q. Xia, L. Lin, Analysis of physicochemical properties, Lipid composition, and oxidative stability of cashew Nut Kernel oil, Foods, 12 (2023) 693. https://doi.org/10.3390/foods12040693

[19] A. Thomas, Fats, and fatty oils, Ullmann's Encyclopedia of Industrial Chemistry, Weinheim, Wiley-VCH, Pp 1-84, 2002. https://doi.org/10.1002/14356007.a10_173

[20] M.M. Chakrabarty, Chemistry and Technology Of Oils and Fats, Wayback Machine, 2018.

https://web.archive.org/

[21] M.A.M. Hassan, Studies on Egyptian sesame seeds (sesamum indicum L) and its products and effect of roasting conditions on peroxide value, free acidity, iodine value and antioxidant activity of sesame seeds, World J. Dairy Food Sci., 8 (2013) 11-17. https://doi.org/10.5829/idosi.wjdfs.2013.8.1.1114

[22] H.A. Zahran, H.Z. Tawfeuk, Physicochemical properties of new peanut (Arachis hypogaea L.) varieties,OilseedsFatsCropsLipids,26(2019)19. https://doi.org/10.1051/ocl/2019018

[23] A. Kaleem, S. Aziz, M. Iqtedar, R. Abdullah, M. Aftab, F. Rashid F, Investigating changes and effect of peroxide values in cooking oils subject to light and heat, FUUAST J. Biol., 5 (2015)191–196. https://fuuastjb.org/index.php/fuuastjb/article/view/106

[24] E.I. Ohimain, C. Daokoru-Olukole, S.C. Izah, E.E. Alaka, Assessment of the quality of crude palm oil produced by smallholder processors in Rivers State, Nigeria, Niger. J. Agri. Food Environ., 8 (2012) 28 - 34. https://catalog.princeton.edu/catalog/99101434973506421

[25] J. M. deMan, Principles of Food Chemistry, Springer New York, NY, 475-489, 1999. https://doi.org/10.1007/978-1-4614-6390-0

[26] F.O. Badmos, N.A. Usman, Q. Onagun, O.A. Arogbokun, G.K. Ezikanyi, M. Jr. Kinta, Determination of some physicochemical parameters of three vegetable oils sold in Bosso Market, Minna, Nigeria, A J. Sci. Technol. Math. Edu., 15 (2019) 1-7. https://searchworks.stanford.edu/view/10376791

[27] C. R. Engler, L. A. Johnson, Effects of processing and chemical characteristics of plant oils on performance of an indirect injection diesel engine, J. Am. Oil Chem. Soc., 60 (1983) 1592-1596. https://doi.org/10.1007/BF02666591

[28] FAO/WHO, Joint FAO/WHO Expert Committee on Food Additives, Ninety-third meeting JECFA, USA, 2022. https://www.who.int/foodsafety/en/

[29] S.J. More, V. Bampidis, D.Benford, C. Bragard, T.I. Halldorsson, A.F. Hernández-Jerez, S.H. Bennekou, K. Koutsoumanis, C. Lambré, K. Machera, E. Mullins, S.S. Nielsen, J.R. Schlatter, D. Schrenk, D. Turck, M. Younes, P. Boon, G.A. Ferns, O. Lindtner, C. Leblanc, Re-valuation of the existing health-based guidance values for copper and exposure assessment from all sources, EFSA J., 21(2023) e07728. https://doi.org/10.2903/j.efsa.2023.7728

[30] S.M. Kithiia, The effects of land use types on hydrology and water quality of upper Athi river basin, Kenya, Publisher: University of Nairobi, 1991. http://erepository.uonbi.ac.ke/handle/11295/21062

[31] Z. Karamzadeh, J. Rakhtshah, N.M. Kazemi, A novel biostructure sorbent based on ysSB/MetSB@ MWCNTs for separation of nickel and cobalt in biological samples by ultrasound assisted-dispersive ionic liquid-suspension solid phase micro-extraction, J. Pharm. Biomed. Anal., 172 (2019) 285-294. https://doi.org/10.1016/j.jpba.2019.05.003

[32] K. Merchant, M.D. Mobarake, Ultrasound-assisted solid-liquid trap phase extraction based on functionalized multi-wall carbon nanotubes for preconcentration and separation of nickel in petrochemical wastewater, J. Anal. Chem., 74 (2019) 865-876. https://doi.org/10.1134/S1061934819090090

[33] N. Esmaeili, Ultrasound assisted-dispersive-modification solid-phase extraction using task-specific ionic liquid immobilized on multiwall carbon nanotubes for speciation and determination mercury in water samples, Microchem. J., 154 (2020) 104632. https://doi.org/10.1016/j.microc.2020.104632

[34] J. Rakhtshah, N. Esmaeili, A rapid extraction of toxic styrene from water and wastewater samples based on hydroxyethyl methylimidazolium tetrafluoroborate immobilized on MWCNTs by ultra-assisted dispersive cyclic conjugation-micro-solid phase extraction, Microchem. J., 170 (2021) 106759. https://doi.org/10.1016/j.microc.2021.106759

[35] M. Habibnia, A. Rashidi, Simultaneously speciation of mercury in water, human blood and food samples based on pyrrolic and pyridinic nitrogen doped porous graphene nanostructure, Food Chem., 403 (2023) 134394. https://doi.org/10.1016/j.foodchem.2022.134394

[36] N. Esmaeili, J. Rakhtshah, E. Kolvari, Rapid speciation of lead in human blood and urine samples based on mwcnts@ dmp by dispersive ionic liquid-suspension-micro-solid phase extraction, Biol. Trace Elem. Res., 199 (2021) 2496-2507. https://doi.org/10.1007/s12011-020-02382-7

[37] Sh. Teimoori, New extraction of toluene from water samples based on nano-carbon structure before determination by gas chromatography, Int. J. Environ. Sci. Technol., 20 (2023) 6589–6608. https://doi.org/10.1007/s13762-023-04906-9

[38] E.I. Adeyeye, A.J. Adesina, M.C. Ginika, H.E. Aiyo, Great Barracuda: Its skin and Muscle fatty acids, phospholipids and Zoosterol composition, Int. J. Chem. Sci., 5 (2012) 18-28. https://www.chemicaljournals.com/

[39] D. William, molecular basis for membrane phospholipids diversity: why are there so many lipids? Annu. Rev. Biochem., 66 (1997)199-232 .https://doi.org/10.1146/annurev.biochem.66.1.199